University of Crete, Department of Biology

PhD Dissertation
Supervisor: Professor Electra Gizeli

# Development of acoustic wave biosensors for application in molecular diagnostics

**Aristea Grammoustianou**


Heraklion, 2018

Trust that your success is well deserved and hard earned.

(Anonymous source)

# Contents

# Aknowledgements

I would like to thank my supervisor Prof. Electra Gizeli, for the guidance, motivation and support she provided throughout the duration of my PhD studies. We met at a very difficult period of my life, and working in her lab, gradually, chased my blues away.

To the rest of you, the very few and special ones of you, thank you for being an important part of my story.

# Abstract

Since the development of the first biosensor by Leland C. Clark in 1962, the progress in the field of biosensors has been phenomenal. The biosensors market is estimated to reach US$ 27.06 billion by the year 2022 and, currently, scientific research is focused on the development of inexpensive, non-invasive, integrated and portable biosensors that will find application in point-of-care diagnostics, food and process control, environmental monitoring, biodefense, and forensics. The present PhD research focused on the development of acoustic wave-based bioassays that can be applied in molecular diagnostics. Acoustic wave biosensors offer real-time and label-free biological sensing. This study made use of the unique characteristics of acoustic wave biosensors in order to develop bioassays for food safety and cancer diagnostics.

The first objective of this thesis was the acoustic detection of the foodborne pathogen *Salmonella* Typhimurium. Two approaches were followed: the first one made use of an acoustic wave immunosensor for the detection of whole *Salmonella* Typhimurium cells. The biosensor developed was able to detect *Salmonella* Typhimurium cells of a concentration of $10^6$ cfu/mL and within 30 min. The second approach employed an acoustic wave biosensor for the solid phase amplification of the gene *invA* of *Salmonella* Typhimurium via the recombinase polymerase amplification and simultaneous detection of DNA amplicons on the device surface. For amplicon detection, a novel methodology was described, where the formation of surface-bound DNA amplicons was detected by using liposomes as an amplification probe. The presented methodology was fast (detection of DNA amplicons after only 5 min of amplification) and simple (it did not require any post-amplification steps).

The second part of the research work focused on the development of acoustic wave biosensors for molecular cancer diagnostics. A DNA-based biosensor was designed for the detection of four miRNAs (miR-21, miR-155, miR-150 and miR-107) considered being dynamic biomarkers of breast cancer. The miRNAs detection was achieved using a single oligonucleotide probe. In fact, the biosensor allowed the rapid, real-time, label-free and simple detection of two miRNAs at the same time.

The final aim of this work was the development of an acoustic wave-based bioassay by which ctDNA carrying KRAS mutations that are characteristic of colorectal cancer would be acoustically detected via their hybridization to a PNA probe immobilized on the acoustic sensor surface; the assay employed a high fundamental frequency acoustic wave device and a patented technology which combines the patented aldehyde-modified SMART nucleobases with unique PNA capture probes synthesized with a “blank” position (DGL probes). This technology introduces an entirely chemical, rather than enzymatic, method for nucleic acid testing. The assay achieved the detection of KRAS mutations present on ctDNA introducing a new alternative to current colorectal cancer diagnostic techniques.

# Περίληψη

Από την ανάπτυξη του πρώτου βιοαισθητήρα από τον Leland C. Clark το 1962, η πρόοδος στον τομέα των βιοαισθητήρων είναι πρωτοφανής. Η αγορά των βιοαισθητήρων εκτιμάται ότι θα κοστίζει 27.06 δισεκατομμύρια δολάρια μέχρι το 2022. Επί του παρόντος, η επιστημονική έρευνα είναι επικεντρωμένη στην ανάπτυξη οικονομικών, μη επεμβατικών, ενσωματωμένων και φορητών βιοαισθητήρων που θα βρουν εφαρμογή στους τομείς της ταχείας διαγνωστικής, της ανάλυσης ποιότητας τροφίμων, του περιβαλλοντικού ελέγχου, της βιοάμυνας και της εγκληματολογίας. Η παρούσα διδακτορική έρευνα επικεντρώθηκε στην ανάπτυξη ακουστικών βιοαισθητήρων που μπορούν να βρουν εφαρμογή στη μοριακή διαγνωστική. Οι ακουστικοί βιοαισθητήρες επιτρέπουν την βιολογική ανίχνευση σε πραγματικό χρόνο και χωρίς την ανάγκη σήμανσης. Η έρευνα χρησιμοποίησε τα μοναδικά χαρακτηριστικά των ακουστικών βιοαισθητήρων για την ανάπτυξη βιοδοκιμών με εφαρμογή στους τομείς της ασφάλειας τροφίμων και της διαγνωστικής καρκίνου.

Ο πρώτος στόχος της διατριβής ήταν η ακουστική ανίχνευση του τροφιμογενούς παθογόνου *Salmonella* Typhimurium. Δύο προσεγγίσεις ακολουθήθηκαν: η πρώτη χρησιμοποίησε έναν ακουστικό ανοσοαισθητήρα για την ανίχνευση ολόκληρων κυττάρων *Salmonella* Typhimurium. Ο βιοαισθητήρας πέτυχε την ανίχνευση των κυττάρων μέσα σε 30 λεπτά και με όριο ανίχνευσης τις $10^6$ μονάδες σχηματισμού αποικίας/mL ($10^6$ cfu/mL). Η δεύτερη προσέγγιση χρησιμοποίησε έναν ακουστικό βιοαισθητήρα για την ενίσχυση και ανίχνευση της ενίσχυσης του γονιδίου *invA* της *Salmonella* Typhimurium επάνω στην ακουστική επιφάνεια. Για την ενίσχυση του γονιδίου χρησιμοποιήθηκε η ισόθερμη τεχνική recombinase polymerase amplification (RPA). Η ταυτόχρονη ανίχνευση των γονιδιακών αμπλικονίων πάνω στην επιφάνεια του βιοαισθητήρα έγινε με τη χρήση λιποσωμάτων που έδρασαν ως ενισχυτικοί ανιχνευτές. Η μεθοδολογία που παρουσιάστηκε για πρώτη φορά σε αυτή την έρευνα ήταν γρήγορη (ανίχνευση των γονιδιακών αμπλικονίων σε 5 μόνο λεπτά) και απλή (δε χρειάστηκαν μετα-ενισχυτικά βήματα επεξεργασίας των αμπλικονίων).

Το δεύτερο μέρος της παρούσας διατριβής ασχολήθηκε με την ανάπτυξη ακουστικών βιοαισθητήρων για τη μοριακή διαγνωστική καρκίνου. Ένας DNA-βιοαισθητήρας σχεδιάστηκε για την ανίχνευση 4 microRNAs (miRNAS: miR-21, miR-155, miR-150, miR-107) που θεωρούνται δυναμικοί βιοδείκτες του καρκίνου του μαστού. Η ακουστική ανίχνευση πραγματοποιήθηκε με τη χρήση ενός μοναδικού ολιγονουκλεοτιδικού ιχνηθέτη. Μάλιστα, ο βιοαισθητήρας επέτρεψε τη γρήγορη, απλή και ταυτόχρονη ανίχνευση δύο miRNAs σε πραγματικό χρόνο και χωρίς τη χρήση μορίων επισήμανσης.

Ο τελικός σκοπός της παρούσας δουλειάς ήταν η ανάπτυξη ενός ακουστικού βιοαισθητήρα για την ανίχνευση KRAS μεταλλάξεων, χαρακτηριστικών του ορθοκολικού καρκίνου, παρόντων σε circulating tumor DNA (ctDNA) μόρια. Η ανίχνευση των KRAS μεταλλάξεων έγινε μέσω της υβριδοποίησης των ctDNA μορίων σε έναν peptide nucleic acid (PNA) ανιχνευτή πάνω στην επιφάνεια του αισθητήρα. Χρησιμοποιήθηκαν ακουστικοί αισθητήρες υψηλούς θεμελιώδους συχνότητας και μία πατενταρισμένη τεχνολογία που συνδυάζει νουκλεοβάσεις με τροποιημένη αλδεΰδη (SMART nucleobases) και μοναδικούς PNA ιχνηθέτες που φέρουν μία «κενή» θέση στον σκελετό τους (DGL probes). Η τεχνολογία που αναπτύχθηκε πέτυχε την ακουστική ανίχνευση KRAS μεταλλάξεων παρόντων σε μόρια ctDNA εισάγοντας μία νέα εναλλακτική στις τρέχουσες μεθόδους διάγνωσης του ορθοκολικού καρκίνου.

# List of Abbreviations

| | |
|---|---|
| Base pairs | bp |
| Bulk acoustic wave | BAW |
| Centers for Diseases Control and Prevention | CDC |
| Circulating tumor DNA | ctDNA |
| Colony forming unit | cfu |
| Complementary DNA | cDNA |
| Deoxyribonucleic acid | DNA |
| Deoxyribonucleotide | dNTP |
| Dissipation | D |
| Dissipation units | DU |
| Double-stranded DNA | dsDNA |
| Ethanol | EtOH |
| Food and Drug Administration | FDA |
| Frequency | F |
| Genetically modified organism | GMO |
| Gold nanoparticle | AuNP |
| Hertz | Hz |
| High fundamental frequency | HFF |
| Interdigital transducers | IDTs |
| International Union of Pure and Applied Chemistry | IUPAC |
| Limit of detection | LOD |
| Lipopolysaccharide | LPS |
| Lithium niobate | $LiNbO_3$ |
| Lithium tantalate | $LiTaO_3$ |
| Lysogeny broth | LB |
| Microgram | µg |
| Microliter | µl |
| Micromolar | µM |
| MicroRNA | mRNA |
| Mililiter | mL |
| Molar | M |
| Nanometre | nm |
| Nucleic acid | NA |
| Nucleotide | nt |
| Optical density | OD |
| Peptide nucleic acid | PNA |
| Phase | Ph or $\varphi$ |
| Phosphate buffer saline | PBS |
| Point-of-care | PoC |
| Polyethylenimine-glutaraldehyde | PEG |

| | |
|---|---|
| Polymerase chain reaction | PCR |
| Polymethylmethacrylate | PMMA |
| QCM with dissipation monitoring | QCM-D |
| Quartz crystal microbalance | QCM |
| Ribonucleic acid | RNA |
| Room temperature | RT |
| Scanning electron microscopy | SEM |
| Self-assembled monolayer | SAM |
| Silicon dioxide | $SiO_2$ |
| Single-stranded DNA | ssDNA |
| Sodium chloride | NaCl |
| Streptavidin | SAv |
| Surface acoustic wave | SAW |
| Thickness shear mode | TSM |
| Viable but non-culturable | VBNC |
| World Health Organization | WHO |

# Introduction

## Biosensors

Biosensors are analytical devices that convert biological interactions into digital signals. In recent years, they have proved their potential to find applications in the fields of medical diagnostics, food quality and safety, environmental monitoring and biodefense (*1-4*).

According to the International Union of Pure and Applied Chemistry (IUPAC) a biosensor is an analytical device which provides quantitative or semi-quantitative information using a biological or biologically derived recognition element that recognizes a specific bio-analyte and that is in contact with a physicochemical transduction element (*5, 6*). The biorecognition element can be a biological material (e.g. enzyme, antibody, nucleic acid or cell receptors), a biologically derived material such as an aptamer or a recombinant antibody, or even a biomimic material (molecularly imprinted polymers and synthetic catalysts). The interaction between the recognition element and the analyte is converted by the transducer into a digital signal, which, in turn, is interpreted by a computer (Fig. 1).

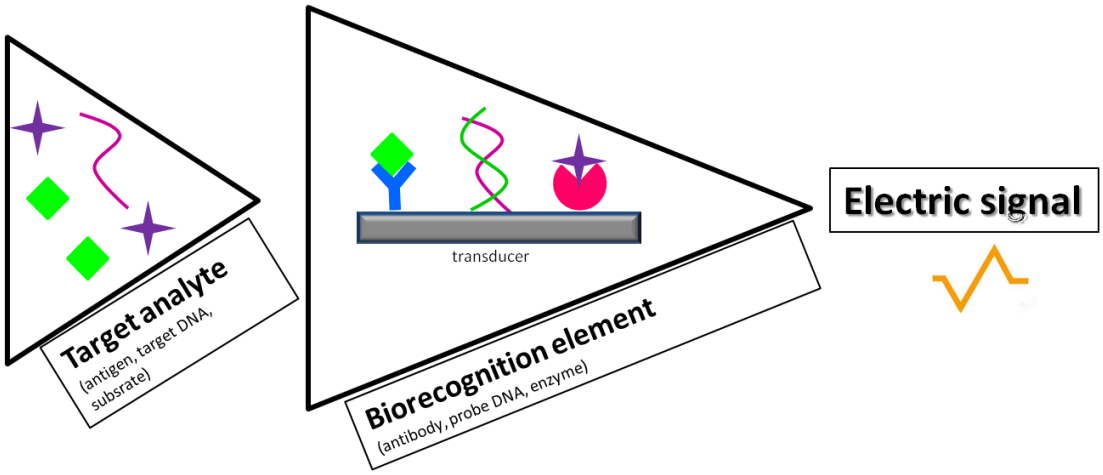


**Figure 1.** Schematic diagram of the working principle of a biosensor

Biosensors can be classified either based on the recognition element which might be an enzyme, a nucleic acid, an antibody, a tissue and even a whole microorganism (enzyme-based, antibody-based, DNA-based e.t.c. biosensors) or based on the type of the transduction element. Based on the type of the transducer biosensors are classified into: piezoelectric/acoustic wave biosensors, electrochemical, calorimetric and optical (Fig. 2).

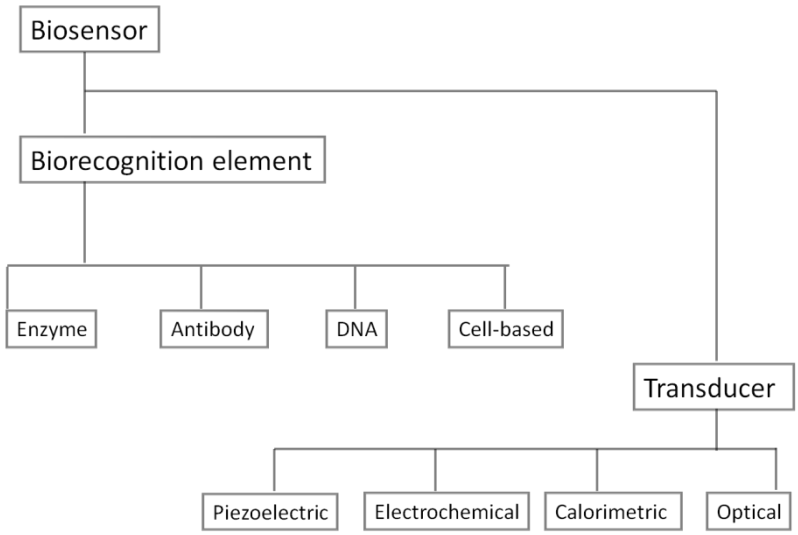


**Figure 2.** Classification of biosensors

For this work, piezoelectric biosensors were used in order to study surface-hybridization and develop molecular diagnostics assays.

## Acoustic wave biosensors

Acoustic wave biosensors are made up of piezoelectric materials. The most commonly used is the quartz because it is abundant in nature and exhibits good meachanical, chemical and thermal properties. Acoustic wave biosensors make use of the piezoelectric effect or, to be more precise, of the converse of the piezoelectric effect. The piezoelectric effect was discovered in 1880 by Jacques and Pierre Curie and it states that anisotropic crystals (crystals without center of symmetry) can generate an electric voltage when mechanical stress is applied to them. The converse piezoelectric effect states than an anisotropic crystal will mechanically deform when voltage is applied to it. In the case of acoustic wave biosensors application of voltage results in the generation of an acoustic wave which is used by the sensor as the detection mechanism. (Fig. 3).

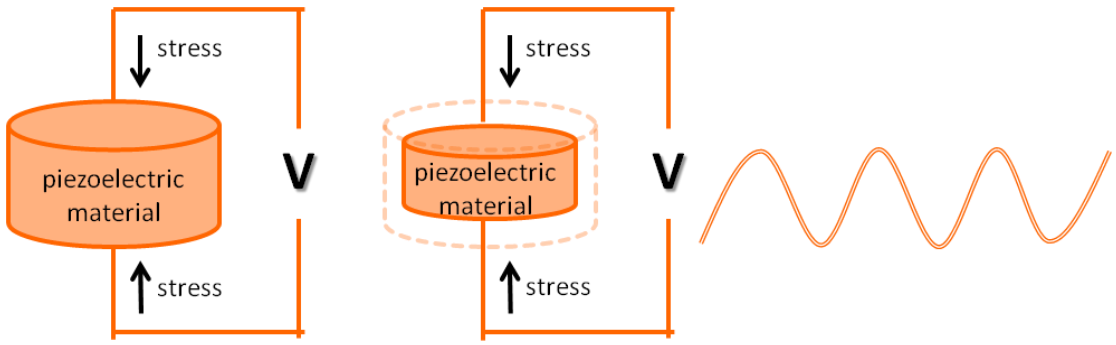


**Figure 3.** Schematic description of the piezoelectric effect

The acoustic wave propagates on the surface of the material and any mass deposition results in changes in the physical properties of the acoustic wave i.e. the velocity and/or amplitude.

According to the type of the acoustic wave generated on the sensor surface acoustic wave biosensors are classified into two main categories. The bulk acoustic wave (BAW) and surface acoustic wave (SAW) devices.

## Bulk acoustic wave (BAW) devices

The Quartz Crystal Microbalance (QCM) or Thickness Shear Mode (TSM) resonator is the most widely used representative of BAW sensors. The QCM (Fig. 4.a) consists of an AT-cut quartz crystal sandwiched between two electrodes (that are usually gold). Application of an alternating voltage through the QCM electrodes causes the crystal to oscillate at a fundamental resonant frequency, with a typical range of 5 to 50 MHz and results in the generation of a standing acoustic wave (Fig. 4.b) inside the crystal. The fundamental resonant frequency (F) of the crystal is sensitive to mass deposition on the crystal surface as Sauerbrey described (*7*):

$$M = -\frac{C}{n}\Delta f \quad (1)$$

where $C$ (17.7 ng cm$^{-2}$ Hz$^{-1}$ for crystals of $f$ = 5 MHz) is the mass sensitivity constant and $n$ (=1, 3, …) is the overtone number.

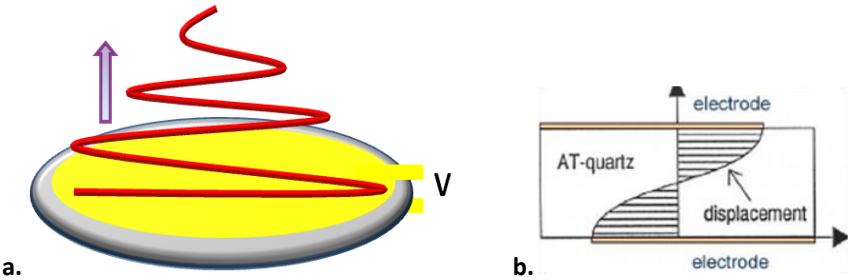


**Figure 4.** Illustration of **a.** a QCM sensor, **b.** the bulk acoustic wave motion

## Surface acoustic wave (SAW) sensors

SAW sensors (Fig. 5. a) consist of two basic components: the first is the piezoelectric substrate, which typically is ST-cut quartz, lithium niobate ($LiNbO_3$) or lithium tantalate ($LiTaO_3$). The second is the photolithographically or ion-beam produced electrodes that are called interdigital transducers (IDTs). Application of an electric potential to the piezoelectric substrate through IDTs creates a shear-horizontal acoustic wave (SH-SAW) (Fig. 5. b) that propagates along the crystal surface and is confined near the surface of the piezoelectric material. SAW devices are advantageous in terms of biosensing since they are highly sensitive to mass

adsorption, owing to the confinement of the acoustic wave to the surface. SAW devices can detect small mass changes at the sensing surface as a frequency response, as the IDTs transmit and receive acoustic waves (*8*). SAW sensors operate at higher frequencies compared to BAW sensors. Such frequencies range from 100 to 500 MHz and depend on the acoustic velocity of the crystal substrate and the IDTs wavelength.

Deposition of a thin film of a polymer (silicon dioxide ($SiO_2$), polymethylmethacrylate (PMMA)) over a quartz-based SH-SAW device results in further confinement of the acoustic wave to the sensing surface. In this case the added material works as a waveguide and the shear-horizontal waves generated are called Love waves (*9*). Love wave SAW (LW-SAW) devices are mainly used in biochemical analysis in solution (*10*).

Obeying to the Sauerbrey equation (1) and equivalently to the QCM, a change in the phase (Ph or $\varphi$) of the acoustic wave on a SAW corresponds to mass deposition on the sensing surface.

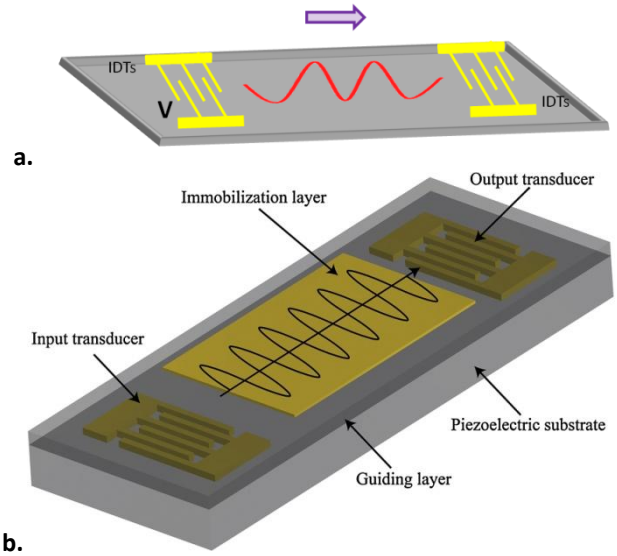


**Figure 5.** Illustration of: **a.** a SAW sensor, **b.** a Love wave SAW sensor

## A closer look into acoustic data interpretation

In principle, mass deposition on the sensor surface affects the velocity of an acoustic wave. Changes in the frequency (ΔF) of the QCM wave or the phase (ΔPh or $\Delta\varphi$) of the SAW correlate to the amount of mass deposited on the sensor surface. The Sauerbrey relationship can be applied when the following three assumptions are fulfilled: first, the adsorbed mass has to be small related to the mass of the quartz crystal; second, the mass adsorbed is a rigid film; and third, the mass adsorbed is homogeneously distributed over the sensing area of the crystal (*11-14*). However, nonrigid, “viscoelastic” films (as are the biomolecular films) will not entirely couple to the oscillation of the crystal, thus the Sauerbrey’s equation will fail to estimate the total mass on the sensor surface (Fig. 6). In addition, viscoelastic films dampen further the frequency of oscillation. This damping or else energy dissipation (D) of

the sensor's oscillation correlates to the film's viscoelasticity. Hence, a different analytical approach is needed to probe the characteristics of a viscoelastic film.

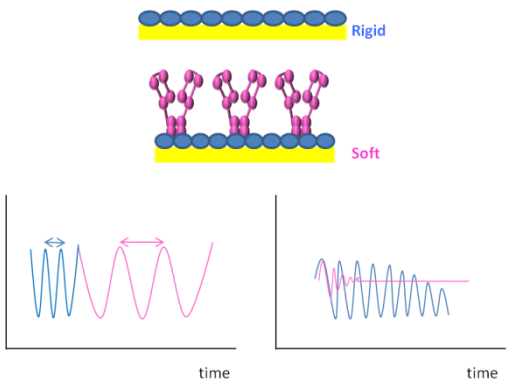


**Figure 6.** The left diagram demonstrates the change of the frequency of the oscillating crystal when the mass is increased by addition of a molecular layer. Here antibodies **(pink)** are added to a layer of protein **(blue)**. The right diagram illustrates the equivalent change in the dissipation signal

The introduction of the QCM with dissipation monitoring (QCM-D) set-up addressed the issue of dissipation (D) due to vscoelastic film adsorption. Simultaneous measurements of changes in both the frequency (ΔF) and dissipation (ΔD) of the quartz crystal increased the information obtained from QCM experiments (Fig.7). Dissipation occurs when the applied voltage to the crystal is shut off and the energy from the oscillating crystal dissipates from the system. D can be calculated by equation (2):

$$D = \frac{E_{lost}}{2\pi E_{stored}} \quad (2)$$

where $E_{lost}$ is the energy lost at one oscillation cycle and $E_{strored}$ is the total energy stored in the crystal oscillator. The combined monitoring of Δf and ΔD using a Voigt-based viscoelastic model provided information on the viscoelastic film thickness ($d_f$), effective density ($\rho_f$), absolute viscosity ($\eta_f$) and elasticity ($\mu_f$), assuming that the adsorbed film is homogeneous (*15*). Moreover, the ratio of DΔ over ΔF (i.e. the measured energy dissipation per surface-coupled unit mass) is used as a qualitative fingerprint of the adsorbed biofilm and relates to the structure of the layer (relative rigidity, water content e.t.c.) (*13, 16*).

Similar to the QCM-D, combined measurement of changes in the phase and amplitude (i.e. energy) (ΔPh and ΔA) of a wave propagating on a SAW sensor provide information about the mass and viscoelastic properties of the deposited film.

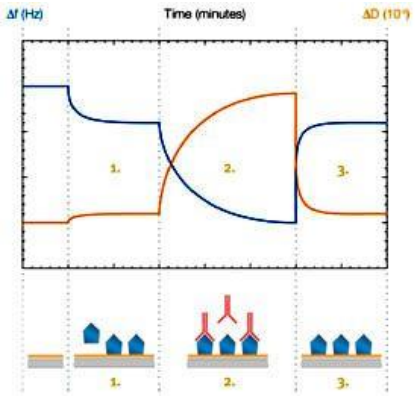


**Figure 7.** Real-time measurements of ΔF and ΔD with a QCM-D device as molecular layers form on the sensor surface. **1)** Binding of a small globular molecule: small ΔF (mass change), insignificant ΔD (rigid film); **2)** Binding of a large elongated molecule: large ΔF (more mass deposited), large ΔD (soft, viscoelastic film); **3)** Rinsing with regenerating buffer washing off elongated molecule: F back to state **1** (mass removal), D back to state **1** (back to the rigid film) (*17*)

### *The "discrete molecule" approach*

In 2008, the Biosensors lab presented a novel way to interpret data derived from acoustic measurements. As opposed to the Voigt model that treats the deposited layer as a homogeneous viscoelastic film, with this approach, the deposited biomass was treated as distinct biomolecules that are attached to the sensor area via an anchor and undergo oscillation which produces a drag force between the moving biomolecule and the surrounding liquid. According to this new approach the ratio of energy dissipation per unit mass, ΔD/ΔF, can be used as a direct measure of the intrinsic viscosity $[\eta]$ of the surface-attached molecules:

$$\frac{\Delta D}{\Delta F} \propto [\eta] \quad (3)$$

The intrinsic viscosity $[\eta]$ is a parameter characteristic of a molecule and depends on its hydrodynamic shape and size, or simply put, its conformation. The "discrete – molecule" model applies to the SAW device as well, where the ΔA/ΔPh ratio is equivalent to the ΔD/ΔF ratio. Experimental data in combination with the model were used to decipher the conformation of surface-attached double stranded (ds)DNA molecules of the same shape (rod) but different size, and also of the same size (90 base pairs (bp)) but of diverse conformations (e.g. ds "straight" and ds "curved") (*18, 19*). Various structures (open or closed "cross" shape) of the DNA Holliday Junction (J1) nanoswitch, as well as the conformation of single stranded (ss)DNAs of varying sizes have been characterized (*20, 21*). The work carried out by the Biosensors lab highlighted the potential of acoustic devices as powerful tools for molecular conformation studies. But besides their employment in biophysical and conformational studies, these tools could be used for the development of diagnostic platforms allowing real-time and label free analyses. Such diagnostic platforms could be broadly applied in the fields of food processing, environmental monitoring and medical diagnostics.

The present PhD deals with the development of acoustic wave – based diagnostic assays which can be applied in the fields of food safety and medical diagnostics. The

dissertation is divided into 2 parts, which, in turn, are subdivided into two chapters. The first part (titled “Acoustic wave biosensors in food safety”) is devoted to the work carried out on the development of acoustic wave platforms for the detection of the food-borne pathogen *Salmonella enterica* serovar Typhimurium. The second part (titled “Acoustic wave biosensors in medical diagnostics) describes the experimental work related to the development of two acoustic wave methodologies for the detection of two types of cancer (breast and colorectal cancer).

# Part 1
# Acoustic wave biosensors in food safety applications

Food is an important aspect of everyone's lives. Foodborne diseases are caused by the consumption of food (including milk, beverages, and alcohol drinks such as beer) or water contaminated with pathogens or their toxins. Pathogens that cause foodborne diseases are called foodborne pathogens and involve bacteria, viruses, fungi and parasites. According to the Centers for Diseases Control and Prevention (CDC) there are 31 identified foodborne pathogens in the United States (U.S.) (*22*). The most common foodborne pathogens are *Listeria monocytogenes*, *Escherichia coli* O157:H7 (*E. coli* O157:H7), *Staphylococcus aureus*, *Salmonella enterica*, *Bacillus cereus*, *Vibrio* spp., *Campylobacter jejuni*, *Clostridium perfingens* and *Shiga* toxin-producing *Escherichia coli* (STEC) (*23-25*).

Approximately 48 million people in the United States get ill, 180.000 are hospitalized and 3.000 die annually due to foodborne illnesses, in spite of the fact that the (U.S.) has the safest food supplies in the world (*22*). Monitoring of safety and nutritional quality of the food are very important for the public health. Food safety as a scientific discipline describes the food handling, preparation and storage for the prevention of foodborne diseases outbreaks (*26*). Foodborne pathogens put at risk food safety at all steps from handling to manufacturing, distribution and consumption.

The global trade of agricultural products (*26*), the increasing amount of street food, and the growing demand for minimally processed ready-to-eat food products (*27*) have alarmed the public health agencies on food safety assurance. In November 2007, the U.S. Food and Drug Administration (FDA) developed a "Food Protection Plan" in which it was stated that food must be considered as a potential vehicle for international contamination (*28*), which could lead to human and/or animal illnesses, deaths and economic losses (*29*). The World Health Organization (WHO) encourages food safety by stating on the World Health Day, 2015: "from farm to plate (and everywhere in between) make food safe" (*30*). The European Union (EU) legislation on microbiological criteria for foodstuffs defines that "foodstuffs should not contain microorganisms or their toxins or metabolites in quantities that present and unacceptable risk for human health" (Regulation (EC) No 2073/2005) (*29, 31*). It becomes apparent that it is of vital importance to test the food for the presence of foodborne pathogens in order to guarantee a safe food supply and to decrease the outbreaks of foodborne diseases (*27*). Current detection methods for monitoring the presence of food pathogens in food include: (a) conventional culturing and colony counting; (b) rapid detection methods.

## *I. Conventional methods for foodborne pathogens detection*

Conventional methods are considered as the gold standard by food inspection authorities and food industry, mostly because they have demonstrated indisputable effectiveness. There are two basic steps in the conventional process of foodborne pathogens detection (Fig. 9):

## 1. Enrichment, Colony Growth, and Purification

A test food sample consists of 25 g (solid) or 25 mL (liquid) which is blended or stomached to assure homogeneity (*32*). This homogenized sample is pre-enriched by combining a portion with a non-selective nutrient broth, usually in a 9:1 (broth: sample) ratio. The mixture is left to incubate at 30-35 $^{o}$C for up to 24 hours. The purpose of the pre-enrichment step is to restore injured cells and elevate the level of the target pathogen in the sample (*33*). This constitutes the primary enrichment culture wherein any bacteria present can reach concentrations ranging between $10^2$ and $10^4$ cfu/mL. Next, a dilution portion of the primary enrichment culture is combined with a selective broth (again in a 9:1, broth: sample ratio) that favors the growth of the target pathogen and suppresses the growth of other microorganisms. After incubation for 24-48 hours, this secondary or selective enrichment results in sufficient growth (up to $10^6$ cfu/mL) so that the target foodborne pathogens can now be isolated. For this purpose, a small amount of culture is plated onto one or more selective agar media and left to incubate for 24-48 hours, to allow for distinct colonies to appear on the agar surface. For certain bacteria (e.g. *Listeria*) this process is repeated by selecting colonies and inoculating another selective medium (followed by a further 24 h incubation period). At this point, foodborne pathogen colonies have been purified and are ready for confirmation tests to determine their nature.

## 2. Confirmation Tests

They are typically grouped into two main categories: a) Morphological: the identification is based on the properties of the pathogen's structure and shape (e.g. rod-shaped, coccus-shaped), and b) Biochemical: the identification relies on the metabolic properties (feeding and oxygen requirements) of the organism (e.g., catalase and oxidase reactions).

Application of a combination of tests discriminates between the organisms, since each pathogen responds to confirmation tests differently. Commercially available miniaturized biochemical test kits such as the API® kits by Biomerieux promote the automation of the process.

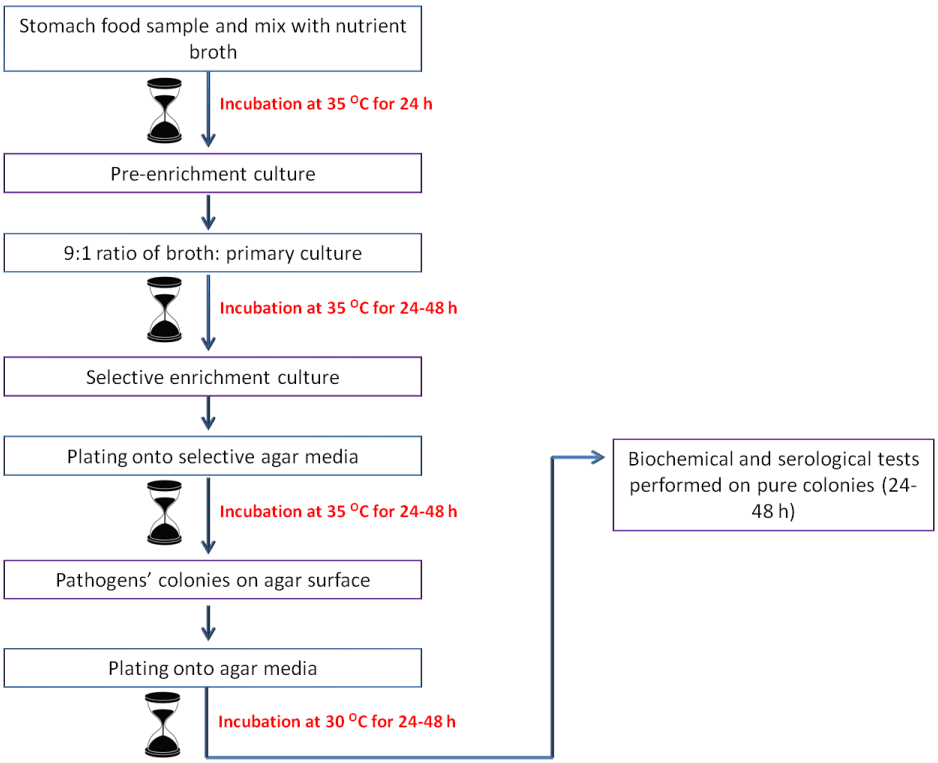


**Figure 9.** General steps involved in conventional methods of foodborne pathogen detection.

Culture-based methods have proved their efficiency in terms of sensitivity and specificity, and are designed to detect a single pathogen cell in the sample tested (*33*). Nevertheless, they are labor-intensive and require trained personnel. Moreover, they are time-consuming since they require 2-3 days for preliminary identification and more than a week for confirmation of the species of the pathogens (*24, 27*). Moreover, false-negative results may occur due to presence of viable but non-culturable (VBNC) pathogens. These are cells that have entered a state wherein they don't undergo division and growth and, hence, are not amplified by the culture and enrichment procedures (*27*).

## *II. Rapid methods for foodborne pathogens detection*

Rapid methods are classified into immunological-based and nucleic acid-based methods. Nucleic acid-based methods detect specific genes of interest in the target pathogens. Immunological-based methods rely on antibody-antigen interactions, through which an antibody will bind to its specific antibody. The most commonly used nucleic acid-based methods are:

### 1. Polymerase chain reaction (PCR)

The PCR is used to amplify a specific target DNA sequence in a cyclic 3-steps process (*27, 34*). Firstly, the double-stranded DNA of interest is denatured at 94-98 $^{O}$C, resulting in the generation of two single-stranded DNA molecules. Secondly, two specific synthetic primers anneal to the DNA strands. Thirdly, elongation occurs, wherein the primers complementary to the single-stranded DNA are extended in the presence of deoxyribonucleotides (dNTPs) and a thermostable DNA polymerase. The PCR amplification products are visualized on electrophoresis gels. PCR has been used

in the detection of *Listeria monocytogenes*, *Escherichia coli* O157:H7, *Staphylococcus aureus*, *Camplylobacter jejuni*, *Salmonella* and *Shigella* spp. (*35-39*).

### 2. Multiplex PCR (mPCR)

Multiplex PCR (mPCR) offers a more rapid detection compared to PCR since it is used for simultaneous amplification of multiple target genes. mPCR uses multiple primer sets within a single PCR mixture to produce amplicons that are specific to different DNA sequences. Primer design is very important for a successful mPCR (*24*). Silva *et al.* detected *Salmonella* spp. and *Salmonella* Enteritidis in food using mPCR (*40*), while Park *et al.* developed an mPCR assay for the simultaneous detection of *Escherichia coli* O157:H7, *Salmonella* spp., *Staphylococcus aureus*, and *Listeria monocytogenes* in one tube (*41*).

### 3. Quantitative PCR (qPCR)

Quantitative or real-time PCR enables the monitoring of the PCR products formed continuously in the entire reaction by measuring the fluorescence signal produced by specific labeled probes or intercalating dyes. Hence, it does not require post-amplification treatment such as gel electrophoresis, reducing the analysis time even further (*24*). Chen *et al.* detected *Salmonella enterica* from artificially contaminated food using qPCR assay (*42*).

### 4. Isothermal Amplification

Isothermal amplification methods have simpler hardware requirements compared to PCR, since they do not require thermal cycling. Therefore, they are appropriate for application in low-resource settings.

#### a) Loop-mediated isothermal amplification (LAMP)

In LAMP, the target sequence is amplified at a constant temperature of 60-65 $^{O}$C. 4-6 primers are used to amplify 6-8 specific regions of the target gene. An additional pair of ''loop" primers can further accelerate the reaction. The amount of DNA produced in LAMP is about $10^3$-fold or higher than the one produced by PCR (*24*). The LAMP amplicons can be monitored by agarose gel electrophoresis or SYBR Green I dye (*24*). Many foodborne pathogens have been detected in naturally or artificially contaminated food samples (*43-46*).

#### b) Nucleic acid sequence-based amplification (NASBA)

NASBA is an isothermal reaction for the amplification of RNA by which the single stranded RNA template is converted into complementary DNA (cDNA) by the reverse transcriptase during the reaction. NASBA is carried out at around 41 $^{o}$C, involves two specific primers and three enzymes: avian myeloblastosis virus (AMV) reverse transcriptase, T7 RNA polymerase and RNase H. The NASBA amplicons are detected by gel electrophoresis (*24, 27*). Min *et al.* developed a NASBA assay for the detection of viable *Escherichia coli* in drinking water (*47*). *Salmonella* Enteritidis and *Listeria monocytogenes* have also been identified by NASBA in artificially contaminated food products (*48, 49*).

#### c) Recombinase polymerase amplification (RPA)

RPA is an isothermal alternative to PCR. Because it is isothermal RPA, uses simpler equipment than PCR. It operates at low temperatures (37-42 $^{O}$C) and is able of working, more slowly of course, at room temperature. RPA is an excellent candidate for the development of low-cost, rapid, and point-of-care molecular tests. RPA has

been used for the detection of foodborne pathogens such as *Salmonella enteritidis* (*50*) and *Staphylococcus aureus* (*51*).

### 5. DNA microarrays

DNA microarrays rely on the hybridization between two DNA strands. A wide range of foodborne pathogens have been detected with DNA microarrays (*52, 53*).

### 6. Enzyme-linked immunosorbent assay (ELISA)

ELISA is one of the most commonly used immunological-based methods for the detection of foodborne pathogens. Sandwich ELISA is widely applied and involves two antibodies; a primary antibody is immobilized onto the walls of a microtiter plate. The antigen (bacterial cells, bacterial toxins) from the food samples bind to the primary antibody. Then a specific detecting antibody is added and binds to the antigen (hence the "sandwich"). Sequentially, an enzyme-linked secondary antibody is added and binds to the detecting antibody. Then a chemical substrate is added and converted by the enzyme into a color or fluorescent or electrochemical signal. Kumar *et al.* (*54*) detected pathogenic *Vibrio parahaemolyticus* in seafood with sandwich ELISA. Shen *et al.* (*55*) detected *Escherichia coli* O157:H7 in artificially contaminated food samples.

### 7. Lateral flow immunoassay (LFI)

Lateral flow immuoassays identify the presence of a target analyte in a sample matrix. LFI devices consist of four parts: the sample pad, the conjugate pad, the nitrocellulose membrane and the adsorbent pad. The sample tested flows through the four parts via capillary action. Once soaked by the sample pad, the fluid meets and mixes with the conjugate which can be antibody or antigen labeled by a color particle; it then passes to the nitrocellulose membrane wherein an antibody or antigen is immobilized. The color particle can bind to the antibody or antigen immobilized at the test line depending on the analytes present in the sample. The detection labels used in LFIs are mainly colloidal gold and monodisperse latex, labeled with colored, fluorescent or magnetic tags (*24*). Most lateral flow assays provide a visual response about 2-10 min after the sample is added **(Zhao, 2014)** (*24*). Shukla *et al. (56)* detected the foodborne pathogen *Salmonella* Typhimurium in artificially contaminated tomato samples using a LFI. Kumar *et al.* employed a lateral flow immunoassay to detect *Salmonella* typhi in artificially contaminated food rinses and at concentrations between $10^4$ and $10^5$ cfu/mL (*57*).

Each of the rapid methods described above have their advantages and limitations. For instance, PCR and its alternatives exhibit a high degree of sensitivity and specificity. However, they are prone to PCR inhibitors, they have a high cost and they need trained personnel. ELISA assays are specific and able to detect bacterial toxins and not only bacterial cells, but they show low sensitivity and they need labeling of the antibodies or antigens involved in the assay (*24, 27, 34, 58*). **Table 1** summarizes the basic advantages and disadvantages of the rapid techniques.

**Table 1. Advantages and limitations of the rapid detection methods**

| | Advantages | Limitations | References |
|---|---|---|---|
| **PCR** | • High sensitivity<br>• High specificity<br>• Automation | • High cost<br>• Affected by PCR inhibitors<br>• Labor-intensive<br>• Requires trained personnel | Law *et al.*, (*27*); Park *et al.*, 2014 (*58*); Mandal *et al.* (*34*) |
| **Multiplex PCR (mPCR)** | • High sensitivity<br>• High specificity<br>• Multiple pathogens detection<br>• Automation | • High cost<br>• Affected by PCR inhibitors<br>• Labor-intensive<br>• Requires trained personnel | Law *et al.* (*27*); Park *et al.* (*58*); Mandal *et al.* (*34*) |
| **Quantitative PCR (qPCR)** | • High sensitivity<br>• High specificity<br>• Real-time monitoring<br>• Does not require post-amplification steps | • High cost<br>• Affected by PCR inhibitors<br>• Labor-intensive<br>• Requires trained personnel<br>• Cross-contamination is probable | Law *et al.* (*27*); Park *et al.* (*58*); Mandal *et al.* (*34*) |
| **LAMP** | • High sensitivity<br>• High specificity<br>• Does not require thermal cycling, hence has a lower cost | • Labor-intensive<br>• Requires trained personnel<br>• Primer design is complicated<br>• Requires post-amplification steps | Law *et al.* (*27*); Zhao *et al.* (*24*) |

| | Advantages | Limitations | References |
|---|---|---|---|
| **NASBA** | • Sensitivity<br>• Specificity<br>• Does not require thermal cycling, hence has a lower cost<br>• Able to detect viable pathogens | • Labor-intensive<br>• Requires trained personnel<br>• Requires viable microorganisms<br>• Difficulties in handling RNA | Law *et al.* (*27*); Zhao *et al.* (*24*); Lauri and Mariani (*59*) |

| | Advantages | Limitations | References |
|---|---|---|---|
| **DNA microarray** | • High sensitivity<br>• High specificity<br>• High throughput<br>• Multiple pathogens detection<br>• Labor-saving | • High cost<br>• Requires trained personnel<br>• Requires oligonucleotide probes and labeling of target genes | Law *et al.* (*27*); Park *et al.* (*58*); Mandal *et al.* (*34*); Lauri and Mariani (*59*) |

| | Advantages | Limitations | References |
|---|---|---|---|
| **ELISA** | • Specificity<br>• Detects bacterial toxins as well | • Low sensitivity<br>• False negative results<br>• Interference from contaminants<br>• Requires trained personnel<br>• Requires labeling of antibodies or antigens<br>• Requires many incubation and washing steps | Law *et al.* (*27*); Park *et al.* (*58*); Zhao *et al.* (*24*); Velusamy *et al.* (*29*) |

| | Advantages | Limitations | References |
|---|---|---|---|
| **LFI** | • Sensitivity<br>• Specificity<br>• Low cost<br>• User-friendliness<br>• Detects bacterial | • Requires labeling of antibodies or antigens | Law *et al.* (*27*); Zhao *et al.* (*24*) |

toxins as well

Biosensors have recently been regarded as attractive alternatives to the existing and established pathogen detection methods. Biosensors have been reportedly applied to the analysis of foodborne pathogens, among which are *Escherichia coli* O157:H7, *Staphylococcus aureus*, *Salmonella* spp. and *Listeria monocytogenes* (*24*). Optical biosensors have been used to detect fordborne pathogens such as *Salmonella* (*60, 61*), and *Listeria* (*62*). Electrochemical biosensors have been shown to detect *Escherichia coli* (*63, 64*), *Salmonella* Typhimurium (*65*) and others (*66*). Acoustic wave biosensors in particular, allow the real-time, label-free, rapid, and selective detection of foodborne pathogens. What is more, they are easy to use without training, their fabrication is easy, and they have proved their cost-effectiveness and their potential of miniaturization and portability for *in-situ* monitoring (*24, 27, 29, 67, 68*). Despite the aforementioned advantageous aspects of acoustic wave biosensors, their application in the field of foodborne pathogen detection is poorer in relation to optical and electrochemical biosensors (*27, 29*). Acknowledging this gap, the present PhD study sought to develop acoustic wave biosensors for the rapid, label-free and real-time detection of the foodborne pathogen *Salmonella* Typhimurium. For this purpose two approaches were followed: the first aimed at the development of an acoustic wave biosensor for whole *Salmonella* Typhimurium cells detection; the second approach intended to design a nucleic acid-based acoustic wave biosensor for the detection of a genetic marker specific for the *Salmonella* Typhimurium pathogen.

# Chapter 1
# Development of an acoustic wave biosensor for whole *Salmonella* Typhimurium cells detection

## *Salmonella*

*Salmonella* species are facultative intracellular gram-negative bacteria found in the grastrointestinal tract of mammalian, avian and reptilian hosts (*69, 70*).

## *Salmonella* Typhimurium

*Salmonella enterica* subsp. *enterica* serotype Typhimurium (or *Salmonella* Typhimurium or *S.* Typhimurium) of the Enterobacteriaceae family are gram-negative bacteria. They are non-spore forming, motile enterobacteria with a diameter of about 0.7 and 1.5 µm, length of 2 to 5 µm and peritrichous flagella. Their cell wall is divided into three sections (Fig. 10.a): **(1)** an inner cell membrane, **(2)** an outer cell membrane and **(3)** a thin peptidoglycan layer sandwiched in between the two cell membranes. The outer membrane contains proteins such as porins and lipopolysaccharides (LPS). LPS act as virulence factors. They consist of three parts (Fig. 10.b): **(i)** lipid A which anchors LPS to the membrane, **(ii)** a lipid core that is highly conserved across *Salmonella* serovars and **(iii)** a polysaccharide side chain, called O-antigen, that is highly polymorphic. Pili and fimbriae are also present on the outer membrane of *Salmonella* Typhimurium. Pili are hair-like protrusions that are responsible for bacterial conjugation. Fimbriae are shorter than pili, consist of fimbrillin and help the attachment of the bacterial cell to the host. The inner membrane contains various proteins.

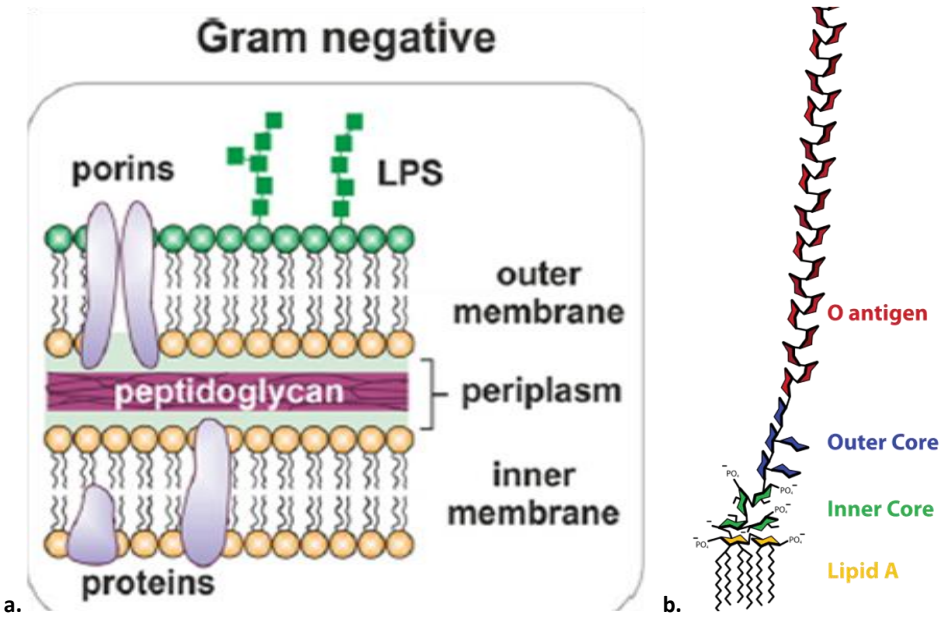


**Figure 10. a.** Architecture of the cell wall of *Salmonella* Typhimurium (*71*); **b.** Structure of the LPS of *Salmonella* Typhimurium (https://en.wikipedia.org/wiki/Lipopolysaccharide#/media/File:LPS.svg)

*Salmonella* Typhimurium is known for causing salmonellosis in humans. Salmonellosis caused by *S.* Typhimurium is characterized by fever, acute abdominal pain, intestinal inflammation and diarrhea (*72*). The onset of salmonellosis symptoms occurs 6-72 hours after *Salmonella* Typhimurium ingestion and the

disease lasts for 2-7 days (*73*). *Salmonella* Typhimurium has developed a range of refined tools to manipulate the cell host and establish an intracellular niche for successful propagation as a facultative pathogen (*69*). Two *Salmonella* pathogenicity islands the SPI-1 and SPI-2 encode two type III secretory systems (T3SS) that are employed in order to transfer bacterial proteins into host cells. In brief, after entering the intestinal lumen, *Salmonella* Typhimurium uses its flagella to move to the intestinal epithelial cells and uses its fimbriae and adhesions (SiiE, BapA) for cell attachment (*72, 74*). The fimbriae bind the extracellular matrix glycoprotein and mediate adhesion to the host cell. After attachment, *Salmonella* Typhimurium mediates cytoskeletal and cell surface rearrangements. The SPI-1 T3SS is related to invasion of epithelial cells. *S.* Typhimurium injects the effector proteins SipA, SopA, SopB, SopD and SopE2 via the SPI-1 T3SS into the host cell. These proteins trigger cytoskeletal rearrangement through actin remodeling and bacterial engulfment. The invasion process results in the rapid formation of membrane ruffles on the surface of the host cell and in the formation of *Salmonella*-containing vacuole (SCV) (*72*). In addition, in concert with the bacterial flagella and lipopolysaccharides (LPS) the SPI-1 T3SS effector proteins promote inflammation (*69, 72*). Within the SCV *S.* Typhimurium motivates the expression of the SPI-2 T3SS system. Proteins secreted via SPI-2 T3SS are required for consecutive steps in the biogenesis of SCV. The majority of SCVs relocate to a juxtanuclear position adjacent to the microtubule organizing center (MTOC) within 1-2 hours after invasion. SCVs at this stage become enriched in proteins such as $Lamp_1$, $Rab_7$, and ATPase which are normally found in late endosomes and lysosomes. Bacterial replication inside the mature SCV begins approximately 4-6 hours following invasion and is escorted by the establishment of a dynamic tubular network that extends from the surface of the SCV. Nonetheless, there are SCVs which don not undergo this maturation process but instead either lyse and release the bacterium in the cytosol or are targeted by the autophagy system (*69*). In the cytosol of epithelial cells *S.* Typhimurium undergoes robust growth and becomes re-induced for SPI-1 T3SS and flagella (*69*). Fig. 11 summarizes the basic steps of *Salmonella* Typhimurium SCV biogenesis.

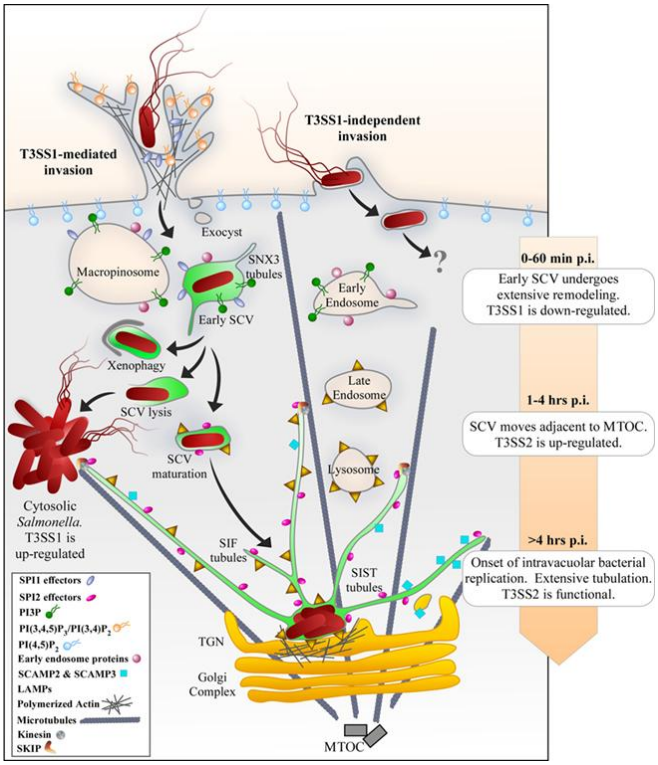


**Figure 11.** *Salmonella* Typhimurium pathogenesis (*69*)

According to the CDC, in the U.S. nontyphoidal salmonellae are estimated to cause 1,000,000 annual illnesses, 19,000 of which end in hospitalizations and 380 in deaths. The current official method for enumerating *Salmonella* in food (ISO 6579-1: 2017) takes more than 4-5 days (*75*). Nevertheless, and despite the safety controls, salmonellosis outbreaks are often phenomena. As reported by the CDC (Fig. 12) the time from when a person is exposed to *Salmonella* till the conformation that this person is a part of an U.S. outbreak is typically about 2-4 weeks (*76*). This delay is caused mainly by **1)** delivering the specimens to a remote laboratory (1-3 days) and **2)** time consuming analyses needed to identify the *Salmonella* strain (*77*). The existence of a portable, real-time, and rapid biosensor for the acoustic detection of whole *S.* Typhimurium pathogens would result in the elimination of this time gap between the first outbreak and its recognition.

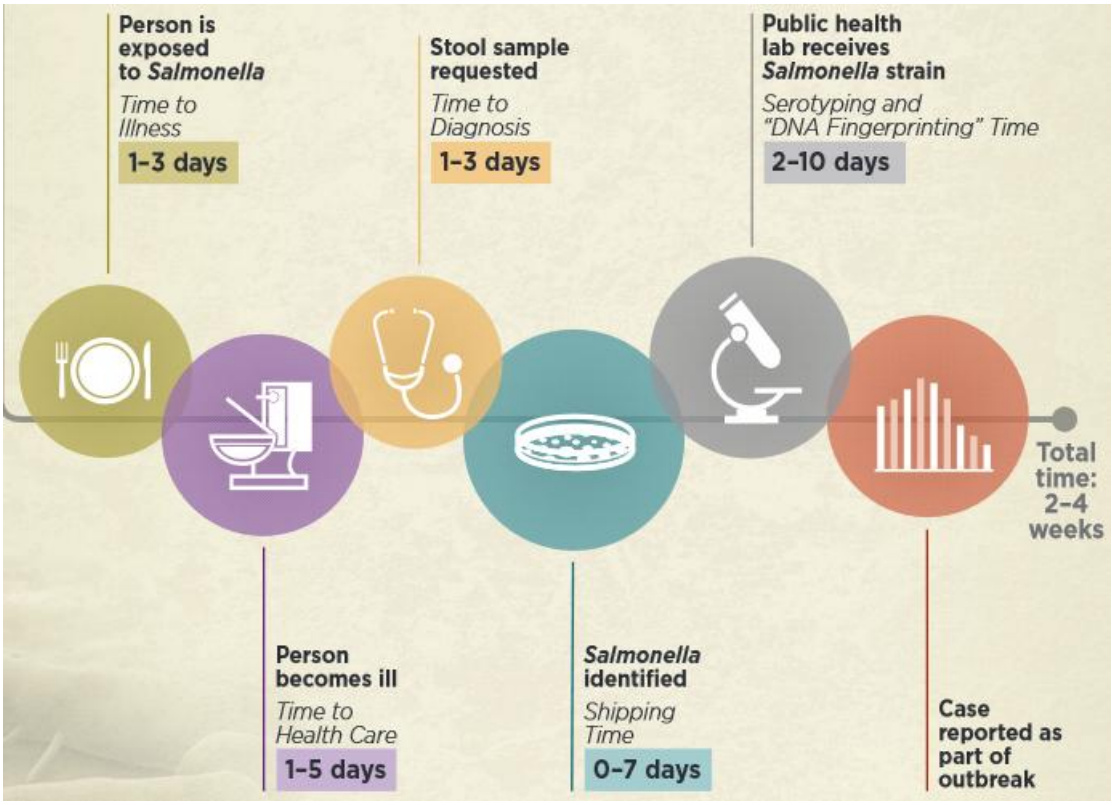


**Figure 12.** Time for reporting cases of *Salmonella* infection (*76*)

## Acoustic wave biosensors for the detection of whole *Salmonella* Typhimurium cells

Admittedly, in terms of whole bacterial pathogens detection, electrochemical and optical biosensors are most common, followed by acoustic wave biosensors (*71*). *Salmonella* Typhimurium has been reportedly detected by acoustic wave immunosensors. Acoustic wave-based immunosensors rely on the specific biochemical interaction between an antibody and an analyte, or in other words between an antibody and the *Salmonella* Typhimurium cell.

Prusak-Sochaczewski and Luong (*78*) developed a QCM immunosensor for the detection of *Salmonella* Typhimurium. The sensor was immersed in a microbial suspension and detected the pathogen at a concentration ranging from $10^5$-$10^9$ cfu/mL. Ye *et al.* (*79*) designed a flow injection system based on a QCM biosensor. An anti-*Salmonella* spp. antibody was immobilized on the gold sensor surface through a polyethylenimine-glutaraldehyde (PEG) linker and dighiobis-succinimidylpropionate

(DSP) coupling. *Salmonella* Typhimurium was identified at concentrations between 5.3 x $10^5$ - 1.2 x $10^9$ cfu/mL. Park and Kim (*80*) designed an antibody coated QCM sensor that was able to detect *Salmonella* Typhimurium in buffer within 30-90 min and at concentrations from 9.9 x$10^5$ -1.8 x $10^8$ cfu/mL. In 2000 the latter immunosensor was applied in the detection of *Salmonella* Typhimurium in artificially contaminated market milk at concentrations of 3.2 x $10^6$ - 4.8 x $10^8$ cfu/mL (*81*). Pathirana *et al.* (*82*), Wong *et al.* (*83*) and Kim *et al.* (*84*) also demonstrated the detection of *Salmonella* Typhimurium using QCM immunosensors. Su and Li (*85*) reported on the whole *Salmonella* Typhimurium detection using a QCM immunosensor with simultaneous measurements of the resonant frequency and motional resistance (ΔF and ΔR). In the direct detection of *Salmonella* Typhimurium in a chicken meat sample ΔF and ΔR were proportional to the cell concentration in the range of $10^5$-$10^8$ and $10^6$-$10^8$ cfu/mL repsectively. Using anti-*Salmonella* magnetic beads as a separator/concentrator for sample pretreatment, as well as a marker for signal amplification the limit of detection was lowered to $10^2$ cfu/mL for ΔR. No interference from *E. coli* K12 or the sample matrix was noticed. Olsen *et al*. (*86*) reported on the use of a philamentous phage-based acoustic wave sensor. The affinity-selected bacteriophage was employed as a specific and selective probe for *Salmonella* Typhimurium instead of an anti-*Salmonella* antibody. Bacteria-phage interaction resulted in resonance frequency changes and in the detection of $10^2$ cells/mL of *Salmonella* in less than 180 s. Salam *et al.* (*87*) developed a QCM immunosensor with nanoparticles amplification for real-time and sensitive detection of *Salmonella* Typhimurium. Magnetic particles and capture aptamer allowed the detection of 100 cfu/mL of *Salmonella* Typhimurium in milk (*88*).

The current study was conducted within the context of the LoveFood and LoveFoodMarket projects and aimed at the development of a bioassay whereby an acoustic wave sensor would detect whole *Salmonella* Typhimurium cells in food sample and would also be integrated in a portable lab-on-chip platform. Pilot experiments (not discussed in detail here) carried out by the Biosensors Lab, made use of a $LiTaO_3$ SAW device operating at 300 MHz and coated with anti-*Salmonella* polyclonal antibody (recognizing *Salmonella* O antigen). When whole *Salmonella* Typhimurium cells were flown over the sensing surface at a range of concentrations, acoustic detection was not possible even at high concentrations such as $10^8$ cfu/mL (Fig. 13 a). However, according to electron microscopy, *Salmonella* cells were captured by the specific antibody and present on the surface (Fig. 13 b). LW-SAW devices with a waveguide layer of PMMA or positive Photoresist S-1805 that are supposed to be more sensitive were also tested but these experiments too were not successful (Fig. 13 c).

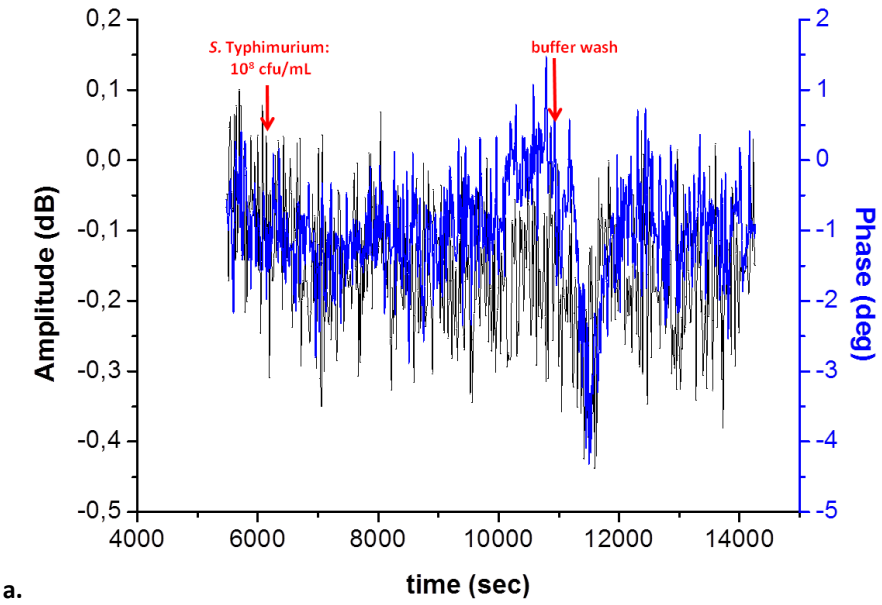


a.

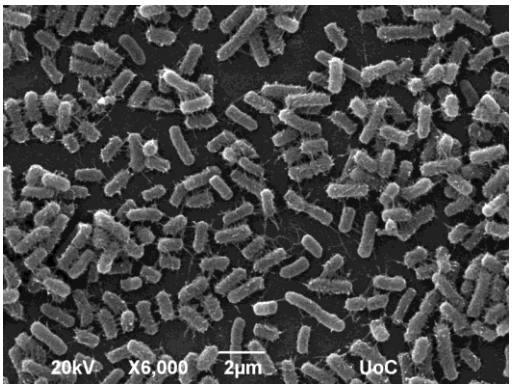


b.

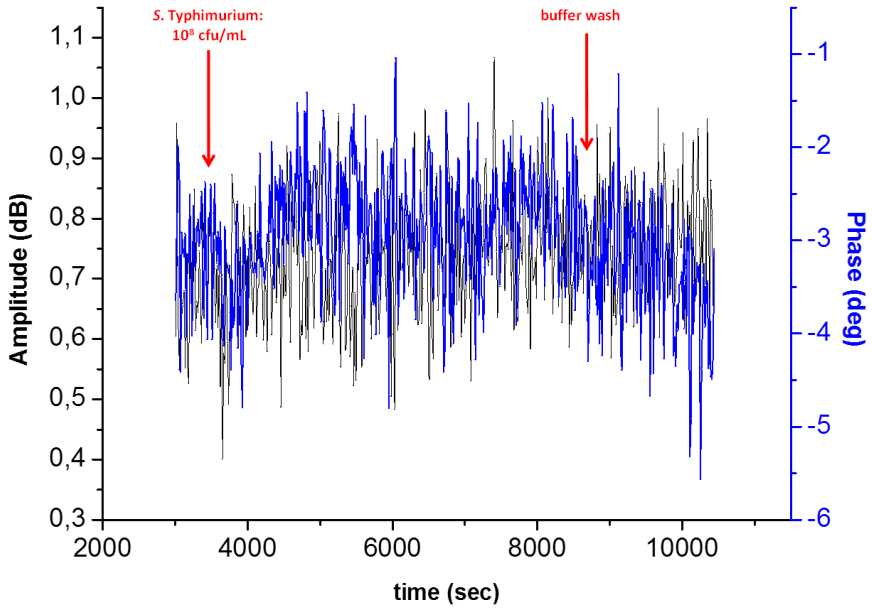


c.

**Figure 13. a)** Real-time graph showing amplitude and phase signals upon the addition of $10^8$ cfu/mL *S.* Typhimurium cells on the sensing surface of a 300 MHz SAW device. No cells detection was achieved; **b)** electron microscopy pictures of the 300 MHz SAW surface after *Salmonella* addition; **c)** Real-time graph showing amplitude and phase signals upon the addition of $10^8$ cfu/mL *S.* Typhimurium cells on the sensing surface of a 300 MHz PMMA LW-SAW device. The sensor did not detect whole cells

Given these preliminary results this PhD study followed three different approaches for the design of an acoustic wave sensor that would detect whole *Salmonella* Typhimurium cells. These approaches are described below.

## Detection of whole *Salmonella* Typhimurium cells using a QCM-D device and biofunctionalized gold nanoparticles (AuNPs)- Approach No. 1

# *Introduction*

As mentioned above, the diameter of the *Salmonella* Typhimurium cell is 0.7-1.5 μm. Instead, the penetration depth of a SAW device in aqueous environment is 50 nm. Hence, it is difficult from a mechanical point of view for a SAW sensor to achieve acoustic detection of whole *Salmonella* Typhimurium cells. Furthemore, the cell wall of such a bacterium is a rigid network wherein even flagellar filaments exhibit a high degree of stiffnes of their own (*89*). This prevents the bacterium from getting close to the sensor surface and forming contact points that would allow it to be sensed by the acoustic device.

For these reasons approach No.1 employed a QCM-D device with a fundamental frequency of 5 MHz which has a penetration depth of 250 nm in aqueous environments (*90*). Alternatively to the antibody-based acoustic wave sensor, a DNA-based acoustic biosensor was developed. DNA-based biosensors rely on the specific hybridization of complementary DNA strands (*91*). DNA base pairing is the basis of the biorecognition process in DNA hybridization biosensors. The signal produced upon hybridization is proportional to the degree of hybridization (*91*). QCM has been extensively used as a DNA hybridization biosensor for the detection of gene mutation, foodborne pathogens and genetically modified organisms (GMOs) (*92*). Gold nanoparticles (AuNPs) are used as amplifiers in QCM DNA hybridization detection since they have a relatively large mass compared to DNA targets.

In our case however, functionalized AuNPs were used as probes (*93*). They were capped with both anti-*Salmonella* antibody and thiolated single stranded oligonucleotides. The antibody targeted *Salmonella* cells and the oligonucleotides were hybridized to complementary oligonucleotides that were surface-immobilized. DNA hybridization was used to detect whole *Salmonella* cells. Figure 14 summarizes the idea behind the experimental design: a QCM sensor chip was modified with a single stranded DNA which was afterward hybridized to a complementary single stranded DNA. Gold nanoparticles (with a diameter of 10 nm) got functionalized with two receptors: a) an anti-*Salmonella* antibody (that would capture the cells) and b) a single stranded DNA complementary to the DNA immobilized on the QCM sensor surface. The idea behind this protocol was to use the nanoparticles to bridge the cells with the surface, since nanoparticles produce a big signal upon binding to the device surface. Acoustic detection of *Salmonella* cells would be performed via the acoustic sensing of the hybridization occurring between the DNA used to cap the AuNPs and the DNA immobilized on the surface (Fig. 14, black dashed rectangle).

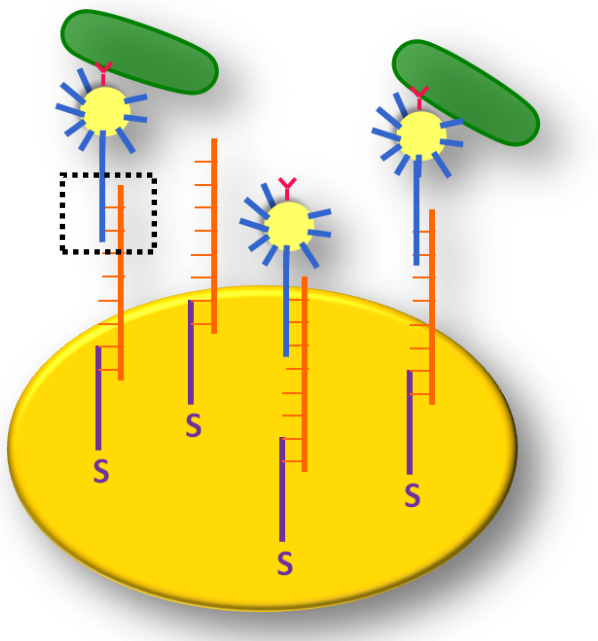


**Figure 14.** Schematic representation of the experimental design described above (not drawn to scale).

# *Materials and methods*

**1. Chemicals**

| |
|---|
| **Gold nanoparticles (10 nm diameter, stabilized suspension in citrate buffer):** Merck KGaA Darmstadt, Germany (Former Sigma-Aldrich) |
| **Olionucleotide probes:** Metabion International AG, Germany |
| **Rabbit anti-*Salmonella* group antigen polyclonal antibody (IgG):** Bio-Rad, Calif., USA |
| **Sodium Chloride (Nacl):** Merck KGaA, Darmstadt, Germany |
| **Sodium phosphate dibasic ($Na_2HPO_4$)**: Scharlau Chemicals, Barcelona, Spain |
| **Sodium hydroxide (NaOH):** Scharlau Chemicals, Barcelona, Spain |
| **Phosphate buffer saline (PBS) tablet:** Merck KGaA, Darmstadt, Germany (Former Sigma-Aldrich |
| **Tween-20:** Merck KGaA Darmstadt, Germany (Former Sigma-Aldrich) |
| **Ethanol absolute, synthesis grade (EtOH):** Scharlab S.L., Barcelona, Spain |
| **Milli-Q water (18MΩ):** Barnstead Nanopure Ultrapure Water Systems (ThermoFisher Scientific, Mass, USA) |

**2. Sequences of the oligonucleotide probes and targets**

| |
|---|
| **P1 (42 nts):** 5'-AGC TCA AGA GTT GCC CAT CCT GCA GCA ATG TTT TTT TTT TTT-3' |
| **P2 (42 nts):** 5'-TTT TTT TTT TTT AAA GTT CAG ATC TTG ATG ACA TTG TAT TTT -3' |
| **T104 (104 nts):** 5'-CAA TTT TTC AGG GAA TAA CAT TGC TGC AGG ATG GGC AAC TCT TGA GCT TCT GTA AAT ATA AAT TTA ATT AAG AGA AAA TAC AAT GTC ATC AAG ATC TGA ACT TT -3' |

**3. Buffers for the functionalization of AuNPs with thiolated oligonucleotides:**

| |
|---|
| 1 M NaCl/100 mM phosphate buffer ($Na_2HPO_4$, pH 7.4) |
| 0.1 M NaCl/10 mM phosphate buffer ($Na_2HPO_4$, pH 7.4) |
| 0.3 M NaCl/10 mM phosphate buffer ($Na_2HPO_4$, pH 7.4) |
| 1 M NaCl/1 mM phosphate buffer ($Na_2HPO_4$, pH 7.4) |
| 0.1 M NaCl/0.01 mM phosphate buffer ($Na_2HPO_4$, pH 7.4) |

## 4. Functionalization of AuNPs with P2 oligonucleotide

Functionalization was performed as described by Chen *et al.* (*92*). 50 µL of 100 µM thiolated P2 oligonucleotides were added to 800 µL of the AuNPs in an eppendorf tube. The tube was placed in a heat block at 37 $^{o}$C for a minimum of 4 h before the addition of 230 µL of Milli-Q (18 MΩ) and 120 µL of 1 M NaCl/100 mM phosphate buffer ($Na_2HPO_4$, pH 7.4). After aging overnight at 37 $^{o}$C excess oligonucleotides were removed by centrifugation (in a Eppendorf® Minispin Plus personal microcentrifuge) at 9500 rpm (7500 *x*g) for 50 min with the removal of supernatant and resuspension of the Au pellet in 0.1 M NaCl/10 mM phosphate buffer ($Na_2HPO_4$, pH 7.4). Centrifugation and resuspension were repeated 3 times. After the final centrifugation, the AuNP pellet was resuspended in 0.3 M NaCl/10 mM phosphate buffer ($Na_2HPO_4$, pH 7.4).

## 5. Functionalization of AuNPs with P2 oligoucleotide and polyclonal anti-*Salmonella* antibody

Preparation of the AuNPs was carried out as described by Chen *et al.* (*94*). Briefly, prior to functionalization, the pH of the AuNPs was adjusted to pH 9.2 with 1 M NaOH. Then, 1 mL of this solution was incubated with 6 µg of rabbit anti-*Salmonella* polyclonal antibody at room temperature (RT) with gently shaking for 30 min. Following, 50 µL of 100 µM thiolated P2 oligonucleotides were added in the solution and incubated for 16 h at 10 $^{o}$C. Subsequently, a salt-aging procedure was performed wherein 2 M NaCl was added in the solution in a six-stepwise-addition within 24 h in order to obtain a final NaCl concentration of 0.1 M. To passivate and stabilize the particles, 0.3 mL (300 µL) of a 10% BSA solution was added in the solution and incubated at RT for 30 min. Later, using a Eppendorf® Minispin Plus personal microcentrifuge, the solution was centrifuged for 20 min at 4 $^{o}$C at 11000 rpm (12581 *x*g) and the supernatant was removed. The particles were resuspended in 0.1 M NaCl/0.01 M phosphate buffer ($Na_2HPO_4$, pH 7.4) and centrifuged once more for further purification. Finally, the particles were resuspended in PBS (0.01 M phosphate buffer, 0.0027 M potassium chloride and 0.137 M sodium chloride, pH 7.4) ontaining 0.01% and 0.1% (w/v) BSA. The functionalized AuNPs were stored at 4 $^{o}$C until they were used.

## 6. *Salmonella* Typhimurium cultures

*Salmonella* Typhimurium (strain: *Salmonella* 6910 = WT ATCC14028) were grown in Lysogeny Broth (LB) medium (Bertani, 2004) (*95*) at 37 $^{o}$C for 16 h. 1 mL of the culture was centrifuged in a microfuge at 4000 rpm for 4 min and the pellet was resuspended in 1 mL PBS solution (0.01 M phosphate buffer, 0.0027 M potassium chloride and 0.137 M sodium chloride, pH 7.4). This procedure was repeated twice. The optical density at 600 nm ($OD_{600}$) was estimated using a Novaspec II spectrophotometer (Pharmacia Biotech, U.K.) in order to get a density of bacterial suspension $OD_{600}$ = 0.2 corresponding to $3.2x10^8$ cfu/mL. Serial dilutions in PBS (0.01 M phosphate buffer, 0.0027 M potassium chloride and 0.137 M sodium chloride, pH 7.4) followed to reach the desired bacterial concentrations (down to $10^5$ cfu/mL). Viable cells number was determined by conventional plate counting on LB agar petri dishes (measurements carried out in triplicates).

## 7. Incubation of functionalized AuNPs with *Salmonella* Typhimurium cells

Functionalized AuNPs solution was added to 200 μL of *Salmonella* Typhimurium (of desired concentration each time) to a final volume of 1 mL. The samples were gently mixed for 30 min at RT. Then, the solution was centrifuged in a microfuge at 4000 rpm for 5 min, in order to remove unbound AuNPs. The remaining pellet was resuspended in PBS (0.01 M phosphate buffer, 0.0027 M potassium chloride and 0.137 M sodium chloride, pH 7.4) and centrifuged again at 4000 rpm for 5 min. After a final resuspension in 1 mL of PBS (0.01 M phosphate buffer, 0.0027 M potassium chloride and 0.137 M sodium chloride, pH 7.4) the functionalized AuNPs were ready to be used.

## 8. Scanning electron microscopy preparation (SEM) of sensor chips

For SEM the samples were placed on ice and rinsed x2 with 0.1 M sodium cacodylate buffer (SCB). Samples were placed at 4 $^{o}$C for 7 min/each. Then, the samples were fixed with 2% glutaraldehyde (GDA), 2% paraformaldehyde (PFA) in 0.08 M SCB, pH 7.4 at 4 $^{o}$C for 15 min. After that, the samples were washed twice with 0.1 M SCB at 4 $^{o}$C for 7 min/each and dehydrated through a grated series of ethanol (EtOH): 30% - 50%- 70% - 90% - 100% at 4 $^{o}$C and 100% dry EtOH twice at RT. Each washing step lasted 7 min. Dehydrated samples were critical point dried (Baltec CPD 030), mounted on a glass slide and sputter coated with 20 nm thickness Au (Baltec SCD 050). Finally, samples were observed under a JEOL JSM-6390LV microscope (JEOL USA, Inc).

## 9. Acoustic device

A QSense Analyzer (4-channel system) (Biolin Scientific, Sweden) acoustic device was employed for real-time simultaneous measurements of frequency and dissipation changes. Au-coated 5 MHz AT-cut quartz crystals (QSensors) were used. Frequency and dissipation responses were recorded at the 35 MHz overtone. Prior to the experiments, the QSensors were first rinsed with Milli-Q (18 MΩ) water and 70% EtOH and then subjected to plasma cleaning for 3 min using a Harrick plasma cleaner PDC – 002 (“Hi” setting) (Harrick Plasma, NY, USA) in order to obtain a clean surface. All measurements, unless otherwise stated, were taken at 25 $^{o}$C. The acoustic device was connected with a Gilson peristaltic pump- MINIPULS® 3 (Wis., USA) through which samples were injected into the system.

## 10. Functionalization of the QCM DNA sensor and acoustic experiments

The first step of the preparation of the QCM DNA sensor was the immobilization of P1 on the gold sensor surface through self-assembly. P1 thiolated ssDNA probes (0.2 μM or 2.77 μg/mL in 1 M NaCl/1 mM phosphate buffer ($Na_2HPO_4$, pH 7.4)) were immobilized via circulating flow (pump speed was set to 0.5 rpm/min) for 30 min. Next, the 104-mer ssDNA (T104) complementary to the P1 was flown over the sensor surface through circulating flow (pump speed: 0.5 rpm/min) at a concentration of 1.5 μM or 51.48 μg/mL (in 1 M NaCl/1 mM phosphate buffer ($Na_2HPO_4$, pH 7.4)) and allowed to hybridize to the P1 probe. Afterwards, the running buffer was changed to the buffer in which functionalized AuNPs were diluted (*i.e.* 0.3 M NaCl/10 mM phosphate buffer ($Na_2HPO_4$, pH 7.4) when functionalized AuNPs with P2 were probed and PBS when functionalized AuNPs incubated with *Salmonella* cells were

probed). As a final step, 1 mL of either functionalized AuNPs or of functionalized AuNPs incubated with *Salmonella* Typhimurium cells were injected in the sensing system and allowed to interact with the modified sensor surface. Each sample addition was followed by buffer washing.

# *Results*

## 1. Acoustic detection of AuNPs functionalized with P2 oligonucleotides

The work was initially focused on the functionalization of AuNPs with the P2 ssDNA and on the immobilization of these functionalized AuNPs on the Qsensor surface (Fig. 15). In brief, AuNPs of a diameter of 10 nm (230 nmol) were capped with the 42-mer thiolated P2 (650 nmol). At the same time a 42-mer thiolated ssDNA named P1 was immobilized on the gold Qsensor surface through self-assembly (SAM). The P1 immobilization was followed by the hybridization of an intermediate 104-mer ssDNA to the P1. Eventually functionalized AuNPs were surface-immobilized via the hybridization of the T104 coating the particles to the T104.

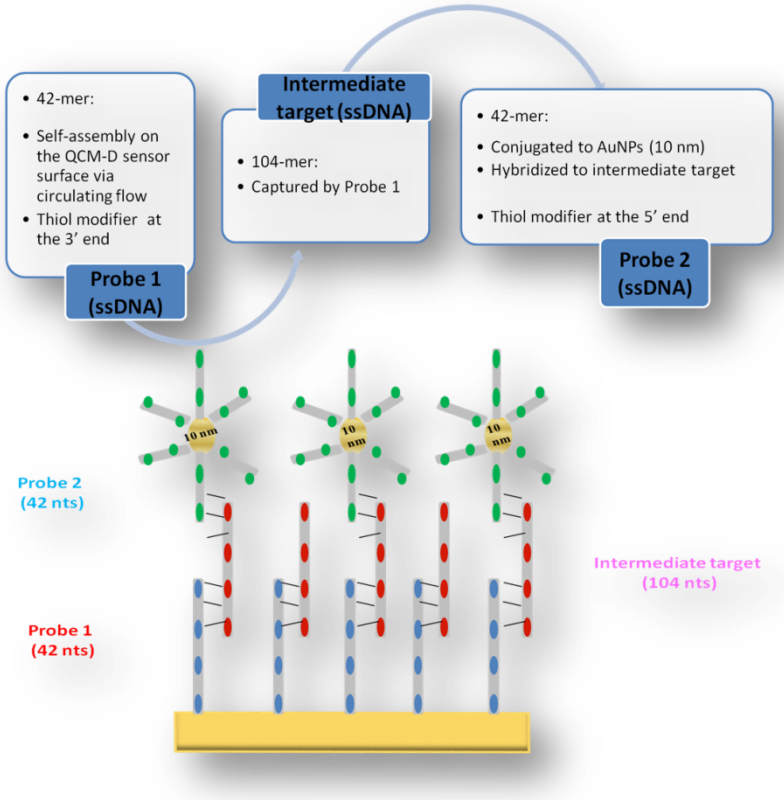


**Figure 15.** Schematic representation of the protocol concerning the acoustic detection of functionalized AuNPs (not drawn to scale)

A frequency decrease of approximately 50 Hz (±13) Hz was observed upon P1 self-assembly immobilization, which suggests that the Au surface was successfully modified. Consecutive hybridization of the T104 intermediate target resulted in an additional frequency decrease of approximately 37 Hz (±17) Hz. Additional treatment of the DNA hybridized sensor with P2-coated AuNPs resulted in amplification and a large frequency shift of 145 Hz (±30) Hz. AuNPs were surface-thethered via hybridization of 30 complementary nucleotides between T104 and P2. Figure 16 shows the frequency and dissipation changes during the process of functionalized AuNPs detection. As a control, the step of T104 hybridization to P1 was omitted. In this case, no frequency or dissipation change was monitored upon AuNPs addition (Fig. 16 b.), verifying that the detection of P2-coated AuNPs was carried out through the hybridization of P2 to the T104 ssDNA.

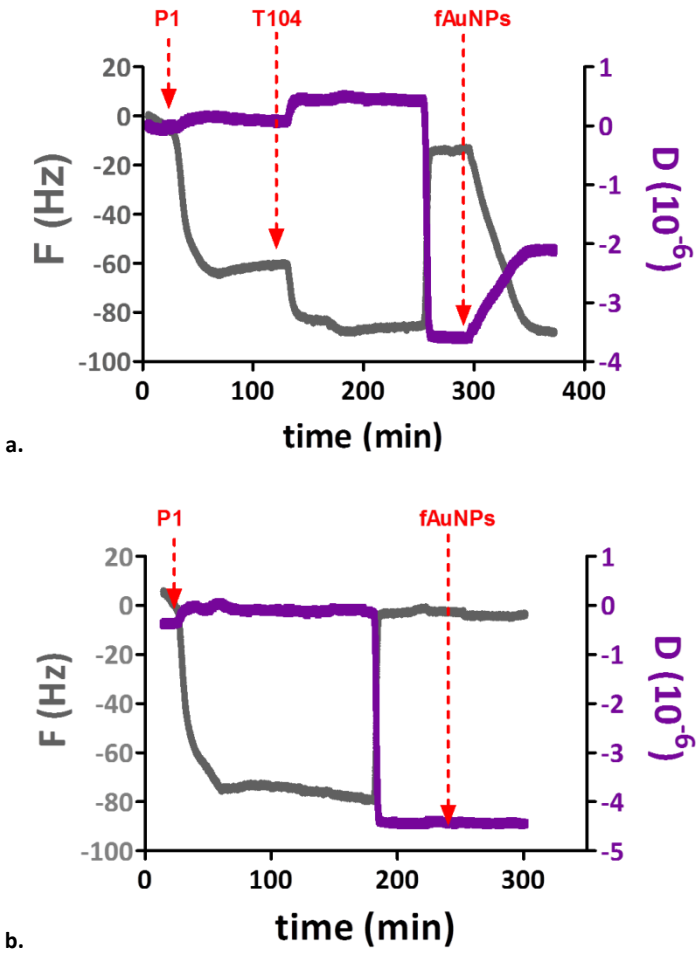


**Figure 16.** Real-time graphs depicting the changes in frequency and dissipation throughout the differet steps of the acoustic detection of functionalized with P2 AuNPs: **a.** sequential addition of P1, T104 and P2-coated AuNPs resulted in frequency and dissipation shifts; **b.** in the absence of the intermediate T104, acoustic detection of functionalized AuNPs was not possible (no frequency and dissipation change). Note: frequency data are not divided by the harmonic number , *i.e.* F/n

## 2. Pre-incubation of AuNPs capped with P2 and anti-*Salmonella* antibody with *Salmonella* Typhimurium cells and acoustic detection of the complex

The experimental process followed for acoustic detection of functionalized AuNPs that were pre-incubated with and were carrying *S.* Typhimurium cells was the same as described for the detection of functionalized AuNPs with P2 alone. While the AuNPs were pre-incubated with the bacterial cells, the gold sensor surface was getting modified with P1 and T104 (process described above). The pre-incubated *Salmonella* cells with the functionalized gold nanoparticles (the red pellet in Fig. 17) were then flowed over the modified sensor surface. Initial experiments were conducted with cells of a concentration of $10^8$ cfu/mL and in a final volume of 1 mL.

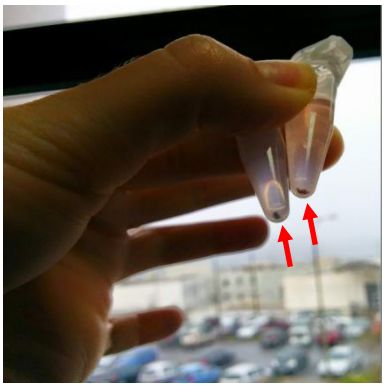

**Figure 17.** Pellets (red arrows) arising after incubation of *Salmonella* cells with functionalized AuNPs

Repetitive experiments confirmed that acoustic sensing of *Salmonella* Typhimurium cells via the use of functionalized AuNPs was not possible. No frequency and dissipation changes were recorded when the complex of functionalized AuNPs and pathogenic cells was flushed through the sensing system (Fig. 18 a.). On the contrary, AuNPs capped with P2 DNA and anti-*Salmonella* antibodies were sensed when added to the DNA sensor (Fig. 18 b.).

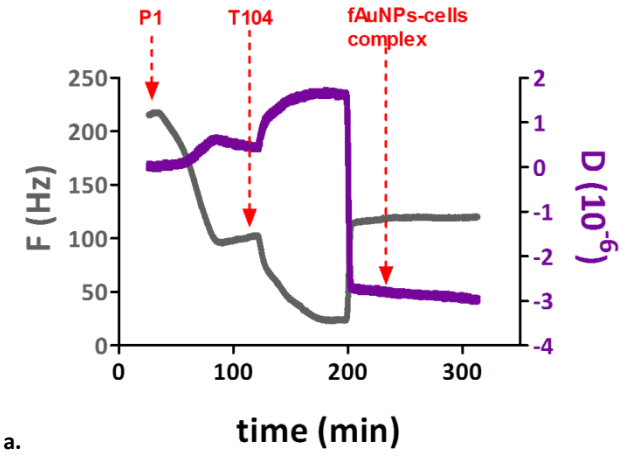


a.

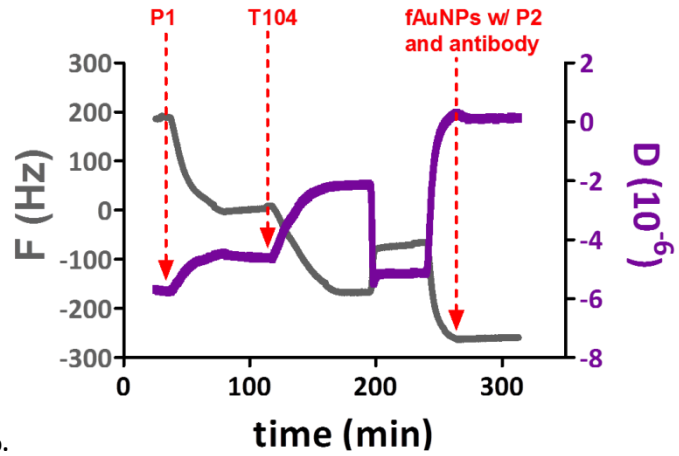


b.

**Figure 18. a.** Real-time graph depicting the absence of changes in frequency and dissipation when the complex of *S.* Typhimurium cells pre-incubated with functionalized AuNPs were added to the sensing system; **b.** Real-time graph depicting the acoustic detection of gold nanoparticles capped with P2 thiolated ssDNAs and anti-*Salmonella* antibodies. Note: frequency data are not divided by the harmonic number , *i.e.* F/n

Observation of the modified sensor surfaces under a SEM microscope revealed a high degree of aggregation between the functionalized AuNPs and *Salmonella* cells (Fig. 19). After this observation, a battery of control experiments was carried out focusing on the elimination of the cells-AuNPs aggregation. These experiments were done in a static mode, using a special holder stage (Fig. 20) Surface modification was followed by SEM.

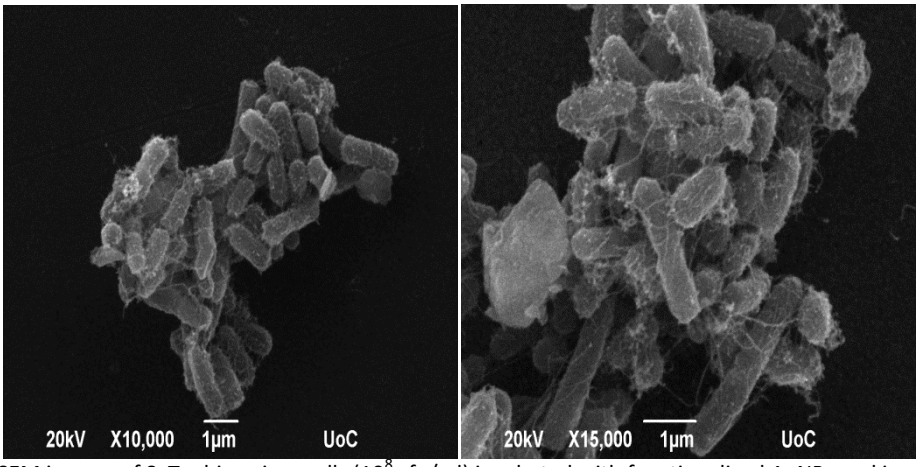


**Figure 19.** SEM images of S. Typhimurium cells ($10^8$ cfu/ml) incubated with functionalized AuNPs and immobilized on the sensor surface through DNA hybridization. Obviously, the gold nanoparticles instead of serving the role of cell carriers, resulted to cell aggregation, hindering their detection

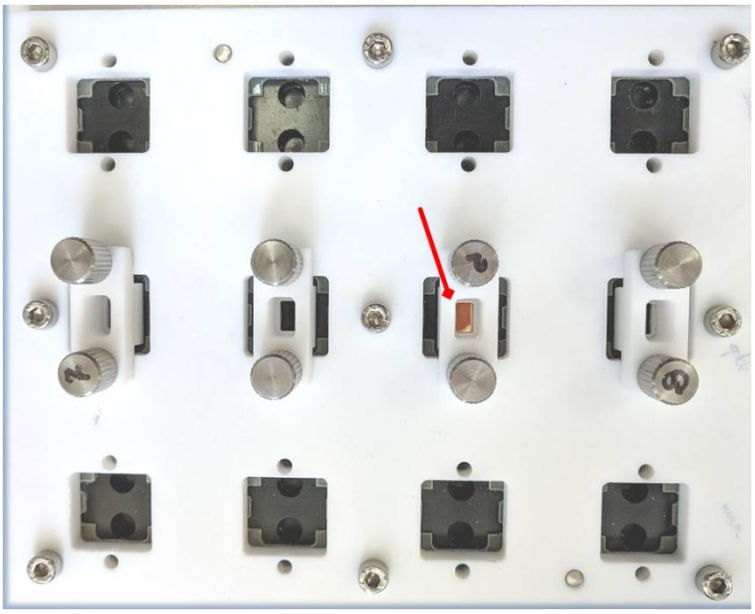

**Figure 20.** The equipment employed to carry out static experiments. The red arrow indicates the position of the gold sensor that was held by the surrounding white upper part of the holder stage

### a) Incubation of functionalized AuNPs with a range of *Salmonella* Typhimurium concentrations

Three concentrations of *Salmonella* Typhimurium cells were tested for their efficiency in eliminating the aggregation between functionalized nanoparticles and bacterial cells. Shortly, functionalized AuNPs were pre-incubated with *Salmonella* cells ranging from $10^4$-$10^8$ cfu/mL (protocol described above, in "Materials and Methods", section 7). The gold sensor surface was modified with thiolated probe P1, then with T104 and finally with the complex of cells and functionalized nanoparticles. Each sample was added to the surface by spiking with a pipette. Between each step the surface was washed with buffer. The sensor surfaces were prepared for SEM microscopy and observed under a JEOL JSM-6390LV microscope (JEOL USA, Inc). What was observed was that at higher cell concentrations (*i.e.* $10^8$ cfu/mL) a high number of cells were surface-tethered; however, these cells looked extremely aggregated and not evenly distributed on the whole surface. Self-aggregated functionalized AuNPs were also present on the surface (Fig 21. c). By way of contrast, at lower cell concentrations such as $10^4$ cfu/mL fewer cells were surface-immobilized and a higher degree of AuNPs self-aggregation was discernible (Fig. 21. b). The concentration of $10^6$ cfu/mL was chosen for onward experiments as the one resulting in the lowest level of aggregation.

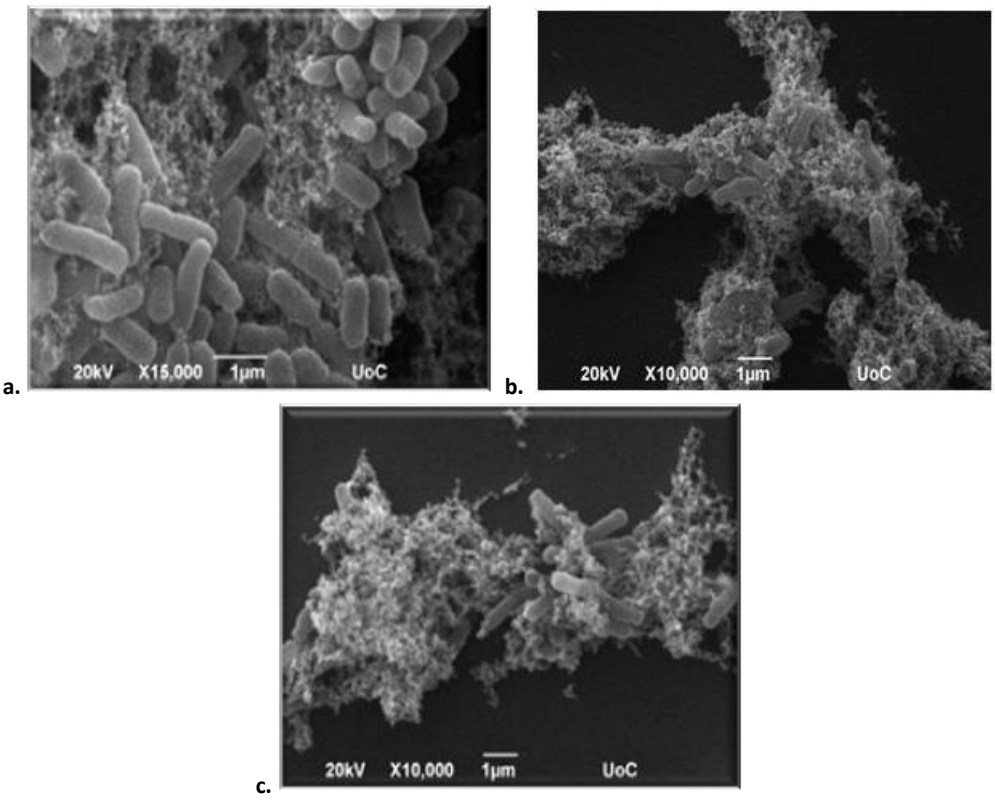


**Figure 21.** SEM pictures portraying the incubation of functionalized AuNPs with different Salmonella cells concentrations and their subsequent immobilization on the chip surface: **a.** functionalized AuNPs incubated with $10^8$ CFU/ml S. Typhimurium cells; **b.** functionalized AuNPs incubated with $10^6$ CFU/ml S. Typhimurium cells; **c.** functionalized AuNPs incubated with $10^4$ CFU/ml S. Typhimurium

### b) Incubation of diluted functionalized AuNPs with $10^6$ cfu/mL *Salmonella* Typhimurium cells

Different dilutions of functionalized AuNPs were pre-incubated with *S.* Typhimurium cells ($10^6$ cfu/mL) and investigated for their ability to decrease the cells-AuNPs aggregation. In short, AuNPs diluted 1,5X (153 nmol), 2X (115 nmol) and 4X (58 nmol) were pre-incubated with $10^6$ cfu/mL *S.* Typhimurium cells and then flown over the DNA hybridization sensor according to the protocol described before. Modified sensor surfaces were observed under a SEM microscope. Overall, gold nanoparticles that had been 2X and 4X diluted were proven incapable of capturing bacteria since no *Salmonella* cell was present on the modified surface (Fig. 22. a). AuNPs that had been diluted 1.5 X and incubated with $10^6$ cfu/mL *S.* Typhimurium cells, were demonstrated to capture the cells and lead them to surface tethering. In fact, the use of 153 nmol functionalized AuNPs led to a lesser degree of cells aggregation (Fig. 22. b, c).

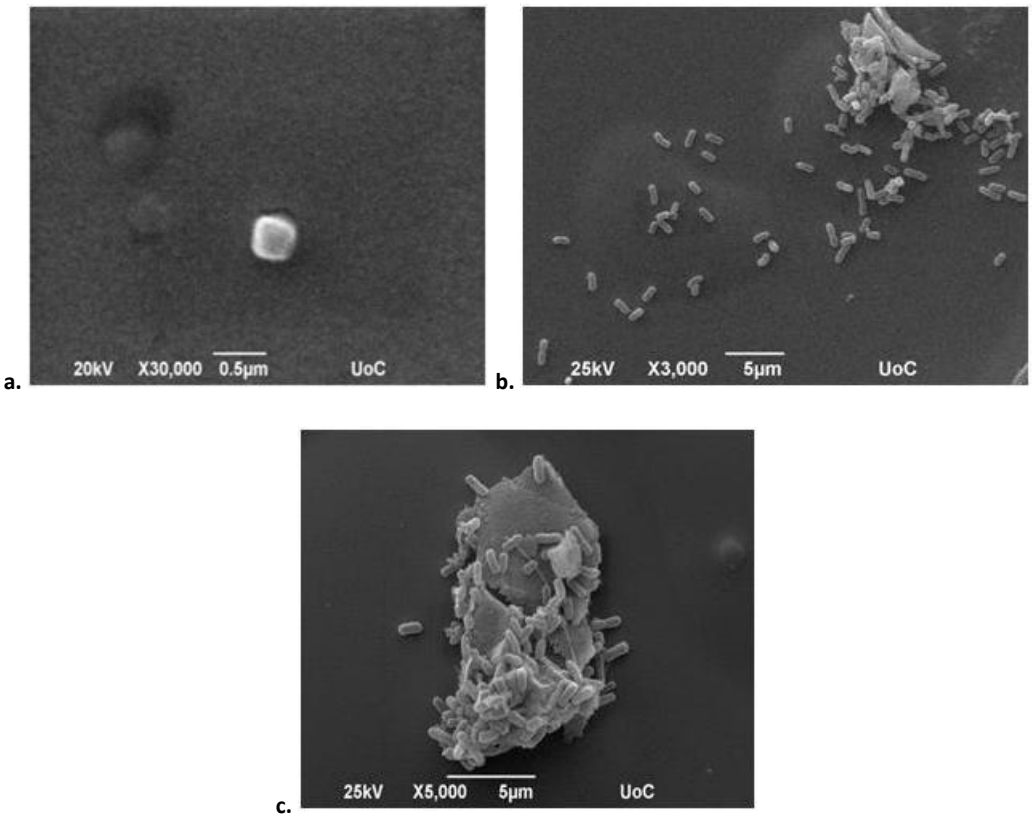


**Figure 22.** SEM pictures depictig the incubation of diluted fAuNPs with *S.* Typhimurium cells. As shown in figure **a.** highly diluted (4X) AuNPs were not able to capture any cells; **b.** functionaized AuNPs diluted 1.5X were able to captures *S.* Typhimurium cells and mediate their surface immobilization. These cells were not aggregated, compared to **c.** the cells captured by non-diluted functionalized AuNPs (230 nmol)

### c) Functionalization of AuNPs with polyclonal anti-*Salmonella* Typhimurium antibody 10X diluted (0.6 µg)

The amount of antibody used for gold nanoprticles functionalization was also probed for its impact on cells aggregation observed on the sensor surface. In the functionalization protocol described in "Materials and Methods" in section 5, the amount of antibody used was 0.6 µg instead of 6 µg. The differentially functionalized AuNPs were pre-incubated with *S.* Typhimurium cells ($10^6$ cfu/mL) and injected in the DNA sensor system. SEM observation of these sensors proved that the application of smaller amount of antibody to the functionalization process did not favor cells capturing. In fact, the sensor surface was completely devoid of bacterial cells (Fig. 23).

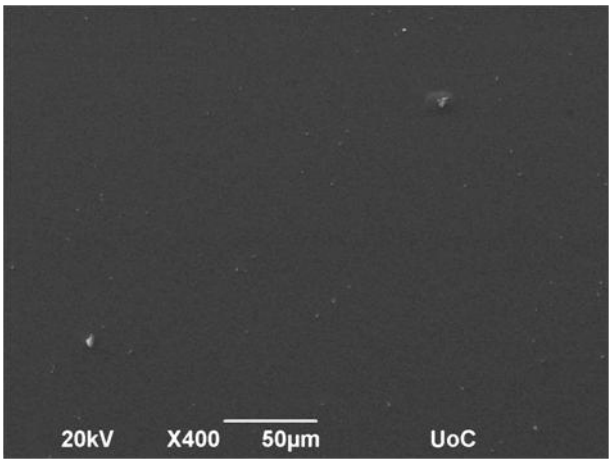


**Figure 23.** SEM picture of a DNA-modified gold surface on which *Salmonella* cells pre-incubated with AuNPs functionalized with 10 times diluted anti-*Salmonella* antibody were added. The surface is empty of cells

### 3. Pre-incubation of AuNPs (1.5X diluted) capped with P2 and anti-*Salmonella* antibody with *Salmonella* Typhimurium cells ($10^6$ cfu/mL) and acoustic detection of the complex

Conclusions drawn from the control experiments mentioned above were applied to acoustic experiments for the detection of whole *Salmonella* Typhimurium cells. AuNPs functionalized with P2 ssDNA and 6µg of polyclonal anti-*Salmonella* antibody were prepared. These functionalized AuNPs were diluted 1.5X (153 nmol) and used for pre-incubateion with *Salmonella* Typhimurium cells of a concentration of $10^6$ cfu/mL. While the AuNPs were pre-incubated with the bacterial cells, the gold sensor surface was getting modified with P1 and T104 (process described above). Finally, the AuNPs-cells complex was injected in the flow cell at a final volume of 1 mL and frequency and dissipation signals were recorded. Unfortunately, despite the fine tuning of the protocol parameters, no frequency and dissipation change were observed upon injection of the complex in the sensing system (Fig. 24), designating that acoustic detection of whole *Salmonella* Typhimurium cells through the use of biofunctionalized AuNPs was not feasible.

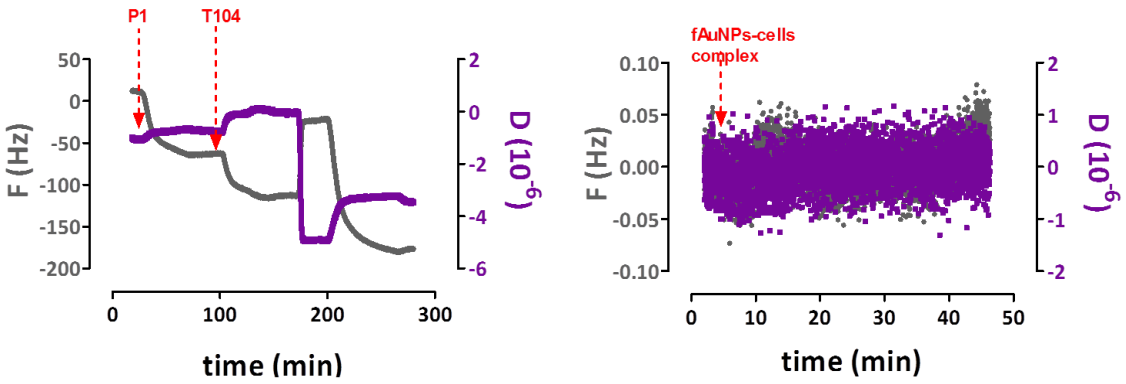


**Figure 24.** Real-time graphs showing the frequency and dissipation changes during the different steps of the process of acoustic detection: **left panel:** upon addition of the thiolated P1 ssDNA and the intermediate T104 ssDNA frequency signal decreased and dissipation signal increased; **right panel:** no acoustic detection (through changes in frequency and dissipation signals) of the cells-AuNPs complex was achieved. Note: frequency data are not divided by the harmonic number , *i.e.* F/n

# Conclusions

Gold nanoparticles have been previously employed for the acoustic detection of whole *Salmonella* bacteria cells (*87*). These gold nanoparticles however, were employed as signal amplifiers in a sandwich assay. They were functionalized with anti-*Salmonella* antibody and used to bind whole cells that had previously been immobilized on a sensor surface coated with anti-*Salmonella* antibody. The nanoparticle-antibody conjugates improved the sensitivity of the assay for bacteria detection.

In the present study, biofunctionalized gold nanoparticles were employed rather as *Salmonella* Typhimurium carriers rather than acoustic signal amplifiers. Functionalized AuNPs used here were successful in capturing and carrying the cells to the surface (control experiments demonstrated that *Salmonela* cells were not immobilized to the DNA sensor surface in the absence of biofunctionalized AuNPs); yet, they resulted in heavily aggregated cells on the sensor surface. It is speculated that the crowded outer mebrane of *S.* Typhimurium cells which is occupied by flagella, fimbriae and pili, in combination with the presence of thiolated oligonucleotides and antibodies on the surface of the gold nanoparticles caused the aggregation observed. The aggregation prevented the acoustic sensing of the cells present on the surface through DNA hybridization sensing. Incubation of the biofunctionalized nanoparticles with *S.* Typhimurium cells without flagella (strain: Salmonella 8941 = delta CSgD delta Cm) was not successful, since whole cells acoustic detection was not possible.

The use of gold nanoparticles of a bigger diameter (30 nm) was also studied. It was hypothesized that bigger particles would result in smaller aggregation of cells, since fewer particles of 30 nm would be bound to the bacterial cell compared to the 10 nm gold nanoparticles (Fig. 25). Unlike 10 nm AuNPs, 30 nm AuNPs that were functionalized with thiolated P2 and surface-immobilized to the sensor surface could not be acoustically sensed. Taking into account that 30 nm nanoparticles capped with proteins such as streptavidin have been acoustically detected in the Biosensors Lab, this result supports the assumption that the oligonucleotide surface coverage of these particles was decreased in comparison to the oligonucleotide surface coverage of the 10 nm AuNPs (*96*). This decreased coverage diminished the probability of the P2 getting hybridized to the surface immobilized T104.

The approach of detecting whole *Salmonella* Typhimurium cells using a QCM-D device and biofunctionalized gold nanoparticles proved unsuccessful and the study proceeded with approach No. 2.

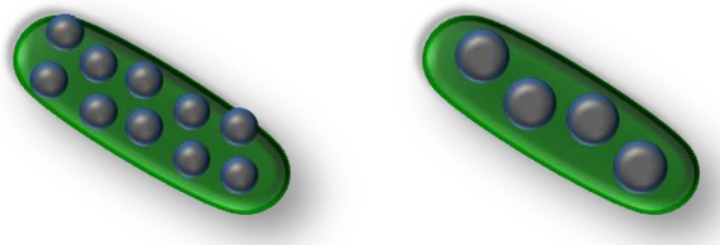

**Figure 25.** Schematic drawing of *Salmonella* Typhimurium interacted with 10 nm (**left panel)** and 30 nm **(right panel)** functionalized AuNPs (not drawn to scale)

## Detection of whole *Salmonella* Typhimurium cells using a QCM-D device with liposomes amplification-Approach No. 2

# *Introduction*

The second approach followed dealt with a type of a "competitive" biosensing assay. Similar to approach No. 1, acoustic detection of whole *Salmonella* Typhimurium cells was "indirect" in that the presence of *Salmonella* cells on the sensor surface was detected via acoustic detection of liposomes that were also present on the surface. For this assay two types of sensor surfaces were investigated: an aptamer-DNA sensor and an antibody-DNA sensor.

More specifically, a QCM sensor surface (QSensor) was used for real-time acoustic detection of whole *Salmonella* cells. On this surface either an anti-*Salmonella* aptamer together with a cholesterol-modified single stranded DNA or an anti-*Salmonella* antibody together with a cholesterol-modified single stranded DNA was immobilized. The anti-*Salmonella* aptamer and anti-*Salmonella* antibody targeted whole bacterial cells. The ssDNA with the cholesterol at its exposed end targeted liposomes. Liposomes are small spherical vesicles made up of one or more lipid bilayers which surround aqueous compartments (*97, 98*). Liposomes have been extensively used in the field of biosensing for signal amplification (*99-101*). In the present study liposomes were employed owing to their small size (smaller than the size of *Salmonella* Typhimurium cells) which falls in the range of the penetration depth of a 5 MHz QCM sensor in liquid environment (as opposed to the size of *Salmonella* Typhimurium cells). They were also chosen for their specific interaction with cholesterol molecules. The logic behind approach No.2 is illustrated in Figure 26: a QCM sensor surface was simultaneously coated either with and anti-*Salmonella* Typhimurium aptamer and a cholesterol-modified ssDNA or with an anti-*Salmonella* Typhimurium antibody and the same cholesterol-modified ssDNA. *Salmonella* Typhimurium cells were flown over the sensing surface (at varying concentrations), followed by injection of liposomes (diameter of 200 nm) at a fixed concentration. All the steps of the assay were recorded in real-time. *Salmonella* Typhimurium cells captured by the aptamer or the antibody occupied a specific surface area. The higher the cells' concentration the bigger the surface area occupied by bacterial cells. Surface-tethered cells due to their big size and number also covered the surface-immobilized ssDNA targeting the liposomes. Consequently, few liposomes would be surface-attached via interaction with the ssDNAs. This would lead to small changes in frequency and dissipation signals upon lipoosomes injection. On the contrary, *S.* Typhimurium cells injected at low concentrations would occupy a smaller surface area and would leave more surface-immobilized ssDNA molecules exposed. These exposed cholesterol-modified DNAs would capture a larger number of liposomes, leading to significant frequency and dissipation changes upon liposomes addition. *Salmonella* cells and liposomes competed for surface occupation; hence the assay is characterized as "competitive bioassay". Comprehensively, the sensing of liposomes would allow the qualitative and quantitative assessment of the presence of bacterial cells on the sensor surface.

The biorecognition elements of the assay (*i.e.* biotinylated aptamer, antibody and cholesterol-modified ssDNA) were surface-immobilized via neutravidin-biotin interaction. This immobilization method was preferred because biotin binds to neutravidin via an exceptionally strong non-covalent interaction. The interaction is rapid and practically insensitive to pH, temperature and denaturing agents. (*102, 103*). In addition it allows the oriented immobilization of the biotinylated molecules.

Two types of probe molecules recognizing *Salmonella* Typhimurium cells were studied for their capturing efficiency and their capability to increase the assay performance. The traditional anti-*Salmonella* antibody and its alternative, an anti-*Salmonella* aptamer. Aptamers are single stranded DNA or RNA molecules of 25-60 bases long with high specificities for a variety of ligands such as small molecules, proteins and whole cells (*104*). The high affinity for their ligands is derived from their ability of folding upon binding with their target molecules (*105*). Often, aptamers are preferred over antibodies because they are not as expensive; they are more stable in a wide range of pH and temperature; and can be selected *in vitro* for any given target (*105, 106*). Min *et al.* (*107*) reported on the employment of a QCM aptasensor to detect interferon-γ (IFN-γ). In 2004 Schlensog *et al. (108)* fabricated and aptamer-based Love-wave sensor that detected human α-thrombin and HIV-1 Rev peptide. In our case, the anti-*Salmonella* aptamer was employed for whole cells detection. It was hypothesized that thanks to its smaller size (compared to the equivalent antibody) it would get surface-immobilized at a higher density, allowing for higher *Salmonella* Typhimurium cells surface-coupling. Furthermore, its conformation and size resembled these of the cholesterol-modified ssDNA and therefore, their behavior regarding surface-immobilization, could be better controlled and predicted. The aptamer used for this assay was derived from literature and it was a 40 bases DNA molecule named Aptamer 33 (Apt33). Apt33 exhibits specific binding affinities to the outer membrane proteins (OMPs) of *Salmonella* Typhimurium (*109*).

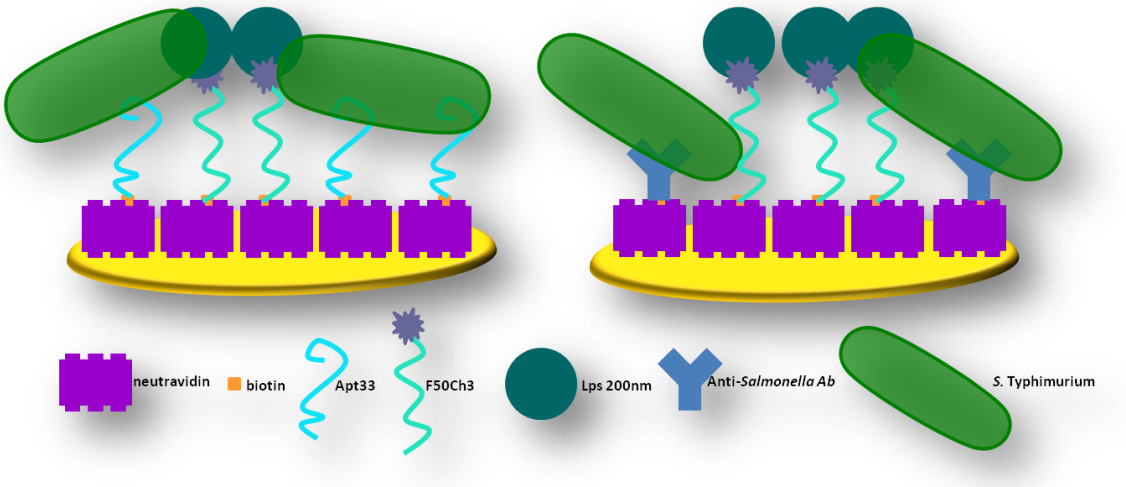


**Figure 26.** Schematic representation of approach No. 2. On the left panel the aptamer/ssDNA biosensor is depicted, while on the right panel the antibody/ssDNA biosensor can be seen (not drawn to scale)

# *Materials and methods*

## 1. Chemicals

| |
|---|
| **Olionucleotide probes:** Eurogentec, Liège, Belgium |
| **Rabbit anti-*Salmonella* group antigen: Biotin polyclonal antibody (IgG):** Bio-Rad, Calif., USA |
| **Avidin, NeutrAvidin®Biotin-binding protein:** ThermoFisher Scientific, Mass., USA |
| **Phosphate buffer saline (PBS) tablet:** Merck KGaA, Darmstadt, Germany (Former Sigma-Aldrich |
| **Ethanol absolute (EtOH) synthesis grade:** Scharlab S.L., Barcelona, Spain |
| **Milli-Q water (18 MΩ):** Barnstead Nanopure Ultrapure Water Systems (ThermoFisher Scientific, Mass., USA) |

## 2. Sequences of oligonucelotide probes

| |
|---|
| **F50Ch3:** 5' biotin TEG- AAT TCA GAG AGG AGG AGA GAG CGG TGC GGT AGG AGA GAG AGA GGA GGA TC –Cholesterol TEG 3' |
| **Apt33:** 5'- biotin TEG- GGT CCT TGT CTT ATG TCC AGA ATG CTA TGG CGG CGT CAC CCG ACG GGG ACT TGA CAT TAT GAC AGA TAA TCC ACC TAT CCC AGT AGG AGA AAT-3' |

## 3. Materials and equipment for liposomes preparation

1-palmitoyl-2-oleoyl-*sn*-glycero-3-phosphocholine (POPC) and Avanti Mini Extruder for large unilamellar vesicles (LUV) preparation were obtained from Avanti Polar Lipids, Inc. (Ala., USA). Polycarbonate (PC) membranes (19 mm in diameter) with a pore size of either 0.2µm were also purchased from Avanti Polar Lipids, Inc. (Ala., USA).

## 4. Liposomes preparation

Liposomes of 50 nm diameter were prepared. 2 mg of POPC lipids were dissolved in chloroform [(Chloroform for analysis EMSURE® Acs, Iso, Reag. Ph Eur. (Merck Millipore, Mass., USA)] in a round-bottom glass vial. The chloroform was homogeneously evaporated and the lipid film was left under nitrogen gas flow for ~60 min to ensure complete evaporation of the organic solvent. Next, the lipid film was rehydrated by the addition of 1 ml of PBS and vortexed for another 60 min. Finally, liposomes were extruded using the Avanti Mini Extruder and the 0.2 µm PC membranes.

## 5. *Salmonella* Typhimurium cultures

*Salmonella* Typhimurium (strain: WT ATCC14028) were grown in Lysogeny Broth (LB) medium (*95*) at 37 $^{o}$C for 16 h. 1 mL of the culture was centrifuged in a microfuge at 4000 rpm for 4 min and the pellet was resuspended in 1 mL PBS solution (0.01 M phosphate buffer, 0.0027 M potassium chloride and 0.137 M sodium chloride, pH 7.4). This procedure was repeated twice. The optical density at 600 nm ($OD_{600}$) was estimated using a Novaspec II spectrophotometer (Pharmacia Biotech, U.K.) in order to get a density of bacterial suspension $OD_{600}$ = 0.2 corresponding to $3.2x10^8$ cfu/mL. Serial dilutions in PBS (0.01 M phosphate buffer, 0.0027 M potassium chloride and 0.137 M sodium chloride, pH 7.4) followed to reach the desired bacterial concentrations (down to $10^3$ cfu/mL). Viable cells number was determined by conventional plate counting on LB agar petri dishes (measurements carried out in triplicates).

## 6. Acoustic device

A QSense Analyzer (4-channel system) (Biolin Scientific, Sweden) acoustic device was used for real-time measurement of frequency and dissipation changes. Au-coated 5 MHz AT-cut quartz crystals (QSensor Gold (Ag), Bioline Scientific, Sweden) were employed. Frequency and dissipation responses were monitored at 35 MHz overtone. Prior to the experiments, the QSensors were first rinsed with Milli-Q (18 MΩ) water and 70% EtOH and then subjected to plasma cleaning for 3 min using a Harrick plasma cleaner PDC – 002 ("Hi" setting) (Harrick Plasma, NY, USA) in order to obtain a clean surface. All measurements, unless otherwise stated, were taken at 25 $^{o}$C. The QSense Analyzer was connected to an IPC Ismatec peristaltic pump (Ismatec, Wertheim, Germany).

## 7. Fabrication of the aptamer/ssDNA biosensor and acoustic detection of whole *Salmonella* Typhimurium cells using a QCM-D device and liposomes amplification

The fabrication of the aptamer/ ssDNA biosensor consisted of the following steps: the Qsensor was coated with 200 μg/mL of neutravidin which was added in order to saturate the surface and enable the oriented immobilization of the biotinylated probes. biotinylated Apt33 and cholesterol-modified ssDNA of 50 nts (F50Ch3) were heated at 95 $^{o}$C for 5 min and placed immediately on ice for a minimum of 10 min, in order to untangle. A mixed solution of Apt33 and F50Ch3 in a 1:1 ratio was created by mixing 0.25 pmol/μl (or 4.13 μg/mL) of Apt33 with 0.25 pmol/μl (or 4,13 μg/mL) of F50Ch3 in PBS (final volume 200 μL). This mixed solution was flown over the sensor surface at a flow rate of 50 μL/min. Next, two dilutions of *Salmonella* Typhimurium cells in PBS, either $10^5$ cfu/mL or $10^3$ cfu/mL, where injected in the system at a final volume of 1 mL and at a flow rate of 50 μL/min. As a final step, a 10% solution of liposomes (200 nm) at a final volume of 500 μL (flow rate of 50 μL/min) was added. Liposomes were diluted in PBS. Between each step the sensor was washed with PBS buffer. Frequency and dissipation signals were monitored in real-time throughout the procedure.

## 8. Fabrication of the anti-*Salmonella* antibody/ssDNA biosensors and acoustic detection of whole *Salmonella* Typhimurium cells using a QCM-D device and liposomes amplification

All the steps of the process were carried out in PBS and at a flow rate of 50 μL/min. The preparation of the antibody/ssDNA biosensor was as follows: the Qsensor was coated with 200 μg/mL of neutravidin which was added in order to saturate the surface and enable the oriented immobilization of the biotinylated probes. The cholesterol-modified ssDNA F50Ch3 was heated at 95 $^{o}$C for 5 min and immediately put on ice in order to unwind. A mixed solution of F50Ch3 and polyclonal biotinylated antibody in a 1:10 ratio was created by mixing 6.6 μg/mL (or 406 pmol/μl) of F50Ch3 with 66 μg/mL of antibody in PBS (final volume 200 μL). These 200 μL were added to the sensing system. Next dilutions of whole *Salmonella* Typhimurium cells in PBS ($10^8$ cfu/mL and $10^5$ cfu/mL) were flown over the sensing system at a final volume of 1 mL. Finally, a 10% solution of liposomes (200 nm) in PBS (500 μL) was added. Between each step the sensor was washed with PBS buffer. Frequency and dissipation signals were monitored in real-time throughout the procedure.

# *Results*

## 1. Fabrication of the aptamer/ssDNA biosensor and acoustic detection of whole *Salmonella* Typhimurium cells using a QCM-D device and liposomes amplification

Figure 27 presents the real-time measurements of frequency and dissipation signals recorded throughout the whole experimental process. The frequency changes of neutravidin adsorption were 480 (±40) Hz. Immobilization of the mixed Apt33 and F50Ch3 caused a decrease in frequency of 203 Hz (±24) Hz. Injection of *Salmonella* Typhimurium cells of a concentration of either $10^5$ or $10^3$ cfu/mL caused no frequency decrease or dissipation increase, confirming that the acoustic detection of whole *Salmonella* cells per se, is impossible. The addition of POPC liposomes (200 nm) following the addition of $10^5$ cfu/mL *S.* Typhimurium gave an average frequency decrease of 334 Hz (±75) Hz. The dissipation change was 19 ± 1.52 ($10^{-6}$) dissipation units (DU). The acoustic ratio obtained was 0.0624 ± 0.0152 ($10^{-6}$/Hz). Addition of the same POPC liposomes in the sensing system after the addition of $10^3$ cfu/mL *S.* Typhimurium led to a frequency decrease of 239 ± 38 Hz and to an acoustic ratio of 0.0735 ± 0.0200 ($10^{-6}$/Hz). The average dissipation change was 17 (±1.73) DU. The acoustic detection of the presence of whole cells on the sensor surface via the acoustic detection of liposomes was not successful since the two cell concentrations studied could not be acoustically distinguished (the frequency and dissipation changes, as well as the acoustic ratio obtained upon liposomes addition could not distinguish the two concentrations ($10^5$ and $10^3$ cfu/mL: Fig. 28).

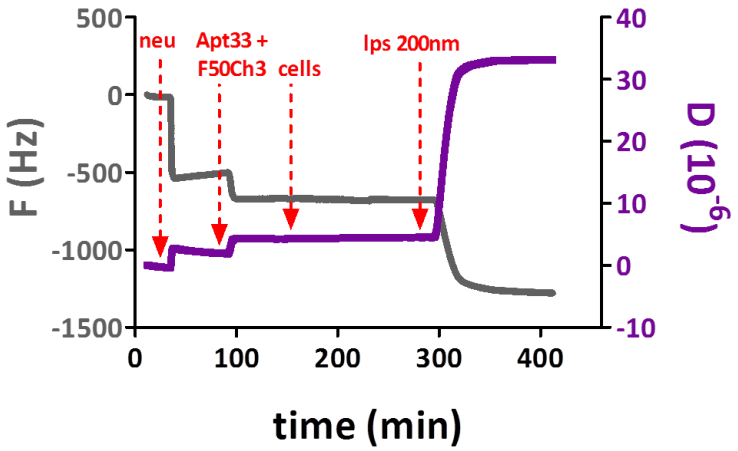


**Figure 27.** Real-time graph presenting the frequency and dissipation changes caused by the addition of neutravidin, mixed solution of Apt33 and F50Ch3, *Salmonella* cells ($10^5$ cfu/mL) and liposomes (200 nm). Note: frequency data are not divided by the harmonic number , *i.e.* F/n

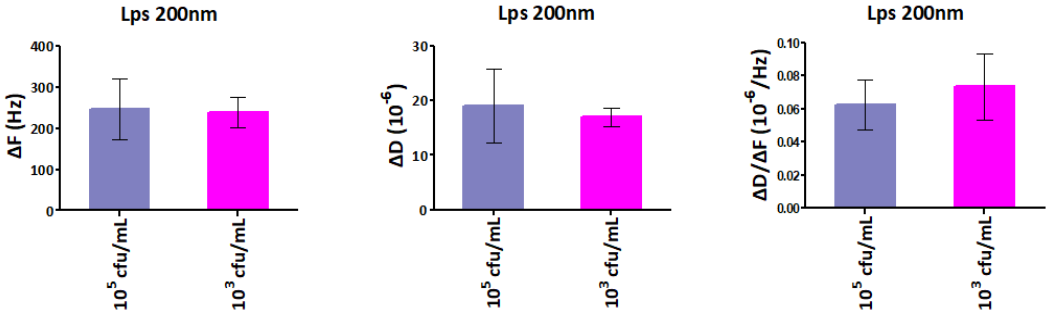


**Figure 28.** Bar graphs representing the frequency change, the dissipation change and the acoustic ratio of the POPC lipoosomes (200 nm) that were added on the sensor surface after the addition of $10^5$ cfu/mL **(purple columns)** and $10^3$ cfu/mL **(pink columns)** *Salmonella* Typhimurium cells

## 2. Fabrication of the anti-*Salmonella* antibody/ssDNA biosensors and acoustic detection of whole *Salmonella* Typhimurium cells using a QCM-D device and liposomes amplification

Figure 29 presents the real-time measurements of frequency and dissipation signals recorded throughout the whole experimental process. The frequency changes of neutravidin adsorption were 450 (±66) Hz. Immobilization of the mixed anti-*Salmonella* antibody and F50Ch3 caused a decrease in frequency of 284 (±79) Hz. Injection of *Salmonella* Typhimurium cells of a concentration of either $10^8$ or $10^5$ cfu/mL caused no frequency or dissipation shift, as usual. The addition of POPC liposomes (200 nm) following the addition of $10^8$ cfu/mL *S.* Typhimurium gave an average frequency change of 215 (±42) Hz. The dissipation change was 16 ± 2.71 ($10^{-6}$) units. The acoustic ratio obtained was 0.0746 ± 0.0096 ($10^{-6}$/Hz). Addition of the same POPC liposomes in the sensing system after the addition of $10^5$ cfu/mL *S.* Typhimurium led to a frequency decrease of 249 ± 37 Hz and to an acoustic ratio of 0.0738 ± 0.0009 ($10^{-6}$/Hz). The average dissipation change was 18 units ($10^{-6}$) units (±2.65). The acoustic detection of the presence of whole cells on the sensor surface via the acoustic detection of liposomes was not successful since the two cell concentrations studied could not be acoustically distinguished. In fact, control experiments wherein the step of cells addition was skipped showed that the biosensor could not distinguish between the presence and absence of cells on the sensor surface. Frequency, dissipation and acoustic ratios calculated for liposomes of 200 nm in diameter that were flown over a surface treated with neutravidin and antibody/ssDNA mixed solution but without cells were the same with the data described four sentences above (Fig. 30).

Control experiments were conducted to test the specificity of the binding of liposomes to the surface. In these experiments, the sensor surface was coated with neutravidin and then the immobilization of the biotinylated anti-*Salmonella* antibody alone and not in a mix with the F50Ch3 followed. Real-time measurements revealed that in the absence of the cholesterol-modified ssDNA, the liposomes could not bind to the surface, since no change in frequency and dissipation signals was recorded (Fig. 31). Therefore, it was confirmed that the binding of the liposomes to the surface was specific.

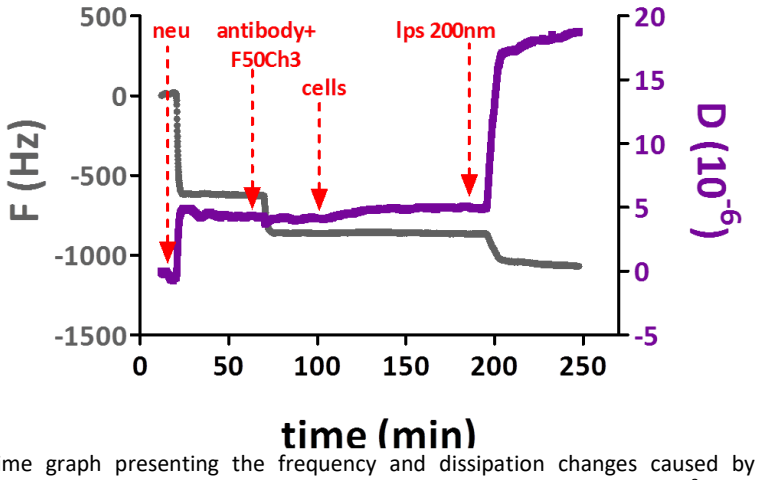


**Figure 29.** Real-time graph presenting the frequency and dissipation changes caused by the addition of neutravidin, mixed solution of anti-*Salmonella* antibody and F50Ch3, *Salmonella* cells ($10^8$ cfu/mL) and liposomes (200 nm). Note: frequency data are not divided by the harmonic number , *i.e.* F/n

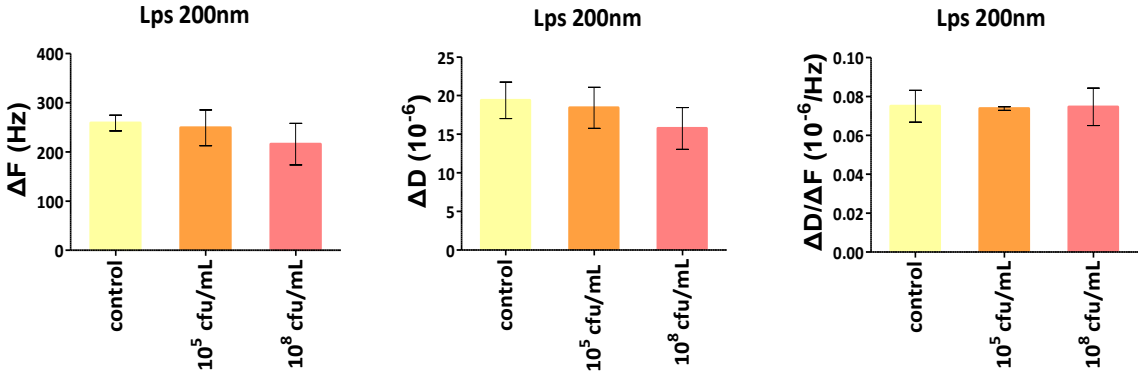


**Figure 30.** Bar graphs representing the frequency change, the dissipation change and the acoustic ratio of the POPC lipoosomes (200 nm) that were added on the sensor surface after the addition of $10^8$ cfu/mL (peach columns) and $10^5$ cfu/mL (orange columns) *Salmonella* Typhimurium cells. Yellow columns represent the control experiments where no bacterial cells were injected in the sensing system

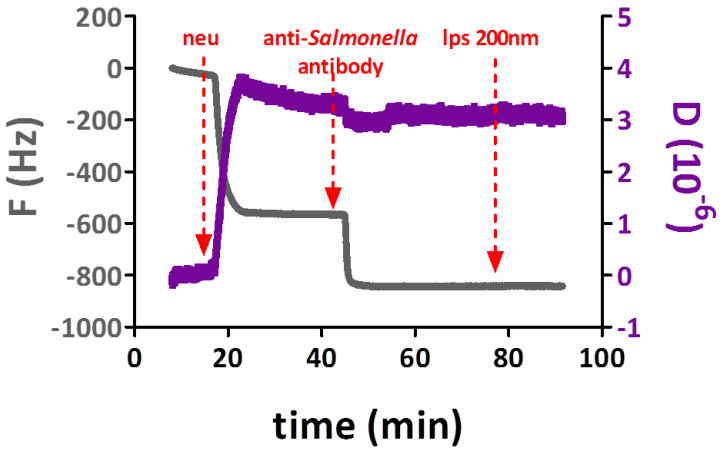


**Figure 31.** Real-time graph showing the absence of frequency and dissipation shift upon liposomes addition in the absence of the F50Ch3 probe. Surface-tethering of liposomes was shown to be specific. Note: frequency data are not divided by the harmonic number , *i.e.* F/n

# Conclusions

Acoustic detection of whole *Salmonella* Typhimurium cells with the use of liposomes was shown to be unsuccessful. The POPC liposomes of a diameter of 200 nm exhibited the same behavior when bound to a sensor surface that had been previously treated with whole *S.* Typhimurium cells at varying concentrations ($10^5$ – $10^8$ cfu/mL). The way the sensor was fabricated, *i.e.* whether it was an aptamer/ssDNA biosensor or an antibody/ssDNA biosensor seemed not to play a significant role in the behavior of liposomes. For the $10^5$ cfu/mL cells for instance, which is a concentration investigated in both types of biosensors, the dissipation change upon liposomes addition was the same.

Efforts to fine-tune the experimental parameters were made. The Apt33:F50Ch3 ratio was changed from 1:1 to 10:1 because it was speculated that an increase in the concentration of the surface-immobilized aptamer would lead to higher cells capturing, but the results were the same. In the case of the antibody/ssDNA biosensor the ratio between the two was fixed at 10:1 to allow for a balanced surface coverage between the bigger antibody and the smaller ssDNA. But, whole *Salmonella* Typhimurium cells of different concentrations could not be sensed through the use of liposomes. Moreover, liposomes had the same response when added on a surface covered with cells and when added on a surface bare of cells. Liposomes of 200 nm are 10 times smaller compared to *Salmonella* cells. For that reason, it was speculated that the smaller liposomes found their way to the cholesterol-modified DNA and were getting captured underneath the cells, hence the inefficiency to distinguish among $10^8$ cfu/mL, $10^5$ cfu/mL and control (no cells). Overall, the multifaceted approach did not achieve real-time acoustic detection of whole pathogens.

## Direct detection of whole *Salmonella* Typhimurium cells using a QCM immunosensor – Approach No. 3

# *Introduction*

In view of the data obtained with experimental approaches 1 and 2 it was decided to return to the fabrication of an acoustic wave-based immunosensor. According to the literature, acoustic wave immunosensors have been extensively used for the detection of bacterial pathogens including *Salmonella* spp. As mentioned before LW-SAW sensors coated with a waveguide layer were used by the Biosensors Lab to develop a "direct" acoustic wave-based immunoassay for the detection of whole *Salmonella* Typhimurium cells. The immunoassay developed however was not successful. Approach No. 3 employed a QCM sensor surface on account of its larger penetration depth compared to the LW-SAW sensor. The assay protocol was the same used with the LW-SAW sensor and will be explained in detail below. In fact, the QCM sensor was coated with the same waveguide layer that was used for the fabrication of the LW-SAW immunosensor, the positive Photoresist S-1805. Even though the practice of coating a QCM sensor with a waveguide layer is not common, we chose to do it because we noticed that *Salmonella* cells were present in bigger numbers on a surface treated with photoresist waveguide (Fig. 32. a), compared to a non-treated surface (Fig. 32. b). Photoresist is a light-sensitive material used mainly in photolithography to form patterned coatings on surfaces.

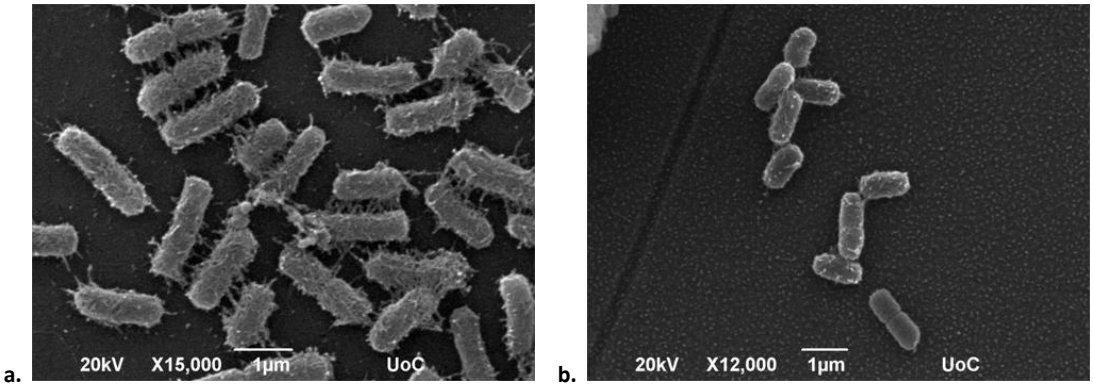


**Figure 32.** SEM pictures showing **a.** Salmonella Typhimurium cells covering a photoresit-treated QCM surface **b.** *Salmonella* Typhimurium cells covering a QCM surface non-treated with photoresist

The QCM immunosensor fabrication consisted of the following steps (Fig. 33): first, the sensor was coated with positive Photoresist S-1805. Then, neutravidin was adsorbed on the surface. A biotinylated anti-*Salmonella* Typhimurium antibody was surface-immobilized through neutravidin-biotin interaction. In a final step, *Salmonella* Typhimurium cells were flown over the immunosensor at concentrations ranging from $10^5$ to $10^8$ cfu/mL.

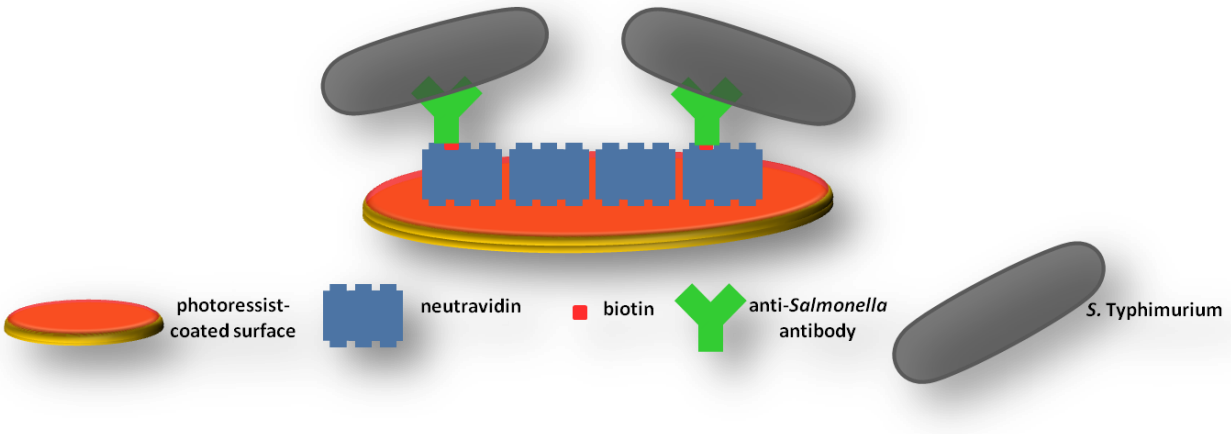


**Figure 33.** Schematic representation of Approach No.3 (not drawn to scale)

# *Materials and methods*

## 1. Chemicals

| |
|---|
| **Rabbit anti-*Salmonella* group antigen: Biotin polyclonal antibody (IgG):** Bio-Rad, Calif., USA |
| **Avidin, NeutrAvidin®Biotin-binding protein:** ThermoFisher Scientific, Mass., USA |
| **Protein G, Recombinant, *E. coli* :** Merck KGaA, Darmstadt, Germany |
| **Phosphate buffer saline (PBS) tablet:** Merck KGaA, Darmstadt, Germany (Former Sigma-Aldrich |
| **Microposit™ S1805™ G2 Positive Photoresist:** Symcon B.V., Veldhoven, The Netherlands |
| **Milli-Q water (18MΩ):** Barnstead Nanopure Ultrapure Water Systems (ThermoFisher Scientific, Mass., USA) |

## 2. *Salmonella* Typhimurium cultures

*Salmonella* Typhimurium (strain: WT ATCC14028) were grown in Lysogeny Broth (LB) medium (*95*) at 37 $^{o}$C for 16 h. 1 mL of the culture was centrifuged in a microfuge at 4000 rpm for 4 min and the pellet was resuspended in 1 mL PBS solution (0.01 M phosphate buffer, 0.0027 M potassium chloride and 0.137 M sodium chloride, pH 7.4). This procedure was repeated twice. The optical density at 600 nm ($OD_{600}$) was estimated using a Novaspec II spectrophotometer (Pharmacia Biotech, U.K.) in order to get a density of bacterial suspension $OD_{600}$ = 0.2 corresponding to $3.2x10^{8}$ cfu/mL. Serial dilutions in PBS (0.01 M phosphate buffer, 0.0027 M potassium chloride and 0.137 M sodium chloride, pH 7.4) followed to reach the desired bacterial concentrations (down to $10^{5}$ cfu/mL). Viable cells number was determined by conventional plate counting on LB agar petri dishes (measurements carried out in triplicates).

## 3. *Escherichia coli* cultures

*Escherichia coli* DH10B were grown in Lysogeny Broth (LB) medium (*95*) at 37 $^{o}$C for 16 h. 1 mL of the culture was centrifuged in a microfuge at 4000 rpm for 4 min and the pellet was resuspended in 1 mL PBS solution (0.01 M phosphate buffer, 0.0027 M potassium chloride and 0.137 M sodium chloride, pH 7.4). This procedure was

repeated twice. The optical density at 600 nm ($OD_{600}$) was estimated using a Novaspec II spectrophotometer (Pharmacia Biotech, U.K.) in order to get a density of bacterial suspension $OD_{600}$ = 0.25 corresponding to $2x10^8$ cfu/mL. Serial dilutions in PBS (0.01 M phosphate buffer, 0.0027 M potassium chloride and 0.137 M sodium chloride, pH 7.4) followed to reach the desired bacterial concentrations (down to $10^5$ cfu/mL). Viable cells number was determined by conventional plate counting on LB agar petri dishes (measurements carried out in triplicates).

**4. Coating of QCM sensors with photoresist**

The QSensors (Gold (Ag), Bioline Scientific, Sweden) were cleaned by sequentially rinsing with Milli-Q (18 MΩ) water and 70% EtOH. Then they were air plasma – cleaned for 3 min using a Harrick plasma cleaner PDC – 002 ("Hi" setting) (Harrick Plasma, NY, USA) in order to obtain a clean surface. After, the sensors were coated with Microposit™ S1805™ G2 Positive Photoresist using a Spincoater Model P6700 SN 136962-15 (Specialty Coating Systems, Inc, Ind., USA) device. The sensor was rotated at 4000 rpm for 1 min and the photoresist was spread by centrifugal force. Finally the sensor was softbaked for 2 min at 115 $^oC$ using the MR 3001 hotplate (Heidolph, Germany). This post-apply bake process reduced the photoresist solvent and dried the photoresist film in order to stabilize it.

**5. Acoustic device**

A QSense Analyzer (4-channel system) (Biolin Scientific, Sweden) acoustic device was used for real-time measurement of frequency and dissipation changes. Au-coated 5 MHz AT-cut quartz crystals (QSensor Gold (Ag), Bioline Scientific, Sweden) were employed. Frequency and dissipation responses were monitored at 35 MHz overtone. Prior to the experiments, the QSensors that were previously coated with photoresist were rinsed with Milli-Q (18 MΩ) water and then subjected to air plasma cleaning for 3 min using a Harrick plasma cleaner PDC – 002 ("Hi" setting) (Harrick Plasma, NY, USA) in order to obtain a clean surface. All measurements, unless otherwise stated, were taken at 25 $^oC$. The QSense Analyzer was connected to an IPC Ismatec peristaltic pump (Ismatec, Wertheim, Germany).

**6. Fabrication of the QCM immunosensor and "direct" acoustic detection of whole *Salmonella* Typhimurium cells**

The photoresist-treated QSensor surface was coated with neutravidin at a final concentration of 200 μg/mL, in PBS. Afterwards, the biotinylated rabbit anti-*Salmonella* group antigen polyclonal antibody was surface-immobilized through neutravidin-binding interaction at a final concentration of 66 μg/mL in PBS. In the end *Salmonella* Typhimurium cells diluted in PBS with concentrations ranging from $10^5$ to $10^8$ cfu/mL were flown over the sensing system. *E.coli* DH10B were used as control bacteria. Unless otherwise stated the volume of the cell sample injected in the system was 1 mL. The flow rate throughout the experimental process was set to 50 μL/min. Between each step of the process the sensor was washed with PBS.

# *Results*

## 1. Direct acoustic detection of whole *Salmonella* Typhimurium cells

The QCM immunosensor developed achieved the detection of whole *Salmonella* Typhimurium cells. For the first time, whole *S.* Typhimurium cells were acoustically detected via monitoring of the dissipation shifts upon cells addition. The immunosensor preparation steps were characterized using the QCM-D device (Fig. 34) with the exception of the coating of the sensor surface with photoresist S1805, which was done *ex-situ*. Adsorption of neutravidin on the photoresist-coated sensor surface caused an average decrease in frequency of 563 Hz (±85.5 Hz) and an average dissipation increase of 10.6 ($10^{-6}$) dissipation units (DU). The ΔD/ΔF acoustic ratio was calculated to be 0.0075 ± 0.0020 ($10^{-6}$/Hz), higher to the acoustic ratio calculated for neutravidin adsorption on a bare gold sensor surface. The higher ratio was attributed to photoresist deposition which alters the surface morphology in terms of thickness, roughness and topology. Sequential addition of the biotinylated anti-*Salmonella* polyclonal antibody caused a frequency decrease of 253 ± 44 Hz. Unexpectedly, upon addition of the antibody the dissipation shift was also negative (instead of positive) with an average of 0.99 ($10^{-6}$) DU. Final injection of whole *Salmonella* Typhimurium cells gave a dissipation increase which was dependent on the cells concentration flown through the sensing system (see below).

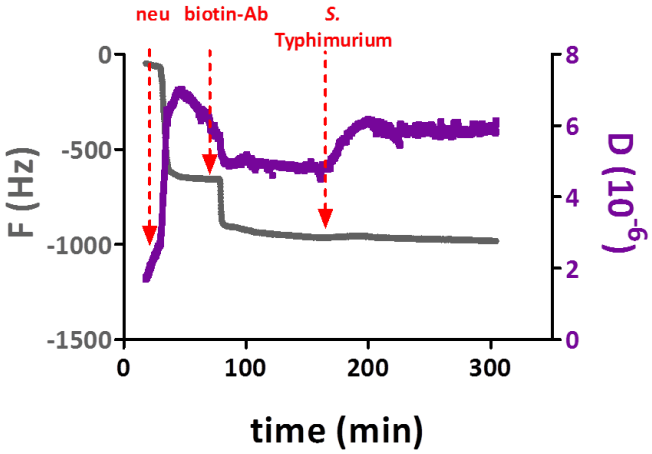


**Figure 34.** Real-time graphs showing frequency (gray line) and dissipation **(purple line)** shifts for the different sensor preparation steps. Note: frequency data are not divided by the harmonic number , *i.e.* F/n

## 2. Dissipation shift as a function of cell concentration

The immunosensor developed achieved the direct acoustic detection of whole *S.* Typhimurium cells at concentrations ranging from $10^6$ to $10^8$ cfu/mL. Concentrations exceeding $10^8$ cfu/mL were obviously detected as well, but not discussed here, since the sensor was fabricated for the detection of whole cells at the lowest concentrations possible. Figure 35 a. summarizes the dissipation shifts upon addition of whole cells at concentrations ranging from $10^6$ cfu/mL to $10^8$ cfu/mL. Addition of $10^6$ cfu/mL *S.* Typhimurium led to an average dissipation increase of 0.21 ± 0.035 ($10^{-6}$) dissipation units. $10^7$ cfu/mL cells increased the dissipation of the crystal by 0.72 ($10^{-6}$) dissipation units. Injection of *Salmonella* Typhimurium cells at a concentration

of $10^8$ cfu/mL led to an average dissipation shift of 1.26 ± 0.40 ($10^{-6}$) dissipation units. Figure 35 b. proves that different cell concentrations could be easily distinguished by the monitoring of the dissipation shift. Cell concentrations below $10^6$ cfu/mL did not cause a dissipation shift and were not detected.

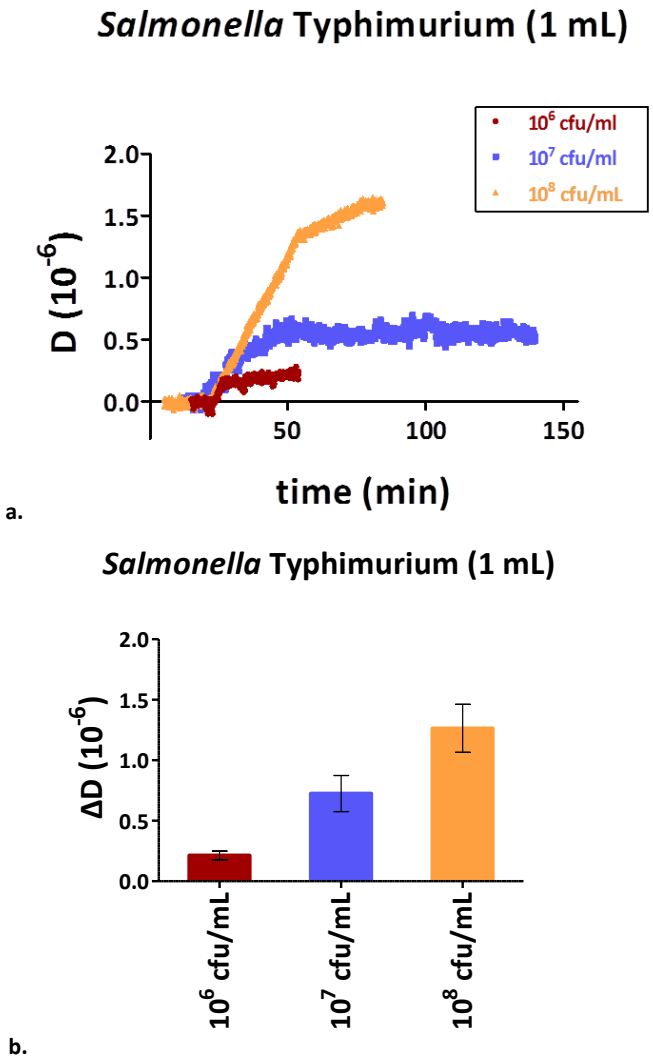


**Figure 35. a.** Real-time dissipation shift caused by different *Salmonella* Typhimurium cell concentrations: $10^6$ cfu/ml **(dark red line)**, $10^7$ cfu/ml **(blue line)** and $10^8$ cfu/ml **(light orange line)**; **b.** mean average dissipation shifts obtained by acoustic sensing of distinct *Salmonella* Typhimurium concentrations

The working range of the current *S.* Typhimurium immunosensor is comparable to some of the working ranges previously reported (*78-81, 85*). However, these traditional QCM-based bacterial biosensors use, in their majority, the frequency shift as the key sensor response signal. This is the first time that a *Salmonella* Typhimurium acoustic immunosensor uses the dissipation shift as the optimal biosensor response, achieving a limit of detection which is line with the detection limits achieved with *Salmonella* Typhimurium acoustic biosensors based on the frequency shift. To date, Poitras and Tufenkji (*110*) are the only ones (besides the

current study) to report on a QCM-based biosensor for *E. coli* O157:H7 detection highlighting the relevance of the dissipation slope as a transduction signal.

### 3. Dissipation shift as a function of the cell sample volume

A range of cell sample volumes flown over the sensor surface was tested in order to conclude whether a bigger dissipation shift would be acquired by adding more sample volume. Figure 36 a. illustrates the real-time dissipation response upon addition of $10^8$ cfu/mL of *S.* Typhimurium at various samples volumes (1 mL to 4 mL). The addition of 2 mL of whole *S.* Typhimurium cells ($10^8$ cfu/mL) raised the dissipation shift to 2.43 ($10^{-6}$) dissipation units from the 1.26 ($10^{-6}$) dissipation units obtained by the addition of 1 mL of whole *S.* Typhimurium cells ($10^8$ cfu/mL) (Fig. 36 b.) The addition of 4 mL of *S.* Typhimurium cells ($10^8$ cfu/mL) caused a further increase in the dissipation shift (2.70 ($10^{-6}$) DU). Nevertheless, this dissipation increased shift was not adequate enough to distinguish between the 2 mL and the 4mL sample, indicating that the sensor surface was saturated at 2 mL. It becomes apparent that 1 mL is sufficient for a rapid and clear *Salmonella* Typhimurium detection ranging from ($10^6$ to $10^8$ cfu/mL). Increasing the cell sample volume increased the shift in the dissipation signal (as predicted), it did not however, decrease the detection of limit.

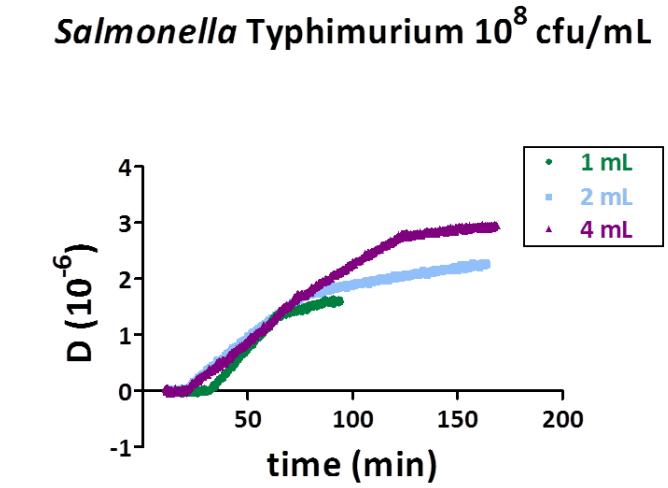


a.

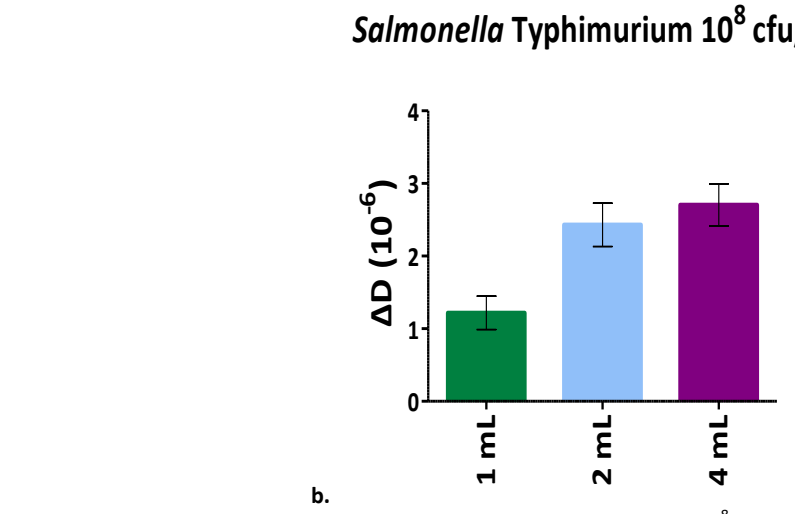


**Figure 36. a.** Real-time dissipation increase caused by the addition of $10^8$ cfu/mL *Salmonella* Typhimurium whole cells at a range of sample volumes: 1 mL **(green line)**, 2 mL **(blue line)** and 4 mL (**purple line)**; **b.** average dissipation shifts obtained upon addition of samples of $10^8$ cfu/mL *Salmonella* Typhimurium at different volumes

## 4. Specificity of the direct QCM immunosensor

To test the specificity of the fabricated acoustic wave immunosensor, detection of the *Escherichia coli* DH10B bacterium was investigated. The experimental procedure was the same as described in the section of *Materials and Methods*, Part 6. At the final step, instead of 1 mL of *S.* Typhimurium, 1 mL ($10^8$ cfu/mL) *E. coli* were added. The results are presented in Figure 37. A slight dissipation increase, in the range of 0.17 ($10^{-6}$) DU, was caused by the addition of the *E.coli* DH10B. The shift was attributed to non-specific binding of the related (both *Salmonella* Typhimurium and *E.coli* are gram-negative bacteria and belong to the *Enterobacteriaceae* family) *E.coli* DH10B to the anti-*Salmonella* polyclonal IgG. Under no circumstances however, could the change in the dissipation signal caused by the addition of *E. coli* be compared to the one caused by the addition of *Salmonella* Typhimurium. Divergent methods for the surface-immobilization of the anti-*Salmonella* Typhimurium were probed in an attempt to minimize the non-specific binding of the *E. coli* DH10B to the anibody. In the first place the antibody was allowed to adsorb on the photoresist-coated sensor surface and 1 mL of either *Salmonella* Typhimuirum or *E. coli* at a concentration of $10^8$ cfu/mL was added. It was shown that in this case the dissipation shifts were similar (2.75 ($10^{-6}$) DU for *Salmonella* and 2.46 ($10^{-6}$) DU for *E. coli*) and the two types of bacteria could not be discriminated. In the second place, the anti-*Salmonella* antibody was surface-immobilized through binding to Protein G. Via this immobilization technique the immunosensor achieved the discrimination between *Salmonella* and *Escherichia coli*, even though the non-specific binding of *E.coli* was shown to be higher (1.20 ($10^{-6}$) DU compared to the 0.17 ($10^{-6}$) DU). It was shown that the antibody immobilization via neutravidin-biotin interaction was the most satisfactory. A more satisfactory specificity could be achieved by testing the addition of a bacterium non-related to the *Salmonella* Typhimurium (*e.g.* the gram-positive *Bacillus subtilis*).

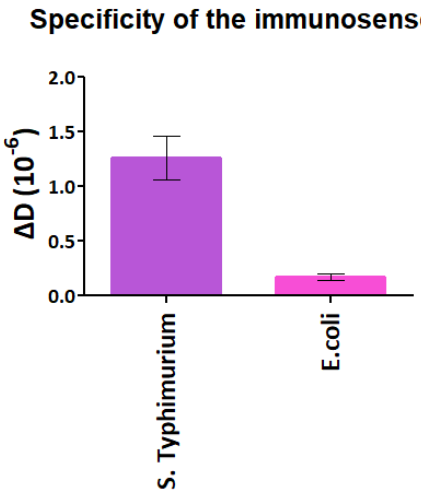


**Figure 37.** Summary of the dissipation shifts obtained upon addition of $10^8$ cfu/mL *S.* Typhimurium and $10^8$ cfu/mL *E.coli* (sample volume: 1 mL)

## 5. Control assays

A number of control experiments were conducted to investigate the specificity of the binding of *S.* Typhimurium to the biotinylated antibody. *S.* Typhimurium did not non-specifically attach to Photoresist S-1805 coated surface. *S.* Typhimurium did not non-specifically attach to neutravidin that was physisorbed on the sensor.

## 6. Direct detection of *Salmonella* Typhimurium in LB

The current acoustic wave-based immunosensor achieved the detection of 1 mL of *Salmonella* Typhimurium of a concentration of $10^8$ cfu/mL in LB (Fig. 38. a). The higher dissipation shift obtained upon addition of *Salmonella* Typhimurium in LB was attributed to the LB matrix. In any case, the LB did not interfere with the acoustic signal (Fig. 38. b). This finding is promising and could pave the way for the application of the immunosensor in real-life scenarios.

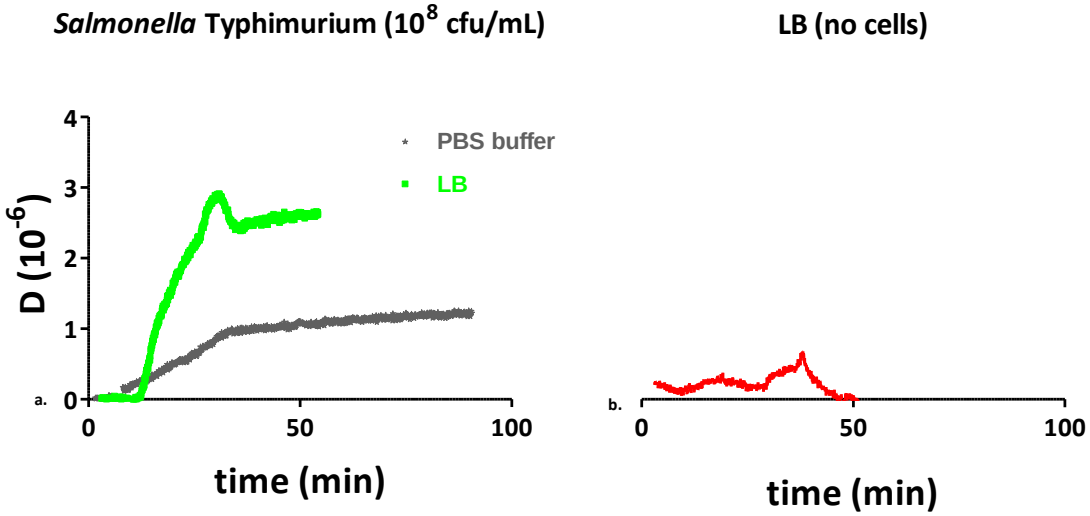


**Figure 38.** Dissipation response upon addition of whole *Salmonella* Typhimurium cells ($10^8$ cfu/mL, 1 mL final volume) in: LB **(light green line)** and PBS buffer **(gray line)**; the **red line** represenst the absence of dissipation shift upon addition of plain LB (LB without *Salmonella* Typhimurium cells)

## 7. Frequency shift upon *Salmonella* Typhimurium addition

An interesting finding of the assay reported here was the frequency response upon cells addition in the sensing system. A frequency increase (instead of a frequency decrease) was recorded for bacterial cells addition (Fig. 39). Addition of $10^8$ cfu/mL *Salmonella* Typhimurium cells resulted in a frequency increase of 12.4 ± 4.8 Hz. Injection of $10^7$ cfu/mL caused the frequency signal to increase by 1.4 ± 2.75 Hz, while addition of $10^6$ cfu/mL *S.* Typhimurium cells caused an insignificant frequency increase of 0.66 Hz. It is obvious that the frequency response was not as sensitive as the dissipation response. Furthermore, the frequency response was not as stable and reliable as the dissipation response and this is why the current study focused on the dissipation signal response for whole *S.* Typhimurium cells acoustic detection.

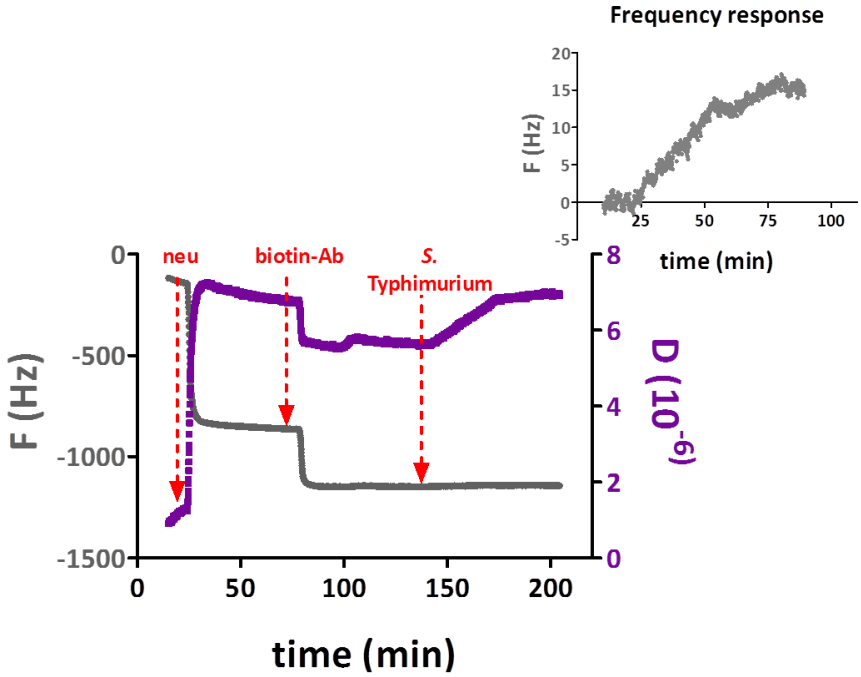


**Figure 39.** Real-time graph depicting the frequency and dissipation responses during the different steps of the assay. The inset zooms in the frequency increase caused by the addition of *S.* Typhimurium cells ($10^8$ cfu/mL, final volume: 1 mL). Note: frequency data are not divided by the harmonic number , *i.e.* F/n

Although rare, it has been noted in the literature that bacterial acoustic detection resulted in positive frequency shifts instead of negative ones (*111, 112*). Conventional mass-loading theory (Sauerbrey equation) cannot explain positive frequency shifts. According to Olsson *et al.* (*111*) and Jiang *et al.* (*113*), positive frequency shifts can be explained by the coupled-oscillator theory. As Dybwad (*114*) showed for the adhesive bonding between a colloid particle and a substrate, the coupling between two oscillators via a small point contact may increase the resonance frequency. According to this coupled-oscillator theory, the resonance frequency is not only governed by the magnitude of adsorbed mass, but also by the stiffness of the contact point between the adsorbed mass and the crystal sensor surface according to:

$$2\,(2\pi f)^2 = (\frac{K}{M} + \frac{k}{M} + \frac{k}{m}) \pm \sqrt{(\frac{K}{M} + \frac{k}{M} + \frac{k}{m})^2 - 4\,\frac{K}{M} \times \frac{k}{m}} \qquad (4)$$

where: *f* is the resonance frequency of the crystal; K is the spring constant; M is the mass of the crystal;k is a spring constant of the stiffness of the paryicle-sensor contact point; m is the mass of the adhering particle.

Bacteria are of the shape and size of large colloidal particles and for this reason are likely to affect the QCM frequency shift according to the coupled oscillator theory. In the assay presented here, the positive frequency shifts recorded might be the result of the stiffness of the contact points bridging the biotinylated anti-*Salmonella* antibody and the O (O polysaccharide) and H (flagellar antigen) antigens of the outer membrane of the bacterial cell.

## 8. Anti-*Salmonella* antibody surface immobilization

Another interesting observation of the current study was the dissipation decrease caused by the anti-*Salmonella* antibody surface-immobilization via neutravidin-avidin interaction. The 150 kDa antibody was expected to be dissipative enough to cause dissipation to increase upon its surface immobilization. Instead, antibody surface-immobilization caused the dissipation signal to decrease (Fig. 40). The decrease in signal was recorded when the antibody was immobilized through neutravidin or protein G. When it was immobilized via physisorption on a photoresist coated sensor surface the dissipation increased as expected. The immobilization of the antibody on neutravidin that had previously been adsorbed on a bare gold sensor surface and on a gold sensor treated with photoresist S-1805 was investigated. The average dissipation obtained by the antibody immobilization in the first case was of -0.41 ± 0.13 ($10^{-6}$) dissipation units and the average frequency was 276 ± 3 Hz. When neutravidin was adsorbed on a photoresist-coated surface, the addition of the antibody resulted in both a dissipation and frequency decrease of -0.99 ± 0.64 ($10^{-6}$) dissipation units and 253 ± 44 Hz respectively. Papadakis *et al.* (*115*) studied the formation of histone Hv1-DNA complexes using a SAW sensor. In this work they reported on an unexpected amplitude increase (instead of the regular decrease) upon Hv1-DNA electrostatic interaction. They attributed this amplitude increase to the formation of compact and rigid layers of DNA/Hv1 complexes. These rigid layers resembled the ones formed by tightly adsorbed proteins on the sensor surface. Figure 40 shows that in the current study the dissipation decrease occurred only when the antibody interacted with another protein (neutravidin or protein G). When it was adsorbed on the photoresist-treated sensor surface, the dissipation increased as it was supposed to do. For this reason, it can be hypothesized that the antibody-neutravidin interaction resulted in the formation of a tight, rigid non-dissipative structure that caused the dissipation to decrease. Another assumption that could be made is that the deposition of the antibody resulted in the removal of neutravidin molecules from the surface. The antibody might have occupied the empty neutravidin spaces, which would explain the frequency decrease (mass loading on the surface).

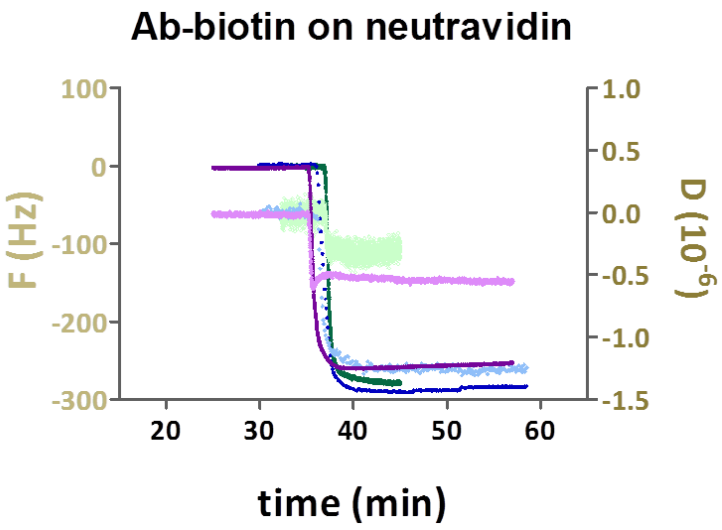


a.

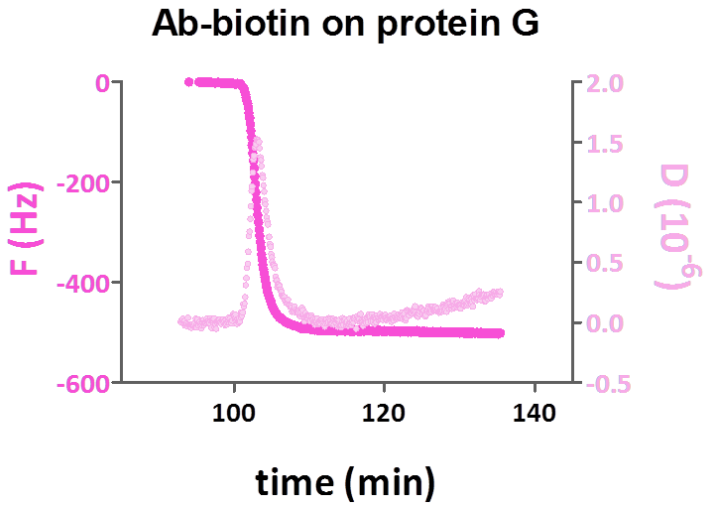


b.

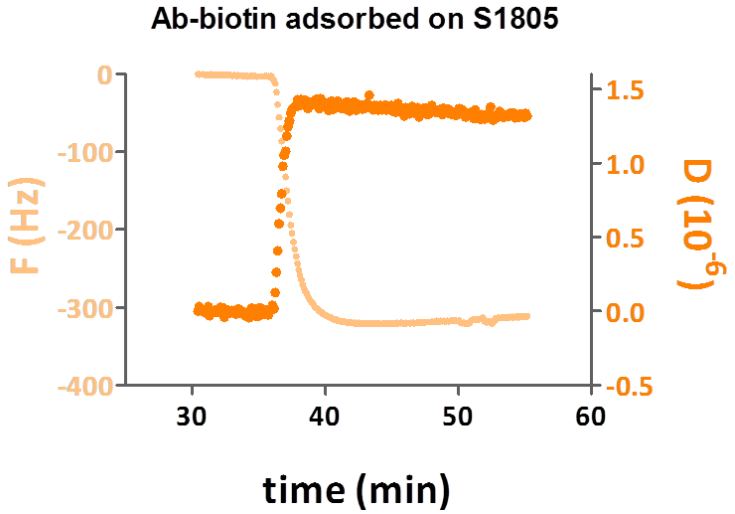


c.

**Figure 40.** Frequency and dissipation responses upon surface immobilization of the anti-*Salmonella* antibody through **a.** neutravidin; **b.** protein G and **c.** on plain photoresist-coated sensor surface

# *Conclusions*

This work was done to develop an improved acoustic wave immunosensor for direct, rapid specific, real-time and label-free detection of whole *Salmonella* Typhimurium cells. A QCM sensor with a photoresist S1805 layer was employed. The limit of detection of the immunosensor was $10^6$ cfu/mL. This detection limit is in agreement with the literature. *Salmonella* Typhimurium cells were detected both in PBS buffer and in LB This study, highlights for the first time, the significance of the dissipation response in the detection of *Salmonella* Typhimurium cells.

The time needed for the real-time acoustic detection of *Salmonella* cells was shown to be 30 min. This short time, combined with the time needed to reach a *Salmonella* Typhimurium cell concentration of $10^6$ cfu/mL (8 hours), starting from a single colony, add up to 6 hours and 30 min. This advantageous characteristic could render the current assay a promising alternative to traditional plate counting.

Since foodborne pathogens are present in very low numbers and in the presence of millions of other bacteria, the immunosensor developed should be tested with a mixed culture of *Salmonella* Typhimurium and other bacteria, not necessarily pathogenic, that are included in food products, to test for its ability to specifically detect *Salmonella* Typhimurium in a complex matrix. In addition, the current immunosensor should be studied for its capability to detect *Salmonella* Typhimurium cells in real samples, such as milk and chicken samples.

# Chapter 2
# Development of an isothermal solid-phase amplification assay for specific and fast acoustic detection of *Salmonella* Typhimurium DNA

## *The emergence of isothermal amplification strategies in foodborne pathogens sensing*

The application of molecular diagnostics for rapid detection of foodborne pathogens is a common practice in the field of food testing. Molecular diagnostics rely upon the detection of pathogenic nucleic acids (NA) and constitute a specific and sensitive alternative to traditional microbiological detection methods for the rapid and on-site detection of foodborne pathogens (*116, 117*). A crucial step in nucleic acids detection is the amplification of the target nucleic acid sequence. This amplification step results in the generation of a large number of target copies, enhancing the assay sensitivity (*116, 117*).

The most widely used amplification technique is the PCR, developed by Kary Mullis in 1983. PCR is based on thermal cycling and on the use of DNA polymerase for primer-directed target amplification (*118*). PCR and its evolved versions (real-time PCR, qPCR) revolutionized the field of molecular diagnostics. PCR, however, is mainly limited by its requirement for precise thermal cycling between three temperatures during the reaction (*116, 117*). The use of this amplification method in miniaturized lab-on-chip devices for point-of-care (PoC) testing is challenging due to the high electricity demand of the thermocycling process (*119*). The problem is even more intense in developing countries where due to the infrastructure, the lack of lab facilities and the skills required to perform PCR analyses, foodborne pathogen detection uses the traditional microscopy or culture and identification methods (when available) (*120*).

In an effort to bridge the gap between traditional methods and PCR, the field of molecular diagnostics has shifted towards the development and use of isothermal amplification methods (*116, 117, 120*). These isothermal amplification techniques are fast and do not require thermal cycling and consequently expensive instrumentation, and therefore, are amenable to low-resource settings. In addition, the reduced complexity of these techniques allows the DNA amplification to be performed on solid surfaces enabling the simultaneous performance of amplification and product detection. This is a key feature that makes the integration of these techniques in PoC diagnostic platforms for on-site detection highly appealing. Some examples of such isothermal amplification techniques are the nucleic acid sequence-based amplification (NASBA) (*121*), the loop-mediated isothermal amplification (LAMP) (*122*), the rolling circle amplification (RCA) (*123*), the helicase dependent amplification (HDA) (*124*) and the recombinase polymerase amplification (RPA) (*125*).

## *Recombinase polymerase amplification (RPA)*

RPA in particular is rather impressive, because it works at an optimal constant low temperature of 37-39 $^{o}$C, and needs not an initial denaturation step (*116*). The RPA (Fig. 41) uses enzymes known as recombinases, which form complexes with oligonucleotide primers and pair the primers with their homologous sequences in dsDNA. A single-strand DNA binding (SSB) protein binds to the displaced DNA strand and stabilizes the formation of a D-loop structure where the primers are introduced at the cognate site of the DNA template, leaving the 3'-end of the oligonucletide accessible to a strand displacing DNA polymerase. The polymerase elongates the

primer according to the template sequence and an exponential amplification of a few target copies is rapidly accomplished by the cyclic repetition of the process (*125*). Several examples of RPA amplification of bacterial and/or viral DNA have been reported (*51, 126, 127*).

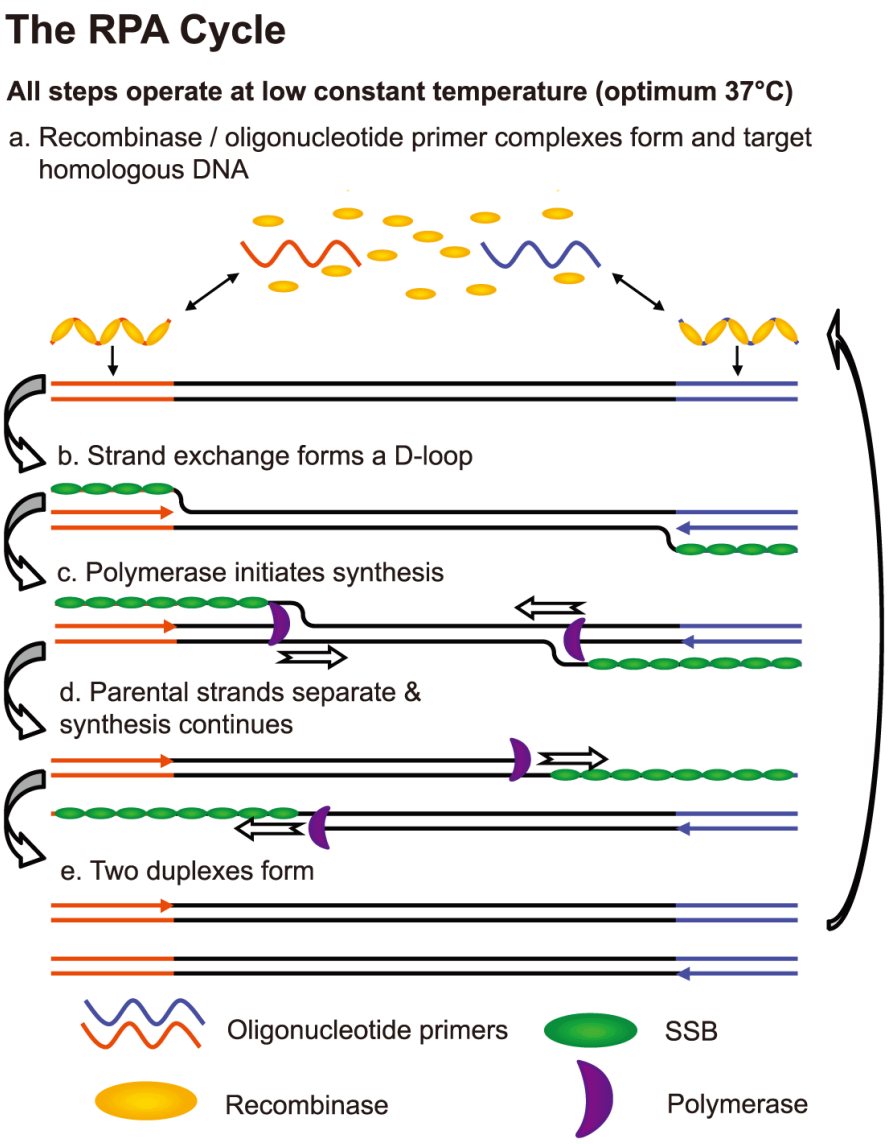


**Figure 41.** RPA scheme. The three main proteins, recombinase, single-strand DNA binding protein (SSB) and strand-displacing polymerase participate in the DNA amplification. The scheme was created by TwistDx Ltd (*128*)

## *Solid-phase RPA*

Another characteristic of RPA that renders this technique particularly attractive is that it can be performed not only in liquid solutions but also on solid surfaces. Solid-phase RPA has been combined with optical/fluorescence (*50, 119, 129-132*), chemiluminescence (*133*), and electrochemical sensors (*134*) for the detection of bacterial pathogens, viruses and genetically modified organisms in food samples. An example is Kersting *et al.* (*119*) who detected three bacterial pathogens at the same time using multiplex RPA and a fluorescence microarray technology for RPA

products' analysis. The bacteria they managed to detect were *Neisseria gonorrhoeae* (implicated in sexual-transmitted diseases), the fodborne pathogen *Salmonella enterica*, and the methicillin-resistant *Stapphylococcus aureus* (responsible for hospital infections). Mayboroda *et al.* (*129*) employed an optical system for the detection of RPA amplified *Yersinia pestis* DNA. *Yersinia pestis* is the causative agent of plague. Kunze *et al.* (*133*) combined the solid-phase RPA with a flow-based chemiluminescence microarray in order to detect viruses (the human adenovirus 41, the Phi X 174) and bacteria (*Enterococcus faecalis*) that are implicated in water hygiene.

## Solid-phase RPA and detection of *Salmonella* Typhimurium DNA on QCM using liposomes and dissipation monitoring

# *Introduction*

As previously mentioned, acoustic wave devices present an attractive alternative to optical and electrochemical sensors thanks to their simplicity in operation, label-free and real-time detection and capacity to be integrated into lab-on-chip platforms (*135-137*). So far, acoustic wave devices have been used for pathogen identification in combination with solid-phase isothermal amplification, based on the use of RCA (*138, 139*) or LAMP (*140*).

The present study combined, for the first time, the RPA method with acoustic biosensing in order to achieve the integrated acoustic amplification and sensing of the gene *invA* from *Salmonella* Typhimurium. *invA* is a critical virulence factor, indispensable for the invasion of cells in the intestinal epithelium. It is specific for *Salmonella* spp. and a suitable PCR target for diagnostic applications (*141, 142*). Among the available isothermal amplification methods, RPA was chosen because it is a straightforward, rapid and specific method of DNA amplification. Compared to the commonly used LAMP for instance, it consumes less power at 37 $^{o}$C as opposed to 65 $^{o}$C; it requires only two primers compared to the six of LAMP; and it can be faster than LAMP (*119, 143*). Figure 42 is a brief illustration of the experimental process followed (which will be described in detail below): in short, *in-situ* RPA was carried out on a QCM sensor surface. The RPA reaction resulted in the generation of multiple copies of the *invA* gene. These copies were surface tethered to the QCM sensor surface via biotin-neutravidin specific interaction. The detection of the RPA *invA* amplicons on the surface was acoustically performed through the use of liposomes (of diameters of 50 and 200 nm) and monitoring of the dissipation changes upon liposomes binding to the surface-bound amplicons. Liposomes were bound to the RPA amplicons because the latter were cholesterol-modified at their 5' ends.

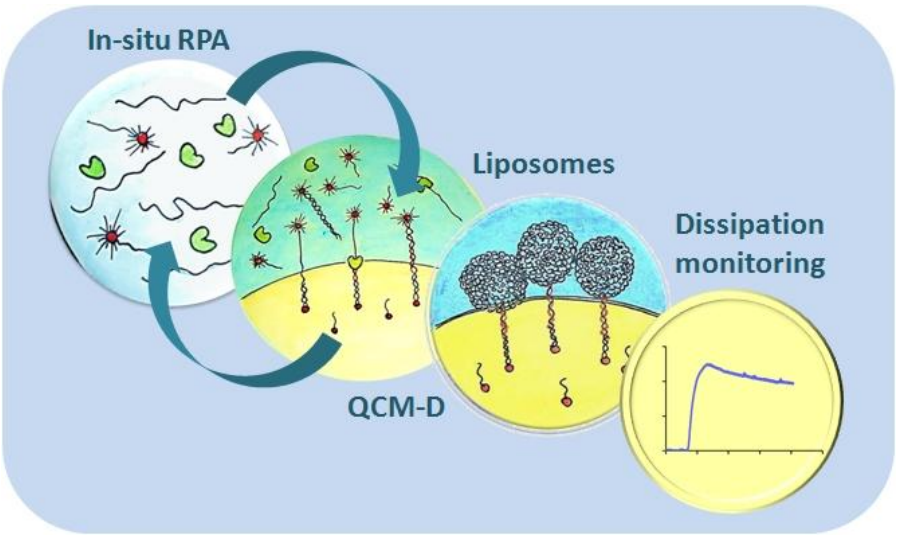


**Figure 42.** Schematic illustration of the steps involved in the solid-phase amplification (RPA) and acoustic detection of *Salmonella* Typhimuirum DNA on a QCM device through the use of liposomes

# *Materials and Methods*

## 1. Chemicals

| |
|---|
| ***invA* synthetic fragment:** Microchemistry Laboratoty, FORTH, Greece |
| **Modified forward and reverse primer:** Eurogentec, Liège, Belgium |
| **RPA kit: RPA TwistAmp® Basic:** TwistDx Ltd., Babraham, Cambridge, U.K. |
| **Avidin, NeutrAvidin®Biotin-binding protein:** ThermoFisher Scientific, Mass., USA |
| **Buffer A: Phosphate buffer saline (PBS) tablet:** Merck KGaA, Darmstadt, Germany (Former Sigma-Aldrich) |
| **Buffer B: Tris HCl 20 mM, NacL 50 mM, MgAc 14 mM in Milli-Q water (18 MΩ)** |
| **Trizma® hydrochloride (Tris HCl) 1 M, pH 7.5:** Merck KGaA, Darmstadt, Germany (Former Sigma-Aldrich) |
| **MgAc (magnesium acetate tetrahydrate):** Merck KGaA, Darmstadt, Germany (Former Sigma-Aldrich) |
| **NaCL:** Merck KGaA, Darmstadt, Germany |
| **Milli-Q water (18 MΩ):** Barnstead Nanopure Ultrapure Water Systems (ThermoFisher Scientific, Mass., USA) |

## 2. Sequences of oligonucelotides

| |
|---|
| ***invA* fragment:**<br>**5**'- GGATCACTAAGCTGTGGATTACCTATTATCTTTTTTTTTTCTAAAGAAATATCCACGCAGGAAATAACAG - **3'** |
| **$SF_3B$ (forward primer): 5' –**Biotin 405.45- -GGATCACTAAGCTGTGGATTACCTATTATC – **3'** |
| **$SR_3$Chol (reverse primer):**<br>**5'** – Cholesteryl-TEG755.97 – CTGTTATTTCCTGCGTGGATATTTCTTTAG – **3'** |

## 3. Materials and equipment for liposomes preparation

1-palmitoyl-2-oleoyl-*sn*-glycero-3-phosphocholine (POPC) and Avanti Mini Extruder for large unilamellar vesicles (LUV) preparation were obtained from Avanti Polar Lipids, Inc. (Ala., USA). Polycarbonate (PC) membranes (19 mm in diameter) with a pore size of either 0.2µm or 0.05 µm were also purchased from Avanti Polar Lipids, Inc. (Ala., USA).

## 4. Liposomes preparation

Liposomes of 50 nm and 200 nm in diameter were prepared. 2 mg of POPC lipids were dissolved in chloroform [(Chloroform for analysis EMSURE® Acs, Iso, Reag. Ph Eur. (Merck Millipore, Mass., USA)] in a round-bottom glass vial. The chloroform was homogeneously evaporated and the lipid film was left under nitrogen gas flow for ~60 min to ensure complete evaporation of the organic solvent. Next, the lipid film was rehydrated by the addition of 1 ml of Buffer A and vortexed for another 60 min. Finally, liposomes were extruded using the Avanti Mini Extruder and the appropriate PC membrane according to the desired diameter of the liposomes.

## 5. Acoustic device

A QSense Analyzer (4-channel system) (Biolin Scientific, Sweden) acoustic device was used for real-time measurement of frequency and dissipation changes. Au-coated 5 MHz AT-cut quartz crystals (QSensor Gold (Ag), Bioline Scientific, Sweden) were employed. Frequency and dissipation responses were monitored at 35 MHz overtone. Prior to the experiments, the QSensors were first rinsed with Milli-Q (18 MΩ) water and 70% EtOH and then subjected to plasma cleaning for 3 min using a

Harrick plasma cleaner PDC – 002 (“Hi” setting) (Harrick Plasma, NY, USA) in order to obtain a clean surface. All measurements were taken at 37 $^{o}$C. The QSense Analyzer was connected to an IPC Ismatec peristaltic pump (Ismatec, Wertheim, Germany).

**6. Solid-phase RPA and acoustic detection of RPA amplicons with liposomes amplification**

The acoustic experiments were performed at a constant temperature of 37 $^{o}$C and at a flow rate of 50 µL/min. A continuous flow of Buffer B was flushed through the acoustic system and allowed to equilibrate prior to the first experimental step, and, in between the following experimental steps. Neutravidin dissolved in Buffer B was physically adsorbed on the sensor surface at a concentration of 200 µg/mL, in order to generate an evenly covered surface. The biotinylated forward primer $SF_3B$ was surface-immobilized via neutravidin-biotin interaction at a concentration of 0.25 µM or 2.48 µg/mL. In the meantime, the cholesterol-modified reverse primer $SR_3Chol$ (0.25 µM or 2.48 µg/mL) and the i*nvA* synthetic target (at concentrations ranging from 0.4 nM to 4000 nM) were added in the TwistAmp® Basic eppendorfs containing all the lyophilized enzymes and regents necessary for the isothermal amplification. After thorough mixing and right before flashing the RPA reaction mix over the acoustic sensor, 14 mM of MgAc were added in the mix. Then, 50 µL of the RPA reaction mix were flown over the sensor and upon reaching the sensor surface, the flow was stopped for time durations of 5, 15, 25, 30, 45 and 60 min. Next, the flow was reestablished and buffer B was allowed to run through until a steady baseline was acquired. Subsequently, Buffer B was changed to Buffer A and 500 µL of of POPC liposomes with diameters of either 50 nm or 200 nm diluted in Buffer A at a percentage of 10% were flushed over the sensor. Changes in dissipation and frequency upon liposomes addition were recorded in real-time for the acoustic detection of the RPA amplicons present on the surface.

# *Results*

## 1. Solid-phase RPA and acoustic detection of the surface-tethered RPA amplicons

Figure 43 illustrates in detail the steps involved in the process of solid-phase RPA and in the acoustic detection of the amplicons through the use of liposomes. In order to perform on-chip RPA, a biotin-labeled forward primer ($SF_3B$) targeting the *invA* gene was immobilized on the sensor gold surface which had been coated with neutravidin (Fig. 43. b). Neutravidin promoted the oriented surface-immobilization of $SF_3B$. The $SF_3B$ immobilization led to a frequency decrease of 97 (± 45) Hz and to a dissipation increase of 1.1 ± 0.60 ($10^{-6}$) dissipation units. At the beginning, the RPA reaction mix containing the RPA reagents (*i.e.,* a recombinase, single-strand DNA binding proteins (SSB), and the strand-displacing polymerase), the single-stranded *invA* targets and the cholesterol-labeled reverse primer ($SR_3Chol$), was flushed over the surface at 37 $^{o}$C. Cholesterol is a hydrophobic anchor frequently used for binding of DNA oligonucleotides to lipid bilayers or liposomes (*144*). The RPA reaction was immediately initiated in the solution, resulting firstly in the generation of double stranded amplicons carrying a molecule of cholesterol at one of their 5' ends (Fig. 43. c). The $SR_3Chol$ reverse primer, together with the recombinase, bound to the double stranded DNA target and released one of the DNA strands. The released DNA strand hybridized to the surface-immobilized $SF_3B$ (Fig. 43. d). The surface-immobilized forward primers ($SF_3B$) along with the strand-displacing polymerase initiated the elongation of the DNA strand and lead to the roduction of RPA amplicons that were cholesterol-labeled at their one end and surface-immobilized through the biotin at their other end (Fig. 43. d). Hence, the RPA amplicons were simultaneously present in the solution and on the surface of the acoustic surface (Fig. 43. c and d). When the solid-phase RPA reaction was completed, the sensor was washed with buffer A followed by the addition of a 10% liposome solution (Fig. 43. e). The liposomes were captured by the cholesterol RPA amplified molecules providing a specific signal for surface-tethered DNA amplicons (Fig. 43. f).

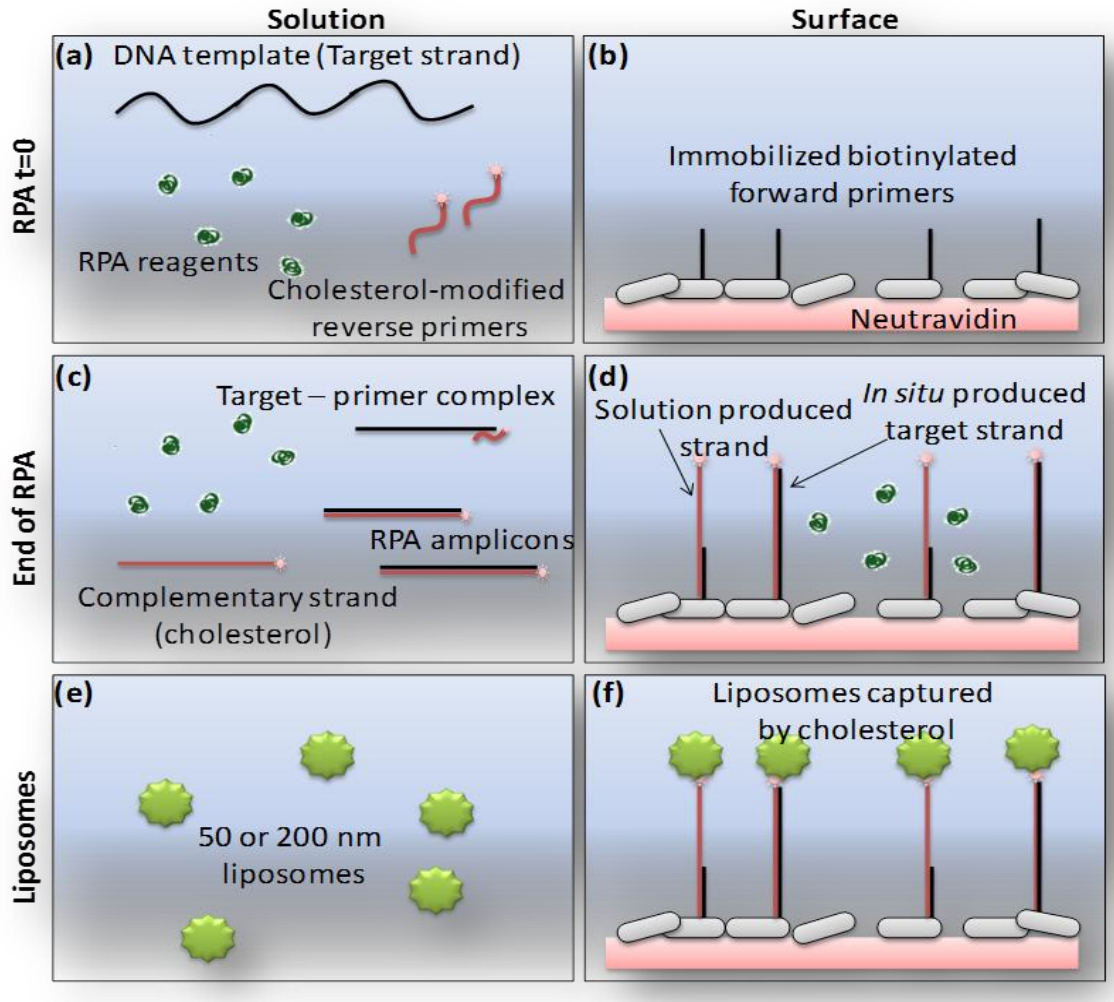


**Figure 43.** Detailed illustration of all the steps of the procedure of the on-chip recombinase polymerase amplification of the *Salmonella* Typhimurium *invA* gene and the subsequent acoustic detection of the RPA amplicons through the use of liposomes

## 2. Direct detection of solid-phase RPA amplicons

Solid-phase RPA was initially carried out for 30 and 60 min and for various *invA* target concentrations which ranged from 0.4 nM to 4000 nM. The changes in the wave frequency and energy dissipation after a washing step showed that direct detection of the surface-immobilized amplicons was not possible (Fig. 44). In the case of RPA, the crowding agents and ingredients included in the reaction mix could have interfered with the direct acoustic detection of RPA products. The direct detection of RPA amplicons in the viscous RPA mixture has been shown to be challenging even with gel electrophoresis, which is why the target purification before detection is needed (*119*). The high sensitivity of acoustic wave biosensors to viscosity changes, could explain the inability of the sensor used here to detect the low amounts of the immobilized DNA amplicons.

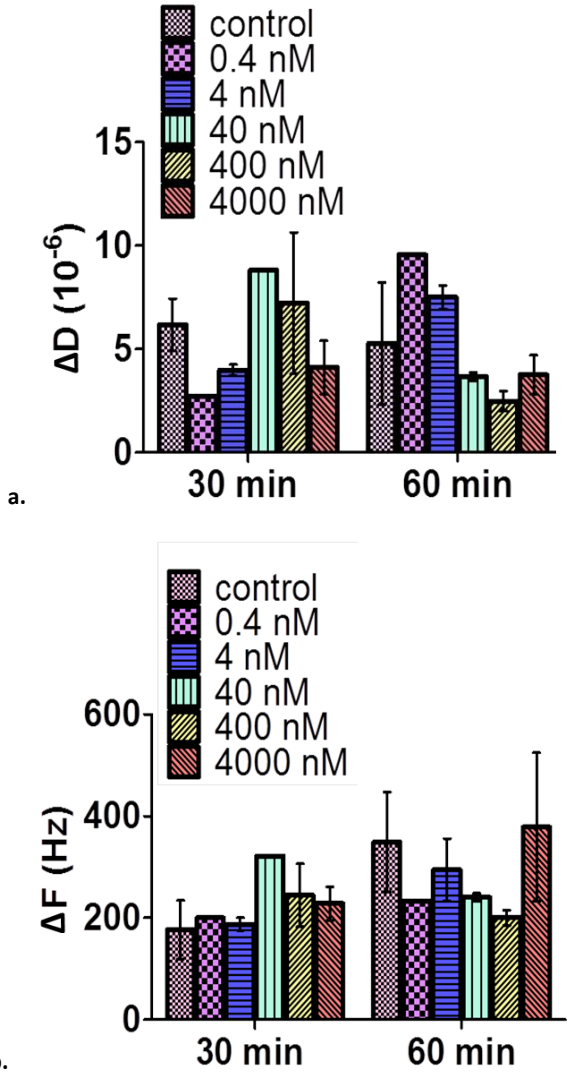


**Figure 44.** Bar charts depicting the measured acoustic signal changes in **a.** dissipation (ΔD) and **b.** frequency (ΔF) after RPA was performed for 30 and 60 min with *invA* target concentrations ranging from 0.4 nM to 4000 nM. Direct acoustic detection of the RPA amplicons generated on the sensor surface was not possible

### 3. Acoustic detection of the surface-immobilized RPA amplicons through the use of liposomes

In order to improve the sensitivity of the on-chip RPA amplicon acoustic detection liposomes were employed, and captured by the cholesterol molecule at the 5' - end of the produced RPA amplicons, for signal enhancement. Real-time monitoring of the whole experimental procedure consisting of, first, RPA amplification on the chip followed by buffer wash and liposomes addition, is shown in Figure 45. Control RPA refers to the case where no *invA* target was included in the initial RPA mix solution. Upon liposomes addition a frequency decrease and a dissipation increase were observed (Fig. 45. a). In the case of control RPA, liposomes addition did not give any detectable signal in frequency or dissipation (Fig. 45. b).

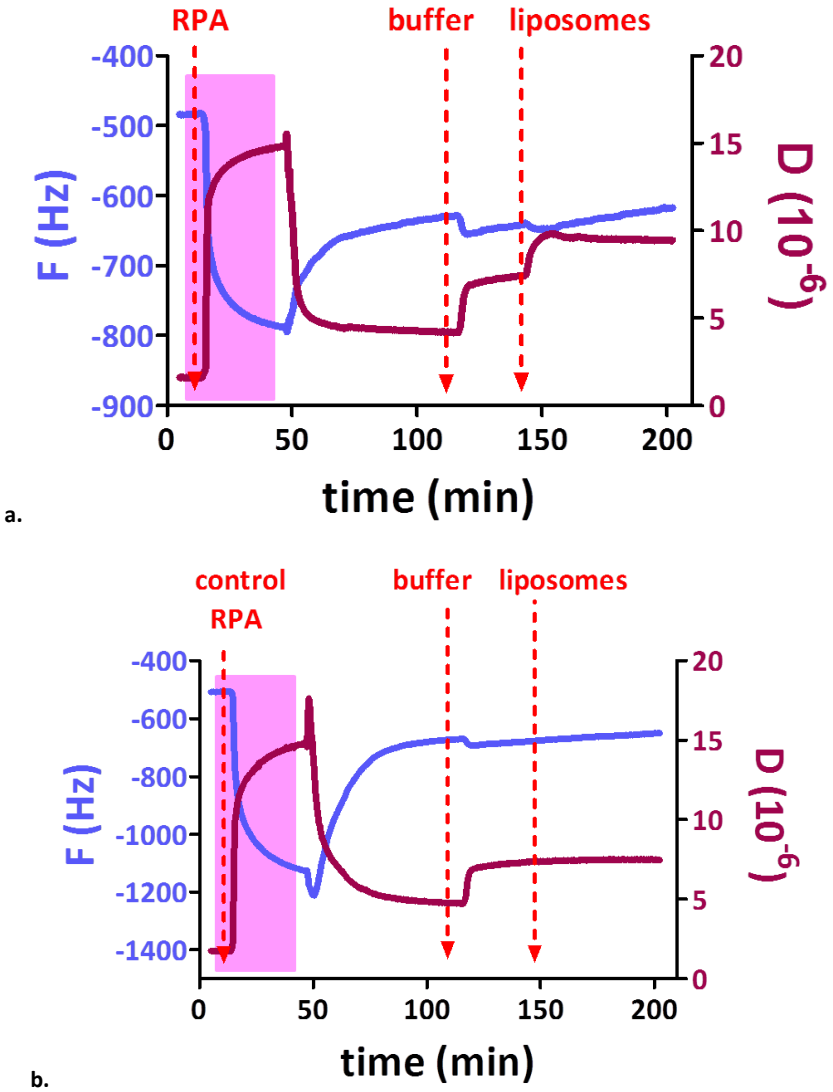


**Figure 45.** Real-time plots of the three key steps of the assay: RPA solution was added in the sensing system and the flow stopped for 60 min (light pink-shadowed part); rinsing of the surface upon completion of the RPA was followed by the addition of the buffer in which lipoosomes were prepared (Buffer A); liposomes were flown over the sensor surface and captured by cholesterol-labeled RPA amplicons, leading to dissipation shift. **a.** results regarding the on-chip RPA of a 4000 nM *invA* gene are shown; **b.** results regarding the control RPA are shown (no dissipation or frequency changes were observed). Note: frequency data are not divided by the harmonic number, *i.e.* F/n

## 4. Specificity of the assay

In order to study the specificity of the assay developed, two different versions of the original RPA mix solution were created. In the first one, a cholesterol-free reverse primer was added in the RPA mixture. It was expected that the non-modified reverse primer would contribute to the formation of solid-immobilized RPA amplicons without the cholesterol label at one of their 5'- ends. Consequently, liposomes would not be captured by the amplicons and their addition would not cause any signal frequency and dissipation shift. In the second version, the biotinylated forward primer $SF_3B$ was not immobilized on the sensor surface, but only included in the RPA mixture. In the absence of the immobilized $SF_3B$, the RPA amplicons would not be

easily surface-tethered through their biotin modification. For this reason, fewer RPA products would be present on the sensor surface and not easily detected by liposomes. The high specificity of the assay was confirmed because in both versions the addition of liposomes resulted in no change in the frequency and dissipation signal (Figure 46).

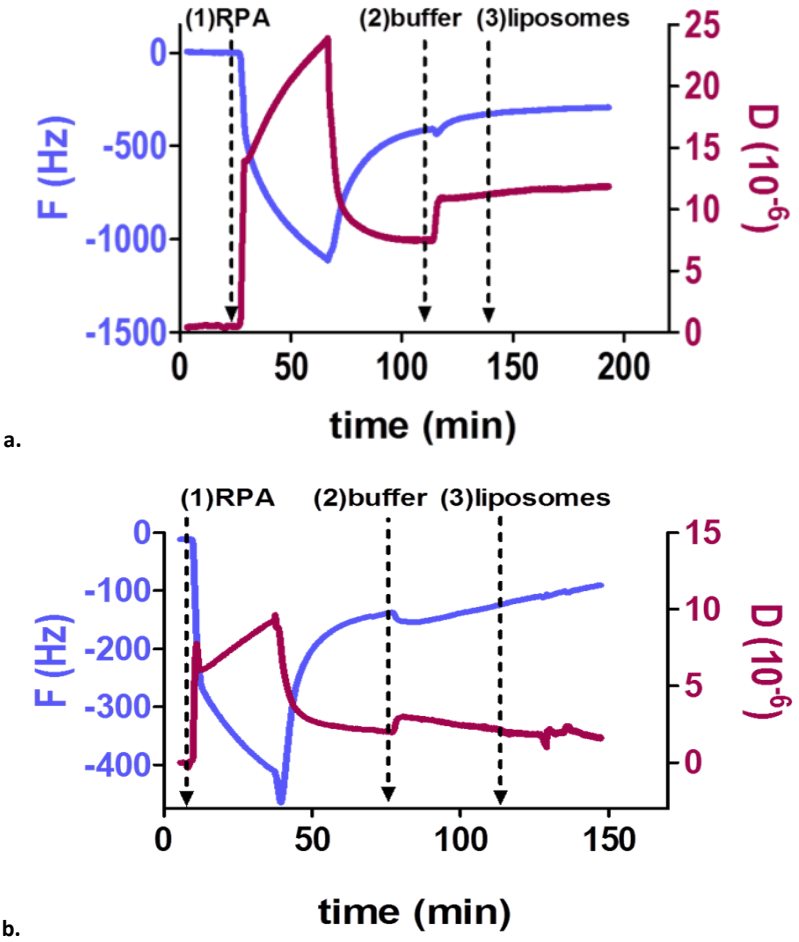


**Figure 46.** Real-time plots highlighting the absence of dissipation and frequency change upon liposomes addition when: **a.** a cholesterol-free primer was used; **b.** the forward primer was not surface-immobilized. Note: frequency data are not divided by the harmonic number, *i.e.* F/n

## 5. Detection of surface-bound RPA amplicons using 50 nm and 200 nm liposomes

Figure 47 provides the measured changes in dissipation (ΔD) and frequency (ΔF) corresponding to binding of liposomes of two different sizes (50 nm and 200 nm) to amplicons produced using DNA targets in the range of 0.4 nM to 4000 nM and for 30 and 60 min of amplification time. Comprehensively, this figure reveals that dissipation changes are more sensitive in comparison to frequency changes with either liposome size. Given that the minimum frequency change that can be reliably detected is 5-10 Hz, frequency changes were significant only when high concentration (4000 nM) of the DNA template was used. Liposomes of 50 nm added after the amplification of 4000 nM DNA target for 30 min, caused a frequency shift

of 27.7 Hz (± 11 Hz). Liposomes of the same size gave a frequency shift of 27 ± 16 Hz when the same 4000 nM of DNA target were amplified for 60 min. Accordingly, liposomes of 200 nm gave a frequency change of 9 ± 10 Hz when the amplification of the 4000 nM target was carried out for 60 min. Amplification of the same target concentration for 30 min was not detected via the use of 200 nm liposomes (Fig. 47. d). The fact that frequency changes were significant only for the highest concentration of the DNA template indicates low yields of the produced amplicons, which is in contrast with previous studies (*101*). It is possible that in the current configuration, the production of RPA amplicons on the sensor surface was less favored than in the solution, probably due to the low surface-to-volume ratio of the QCM set-up. Kersting *et al.* (*119*) suggested that in solid-phase amplification assays with reduced volumes or with three-dimensional surface structures, the rates of the amplification in solution and on the surface may result in enhanced solid-phase amplification.

Based on the results on dissipation obtained using a two-way ANOVA analysis, it was concluded that, with the exception of 400 nM DNA template, increasing the time from 30 to 60 min did not make a significant difference in the acoustic signal when large liposomes (200 nm) were used for the detection (Fig. 47. b). On the contrary, time plays a crucial role when it comes to RPA amplicon acoustic detection with the use of smaller liposomes (50 nm). Using the 50 nm liposomes, it was not possible to detect the on-chip amplification of 0.4 nM, 4 nM and 40 nM DNA template within 30 min; instead, amplification of these concentrations was detected only after 60 min of the RPA reaction (Fig. 47. a). In terms of resolution, quantitative results could be obtained after 60 min amplification using the 50 nm liposomes and in the range of 4 nM to 4000 nM, and after 30 min amplification using the 200 nm liposomes and in the range of 0.4 nM to 4000 nM. In both cases, the two lowest concentrations could not be distinguished from each other (*i.e.*, 4 from 40 nM for the 50 nm liposomes and 0.4 from 4 nM for the 200 nm liposomes).

Interestingly, it was observed that the change in the dissipation signal obtained during the amplification of the 4000 nM template, was larger with the 50 nm liposomes (4.25 ± 0.35 ($10^{-6}$) dissipation units for 30 min amplification; 6.62 ± 0.01 ($10^{-6}$) dissipation units for 60 min amplification) than with the 200 nm liposomes (3.64 ± 0.60 ($10^{-6}$) dissipation units for 30 min amplification; 4.62 ± 0.25 ($10^{-6}$) dissipation units for 60 min amplification). This could be attributed to steric hindrance effects present during the binding of the larger liposomes. Indeed, liposomes of 50 nm seem to have improved the resolution of the assay for higher surface DNA densities, while liposomes of 200 nm offered a better limit of detection, improving the sensitivity of the assay.

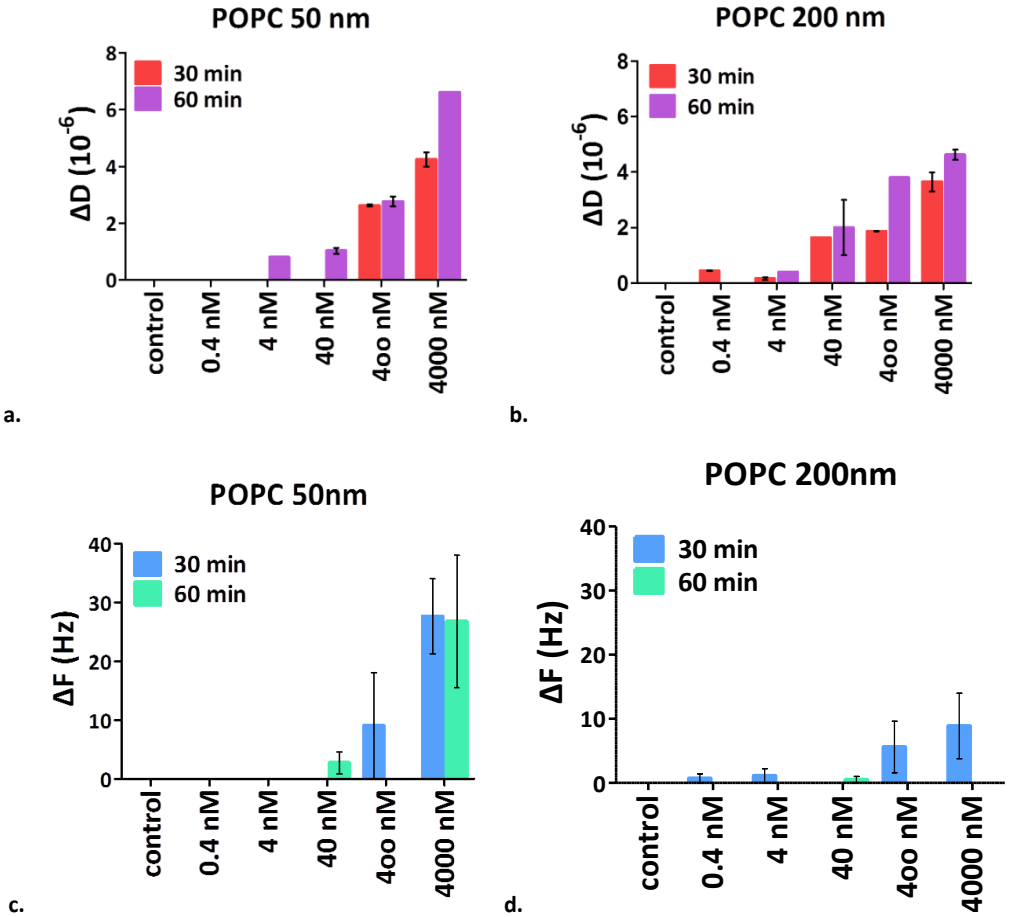


**Figure 47.** Bar charts illustrating the measured acoustic signal changes (ΔD and ΔF) caused by liposomes addition in the sensing system; liposomes targeted cholesterol-modified RPA amplicons. Starting concentrations of the RPA target (0.4 nM – 4000 nM), duration of the on-chip RPA reaction (30 and 60 min) and liposomes sizes (50 nm 200 nm) are plotted

## 6. The effect of the RPA reaction time

For the investigation of the effect of the RPA reaction time, 4000 nM of DNA template were used and solid-phase RPA was carried out for time durations of 5, 15, 25, 30, 45 and 60 min. Amplicons produced within these times were then acoustically detected via the use of 200 nm liposomes and by monitoring the change in the dissipation signal. As shown in Figure 48, frequency changes were once again not sensitive enough to distinguish between different conditions (Fig. 48. b). However, we managed to detect the on-chip RPA products within only 5 min by monitoring the dissipation changes (Fig. 48. a). On-chip RPA reactions performed for more than 30 min appeared to reach a plateau, when detected through the use of 200 nm liposomes. Taking into account that RPA in solution saturates within 10 min (*134*), the 30 min within which the less favored solid-phase RPA was shown to saturate here, are a reasonable time for saturation.

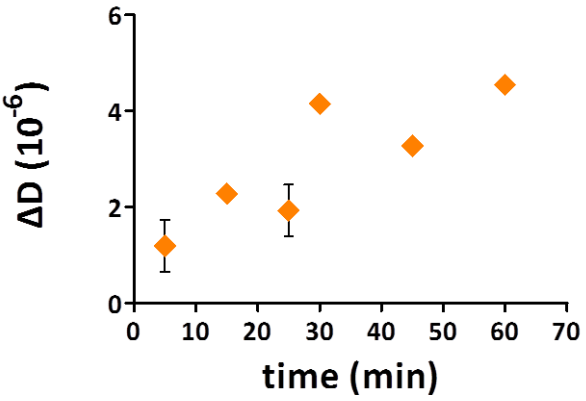


a.

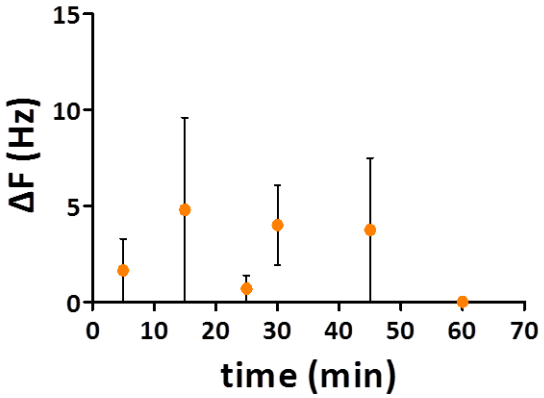


b.

**Figure 48.** Plots of dissipation and frequency changes measured during the acoustic detection of 200 nm liposomes that bound RPA amplicons of *S.* Typhimurium produced at different time intervals. Starting concentration of the RPA template was 4000 nM

# *Conclusions*

In the assay developed here, the QCM device was employed for the first time for the simultaneous solid-phase amplification via RPA and subsequent acoustic detection of DNA amplicons on the sensor surface. The described method is simple and straightforward, since there is no need for post-amplification purification, post-amplification denaturation and subsequent hybridization of the amplification products, reducing analysis time and reagents consumption. Moreover, the assay is rapid (acoustic detection of RPA amplicons on the surface within 5 min), sensitive and specific. The current solid-phase RPA could be further improved by either adding the forward primer in the solution under asymmetric conditions (*119*), or using a dsDNA template (*129*) instead of the ssDNA that was used here.

On the other hand, the solid-phase RPA described here, with its forward primer immobilized on the surface, addressed the problem of the formation of primer-dimers which is a typical drawback of liquid-phase RPA. This feature renders the solid-phase RPA a suitable candidate for integration in lab-on-chip acoustic platforms. The use of a SAW device with microfluidics and on-chip amplification could be an example of such an integrated platform for on-site pathogen detection (*135, 136, 145*).

The results presented in this study, provide a novel insight on the use of liposomes and dissipation monitoring for the acoustic detection of the RPA amplicons produced on the sensor surface. As previously stated, liposomes are spherical vesicles made up of one or more lipid bilayers which surround aqueous compartments (*97, 98*). They have been broadly used in the field of biosensing owing to their small sizes and ease of manipulation. Patolsky *et al. (99, 101)* where the first to use functionalized liposomes to enhance the acoustic signal during DNA hybridization on a QCM surface. Willner *et al.* (*100*), used liposomes for the detection of a single-base mismatch employing a QCM acoustic device. In both cases the use of liposomes for acoustic signal amplification was monitored through frequency changes. Data from the current work suggest that monitoring the dissipation change upon liposomes addition can be a more sensitive approach for the detection of surface-immobilized DNA molecules. In fact, dissipation monitoring during liposome addition was shown to be 4 orders of magnitude more sensitive than frequency.

The solid-phase RPA assay developed here, needs to be tested with genomic and not synthetic *Salmonella* Typhimurium DNA. It could also be carried out in a complex matrix, where the target DNA would coexist with non-specific DNAs and substances, to determine their inhibitory effect for a PoC testing application.

# Part 2
# Acoustic wave biosensors in cancer molecular diagnostics

Cancer is the second leading cause of death globally (*146*). According to the WHO, cancer accounted for 8.8 million deaths only in 2015. The economic burden of cancer is serious and constantly increasing. The total economic cost of cancer in 2010 was approximately U.S. $ 1.16 trillion. Lung, prostate, colorectal, stomach and liver cancer are the most common types of cancer in men; breast, colorectal, lung, cervix and stomach cancer are the most common types among women. WHO predicts that the number of new cancer cases will increase by 70% in the next two decades. It becomes apparent that the diagnosis of cancer at early stages is crucial for patient survival and successful prognosis of the disease. Prognosis is the monitoring of the natural course of the disease in the absence of treatment or the prediction of treatment outcomes. Furthermore, prognosis refers to the ability of determining whether an existing cancer will recur after treatment (*147*).

Conventional methods for cancer diagnosis are the: **a)** tissue biopsy which relies heavily on traditional methods that are based on cell morphology using staining and microscopy. A small tissue is removed from the body and examined under a microscope after cell fixation; **b)** magnetic resonance imaging (MRI): an imaging test where a powerful magnetic field and radio waves produce detailed, computer-generated pictures of organs and tissues; **c)** ultrasound: it is also an imaging test that uses high-frequency sound waves to create pictures of internal organs, locating in this way possible tumors. These diagnosis techniques are commonly used by clinicians for cancer diagnosis; however, they are inefficient for early stage cancer diagnosis because they are based on the phenotypic properties of the tumors detected (*148, 149*).

Besides traditional cancer diagnosis methods there are the more present-day ones. Immunodiagnostic assays that use the antibody-antigen interaction in order to detect cancer biomarkers (*e.g.* hormones, proteins etc.) belong to this group of the more recent diagnostic techniques. Radioimmunoassay (that uses radiolabeled molecules in a stepwise formation of immune complexes), immunohistochemistry, ELISA and fluoroimmunoassay are the most commonly used immunoassays in the field of cancer diagnosis. These immunoassays are very sensitive and selective, but they are expensive, time-consuming, need trained personnel, and complicated labeling processes (*149, 150*). In addition, and despite their high sensitivity, some ELISA tests for example, are not adequately sensitive for the detection of cancer biomarkers of low concentrations occurring at the early stages of the disease.

More sensitive, rapid and label-free diagnostic platforms are needed to meet the demanding requirements in cancer diagnostics. The “omics” revolution led to the indispensable use of molecular diagnostics techniques in the field of cancer diagnosis. The term “molecular diagnostics” defines the tests that detect genetic material (DNA, RNA), proteins, or related molecules which provide information about health or disease (*147*). Molecular diagnostic testing is a fundamental part of medical practice (*151*) and constitutes an essential aspect of “personalized” medicine in cancer treatment (*147*). Molecular diagnostics are predicted to play an ever significant role in cancer management in the future, helping in **a)** evaluating the risk assessment, **b)** differential diagnosis, **c)** prognosis, **d)** predicting the treatment response, **e)** pharmacokinetics, **f)** monitoring of the treatment response, and **g)** monitoring recurrence in patients without symptoms of cancer (Fig. 49) (*147*).

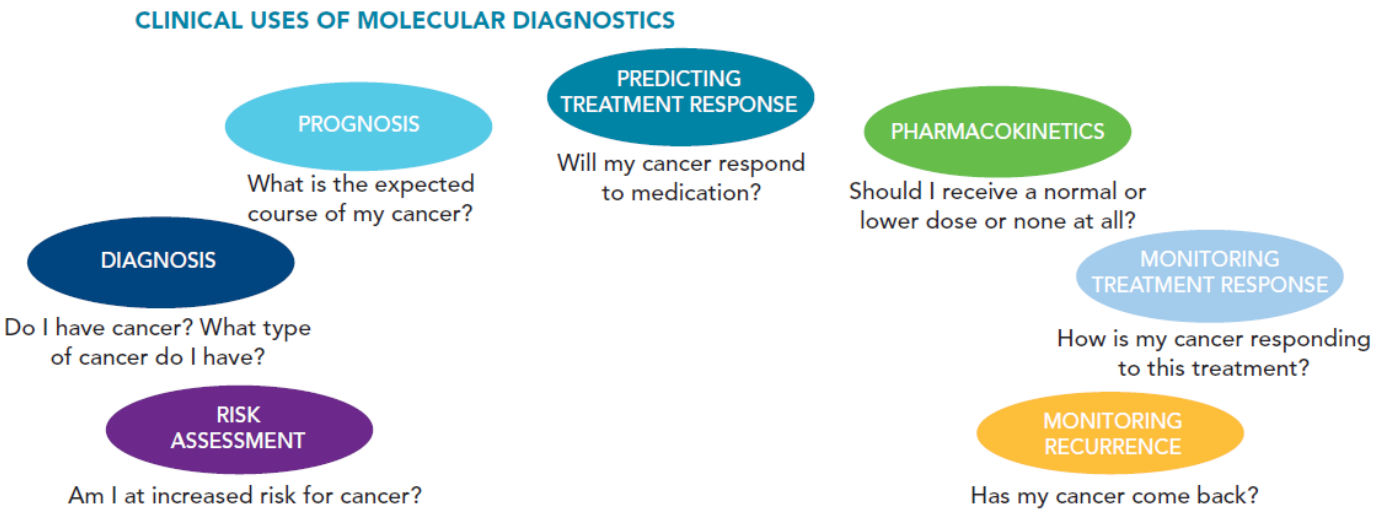


**Figure 49.** Schematic presentation of the main uses that molecular diagnostics find in the field of cancer management (*147*)

Molecular biomarkers are certain mutations in chromosomes, DNA, RNA, proteins and related molecules which have the potential to cause cancer. Nucleic acid-based biomarkers (NA-based) in particular, are of significant importance in the field of cancer diagnosis, because they boost the early detection of cancer, even in the absence of physical symptoms (*147, 148*).

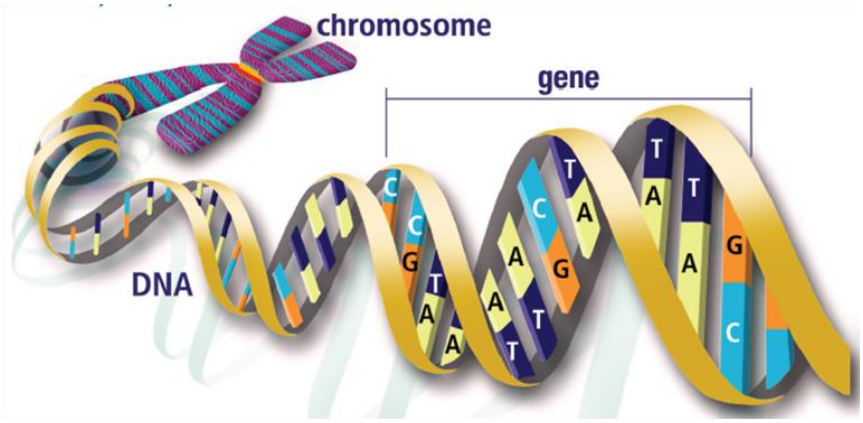


**Figure 50.** Chromosomes consist of DNA and certain species of DNA make up genes (*152*)

Currently, the most widely used methods applied to detect NA-based cancer biomarkers are: **a)** PCR and real-time (RT)-PCR, **b)** Southern blot, **c)** DNA microarrays, and **d)** DNA sequencing. They are undoubtedly sensitive and selective, but they are expensive, time-consuming, complex, and laboratory-based and demand trained personnel.

On account of the increasingly demand for cancer molecular diagnostic platforms that will be able to function in settings with limited access to a central lab (*151*), it is apparent that the methods described above, cannot meet this requirement. By way of contrast, biosensors, in general, can form platforms for cancer biomarkers analysis

which will allow on-site detection and will be accessible to a large portion of the population (*153*). The current PhD study investigated the potential application of acoustic wave biosensors in cancer molecular diagnostics. As previously mentioned, acoustic wave biosensors provide the inexpensive, real-time, label-free, rapid and specific detection of molecular biomarkers. In addition, they are easy to use, they have proven their ability to get integrated in diagnostic platforms for on-the-spot detection (*137, 145*), and have shown multi-analyte testing ability (*136*). This latter characteristic of acoustic wave biosensors could be very useful for cancer diagnosis, since cancer is a complex genetic disease (*154*) and the multi-biomarker diagnosis using a multi-array acoustic wave diagnostic platform could fulfill the demands of the modern cancer molecular diagnostics field. Chapter 3 describes the work carried out on the fabrication of an acoustic wave DNA-hybridization biosensor for the detection of four breast cancer molecular biomarkers. Chapter 4 deals with the experimental work focused on the development of an acoustic wave diagnostic platform for the detection of molecular biomarkers associated with colorectal cancer.

# Chapter 3
# Detection of multiple miRNA breast cancer biomarkers with a single probe using a conformation-sensitive acoustic sensor

# *Introduction*

Breast cancer is the most common type of cancer in women. Every year 1.6 million cases of breast cancer are reported globally (*155*). Breast cancer is considered to be the main cause of death among women from cancer (*156*). Most breast cancers occur in women without traceable risk factors, while hereditary disposition makes up for only 5%-10% of the cases (*157*). Etiological factors that have been involved in the occurrence of breast cancer include: age at menarche and menopause **(*158*)**, childbearing (*159*), breastfeeding (*158*), hormonal status (*158*), alcohol consumption (*160, 161*), type of diet (*162*), obesity (*163*), radiation (*164*) and genetic susceptibility (*165*). Breast cancer affects men as well (1% of all cases), occurs in both young and old people and affects people of all the races and nationalities (*166*). It has been suggested in the literature that early breast cancer diagnosis in combination with suitable treatment could significantly reduce the deaths caused by this disease in the long-term (*150*). To date there exist a wide range of biomarkers which have been identified with breast cancer. Recently, microRNAs have attracted the scientific attention for their potential role as novel breast cancer biomarkers and targets for breast cancer treatment (*167*).

## *microRNAs in breast cancer*

Mature microRNAs (miRNAs) are a class of evolutionary conserved, small, (19-23 nucleotides), endogenous, single-stranded and non-coding RNAs which regulate gene expression at the post-transcription level, in animals, plants and viruses (*168, 169*). The biogenesis cascade of miRNAs (Fig. 51) starts in the cell nucleus where miRNAs are initially transcribed from intra- or intergenic regions by RNA polymerase II to form primary miRNAs (pri-miRNAs) (1-3 kb). These pri-miRNAs are cleaved in the nucleus by the RNase III enzyme Drosha and a double-stranded RNA-binding protein Pasha into approximately 70 nucleotide-long stem-loop structures, the pre-miRNAs. The pre-miRNAs are then exported in the cytoplasm by Exportin-5, where they are further processed into the 18-24 double-stranded oligonucleotides by the RNase III enzyme Dicer into mature double-stranded miRNA:miRNA. After strand separation, one of the strands becomes a mature miRNA incorporated into RNA-induced silencing complex (RISC); the other strand is usually degraded. The RISC complex operates by perfectly or imperfectly matching with its complement mRNA target and induces target degradation or translational suppression of mRNAs (*154, 168*).

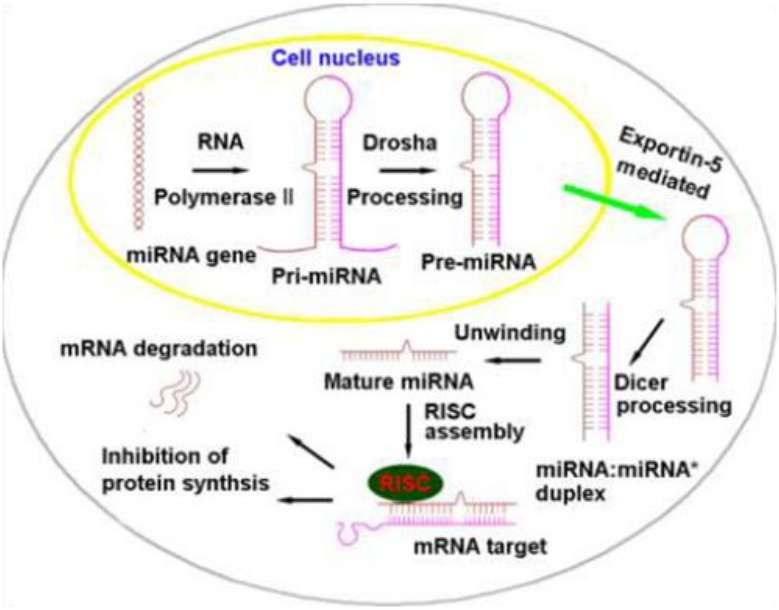


**Figure 51.** schematic presentation of the biogenesis of miRNAs process. The differential steps are explained in the text above. Reprinted from reference (*168*)

miRNAs are regulators of almost every biological process, including cell fate determination, proliferation and cell death (*154, 168, 170*). Recent genome-wide analyses have discovered deregulated miRNAs expression in human malignancies (*168*). Lawrie *et al.* (*171*) were the first to observe elevated levels of the miRNA-21 (miR-21) in the serum of large B-cell lymphoma patients. Mitchell *et al.* (*172*) reported the association between miR-141 and prostate cancer. An explanation for this may be the fact that about 50% of all human miRNAs are located in genome areas known as "fragile sites" that are linked to cancer *(173).* The function of analogous miRNAs in breast cancer has been studied (*174*). MiRNAs implicated in breast cancer have been shown to either modulate oncogenic or tumor suppressor pathways; miRNAs themselves can be regulated by oncogenes or tumor suppressor genes (*168, 169*). Circulating miRNAs, present in the cell-free component of blood and body fluids of breast cancer patients can serve as novel diagnostic biomarkers to assist in the diagnosis, prognosis and prediction about the treatment responses (*168, 169, 175*). Moreover, they could be treated as novel therapeutic targets (*169*). In light of these discoveries, and within the last decade, research efforts have focused on the development of bioassays for the rapid and sensitive detection of miRNAs implicated in breast cancer.

miRNAs related to breast cancer are detected by three widely applied methods which include: **a)** Northern blot, **b)** miRNA microarrays and **c)** quantitative reverse transcriptase PCR (qRT-PCR). Northern blotting is the gold-standard approach that validates data obtained from more state-of-the-art and sensitive detection techniques. However, Northern blotting is low-throughput, time-consuming, exhibits low sensitivity, requires a large amount of RNA (hundreds of micrograms) and it oftenly fails to detect miRNAs at low concentrations. miRNA microarrays offer high throughput, but tend to have lower sensitivity and dynamic range; qRT-PCR finally, is based on the reverse transcription of miRNA to complementary DNA (cDNA), which is followed by qPCR with real-time monitoring of produced products. qRT-PCR

exhibits a wide dynamic range, high sensitivity, but suffers from low throughput. Overall, the three techniques are expensive, laboratory-based, and time-consuming and require sophisticated equipment and trained personnel (*168, 176*). These key characteristics constitute an obstacle which prevents the application of these techniques in platforms that will rapidly, specifically, robustly and inexpensively detect the presence of breast cancer-related miRNAs in clinical samples.

## *Acoustic wave biosensors in the detection of miRNAs associated with breast cancer*

Acoustic wave biosensors have generally been used for the detection of cancer biomarkers. Piezoelectric immunosensors (both QCM and SAW) detecting cancer protein markers have been presented by Arif *et al.* (*158*)**,** Su *et al.* (*177*)**,** Gruhl *et* al. (*178*), Ding *et al.* (*179*) and Chou *et al.* (*180*). Numerous QCM and SAW DNA-based sensors have been developed for the detection of specific mutations in gene fragments (BRCA1, BRCA2, p53) that play a crucial role in the biogenesis of breast cancer (*181-185*). Not so unexpectedly, since miRNAs have only recently began to gain attention as breast cancer biomarkers, there are not many reports in the literature regarding the application of acoustic wave biosensors in the detection of breast cancer biomarkers. Premaratne *et al.* (*186*) used a QCM DNA-based sensor to detect an oligonucleotide mimic of a miR-21 biomarker by monitoring the mass (frequency) response. Palaniappan *et al.* (*187*) developed a QCM-based multistep protocol which, among others, included signal amplification by avidin-coated nanoparticles in order to acoustically detect the miR-21 breast cancer biomarker. QCM frequency responses were correlated to the miRNA concentration.

The current PhD study presents the design of a DNA-based acoustic wave biosensor and its application to the detection of four miRNAS that are considered to be dynamic biomarkers of the breast cancer disease. The biosensor presented here relies on DNA-hybridization and is sensitive to binding-induced conformational change events occurring on the sensor surface upon probe-target hybridization. This relatively new type of biosensors was initially presented for electrochemical and optical biosensing devices (*188, 189*). This method exploits specific DNA probes, such as beacons (*190*), stem loops (*191*), flexible bulge-containing duplexes (*192*), hairpins (*193*), two single-stranded DNA pieces connected through PEGS (*193*), and clamp-like DNAs (*194, 195*) all of which undergo a significant conformational change upon target binding. Nevertheless, in reality, both optical and electrochemical sensors do not measure the conformation of the surface-immobilized DNA *per se*; instead they exploit the sensor's sensitivity to the distance of a probe from another probe or the device surface, respectively, which changes as a result of target binding. Moreover, optical and biochemical biosensors require laborious labeling.

The conformation-sensitive acoustic sensor described here makes use of the "discrete molecule" approach presented by the Biosensors Group (*18*). As previously explained, it was shown that acoustic biosensors can sense the hydrodynamic volume of a biomolecule attached to the device surface (*18*). Since the hydrodynamic volume is a measure of the shape and size of a molecule, it was possible to characterize and even predict DNA geometry through acoustic measurements (*21*). The biophysical explanation is: single-point surface-attached

DNAs are driven to oscillation by the acoustic wave. This generates a dragging force between the biomolecule and the surrounding liquid which results in energy dissipation. Theoretical modeling and experimental results showed that the ratio ΔD/ΔF (where ΔD and ΔF are the wave energy dissipation and frequency changes, respectively) observed during molecular binding to the surface of a QCM is a measure of the molecule's intrinsic viscosity [$\eta$] (*i.e.* ΔD/ΔF ~ [$\eta$]). The latter is mathematically related to the geometrical features of the molecule, *i.e.* its conformation. The approach presented in this chapter aimed at designing a DNA detection assay where multiple targets could be acoustically detected (through the acoustic ratio) with a single probe, simply by producing hybridization products of a different geometry each time. The simultaneous detection of two targets was also a goal, setting the challenge for designing a probe where its conformation upon binding of two targets would be distinctly different to that produced by the binding of either one of them.

Four miRNAs acknowledged as early breast cancer biomarkers were studied: **1)** the **miR-21** (gene locus: 17q23.2) which has been shown to act as an anti-apoptotic, oncogenic factor and is upregulated in breast cancer (*173, 196, 197*); **2) the miR-155** (gene locus: 21q21) that is consistently upregulated in breast cancer and acts as an oncogenic factor (*154, 169, 173, 196*); **3)** the **miR-150** (gene locus: 19q13.33) that was found to be over-expressed in breast cancer cell lines and tissues and promoting human breast cancer growth and malignant behavior (*170*), and **4) the miR-107** (gene locus: 10q23.31) which is over-expressed and serves as an oncogene for promoting tumor invasion and metastasis in breast cancer (*198, 199*)**.** In the current proof-of-principle study, synthetic oligonucleotide mimics of the miR-21, miR-155, miR-150 and miR-107 biomarkers with a thymine in the place of uracil were used.

Figure 52 illustrates the assay design: a linear ssDNA probe of 86 nucelotides (nts) (Probe-86) was employed consisting of the following areas: four target recognition regions each one of 14 nts of a different sequence placed at positions P1, P2, P3 and P4.; three intermediate regions consisting of 10 poly-cytocines (polyC); and one surface link region comprising a biotin at the 5' end of the probe. Each oligonucleotide mimic of the four miRNAs comprised a 14 nts recognition target sequence complementary to one of the regions of the probe: miR-21 mimic (T1) bound to P1; miR-155 mimic (T2) bound to P2; miR-150 mimic (T3) bound to P3, and miR-107 mimic (T4) bound to P4. Each of the miRNAs mimics carried a poly-thymine (polyT) tale of variable lengths, *i.e.* 20, 30, 40 and 50 nts. The flexible polyT tails (and not tails of a random sequence were chosen) in order to: **a)** construct targets of different shapes and sizes and **b)** minimize non-specific interactions with the Probe-86. The combination of the four target sequences with each one of the polyT tails resulted in a total number of 16 analytes. Figure 52 illustrates the case where all the binding sites of the Probe-86 were hybridized to their targets.

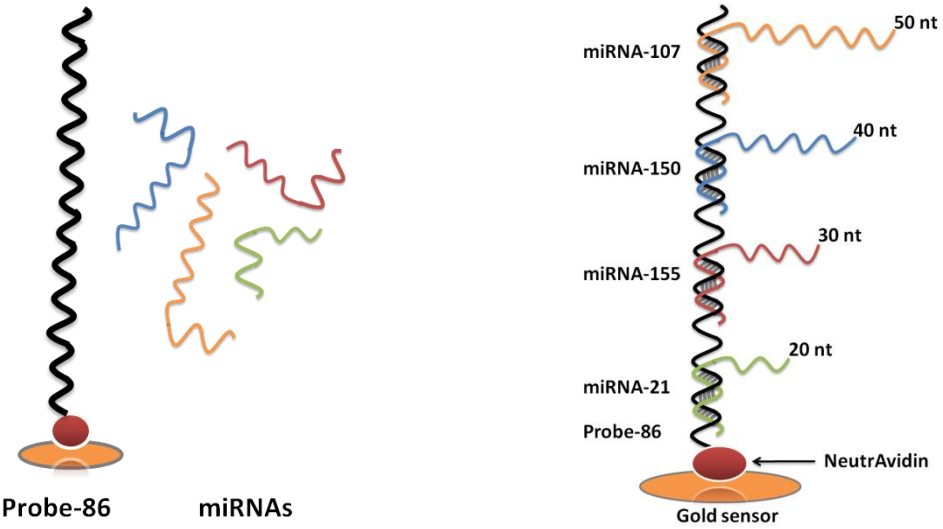


**Figure 52.** Schematic representation of the probe and miRNA targets used in the design of the bioassay

# *Materials and methods*

## 1. Chemicals

| |
|---|
| **Olionucleotide probe (Probe-86) :** Integrated DNA Technologies (IDT), Iowa, USA |
| **Oligonucleotide probe with a random sequence in between its target hybridization regions (Probe-86b):** Integrated DNA Technologies (IDT), Iowa, USA |
| **Oligonucleotide miRNA mimics (T1,T2,T3, T4):** Microchemistry Laboratoty, FORTH, Greece |
| **Avidin, NeutrAvidin®Biotin-binding protein:** ThermoFisher Scientific, Mass., USA |
| **Phosphate buffer saline (PBS) tablet:** Merck KGaA, Darmstadt, Germany (Former Sigma-Aldrich |
| **Ethanol absolute (EtOH) synthesis grade:** Scharlab S.L., Barcelona, Spain |
| **Milli-Q water (18 MΩ):** Barnstead Nanopure Ultrapure Water Systems (ThermoFisher Scientific, Mass., USA) |

## 2. Sequences of oligonucelotide probes and oligonucleotide miRNA mimics

| |
|---|
| **Probe-86:**<br>**5'** biotin- AGCTTATCAGACTGCCCCCCCCCCCTCCTACATATTAGCCCCCCCCCCCTCCCAACCCTTGTCCCCCCCCCCTATCAAAGCACAGA- **3'** |
| **Probe-86b:**<br>**5'** biotin- AGCTTATCAGACTGGCATCATCAACTCCTACATATTAGTCATCATCAACTCCCAACCCTTGTTCATCATCAATATCAAAGCACAGA- **3'** |
| **miRNA-21 (T1)+polyT20:**<br>**5'**- TTTTTTTTTTTTTTCCCCCCAGTCTGATAGCT- **3'** |
| **miRNA-155 (T2)+polyT30:**<br>**5'**- TTTTTTTTTTTTTTTTTTTTTTTTCCCCCCTAATATGTAGGAG- **3'** |
| **miRNA-150 (T3)+polyT40:**<br>**5'**- TTTTTTTTTTTTTTTTTTTTTTTTTTTTTTTTTTTTCCCCCACAAGGGTTGGGAG- **3'** |
| **miRNA-107 (T4)+polyT50:**<br>**5'**- TTTTTTTTTTTTTTTTTTTTTTTTTTTTTTTTTTTTTTTTTTTTTTTCCCCCTCTGTGCTTTGATA- **3'** |

Note: each one of the miRNA targets is depicted combined with only one of the available polyT tails

### 3. Acoustic device

A QSense Analyzer (4-channel system) (Biolin Scientific, Sweden) acoustic device was used for real-time, simultaneous measurement of frequency and dissipation changes. Au-coated 5 MHz AT-cut quartz crystals (QSensor Gold (Ag), Bioline Scientific, Sweden) were employed. Frequency and dissipation responses were recorded at 35 MHz overtone. Prior to the experiments, the QSensors were first rinsed with Milli-Q (18 MΩ) water and 70% EtOH and then subjected to plasma cleaning for 3 min using a Harrick plasma cleaner PDC – 002 ("Hi" setting) (Harrick Plasma, NY, USA) in order to obtain a clean surface. All measurements, unless otherwise stated, were taken at 25 $^{o}$C. The QSense Analyzer was connected to an IPC Ismatec peristaltic pump (Ismatec, Wertheim, Germany).

### 4. Hybridization of the miRNA targets to the single-stranded, surface-immobilized Probe-86

A continuous flow of PBS buffer was flushed through the system at a flow rate of 50 μL/min and allowed to equilibrate prior to the first addition. The same flow rate of 50 μL/min was used throughout the experimental process. Neutravidin, dissolved in PBS (final concentration: 200 μg/mL), was physically adsorbed on the QSensor in order to produce a fully saturated surface. After buffer rinse, the QSensor was exposed to the oligonucleotide probe (Probe-86 or Probe-86b) which was introduced at a concentration of 0.2 μM or 5.68 μg/mL in PBS, and in a total sample volume of 200 μL. Probe-immobilization took place through avidin-neutravidin interaction, and was followed by buffer rinse and the addition of the target miRNA mimics. Each of the miR-21+polyT, miR-155+polyT, miR-150+polyT and miR-107+polyT targets was diluted in PBS at a final concentration of 4 μM and was added in a volume of 200 μL; hybridization was performed at room temperature. Before adding the probe and target oligonucleotides on the sensor surface, both were heat-denatured at 95 $^{o}$C for 5 min and placed immediately on ice for a minimum of 5 min in order to untangle.

To detect the simultaneous binding of two miRNA mimics on the same probe, the same procedure was followed. After neutravidin physisorption and probe surface-immobilization, miRNA-21+polyT20 (4μM) and miRNA-107+polyT50 (4μM) were mixed in PBS buffer in two ratios (1:1 and 1:10) and injected in the sensing system in a final volume of 200 μL. The sensor surface was exposed to the sample solution and the miRNA targets were allowed to hybridize at room temperature. Prior to their addition to the sensor surface, the probe and the miRNA mimics were heat-denatured as described above.

# *Results*

## 1. Acoustic sensing of the Probe-86 surface-immobilization and subsequent sequential hybridization of miRNA targets

The experimental protocol consisted of the addition of neutravidin on a QCM device surface to produce a fully covered sensing substrate, followed by the immobilization of the biotinylated probe and sequential addition of the four miRNA targets (Figure 53). The sequential addition of the miRNA mimics on the same surface is possible, since the acoustic ratio is independent of previous additions, order of target addition, or amount of added mass. This is due to the fact that the acoustic ratio reflects intrinsic properties (conformation) of the attached molecules (*18, 19*). It is, therefore, characteristic for each DNA structure and does not change with surface coverage. This assumes that the conformation of the bound oligonucleotide molecules is not affected by lateral interactions with neighboring molecules or the sensor surface (*18*).

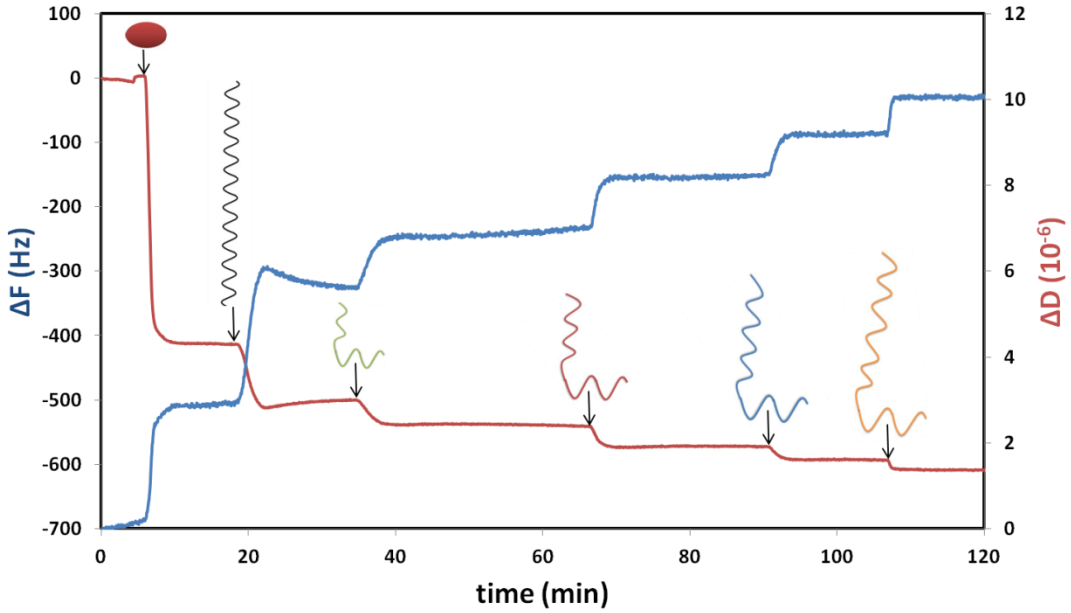


**Figure 53.** Real-time graph representing dissipation and frequency changes upon the addition of neutravidin, Probe-86, miRNA21polyT20, miRNA-155+polyT30, miRNA-150+polyT40 and miR-107+polyT50. Note: frequency data are not divided by the harmonic number, *i.e.* F/n

## 2. Acoustic sensing of the acoustic ratio (conformational changes) obtained upon miRNA targets hybridization to Probe-86

Figure 54 presents the acoustic ratio of Probe-86 after hybridization with each one of the 16 miRNA mimics, as a function of the length of the attached polyT tail. As can be seen in the figure, varying the length of the polyT tail at the same position had no effect on the acoustic ratio of the final hybridized product. The acoustic ratio obtained upon hybridization of the T1+polyT20 at P1 was 0.0301 ± 0.0010 ($10^{-6}$/Hz); hybridization of the T2+polyT30 at P1 gave an acoustic ratio of 0.0296 ± 0.0002 ($10^{-6}$/Hz); the acoustic ratio observed during the addition of T3+polyT40 at P1 was 0.0339 ± 0.0006 ($10^{-6}$/Hz), and, finally, the ratio obtained from the hybridization of

the T4+polyT50 at P1 was 0.0316 ± 0.0003 ($10^{-6}$/Hz). This result implied that the emerging structures were hydrodynamically indistinguishable. It was hypothesized that the miRNA mimics were not extended, as schematically depicted in Figure 52, but rather adopted a shape closer to that of a compact coil, of a diameter increasing with the size of the polyT tail. This shape induced a negligible change on [$\eta$] that did not allow the conformation-based acoustic discrimination of the four miRNA targets.

By way of contrast, a clear distinction among the four miRNA mimics was observed when the target was placed at different positions along the Probe-86 backbone (Fig. 54). For instance, the hybridization of the T1+polyT20 at P1 was distinguished from T2+polyT30 when the latter was hybridized at P2 [(acoustic ratios: 0.0301 ± 0.0010 ($10^{-6}$/Hz) and 0.0412 ± 0.0010 ($10^{-6}$/Hz), respectively]. Similarly, the T3+polyT40 mimic placed at position 3 (P3) was distinguished from the T4+polyT50 one, when the latter was hybridized at P4 [acoustic ratios obtained were: 0.0395 ± 0.0023 ($10^{-6}$/Hz) and 0.0504 ± 0.0041 ($10^{-6}$/Hz)]. Even the placement of the same miRNA mimic at different hybridization positions of the probe resulted in versatile acoustic ratios that could be used to determine at which site of the probe the same target was hybridized each time (*e.g.* ΔD/ΔF: 0.0301 ± 0.0010 ($10^{-6}$/Hz) at P1 and ΔD/ΔF: 0.0429 ± 0.0031 ($10^{-6}$/Hz) at P4]. The distance of each polyT miRNA mimic with respect to the device surface was, apparently, the most crucial parameter in obtaining hybridized DNA products of different conformations. Furthermore, the exact location of the polyT tail appears to be crucial as well; miRNA targets with their polyT tails at position P2 and P3, *i.e.*, 28 and 42 nts away from the surface, could not be acoustically distinguished. This, according to the theory (*18*), suggests that the two constructs are very similar regarding their structure, to be hydrodynamically distinct.

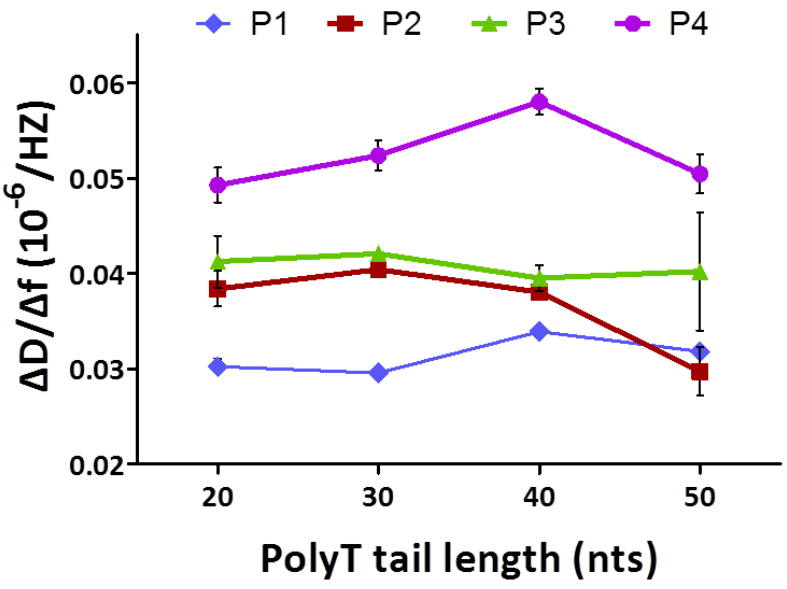


**Figure 54.** Acoustic ratios of hybridized miRNA targets to Probe-86, as a function of the polyT tail attached to each target, and the distance of the miRNA from the sensor surface.PolyT tail lengths of 20, 30 40 and 50 nts refer to: miR-121+polyT20, miR-155+polyT, miR-150+polyT and miR-107+polyT50 mimcs , respectively

## 3. Control assay

To study the effect of the probe sequence on the previous findings, we used an alternative probe, Probe-86b. Probe-86b had its polyC regions replaced by random nucleotide sequences. The rest experimental steps of the fabrication of the DNA-based sensor were the same as the ones described in the "Materials and methods" section, part 4. It was shown (Fig. 55) that the relative differences among the acoustic ratios of the hybridized targets were similar to the ones obtained with the original Probe-86, confirming that the sequence composition of the probe did not affect the measurements.

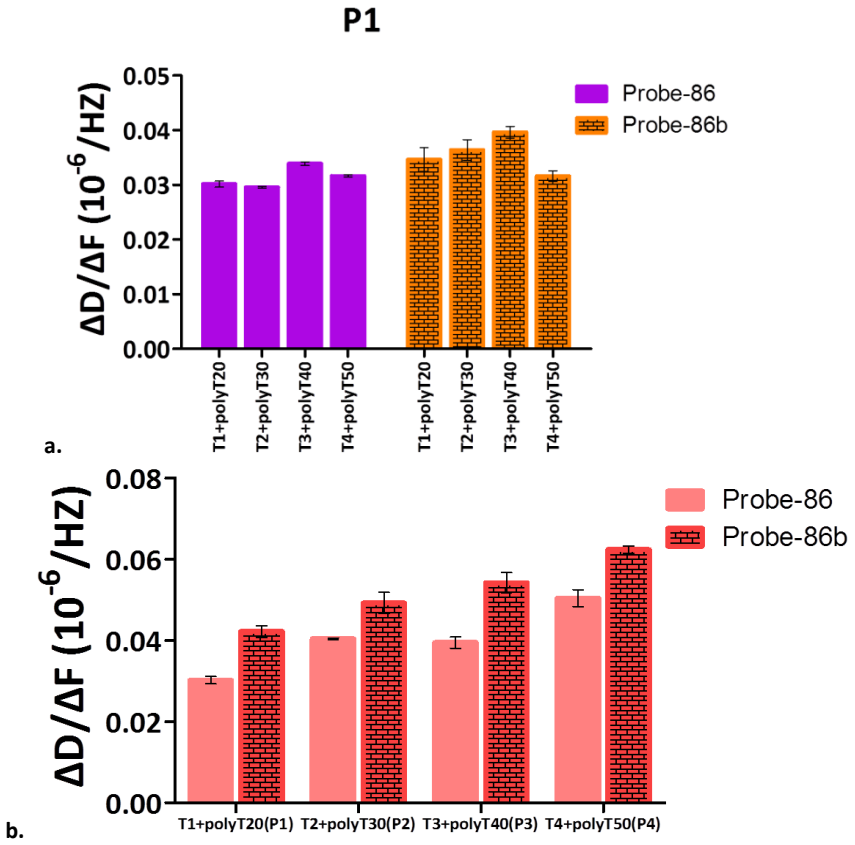


**Figure 55**. Bar charts presenting the acoustic ratios upon hybridization of **a.** T1+polyT20, T2+polyT30, T3+polyT 40 and T4+polyT 50 at position 1 (P1) of Probe-86 **(purple bars)** and Probe-86b **(shadowed orange bars)**; **b.** acoustic ratios obtained upon hybridization of T1+polyT20 at P1, T2+polyT30 at P2, T3+polyT 30 at P3 and T4+polyT 50

## 4. Simultaneous acoustic detection of two miRNA targets

Figure 54 showed that an optimum discrimination was observed when miRNA targets were hybridized at positions P1 and P4 of Probe-86. To test this, T1+polyT20 complementary to P1 and T4+polyT50 complementary to P4, were simultaneously added to the surface-immobilized Probe-86. To achieve this, T1+polyT20 and T4+polyT50 were mixed in a PBS solution at two different ratios (1:1 and 1:10) and the mixture was injected in the sensing system. It was expected that the acoustic ratio obtained upon simultaneous hybridization of the two would be in between the values of the acoustic ratios obtained upon hybridization of T1+polyT20 at P1 and T4+polyT50 at P4 separately, as a result of the relative number of each target on the

probe, as previously demonstrated during the simultaneous binding of dsDNAs of different lengths (*20*). Figure 56 provides the data acquired from this detection. Indeed, applying the two miRNA at two different ratios (1:1 and 1:10) gave an acoustic ratio lying between the ones obtained for each pure sample [0.0301 (±0.0010) ($10^{-6}$/Hz) for T1+polyT20 at P1; 0.0360 (±0.0024) ($10^{-6}$/Hz) for simultaneous T1+polyT20 at P1 and T4+polyT 50 at P4 at a 1:1 ratio; 0.0431 (±0.0017) ($10^{-6}$/Hz) for T1+polyT20 at P1 and T4+polyT 50 at P4 at a 1:10 ratio; 0.0504 (±0.0041) ($10^{-6}$/Hz) for T4+polyT 50 at P4]. In this way, the presence of the two miRNA mimics in the solution and their simultaneous hybridization to the Probe-86 was successfully detected with the QCM sensor.

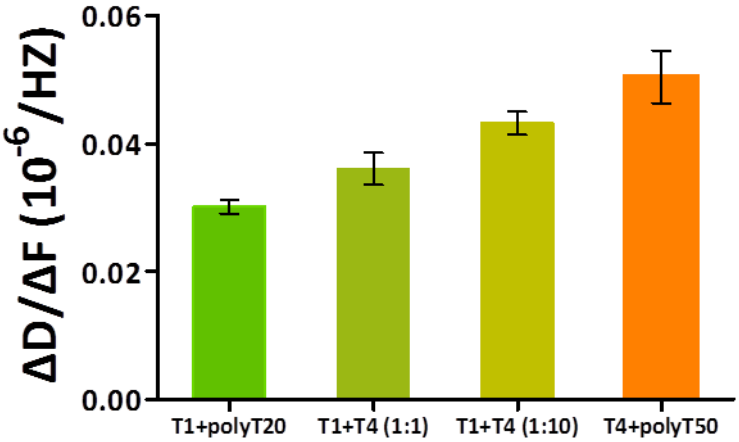


**Figure 56.** Acoustic ratios corresponding to the hybridization of target T1+polyT20 at P1, T4+polyT50 at P4 and a combination of the two hybridized simultaneously with the surface-immobilized Probe-86 at a mole ratio of 1:1 and 1:10

# *Conclusions*

The current assay achieved the detection and identification of different miRNAs implicated in breast cancer using a single probe. The underlying scientific principle is related to a new sensing mechanism which correlates the acoustic measurements and, more specifically the acoustic ratio measurements, with the conformation of surface-bound molecules.

Real-time acoustic detection of the simultaneous hybridization of two miRNAs (miR-21 and miR-107) with the same probe was also achieved. The developed sensor was easy to use and allowed the rapid, real-time, label-free and simple detection of two miRNAs at the same time. The current dual-miRNA marker diagnosis provides guidelines for the design of a probe that could detect more than 3 different miRNA targets at the same time. The ability of acoustic wave sensors to get integrated in diagnostic platforms suitable for on-site detection (*137, 145*) and their proven multi-analyte testing ability (*136*) indicate that the strategy developed here can be extended to other targets and layouts.

The sensor presented here has the potential to make use of the extreme stability of extracellular miRNAs (*168*) circulating in the blood of diseased people and form the basis for the development of an acoustic wave integrated platform that will offer a non-invasive (compared to tissue biopsies for instance) method for the multi-marker diagnosis (multiplexing ability) of miRNAs involved in cancer. Ideally, the detection will be carried out on-site, in real-time, inexpensively and non-laboriously. Circulating miRNAs implicated in other diseases, such as cardiovascular diseases (*200*), diabetes (*201*) and Alzheimer's disease (*202*) could also be detected by such a platform.

# Chapter 4
# Acoustic detection of KRAS mutations in colorectal cancer using blood liquid biopsy

# Introduction

Colorectal cancer (CRC) represents a major cause of morbidity and mortality both in men and women in developed countries (*203, 204*). CRC is the third most common cancer globally. Over 50% of all the CRC patients will die within five years from diagnosis, due to the development of metastatic disease (*204*). According to the WHO, the cancer burden can be reduced through early detection of cancer and management of patients who develop the disease. Many cancers, including CRC, have high cure rates when detected early and treated adequately (*205*).

## Liquid biopsy using circulating tumor DNA (ctDNA) in blood

Currently, tissue biopsies are the gold standard of cancer diagnosis (*206, 207*). In tissue biopsies a small sample of tissue is taken from the suspected tumor and histologically examined. This procedure can provide important information about the patient disease; however, direct tissue biopsies are limited in utility by a range of factors including: **a)** difficulty in obtaining abundant amounts of tissue, **b)** limited repeatability, **c)** biases due to the fact that tissue biopsies reflect a single point in time of a single site of the tumor, **d)** patients' comorbidities and lack of patients' compliance. Although surgical biopsies typically provide the greatest amount of intact tumor tissue for analysis, the procedure is invasive, costly and time-consuming. Clinical complications should not be ignored either, with one study reporting on a 17.1% rate of complications for intrathoracic biopsies and 1.6% for abdominal/pelvic biopsies, plus an overall major complication rate of 0.8% (*208*). Moreover, most tumor tissue samples are preserved in formalin-fixed paraffin embedded (FFPE) blocks, which cross-link DNA and make it inadequate for molecular analysis by routine techniques such as PCR (*206, 207*).

Liquid biopsy has gained plenty of attraction in the last few years and the method has been listed as a top ten technology breakthrough in 2015 by the MIT Technology Review (*209*). A liquid biopsy is a minimally invasive method that monitors tumor development and progression, as well as response to treatment. The method detects either circulating tumor DNA (ctDNA) or intact circulating tumor cells (CTCs) in blood (and other body fluids such as saliva and urine). Tumor cells are thought to release ctDNA in the bloodstream by three mechanisms (Fig. 57): **a)** secretion, **b)** apoptosis and **c)** necrosis. The majority of ctDNA detectable in the blood however, is highly fragmented measuring between 180 and 200 base pairs (bp) which is indicative of apoptotic DNA, rendering apoptotic cells the most important source of ctDNA in the blood (*203, 207*). CTCs detection has already been approved by the FDA for prognosis and monitoring in CRC patients. However, ctDNA is sooner detectable than CTCs in the blood and has been found to harbor the genetic and epigenetic alterations, such as point mutations and methylation from CRC tumor cells (*210*). Hence, it could be used as a biomarker for the early detection of CRC (*203*).

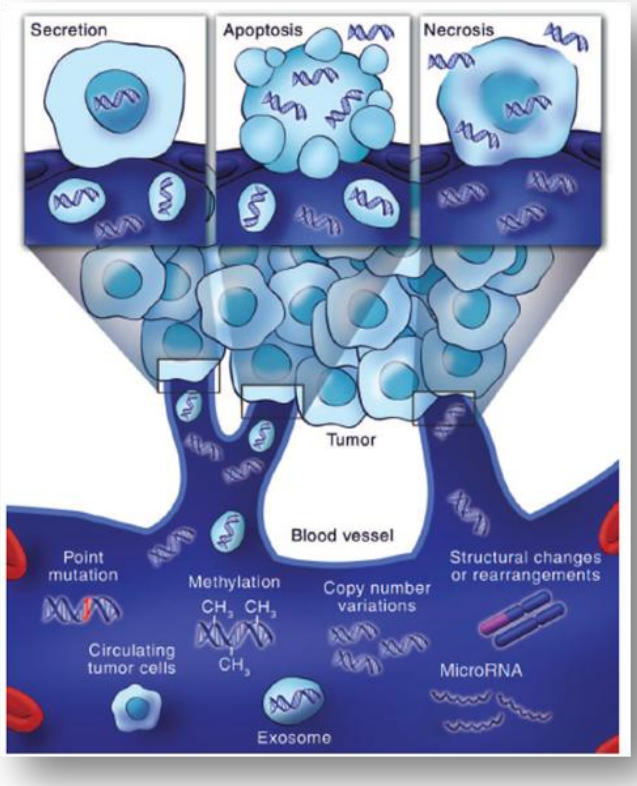


**Figure 57.** ctDNA is released in the bloodstream by tumor cells undergoing a**)** secretion, **b)** apoptosis or **c)** necrosis (*207*)

## *ctDNA detection methods*

Current methods for the detection of ctDNA involved in CRC can be classified in targeted and untargeted. Targeted methods (Fig. 58) analyze single nucleotide mutations or structural chromosomal rearrangements in specified genomic regions and estimate the allelic frequency of a particular mutation within a sample. Targeted methods include: **a)** quantitative and digital PCR, **b)** beads, emulsion, amplification, and magnetics (BEAMing), **c)** personalized analysis of rearranged ends (PARE), **d)** next generation sequencing (NGS), **e)** pyrosequencing **f)** Sanger sequencing **g)** tagged amplicon deep sequencing (Tam-Seq), and **h)** cancer personalized profiling by deep sequencing (CAPP-Seq). The untargeted methods aim at an inclusive analysis of the tumor genome; whole-genome sequencing and whole-exome sequencing belong to this class of ctDNA detection methods (*206, 207*). Although the above analytical methods exhibit suitable clinical sensitivity and specificity, they are laboratory-based, complex, too time-consuming and costly for actual application in a diagnostic setting remote from a central laboratory (*206, 207, 210, 211*). Furthermore, all NGS-based methods depending on amplification of sensitivity are limited by the error rate of DNA polymerases (0.01%).

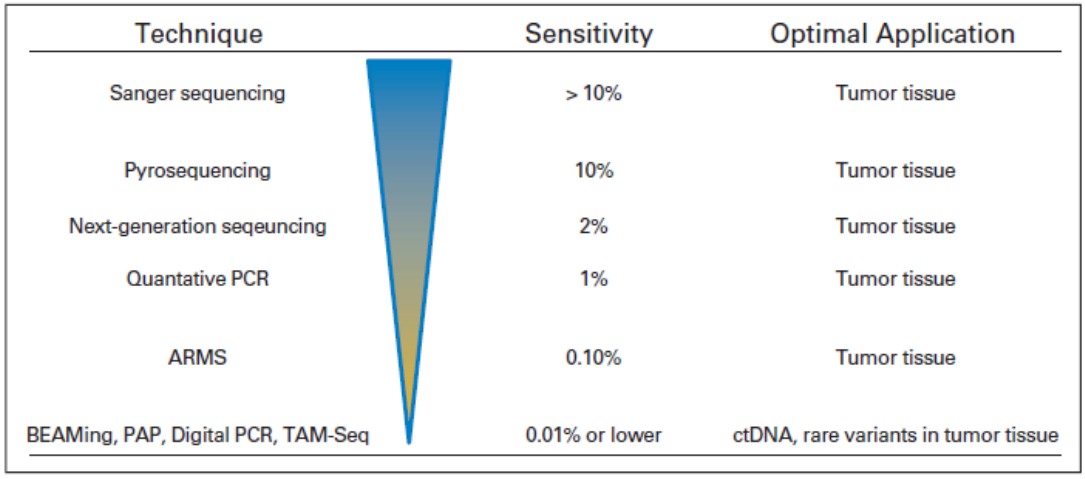


**Figure 58.** An overview of the current techniques applied in targeted ctDNA detection (*207*)

For all these, reasons, the development of a reliable, robust, cost-effective platform for the early, rapid, non-invasive, sensitive and specific detection of CRC ctDNA is necessary. The last chapter of the current PhD thesis discusses the research work that was focused on the development of a bioassay for the acoustic detection of CRC-characteristic KRAS mutations in ctDNA sampled from the blood (liquid biopsy). The ultimate goal is the integration of the bioassay in a diagnostic platform which will be applied in the early detection of colorectal cancer.

## *Acoustic detection of ctDNA harboring KRAS mutations associated to CRC through blood samples using the DGL© technology and high fundamental frequency (HFF) QCM sensors*

The work described here was carried out as part of the project "Reliable novel liquid biopsy technology for early detection of colorectal cancer –Liqbiopsens" (H2020-ICT-2015-GA687785). The project aims at the development and validation, in real settings, of a novel diagnostic platform for the early and fast detection of ctDNA and their KRAS mutations associated to colorectal cancer through blood samples. The current PhD work dealt with the development of a bioassay where ctDNA carrying KRAS mutations that are characteristic for CRC would be acoustically detected through their hybridization to an appropriate probe immobilized on an acoustic sensor surface.

In CRC, 30-40% of patients carry a KRAS hotspot mutation as determined from 34,958 cases in the Sanger Cosmic Database (*204, 210*). The KRAS mutations in CRC are thought to occur early, and have been linked to poorer survival and increased tumor angiogenesis. In addition, KRAS mutations in CRC result in the resistance to selected treatments (*204, 212*). KRAS is located at 12p12.1 and encodes a 188 amino acids small protein with a molecular weight of 21.6 kDa (*204*). Normally, KRAS, as a member of the Ras/Raf/MAPK signaling pathway, transduces signals from the extracellular environment to the cell nucleus where specific genes are activated for cell growth, division and differentiation (*204, 213*). Activation of the pathway (Fig.

59) begins with the binding of a signal to the protein tyrosine kinase receptor called epidermic growth factor receptor (EGFR). The binding induces the oligomerization of the receptor and the activation of its kinase activity that eventually results in the recruitment of guanine nucleotide exchange factors (GEFs) to the cell membrane. The GEFs interact with the Ras protein at the cell membrane promoting a conformational change and the transition from its inactive GDP-bound state to the active GTP-bound state. Sequentially, Raf is recruited to the cell membrane through its binding to Ras and also by lipid binding. Raf activation stimulates a signaling cascade by phosphorylation of MAPK which, in turn, phosphorylates and activates downstream proteins such as ERK1 and ERK2. MAPK appears to induce apoptosis by dysregulation of a range of pathways including ERK, JNK and p38. Mutations in KRAS result in the altered activation of Ras which develops resistance to the GTPase activity and remains in an active GTP-bound state, which has a higher tendency to activate downstream effectors, conferring a proliferative advantage to tumors. Overall, the altered activation of Ras results in inappropriate cellular activities, including cell growth, differentiation and survival, and, ultimately, cancer (*204, 213, 214*).

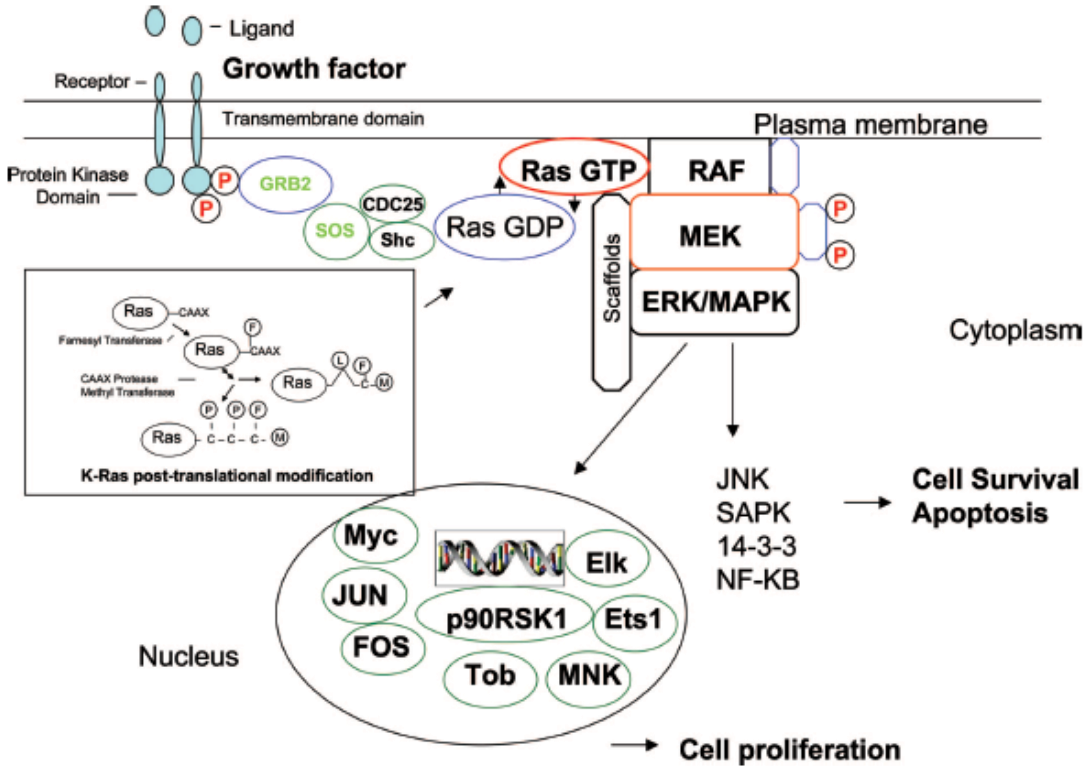


**Figure 59.** The Ras/Raf/MAPK pathway. Reporduced by (*213*)

KRAS gene mutations are mainly present in codons 12 and 13 of exon 1. 80% of them are present in codon 12, and 15% in codon 13. Other mutations in codons 61, 146 and 154 appear rarely, representing a 5% of all the mutations. The most frequent mutations in codon 12 are: **the G12V**: where in the KRAS gene, at position

35, a Guanine (G) nucleotide is replaced by a Thymine (T) one, and in the equivalent protein a glycine (G) is substituted by a valine (V); **the G12D**: where in the KRAS gene, at position 35, a G is replaced by an Adenine (A) nucleotide, and in the corresponding protein, a glycine (G) is substituted by an aspartic acid (D). The most frequent mutation in codon 13 is the **G13D** wherein, the mutation of a guanine (G) to an Adenine (A) at position 38, leads to the substitution of a glycine (G) by an aspartic acid (D) (*204*). ctDNA carrying these mutations has been identified in the blood of CRC patients. This certain type of ctDNA is currently detected with routine detection methods described above, with all their advantages and limitations. The present work, for the first time, set to detect and identify ctDNA with its KRAS mutations implicated in CRC employing an acoustic wave device. The steps followed in order to achieve this, together with the novelties that this work introduced are explained below.

The Liqbiopsens operating concept includes the following steps: **1)** the sampling of purified cell-free DNA (cfDNA) from 2-5 mL of blood plasma aliquots using commercially available DNA extraction kits. This cfDNA contains the ctDNA with the KRAS mutations. However, ctDNA represents only a small fraction (<1%) of the total cfDNA and sometimes this fraction drops to <0.01% (*215, 216*). For instance, in 5 mL of plasma there exist approximately 2-2000 copies of mutated ctDNA among 2000-12000 cfDNA fragments. For this reason, the DNA samples are to be subjected to DNA amplification techniques in order to enrich the mutated targets of interest. The present study tested two amplification methods the PCR and the isothermal RPA for their efficiency in adequately amplifying the DNA fragments of interest; **2)** then, the amplified fragments are to be subjected to a denaturation step at 95 $^{o}$C to produce two single strands. The single strands produced are to be transferred to an acoustic wave sensor device, on which they will be hybridized to their corresponding probe. The current work focused on the optimization of the immobilization process of the probes targeting the mutant ssDNAs. In addition, it used the DGL© technology developed by DestiNA Genomics Ltd (Edinburgh, UK) (Fig. 60). DGL© technology takes advantage of dynamic chemistry for nucleic acid sequence specific recognition using aldehyde-modified natural nucleobases (SMART nucleobases) and probes based on peptide nucleic acid (PNA) containing an abasic “blank” position (DGL probes) opposite the mutation of interest. PNAs are DNA mimics in which the sugar-phosphate backbone is replaced with N-(2-aminoethyl) glycine backbone (*217*). PNAs exhibit excellent thermal stability, stronger binding ability in high ionic strength, greater interaction specificity and resistance to nucleases and proteases (*218*). The reversible reaction between an aldehyde-modified SMART nucleobase and a free secondary amine on the PNA DGL probe generates an iminium intermediate that can be reduced to a tertiary amine by a reducing agent (chemical lock-up). Different iminium species (in particular four, one for each nucleobase) can be generated, but the one with the correct hydrogen bonding motif (according to the Watson-Crick base-pairing) will be the most thermodynamically stable product (*217*). Complementary nucleic acid strands also act as catalysts to accelerate the rate of reductive amination; in the absence of complementary nucleic acids, reductive aminations do not occur within the hybridization assay time-frame (*219*). DGL© technology ensures in this way that mutant targets detection is only sensed when the target nucleic acid binds in perfect alignment to the DGL probe, when the correct

SMART nucleobase seats into the “blank pocket” formed by the duplex, and when the SMART nucleobase is “locked in” chemically. A major characteristic of the DGL© technology is that false positives are difficult, if not impossible to create, as SMART nucleobase incorporation occurs only when the target templating nucleic acid strands are present (*220*). So far, DGL© technology has been used in combination with mass spectrometry (*219*), DNA microarrays (*220*), bead-based methods (*221*) and matrix-assisted laser desorption/ionization – time of flight mass spectrometry (MALDI-ToF) (*222*) and its genotyping ability has been proven; **3)** the mutant targets are to be acoustically detected. To accomplish this, the SMART nucleobases tested in this work were modified with either biotin or cholesterol molecules, and acoustic detection of the perfectly hybridized mutant ssDNA targets was carried out through either the addition of streptavidin oor liposomes and through the recording of the acoustic signal response upon addition of the latter. According to our knowledge the current study reports, for the first time, on the combination of the DGL© technology with an acoustic wave sensor device. What is more, in the present work, a high fundamental frequency (HFF) QCM sensor device was employed. (*223*) were the first to develop a HFF-QCM biosensor (fundamental frequency of 39-110 MHz) for phage detection in liquids, but very few research groups have reported on working with HFF resonators since. The HFF QCM sensors employed here, were developed by the AWSensors S.L. (Valencia, Spain) and based on a patented characterization method of acoustic sensors at high frequency, with a low noise level, which allows for higher sensitivity and lower limit of detection (LOD). These HFF-QCM sensors (fundamental frequency of 100 MHz) have been applied in the detection of carbaryl and thiabendazole pesticides exhibiting an improvement of about one order of magnitude for sensitivity and two orders of magnitude for the LOD when compared to a conventional 9 MHz QCM sensor. The analytical performance achieved was superior to the ones previously reported for conventional QCM and SPR under the same experimental conditions, and approached the most sensitive ELISA assays (*224, 225*).

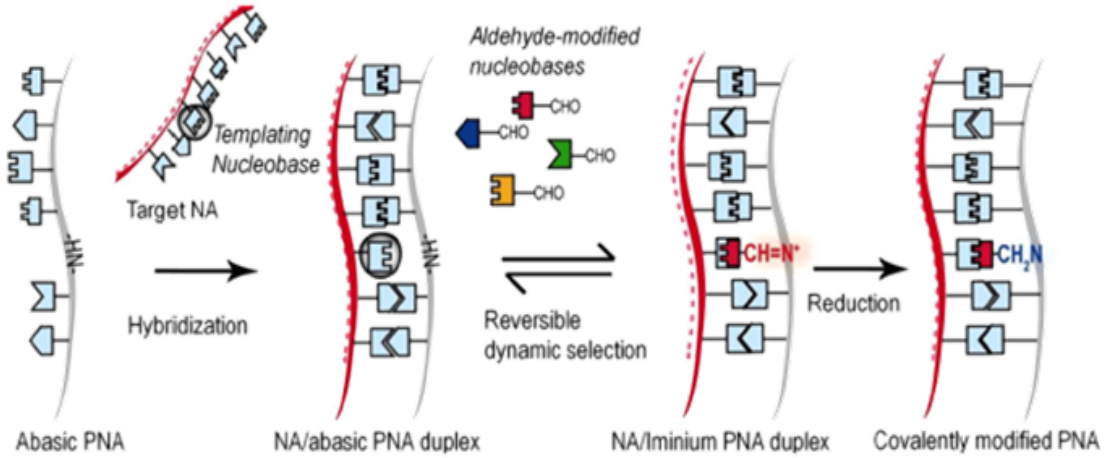


**Figure 60.** Schematic representation of the DGL© technology (*219*)

# *Materials and methods*

## 1. Chemicals

| |
|---|
| **PNA probes**: Destina Genomics Genomics Ltd, Edinburgh, UK |
| **SMART nucleobases:** Destina Genomics Genomics Ltd, Edinburgh, UK |
| **Synthetic KRAS gene:** Metabion International AG, Germany |
| **Short synthetic oligonucleotides mimicking KRAS mutant ssDNAs:** Microchemistry Laboratoty, FORTH, Greece |
| **5mer-SH, 2mer thiol TT, 2mer-thiol AA:** Metabion International AG, Germany |
| **RPA and PCR primers:** Metabion International AG, Germany |
| **RPA kit: RPA TwistAmp® Basic:** TwistDx Ltd., Babraham, Cambridge, U.K. |
| **2X KAPA HiFi HotStart ReadyMix:** Kapa Biosystems, Mass. USA |
| **HpyCH4IV restriction enzyme:** New England BioLabs Inc., Mass., USA |
| **10X CutSmart® Buffer:** New England BioLabs Inc., Mass., USA |
| **Nucleospin® Gel and PCR Clean-up kit:** Macherey-Nagel, Düren, Germany |
| **Avidin, NeutrAvidin®Biotin:** ThermoFisher Scientific, Mass., USA |
| **Streptavidin protein:** ThermoFisher Scientific, Mass., USA |
| **Biotin ≥99% (TLC), lyophilized powder:** Merck KGaA, Darmstadt, Germany (Former Sigma-Aldrich) |
| **Phosphate buffer saline (PBS) tablet:** Merck KGaA, Darmstadt, Germany (Former Sigma-Aldrich) |
| **2X saline-sodium citrate (SSC) buffer contained 0.3M NaCl and 30 mM trisodium citrate ($Na_3C_6H_5O_7$):** Merck KGaA, Darmstadt, Germany (Former Sigma-Aldrich) |
| **Ethanol absolute (EtOH), synthesis grade:** Scharlab S.L., Barcelona, Spain |
| **Milli-Q water (18 MΩ):** Barnstead Nanopure Ultrapure Water Systems (ThermoFisher Scientific, Mass., USA) |

## 2. Sequences of the oligonucleotide probes, targets and primers

| |
|---|
| **G12D: 5'-** TTAGCTGTATCGTCAAGGCACTCTTGCCTACGCCA**T**CAGCTCCAACTACCACAAGTTTATATTCAGTCATTTTCAGCAGGCCTTA- **3'** |
| **G13D: 5'-** TTAGCTGTATCGTCAAGGCACTCTTGCCTACG**T**CACCAGCTCCAACTACCACAAGTTTATATTCAGTCATTTTCAGCAGGCCTTA- **3'** |
| **RCDestinaWT2: 5'-** TAAGGCCTGCTGAAAATGACTGAATATAAACTTGTGGTAGTTGGAGCTGGTGGCGTAGGCAAGAGTGCCTTGACGATACAGCTAA- **3'** |
| **Set1fw (forward primer): 5'-** TTAGCTGTATCGTCAAGGCACTCTTGCCTA- **3'** |
| **Set1rv (reverse primer): 5'-** TAAGGCCTGGTGAAAATGACTGAATATAAA- **3'** |
| **Set2fw (forward primer): 5'-** TTAGCTGTATCGTCAAGGCACTCTTGCCTA- **3'** |
| **Set2rv (reverse primer): 5'-** ATGACTGAATATAAACTTGTGGTAGTTGGA- **3'** |
| **DGL probe K12DAV 3RCC_SH (C-N sequence):** Hac Cys x x AACCTCGgluAC*GL*AgluCCGCAT-$NH_2$-Thiol |
| **DGL probe K13DAV 3RCC_SH (C-N sequence):** Hac Cys x xTCGACCgluAC*GL*GgluCATCCGTT-$NH_2$-Thiol |
| **DGL probe K12_2.2 (C-N sequence):** Hac Cys x x GATGCGgluGT*GL*GgluTCGAGGTT-$NH_2$-Thiol |
| **DGL probe K12_2.4 (C-N sequence):** Hac Cys x x GATGCGgluGT*GL*GgluTCGAGGTT-$NH_2$-biotin |
| **PNA HybC-DGL K12DAV (PNA chimera complex) (C-N sequence):** CTCACAATCGACACTC-M-S-x x CTACGCCA*CAGCTCCAA |

| |
|---|
| **DNA Capture C biotin: 5'** – GAGTGTTAGCTGTGAG- **3'** |
| **5mer-SH: 5'**- Thiol-C6-TTT-TT- **3'** |
| **2mer-thiol TT: 5'**- Thiol-C6-TT- **3'** |
| **2mer-thiol AA: 5'**- Thiol-C6-AA- **3'** |
| **ssDNA KWT: 5'**- TTGGAGCTGGTGGCGTAGGCAA- **3' (KRAS wild type)** |
| **ssDNA K12V: 5'**- TTGGAGCTG**T**TGGCGTAG- **3' (KRAS G12V mutation)** |
| **ssDNA K13V: 5'-** AGCTGGTG**T**CGTAGGCAA- **3' (KRAS G13V mutation)** |
| **ssDNA DGL K12_2.2 WT: 5'**- TTGCCTACGCCACCAGCTCCAA- **3' (KRAS wild type)** |
| **ssDNA DGL K12_2.2 MUT: 5'**-TTGCCTACGCCA**T**CAGCTCCAA- **3' (KRAS G12V mutation)** |

***GL* charged pocket: Aglu, Cglu, Tglu, Gglu are charged monomers**

## 3. Acoustic device

The AWS A20-F20 platform (AWSensors, Valencia, Spain) was employed. The platform included 4 measurement modules and built-in thermostatic system for temperature control of liquid samples. Each module included one syringe pump (Hamilton, Bonaduz, GR, Switzerland), one 6-5 distribution valve, one injection valve for sample injection and one solenoid pump for precise sampling. AWS-HFF-QCM AT-cut gold sensors (AWSensors, Valencia, Spain) of two distinct fundamental frequencies (100 and 150 MHz were used. Frequency and resistance responses were recorded. Prior to the experiments, the AWS-HFF QCM sensors were first rinsed with Milli-Q (18 MΩ) water and 70% EtOH and then either subjected to plasma cleaning for 3 min using a Harrick plasma cleaner PDC – 002 ("Hi" setting) (Harrick Plasma, NY, USA) in order to obtain a clean surface, or subjected to UV ozon cleaning, in a UV ozone cleaner E511 machine (Ossila, Sheffield, UK), for 10 min, rinsed with Milli-Q (18 MΩ) water and 70% EtOH, and again subjected to UV ozon cleaning for another 10 min. All measurements, unless otherwise stated, were taken at 25 $^{o}$C.

The QSense Analyzer (4-channel system) (Biolin Scientific, Sweden) was used in parallel for real-time, simultaneous measurements of frequency and dissipation changes. The QSense Analyzer is a well-established device which, in comparison to the newly developed AWS A20-F20 platform, increases the throughput. Au-coated 5 MHz AT-cut quartz crystals (QSensor Gold (Ag), Bioline Scientific, Sweden) were utilized. Frequency and dissipation responses were recorded at 35 MHz overtone. Prior to the experiments, the QSensors were first rinsed with Milli-Q (18 MΩ) water and 70% EtOH and then subjected to plasma cleaning for 3 min using a Harrick plasma cleaner PDC – 002 ("Hi" setting) (Harrick Plasma, NY, USA) in order to obtain a clean surface. All measurements, unless otherwise stated, were taken at 25 $^{o}$C. The QSense Analyzer was connected to an IPC Ismatec peristaltic pump (Ismatec, Wertheim, Germany).

## 4. Materials and equipment for liposomes preparation

1-palmitoyl-2-oleoyl-*sn*-glycero-3-phosphocholine (POPC) and Avanti Mini Extruder for large unilamellar vesicles (LUV) preparation were obtained from Avanti Polar Lipids, Inc. (Ala., USA). Polycarbonate (PC) membranes (19 mm in diameter) with a pore size of 0.03 µm were also purchased from Avanti Polar Lipids, Inc. (Ala., USA).

## 5. Liposomes preparation

Liposomes of 30 nm in diameter were prepared. 2 mg of POPC lipids were dissolved in chloroform [(Chloroform for analysis EMSURE® Acs, Iso, Reag. Ph Eur. (Merck

Millipore, Mass., USA)] in a round-bottom glass vial. The chloroform was homogeneously evaporated and the lipid film was left under nitrogen gas flow for ~60 min to ensure complete evaporation of the organic solvent. Next, the lipid film was rehydrated by the addition of 1 ml of 2X SSC (pH 6) buffer and vortexed for another 60 min. Finally, liposomes were extruded using the Avanti Mini Extruder and the appropriate PC membrane according to the desired diameter of the liposomes.

**6. PCR amplification of a synthetic KRAS gene mimic**

Two synthetic ssDNA oligonucleotides of 85 nts mimicking the KRAS gene target and carrying a mutation at two different positions (G13D) were purchased. Two sets of primers that could amplify G13D and generate DNA amplicons of distinct lengths (85 and 70 bp long) were also designed and purchased. Set 1 containing Set1fw and Set1rv primers produced an amplicon of 85 bp, and Set 2 including Set2fw and Set2rv primers could produce an amplicon of 70 bp. G13D was successfully amplified by PCR reaction using the KAPA HiFi HotStart polymerase ReadyMix. The reaction included: 1 ng of the G12D and G13D targets, 10 µM of each of the Set1 and Set2 primers, and 2X KAPA HiFi HotStart polymerase ReadyMix in a total reaction volume of 10 µL. The PCR protocol consisted of two temperatures: 92 $^{O}$C for 1 sec and 65 $^{O}$C for 2 sec, cycled for 30 times. The negative controls lacked the G12D and G13D targets. The total reaction protocol was approximately 18 min. The PCR results were verified by a 2% gel electrophoresis.

**7. RPA amplification of a synthetic KRAS gene mimic**

Two synthetic ssDNA oligonucleotides of 85 nts mimicking the KRAS gene target and carrying a mutation at two different positions (G12D and G13D) were purchased. Set 2 of primers including Set2fw and Set2rv primer was used to produce amplicons of 70 bp. Both targets were successfully amplified by RPA reaction. The reaction included: 1.6 ng of either the G12D or G13D targets, 10 µM of each of the Set2 primers, 29.5 µL RPA rehydration buffer and 16 µL Milli-Q (18 Ω) in a total volume of 47.5 µL. 2.5 µL of 280 mM MgAc were added in the reaction, mixed in a total volume of 50 µL and incubated at one single temperature of 37 $^{O}$C for 20 min. The produced amplicons were cleaned with the Nucleospin® Gel and PCR Clean-up kit and eluted in 15 µL Milli-Q. The restriction digestion HpyCH4IV enzyme was used to digest the RPA amplicons. The restriction digestion reaction contained: 7.5 µL of either of the RPA G12D and G13D amplicons, 0.5 µL of HpyCH4IV enzyme, 1 µL of 10X NEBuffer and 1 µL of Milli-Q, in a total volume of 10 µL according to the manufacturer's instructions. The reactions were incubated for 15 min at 37 $^{O}$C and the digested products were run on a 2% agarose gel for verification. A mixed population of G12D and G13D in a ratio of 1000 : 10 copies/µL was also RPA amplified. The reaction contained: 1 µL G12D corresponding to 1000 copies/ µL, 1 µL of G13D corresponding to 10 copies/ µL, 0.5 µL of 10 µM Set2fw primer, 10 µM of Set2rv primer, 29.5 µL of RPA rehydration buffer and 15 µL of Milli-Q in a total volume of 47.5 µL. 2.5 µL of 280 mM MgAc were added in the reaction, mixed in a total volume of 50 µL and incubated at one single temperature of 37 $^{O}$C for 20 min. The produced amplicons were cleaned with the Nucleospin® Gel and PCR Clean-up kit and eluted in 15 µL Milli-Q. The restriction digestion HpyCH4IV enzyme was used to digest the RPA amplicons. The restriction digestion reaction contained: 7.5 µL of the mixture of

G12D and G13D RPA amplicons, 0.5 μL of HpyCH4IV enzyme, 1 μL of 10X NEBuffer and 1 μL of Milli-Q, in a total volume of 10 μL according to the manufacturer's instructions. The reactions were incubated for 15 min at 37 $^{O}$C and the digested products were run on a 2% agarose gel for verification. The negative control reactions lacked either the G12D, or the G13D or the mixture of G12D and G13D targets.

**7. Immobilization of thiolated PNA probes on a 100 MHz AWS-HFF QCM sensor, DGL reaction performed with mutant KRAS targets and acoustic detection of the incorporation of SMART-C$_{cholesterol}$ modified nucleobase via the use of 30 nm liposomes**

Thiolated PNA probes were surface-immobilized through the formation of self-assembly monolayer (SAM). For this purpose a DGL probe K13DAV 3RCC_SH: 5mer-SH mixture was prepared at a ratio of 1 : 10 in PBS. The HFF-QCM sensors were placed in functionalization chambers used for performance of static experiments. 50 μL of the SAM mixture was pipetted over the sensor's surface and left to incubate overnight (O/N) at room temperature. The next morning, the sensor was washed with SSC 2X (pH 6) buffer and filled with the DGL reaction which included: 1 μM ssDNA KWT, 1 μM SMART-C$_{cholesterol}$, 1 mM $NaBH_3CN$, and 21 μL of 2X SSC (pH 6) buffer in a final volume of 30 μL. SMART-C$_{cholesterol}$ recognized the **G** nucleotide opposite the "blank" position of the PNA probe; hence hybridization between the probe and the ssDNA KWT is considered a match (positive reaction). The mismatch case was also tested and for this reason the ssDNA K13V bearing a **T** mutation opposite the "blank" position of the probe was added in the mismatch DGL reaction, where all the reagents were the same, except for the SSDNA KWT which was replaced by the ssDNA K13V. SMART-C$_{cholesterol}$ was not going to recognize the T mutation. These 30 μL were pipetted over the sensor's surface, the functionalization chambers were placed in an oven and left to incubate at 40 $^{O}$C for 1 hour. Then, the sensors were rinsed with 2X SSC (pH 6), dried under a mild nitrogen gas stream, removed from the functionalization chambers and placed in the measurement chambers. The measurement chambers were inserted in the A20-F20 platform and real-time measurements were performed. The flow rate was set to 15 μL/min, a continuous flow of SCC 2X was flushed throught the system and allowed to equilibrate prior to addition of liposomes. A 10% solution of POPC liposomes of a diameter of 30 nm diluted in 2X SSC (pH 6) was injected in the sensing system, and frequency and resistance responses were recorded in real-time.

**8. Immobilization of thiolated PNA probes on a 100 MHz AWS-HFF QCM sensor, DGL reaction performed with mutant KRAS targets and acoustic detection of the incorporation of SMART-C$_{biotin}$ modified nucleobase via the use of streptavidin**

The procedure described above was repeated in order to determine what the best ratio of the SAM mixture of K13DAV 3RCC_SH: 5mer-SH was. Different ratios of K13DAV 3RCC_SH : 5mer-SH were investigated, namely 1 : 1, 1 : 10, and 1 : 100. SAM was left to incubate O/N and the next morning the exact same procedure with the one described above was followed, where both DGL positive and control (without the mutant target) reactions were carried out on the sensor surface and

incorporation or not of the SMART-$C_{biotin}$ modified base was monitored through acoustic sensing of streptavidin (SAv) addition (20 μg/mL), diluted in 2X SSC (pH 6).

**9. Immobilization of thiolated PNA probes on a 100 MHz AWS-HFF QCM sensor, DGL reaction performed with the PCR produced G13D KRAS gene mimic and acoustic detection of the incorporation of the biotin modified SMART-A nucleobase via streptavidin**

K13DAV 3RCC_SH : 5mer-SH were mixed in PBS and at a ratio of 1 : 10. The mix was pipetted over the surface of a HFF-QCM sensor that was placed in a static functionalization chamber in a final volume of 50 μL. The SAM layer was left to self-assembly O/N at room temperature. The next morning, the sensor was washed with 2X SSC (pH 6) and filled with the DGL reaction which included: the 70bp PCR-amplified G13D KRAS ("Materials and methods", section 4, page 104) gene mimic with the T mutation. The PCR product was boiled at 95 $^{O}$C for 5 min and immediately placed on ice for a minimum of 5 min in order to heat-denature. The denatured PCR product was added in the DGL reaction in a variety of concentrations ranging from 8-32 ng. Additionally, the reaction contained 1μM of the SMART-$A_{biotin}$ modified nucleobase, 1 mM of the $NaBH_3CN$ reducing agent and 15 μL of 2X SSC (pH 6) in a total volume of 30 μL. The corresponding control DGL reaction consisted of all the regular DGL reaction reagents, but lacked the PCR-amplified G13D gene mimic which was replaced by Milli-Q water. Following the pipetting of the 30 μL of the DGL reaction over the HFF-QCM sensor's surface, the functionalization chambers were placed in an oven and incubated at 40 $^{O}$C for 1 hour. Sequentially, the sensor was washed with 2X SSC (pH 6), dried under a mild nitrogen gas stream, removed from the functionalization chamber, and placed in the measurement chamber. The latter, in turn, was mounted in the A20-F20 and the real time acoustic sensing of the addition of streptavidin (20 μg/mL) in 2X SSC (pH 6) buffer was performed by recording frequency and resistance changes. The flow rate was set to 15 μL/min.

**10. Immobilization of thiolated PNA probes on a 100 MHz AWS-HFF QCM sensor, DGL reaction with mutant KRAS targets and acoustic detection of the incorporation of the biotin modified SMART-A nucleobase via streptavidin**

K13DAV 3RCC_SH:5mer-SH were mixed in PBS and at a ratio of 1:10. The mix was pipetted over the surface of a HFF-QCM sensor that was placed in a static functionalization chamber in a final volume of 50 μL. The SAM layer was left to self-assembly O/N at room temperature. The next morning, the sensor was washed with 2X SSC (pH 6) and filled with the DGL reaction which included: either the short ssDNA KWT or the ssDNA K13V; 1μM of either the SMART-$A_{biotin}$ modified nucleobase or the SMART-$C_{biotin}$ modified nucleobase; 1 mM of the $NaBH_3CN$ reducing agent and 15 μL of 2X SSC (pH 6) in a total volume of 30 μL. Following the pipetting of the 30 μL of the DGL reaction over the HFF-QCM sensor's surface, the functionalization chambers were placed in an oven and incubated at 40 $^{O}$C for 1 hour. Sequentially, the sensor was washed with 2X SSC (pH 6), dried under a mild nitrogen gas stream, removed from the functionalization chamber, and placed in the measurement chamber. The latter, in turn, was mounted in the A20-F20 and the real time acoustic sensing of the addition of streptavidin (20 μg/mL) in 2X SSC (pH 6) buffer was performed by recording frequency and resistance changes. The flow rate was set to 15 μL/min.

## 11. Immobilization of thiolated PNA probes on a 150 MHz AWS-HFF QCM sensor, DGL reaction with short single-stranded mutant targets and acoustic detection of the incorporation of the biotin modified SMART-A nucleobase via streptavidin

A new batch of HFF-QCM sensors operating at a higher fundamental frequency of 150 MHz was tested. The DGL probe K12_2.2 which is the regular DGL probe with the "blank position", the thiol at the $NH_2$ terminal and a longer spacer at the $NH_2$ terminal in order to have a distance from the sensor surface when immobilized to it was constructed. The K12_2.2 probe was surface-immobilized through SAM in a PBS mix containing a 2mer thiolated intermediate oligonucleotide, the 2mer-thiol AA in a ratio of 1:20 (16 nM : 320 nM). Preparation of O/N SAM has been described above. The next morning the DGL reactions were prepared by adding the short ssDNA mutants as follows: 1 μM ssDNA ssDNA DGLK12_2.2 MUT, 1 μM SMART-$A_{biotin}$, 1 mM $NaBH_3CN$, and 21 μL of 2X SSC (pH 6) buffer in a final volume of 30 μL. SMART A recognizes the **T** mutation of the ssDNA DGLK12_2.2 MUT opposite the "blank" position of the DGL probe and gets incorporated. The mismatch reaction was prepared when instead of adding 1 μM of the DGLK12_2.2 MUT, 1 μM of the DGLK12_2.2 WT was added which opposite the abasic position of the probe has a **C** nucleotide that cannot get recognized by the SMART-$A_{biotin}$. The reactions were pipetted over the acoustic wave sensor surfaces and incubated for 1 hour at 40 $^{O}$C. Sequentially, the sensors were washed with PBS, dried under a mild nitrogen gas stream, removed from the functionalization chambers, and placed in the measurement chamber. The latter, in turn, were mounted in the A20-F20 and the real time acoustic sensing of the addition of streptavidin (20 μg/mL) in PBS was performed by recording frequency and resistance changes. The flow rate was set to 15 μL/min.

## 12. Real-time monitoring of the immobilization of thiolated PNA probes on a 5 MHz QSensor and of the hybridization of short single-stranded mutant and wild type targets

The QSense Analyzer was used for the real-time recording of the PNA probes surface immobilization and of the hybridization of their complementary targets. PNA probe DGL K12_2.2 was immobilized on the sensor surface under a variety of experimental conditions that included three different concentrations (16 nM, 160 nM and 0.5 μM); two different flow modes (stop flow and continuous flow at a rate of 3 μl/min); two different buffers (PBS and SSC 2X, pH 6) and two different temperatures (25 and 40 $^{o}$C). Direct hybridization of either the mutant or wild type target (DGL K12_2.2 MUT and DGL K12_2.2 WT respectively) at a concentration of 1 μM was then followed in real-time and under a number of conditions: two flow modes [stop flow and continuous flow (flow rate: 50 μl/min)]; two different buffers (PBS and SSC 2X, pH 6) and two different temperatures (25 and 40 $^{o}$C).

Another probe, the K12_2.3 DGL probe was also tested. This probe contained a thiol at both N- and C-terminal and a longer spacer. The idea was to follow the probe immobilization and the target hybridization in real-time through monitoring of the acoustic signal. The K12_2.3 probe was surface-immobilized in a mix with the 2mer-thiol AA in a 1 : 1 ratio (0.5 : 0.5 μM) in PBS, at 25 $^{o}$C and at a flow rate of 50 μl/min.

Hybridization of either the mutant (DGL K12_2.2 MUT) or the wild type (DGL K12_2.2 WT) target to the K12_2.3 probe was also followed in real-time. Both targets were flown over the sensor surface (after the latter had been treated with the DGL K12_2.3 : 2merAA-thiol mix) at a concentration of 5 μM, in PBS and at 25 $^{o}$C.

Hybridization of a non-complement oligonucleotide (LFChen) to the DGL K12_2.3 probe was also investigated in real-time.

**13. Acoustic detection of the DGL reaction completion (SMART-A*biotin* incorporation) using streptavidin and the QSense Analyzer**

The DGL K12_2.2 probe was surface-immobilized through SAM formation in a PBS mix containing the 2merAA-thiol intermediate, at a ratio of 1:20 (16 nM:320 nM). SAM formation was performed at stop flow for 90 min. The running buffer was SSC 2X, pH 6 and the temperature was set to 25 $^{o}$C. Following the probe immobilization, the surfaces were washed with SSC 2X, pH6, and DGL reactions containing either the mutant or the wild type target were added in the sensing system in a continuous flow of 50 μl/min. The DGL reactions contained: 1 μM of mutant target (K12_2.2MUT) or wild type target (K12_2.2WT), 10 μM SMART-A$_{biotin}$, and 1 mM $NaBH_3CN$ in 50 μl SSC 2X, pH6. SMART-A$_{biotin}$ is supposed to recognize the **T** mutation of the ssDNA DGLK12_2.2 MUT opposite the "blank" position of the DGL probe and get incorporated. The same is not expected to happen with the DGL reaction including the wild type target that bears a **C** nucleobase opposite the "blank" position of the DGL probe. Sequentially, the sensors were washed with SSC 2X, pH 6, the runnibg buffer was changed to PBS and real time acoustic sensing of the addition of streptavidin (20 μg/mL) in PBS was performed by recording frequency and dissipation changes. The flow rate for SAv addition was set to 50 μl/min.

**14. Real-time monitoring of the immobilization of biotinylated PNA probes on a 5 MHz QSensor and of the hybridization of short single-stranded mutant targets**

The experimental set-up described above was slightly modified, so that DGL probes with a biotin instead of a thiol at their N termini were immobilized on a QCM sensor treated with neutravidin. The biotinylated probes shared the same longer space and same sequence with the thiolated ones. A surface treated with neutravidin, on which a single-strande probe attaches, has been extensively studies by the Bisoensors Lab and more solid conclusions could be drawn from this set of experiements. Neutravidin (200 μg/mL) dissolved in PBS (pH 7.4) was physisorbed on the sensor surface. The biotinylated K12_2.4 probe was surface-immobilized through neutravidin-biotin interaction at a aconcentration of 15 μg/mL (or 2.5 pmol/μl), in PBS (pH 7.4). the hybridization of the mutant (DGL K12_2.2MUT) target to the K12_2.4 probe was also followed in real-time. The target was flown over the sensor surface at a concentration of 30 μg/mL, in PBS (pH 7.4). All the experimental steps Were carried out at 25 $^{o}$C and with a flow rate of 50 μl/min.

**15. Acoustic detection of the DGL reaction completion (SMART-A*biotin* incorporation) using the biotinylated DGL probes, streptavidin and the QSense Analyzer**

The flow rate was set to 50 μl/min. 200 μg/mL of neutravidin were adsorbed on the surface in PBS (pH 7.4) and at 25 $^{o}$C. 15 μg/mL of the biotinylated K12_2.4 probe

were immobilized under the same conditions. Then, the surface was treated with biotin (10 mM in PBS). Biotin was used as a blocking agent. Experiments in which the surface was not blocked with biotin after the probe immobilization were also conducted. The temperature was set to 40 $^{o}$C and the buffer was changed to SSC 2X, 0.1% SDS, pH6. DGL reactions containing either the mutant or the wild type target wer added in the sensing system. The DGL reactions contained: 1 µM of mutant target (K12_2.2MUT) or wild-type target (K12_2.2WT), 10 µM SMART-$A_{biotin}$, and 1 mM $NaBH_3CN$ in 50 µl SSC 2X, 0.1% SDS, pH6. The DGL reactions were carried out at a stop flow for 1 hour. Sequenctially, the flow was adjusted to 50 µl/min, the sensors were washed with SSC 2X, 0.1% SDS, pH6, the running buffer was changed to PBS, and the real time acoustic sensing of the addition of streptavidin (20 µg/mL in PBS pH 7.4) was performed by recording frequency and dissipation changes.

**16. Acoustic detection of the DGL reaction completion (SMART-$C_{biotin}$ incorporation) using the PNA chimera complex, streptavidin and the QSense Analyzer**

The flow rate was set to 50 µL/min. 200 µg/mL of neutravidin were adsorbed on the surface in PBS (pH 7.4) and at 25 $^{o}$C. 2.64 µg/mL of the biotinylated Capture Cbiotin DNA were immobilized under the same conditions. Then, the surface was treated with biotin (10 mM in PBS). Biotin was used as a blocking agent. At the same time DGL reactions were performed in PCR tubes, in a PCR thermocycler, at a final volume of 50 µl. The reactions were left to incubate for 1 h at 40 $^{O}$C. The reactions contained: 20 µM of the PNA Chimera complex; 5 µM of SMART-$C_{biotin}$; 1 mM of $NaBH_3CN$; 400 nM of either KWT or K12V synthetic single-stranded oligos and 37 µl of SSC 2X/0.1% SDS buffer. Alternatively, the reactions contained G13D- or RCDestinaWT2- PCR products of 70 bp produced by the PCR protocol described in Part 6. Concentrations of the PCR products in the DGL reactions varied from 0.5 to 45 ng. Upon completion of the DGL reactions in the cycler, they were diluted in PBS pH 7.4 at a final volume of 200 µl and flushed over the sensor surface at a flow rate of 20 µL/min. The acoustic sensing was carried out through the addition of streptavidin (20 µg/mL in PBS pH 7.4) (flow rate: 20 µL/min). Real-time monitoring of frequency and dissipation changes was performed.

# *Results*

The ultimate goal of the current bioassay is the detection of single-base mutations that happen on the KRAS gene and are associated with CRC. The biosassay intends to use ctDNA bearing such single-base mutations sampled from the blood of CRC patients (liquid biopsy) for the early and rapid CRC diagnosis. Two basic technologies were comnined for the first time: the DGL© technology and the use of HFF-QCM acoustic wave biosensors (both of them described above). For the proof-of-principle the research work reported herein, used synthetic ssDNA oligonucleotides that mimicked KRAS genes (their sequences and their single-base mutations). In order to test the efficiency and performance of both DGL PNA probes and aldehyde modified SMART nucleobases experiments were carried out with short synthetic ssDNAs that were perfectly matching or mismatching by a single base the DGL probes.

The general working principle of the process used here, for the acoustic detection of single-base mutations mimicking KRAS mutations implicated in CRC, is illustrated in Figure 61. a. The surface-immobilized DGL probe (in purple) bears a "blank" position that recognizes the KRAS mutated nucleotide. When the mutant target (in red) is added in the DGL reaction and allowed to incubate, hybridizes perfectly with the probe. This perfect match leads to the formation of a "pocket" in which the SMART nucelobase (in light blue) that specifically recognizes the KRAS mutation seats. The incorporation of the SMART nucleobase in the "pocket" is acoustically sensed through the sensing of either SAv or liposomes, whose addition in the sensing system causes the acoustic signal properties to change. When the target included in the DGL reaction bears a single mismatch in relation to the DGL probe, the SMART nucleobase is not locked in the pocket and addition of either SAv or liposomes causes no change in the properties of the acoustic signal (Fig. 61. b).

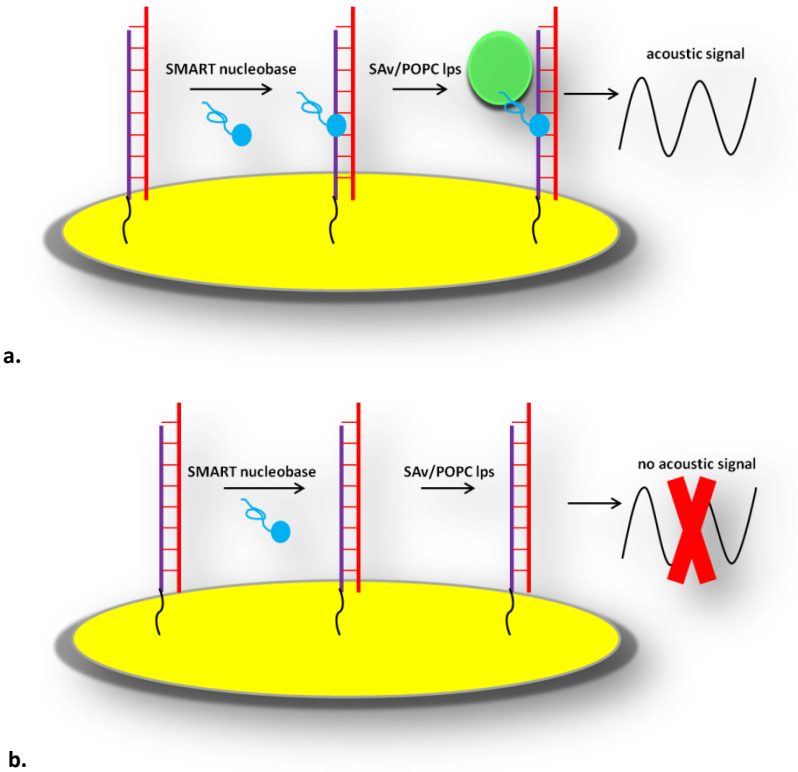


**Figure 61.** Schematic representation of the working principle of the bioassay (not drawn to scale)

## 1. PCR and RPA amplification of a synthetic KRAS gene mimic

The current bioassay aims to analyze ctDNA with its KRAS mutations taken form the blood of CRC patients. However, as previously discussed, the amount of ctDNA in the bloodstream is very low (<1% of the total cfDNA) and hence, ctDNA will need to be amplified. PCR and isothermal RPA amplifications were tested here. A synthetic oligonucleotide mimicking a KRAS gene with a **T** mutation was successfully amplified using PCR by two sets of primers, one producing an amplicon of 85 bp and the other producing an amplicon of 70 bp. The whole protocol lasted 18 min and PCR products were visualized with a 2% agarose gel (Fig. 62). Control PCR reactions were missing the G13D template.

RPA reaction was also proven to amplify the G13D target. Moreover, RPA was applied in the amplification of G13D that coexisted with a not mutated synthetic oligonucelotide, the G12D. The ratio of G12D over G13D was 1000:10 copies/μL. Set2 of primers producing 70 bp RPA amplicons were applied. Given the fact that the two synthetic oligoucleotides were different in one base only, it was expected that both of them would get amplified. To discriminate between the two amplicons, the restriction digestion HpyCH4IV was used. The enzyme recognizing the sequence depicted in Figure 63 was expected to digest only the G13D RPA amplicon and not the G12D. Indeed, 2% agarose gel electrophoresis (Fig. 64) verified the digestion of the G13D RPA product. Overall, it was shown that the amplification of a synthetic KRAS gene was successful with two techniques, the PCR and the RPA. The RPA in particular achieved the detection of the KRAS mimic in a mixed population. 10 copies of the G13D were amplified in a single-step process, at 37 $^{O}$C and within 20 min. These results are encouraging for the direct amplification of ctDNAs in crude samples.

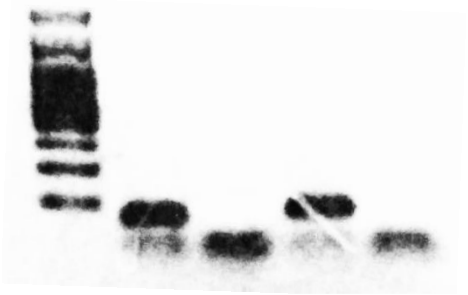

**Figure 62.** Visualization of a 2% gel electrophoresis. G13D PCR amplification is depicted. Lane 1: 100 bp DNA ladder; lane 2: Set2 primers amplified G13D producing a 70 bp product; lane 3: negative control of the Set2 primers; lane 4: Set1 primers amplified G13D producinh a 85 bp product; lane 5: negative control of the Set1 primers

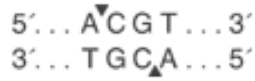


**Figure 63.** T he sequence recognized by the HpyCH4IV enzyme

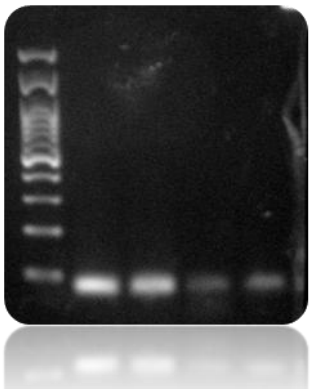

**Figure 64.** 2% agarose gel visualization. G13D was amplifief by PCR while in a mixed population of G12D:G13D in a ratio of 1000:10 copies/μL. Lane 1: 100 bp DNA ladder; lane 2 : RPA amplification of 10 copies/μL of G13D; lane 3: RPA amplification of 1000 copies/μL of G12D; lane 4: RPA amplification of a mixed population of G12D:G13D in a ratio of 1000:10 copies/μL. The RPA product was subsequently digested by the HpyCH4IV; lane 5: negative control where the RPA reaction had no target. Negative control was also digested

## 2. Immobilization of thiolated PNA probes on a 100 MHz AWS-HFF QCM sensor, DGL reaction performed for the hybridization of mutant KRAS targets and incorporation of SMART-C cholesterol modified nucleobase and acoustic detection with 30 nm liposomes

The thiolated DGL probe K13DAV 3RCC_SH was tested for its efficiency to capture a short ssDNA carrying a **G** opposite the probe's "blank" position. The perfectly matched ssDNA was the short synthetic 22 nts KWT. Its G base would be recognized by the cholesterol modified SMART-C nucleobase that would seat in the pocket. And the lock in of the SMART base would be sensed through addition of liposomes of 30 nm that would be captured by the cholesterol modified **SMART-C**. On the contrary, the single-base mismatch K13V synthetic oligonucleotide with its **T** base opposite the "blank" position of the probe would not cause the incorporation of the SMART-C nucleobase in the hybridized duplex, and the subsequenct acoustic detection of the liposomes addition.

The thiolated probe was surface-immobilized via self-assembled monolayers (SAM). Nevertheless, the SAM used here, did not resemble the conventional ones which make use of the alkanethiols' spontaneous assembly on noble metals (*226-228*). Mainly because of the small length of the DGL probe (18 nts), it was decided that the SAM would be performed by mixing the K13DAV 3RCC_SH with a short thiolated 5 nts oligoucleotide in a ratio of 1:10 in order to create some space between the surface-immobilized probes. The SAM was incubated to allow the thiolated oligonucleotides to form a well-organized layer on the gold sensor surface. After this step, the DGL reaction and acoustic sensing of liposomes addition in the sensing system were carried out as described in section 6 of "Materials and methods".

Figure 65 summarizes the frequency and resistance responses upon addition of 30 nm liposomes in the sensing system. It is obvious that the perfect match case (**G base)** could not be distinguished from the single mismatch (**T base)**, most probably due to liposomes' non-specific binding on the surface.

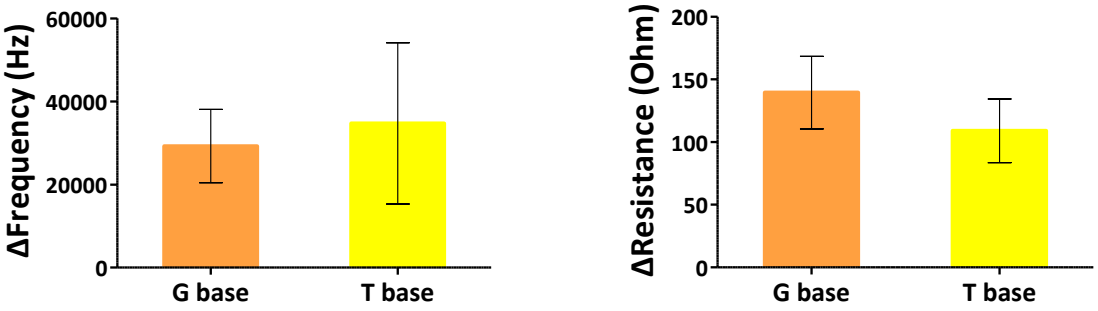


**Figure 65.** Bar graphs summarizing frequency and resistance responses upon addition of liposomes (30 nm) in the sensing system. Prior to this addition, DGL probe was surface-immobilized through SAM formation, and the DGL reaction containing either the perfectly matching target (G base) or the single-base mismatch target (T base) was incubated on the HFF-QCM sensor coated with the DGL probe. Perfect match could not be distinguished from single mismatch using liposomes

### 3. Immobilization of thiolated PNA probes on a 100 MHz AWS-HFF QCM sensor, DGL reaction performed for the hybridization of mutant KRAS targets and incorporation of SMART-C $_{biotin}$ modified nucleobase and acoustic detection with streptavidin protein

In order to avoid liposomes' non-specific binding, the incorporation of the SMART-C biotin-modofied nucelobase in the "pocket" created by the perfectly aligned hybridization between the K13DAV 3RCC_SH and the ssDNA KWT was sensed through the acoustic detection of SAv. SAv was captured by the biotin-modified SMART nucelobase thanks to the affinity of SAv for biotin, which is the strongest non-covalent biological interaction known.

SAv was also employed thanks to its smaller diameter (~ 6 nm) compared to the liposomes diameter (30 nm). The SAM mixture of K13DAV 3RCC_SH: 5mer-SH in a 1:10 ratio was calculated to create a distance of ~ 10 nm between the PNA probes (the diameter of an ssDNA is approximately 1 nm). SAv had better chances to enter in between the DGL probes compared to liposomes. In order to aid further the results obtained by SAv addition, different SAM ratios were prepared and allowed to cover the gold HFF-QCM surface; K13DAV 3RCC_SH: 5mer-SH in a 1:1 ratio and K13DAV 3RCC_SH: 5mer-SH in a 1:100 ratio were also tried. DGL reactions with perfect match target (positive reactions) and without any target that would hybridize to the DGL probe (control reactions) were performed and SAv was added. Table 2 summarizes the results obtained with this experimental set-up. It was concluded that the K13DAV 3RCC_SH: 5mer-SH of 1:10 ratio provided the best results, allowing for a safe discrimination between positive and control DGL reactions.

| DGL probe: 5mer-SH ratio 1:1 | | DGL probe: 5mer-SH ratio 1:10 | | DGL probe: 5mer-SH ratio 1:100 | |
|---|---|---|---|---|---|
| **Positive** | **Control** | **Positive** | **Control** | **Positive** | **Control** |
| < 1 KHz | < 1 KHz | 11-35 KHz | 1-6 KHz | 4-20 KHz | 0 KHz |

**Table 2.** Summary of the results provided when DGL probe was surface-immobilized in distinct SAM mixture ratios. The 1:10 ratio allowed the safest discrimination between positive and control DGL reactions performed on the HFF-QCM surface

## 4. Immobilization of thiolated PNA probes on a 100 MHz AWS-HFF QCM sensor, DGL reaction performed for the hybridization of the PCR produced G13D KRAS gene mimic and incorporation of the biotin modified SMART-A nucleobase, and acoustic detection with streptavidin protein

Based on the results presented in section 3, the thiolated DGL K13DAV 3RCC_SH probe was surface-immobilized through SAM formation in a SAM mix containing also the short 5mer-SH in a ratio of 1 : 10. The probe and the biotin-modified SMART-A nucleobase were tested for their ability to detect a single-base mutation present on a PCR-amplified synthetic oligonucleotide. The 70 bp G13D KRAS gene mimic carried a **T** mutant base opposite the abasic position of the probe. The hybridization between the G13D and the probe caused the **SMART-A** base to get incorporated in the pocket created by the duplex. SAv, captured by the biotin labeled SMART nucleobase, caused a change in the frequency which was monitored in real-time. The G13D was added in the DGL reaction at distinct concentrations ranging from 8-32 ng. As can be seen in Figure 66 the highest frequency change (9900 Hz) was obtained when 8 ng of PCR-amplified G13D was included in the reaction. Raising the G13D amplicon's concentration to 32 ng resulted in a smaller frequency change (4600 Hz), probably due to saturation of the surface. The frequency change caused by a control DGL reaction (no G13D amplicon included) was negligible (1 KHz). The most important observation is that different concentrations of G13D amplified by PCR carrying a single KRAS mutation could be acoustically detected, identified and distinguished from each other.

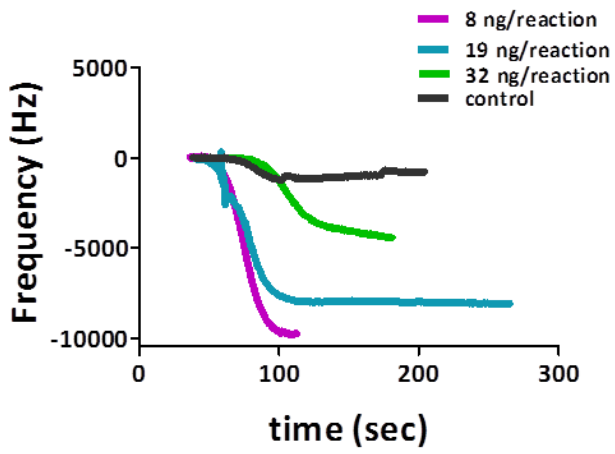


a.

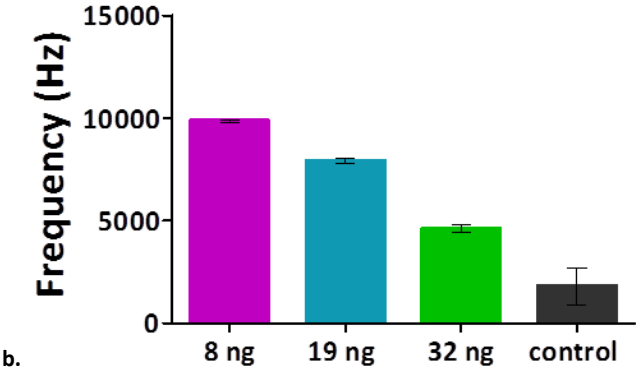

b.

**Figure 66. a.** Real time graph of frequency response upon SAv addition that followed DGL reaction containing a range of G13D amplicons concentrations (8-32 ng); **b.** the biggest frequency response was obtained with the 8 ng G13D amplicon

## 5. Immobilization of thiolated PNA probes on a 100 MHz AWS-HFF QCM sensor, DGL reaction performed for the hybridization of mutant KRAS targets and incorporation of the biotin modified SMART-$C_{biotin}$ nucleobase, and acoustic detection with streptavidin protein

The SAM ratio used for these experiments was K13DAV 3RCC_SH : 5mer-SH = 1 : 10 mixed in PBS buffer. Two different aldehyde-modified nucleobases the SMART-C biotin and the SMART-A biotin were tested for their capacity to detect mutant targets with a single base mutation. **SMART-C** recognizes the ssDNA KWT (**G base**) and the **SMART-A** recognizes the ssDNA K13V (**T base**). Consequently, KWT was the single mismatch for SMART-A biotin and K13V was the single mismatch for SMART-C biotin. DGL reactions were performed as described in the "Matrials and methods, section 9) and acoustic measurements were taken upon SAV addition in SSC 2X (pH 6) in real time. Figure 67 presents the results taken with K13DAV 3RCC_SH, SMART-C biotin nucleobase, and its match and mismatch targets KWT and K13V (results obtained with the SMART-A biotin were eguivalent). As can be seen, the use of K13DAV 3RCC_SH in combination with SMARTC-biotin resulted in the acoustic detection and discrimination of perfectly matched and single mismatched targets. Hybridization of the perfect match KWT to the DGL probe resulted in a frequency change of 30600 Hz upon SAv addition and in a resistance increase of 6.15 Ohm. The hybridization of the single mismatch K13V to the probe resulted in a frequency decrease of 1328 Hz and in a resistance increase of 0.92 Ohm. These two were attributed to non specific binding of SAv which is always present, by default. SAv for instance, might bind to the backbone of the probes, or to SMART-C bases. A closer look at the real-time graph (Fig. 68) however, reveals that the SAv binding was reversible, meaning that the buffer washing step following SAv addition, removed the majority of the SAv bound to the surface. Same real-time responses were observed with SAv addition in the experimental set-up described in section 4. The reasons for this washing off of the SAv remain unclear. Further experiments are needed to elucidate the reasons behind this observation.

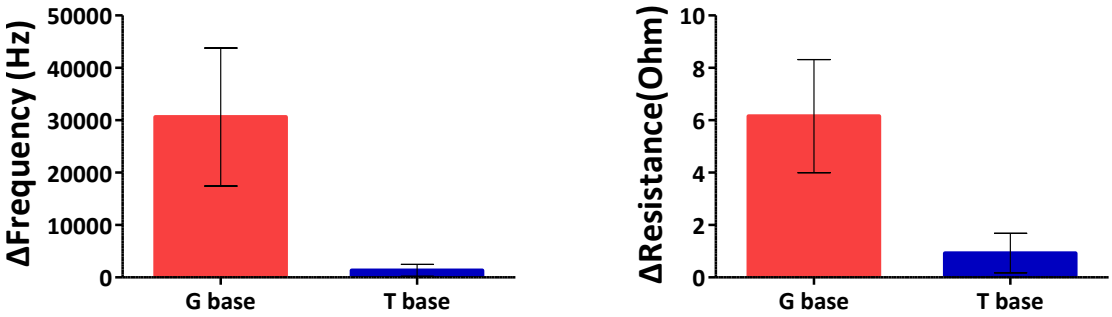


**Figure 67.** Bar graphs illustrating the clear discrimination, using frequency and resistance changes, between perfect match (G base, KWT) and single mismatch (T base, K13V) hybridization to the DGL thiolated probe

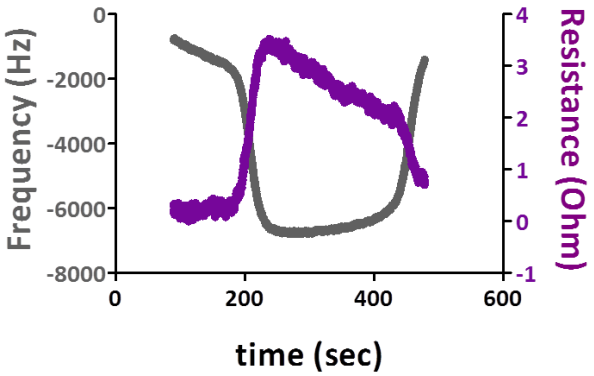


**Figure 68.** Real-time frequency and resistance responses revealing the non-specific nature of the binding of SAv to the functionalized sensing surface

## 6. Immobilization of thiolated PNA probes on a 150 MHz AWS-HFF QCM sensor, DGL reaction performed for the hybridization of short single-stranded mutant targets and incorporation of the biotin modified SMART-C nucleobase, and acoustic detection with streptavidin protein

A new version of HFF-QCM gold sensors operating at the higher fundamental frequency of 150 MHz and, therefore, being more sensitive was introduced. At the same time a different thiolated DGL probe with a longer spacer was employed in order to eliminate steric hindrances occurring when the probes are too close to the sensing surface. The new probe was surface-immobilized through SAM formation but a shorter thiolated intermediate, the 2mer-thiol AA of only two nts was chosen and the SAM mixture ratio was set to 1:20 (DGL probe:2mer-thiol AA) in order to create a larger distance (20 nm) in between the probes. Perfect match (DGLK12_2.2 MUT carrying a **T** base opposite the "blank" position of the probe) and single mismatch (DGLK12_2.2 WT with a **C** base opposite the "blank" position) were cobined with SMART-A biotin nucleobase. SAv was added in PBS and acoustic measurements were taken in real-time. Unfortunately, the perfect from the single mismatch could not be discriminated with this configuration (Figure 69 and Table 3). Frequency changes were expected for the non-specific binding of SAv occurring in the presence of single mismatches, but the frequency responses corresponding to the expected specific binding of SAv in the presence of perfect mismatches, were not high enough. The speculation that the SAM layer was not properly formed was

partially disproved; since control experiments where SAv was added in the sensing system immediately after the SAM formation showed that no change in frequency or resistance was caused, indicating that SAv did not non-specifically bind to the gold surface which was covered by the SAM layer. Besides, results presented in section 5 encourage the idea that SAM formation and probe-target hybridization do occur on the surface under the described experimental conditions. Perhaps the SAv does not have enough space in between the probes in order to get specifically captured by the SMART-A biotinylated nucleobase (Fig. 70).

| Probe | Target | Frequency (KHz) |
|---|---|---|
| DGL probe K12_2.2 | DGLK12_2.2 MUT (perfect match) | 3.1-4 |
| DGL probe K12_2.2 | DGLK12_2.2 WT (single mismatch) | 0-2.4 |

**Table 3.** Summary of the frequency changes obtained upon SAv addition following the performance of DGL reaction

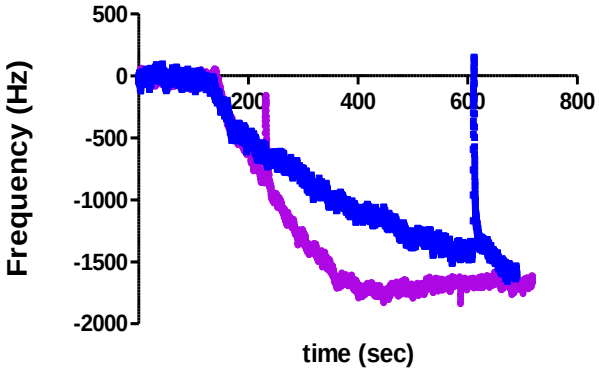


**Figure 69.** Real-time frequency response during addition of SAv after DGL reaction was carried out with the perfect match DGLK12_2.2 MUT **(purple line)** and the single mismatch DGLK12_2.2 WT **(blue line)**

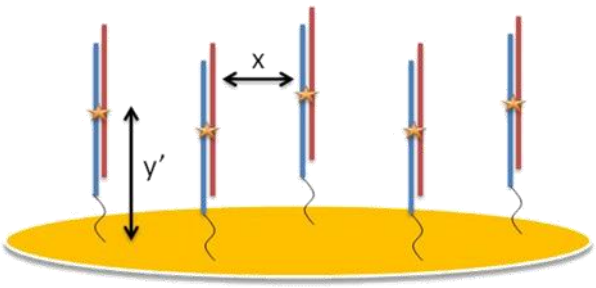


**Figure 70.** Schematic description of the distance of the DGL probes from the surface and the distance in between the DGL probes. Not drawn to scale

## 7. Real-time monitoring of the immobilization of thiolated PNA probes on a 5 MHz QSensor and of the hybridization of short single-stranded mutant and wild type targets

The immobilization of the K12_2.2 DGL probe with one thiol and the longer spacer could not be acoustically followed in real-time. Subsequent direct hybridization of either the mutant or the wild type target (1μM) to the immobilized K12_2.2 probe could not be acoustically sensed since any change in the frequency or dissipation signal was observed.

The surface immobilization of the K12_2.3 DGL probe on the contrary, was sensed by the QSense Analyzer. The immobilization of the K12_2.3 probe in a mixture with the 2mer-thiol AA (0.5 : 0.5 μM) resulted in an average dissipation increase of 0.15 ($10^{-6}$) (±0.07) DU and an average frequency decrease of 31 (±5.5) Hz. Possibly, 90 min incubation of the K12_2.2 probe with one thiol at the N terminal is not enough for it to get strongly immobilized on the surface. An overnight incubation as the one described for the AWS A20-F20 platform might be more suitable, but then real-time monitoring of surface immobilization becomes not feasible. The K12_2.3 probe with the thiols at its two ends seems to get surface-immobilized faster and more acutely compared to the probe with one thiol.

Following hybridization of either the mutant or wild type target to the K12_2.3 was also acoustically detected. The average dissipation change obtained upon mutant (K12_2.2MUT) hybridization to the K12_2.3 probe was 0.49 ($10^{-6}$) DU (±0.08). The respective dissipation change obtained upon wild type (K12_2.2WT) hybridization to the DGL probe was 0.34 ($10^{-6}$) DU (±0.07). Mutant target hybridization led to a frequency shift of 25 Hz (±3.8) and the wild type hybridization led to a frequency change of 17 Hz (±9.5). Hybridization of the mutant target could not be distinguished from the hybridization of the wild type target by the acoustic ratio (Fig. 71). The targets shared the same oligonucleobase sequence, and they differed in only one base opposite the “DGL pocket” of the probe. Hybridization of two oligonucleotides differing in only one base is not expected to result in distinct acoustic ratios.

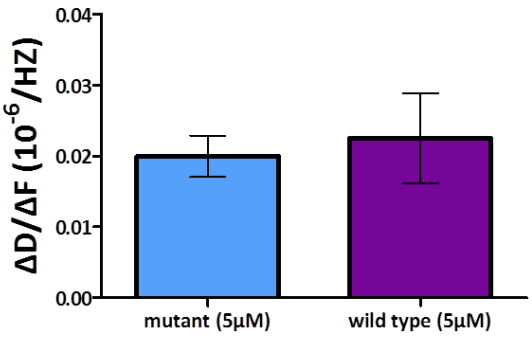


**Figure 71.** Bar graph representing the acoustic ratios obtained upon mutant and wild type target hybridization to the K12_2.3 surface-immobilized probe. As expected, mutant hybridization could not be acoustically discriminated from wild type hybridization using the acoustic ratio [0.0200 ($10^{-6}$/Hz) versus 0.0225 ($10^{-6}$/Hz)]

## 8. Acoustic detection of the DGL reaction completion (SMART-$A_{biotin}$ incorporation) using streptavidin and the QSense Analyzer

As already mentioned for the experiments carried out using the 150 MHz AWS-HFF QCM sensors, DGL reactions occurring on the 5 MHz Qsensor surface and containing the mutant (K12_2.2MUT) target could not be acoustically distinguished from the ones containing the wild type (K12_2.2WT) target. This observation applies to sensor surfaces treated with both K12_2.2 and K12_2.3 probe and for all the experimental conditions described in Part 12 of Materials and Methods section.

## 9. Determination of the binding kinetics of streptavidin addition after injection of DGL reactions using the QSense Analyzer

Since the frequency shift obtained upon SAv addition that followed the addition of DGL reactions was not adequate to distinguish between the mutant and the wild type target, the QSense Analyzer was used to probe the rate of binding of SAv. QCM devices apart from studying molecular binding/interaction processes and conformational changes are also suitable for determining binding kinetics (*229, 230*). The rate of SAv surface-binding after the completion of the DGL reactions including the mutant and the wild type target was probed for its capacity to distinguish between the two DGL reaction cases. The binding rate of SAv was investigated after DGL reaction addition on 5 MHz QSensor surfaces previously treated with either the DGL K12_2.2. or the DGL K12_2.3 probe and under a variety of experimental conditions (that have been explained above). Unfortunately, neither the binding rate was sufficient to differentiate the incorporation of the SMART-$A_{biotin}$ nucleobase in a PNA-DNA dublex formed by the probe and the mutant target from the equivalent non-incorporation in a duplex formed by the probe and the wild type target. Figure 71 portrays the almost identical slopes obtained after a linear regression analysis performed with the Origin Pro 8.0 software. Each slope corresponds to the initial binding rate of SAv (Hz/min) on a surface pre-treated with K12_2.2 probe and then with DGL mutant and DGL wild type reaction (Fig. 72.a) and on a surface pre-treated with K12_2.3 probe and again with DGL mutant and DGL wild type reaction (Fig. 72. b). The figure inlet graphs prove that the SAv binding rate was the same for SAv added on the sensing surface after DGL mutant and DGL wild type reaction, suggesting that the SMART-$A_{biotin}$ incorporation and the subsequent SAv surface-binding were not specific.

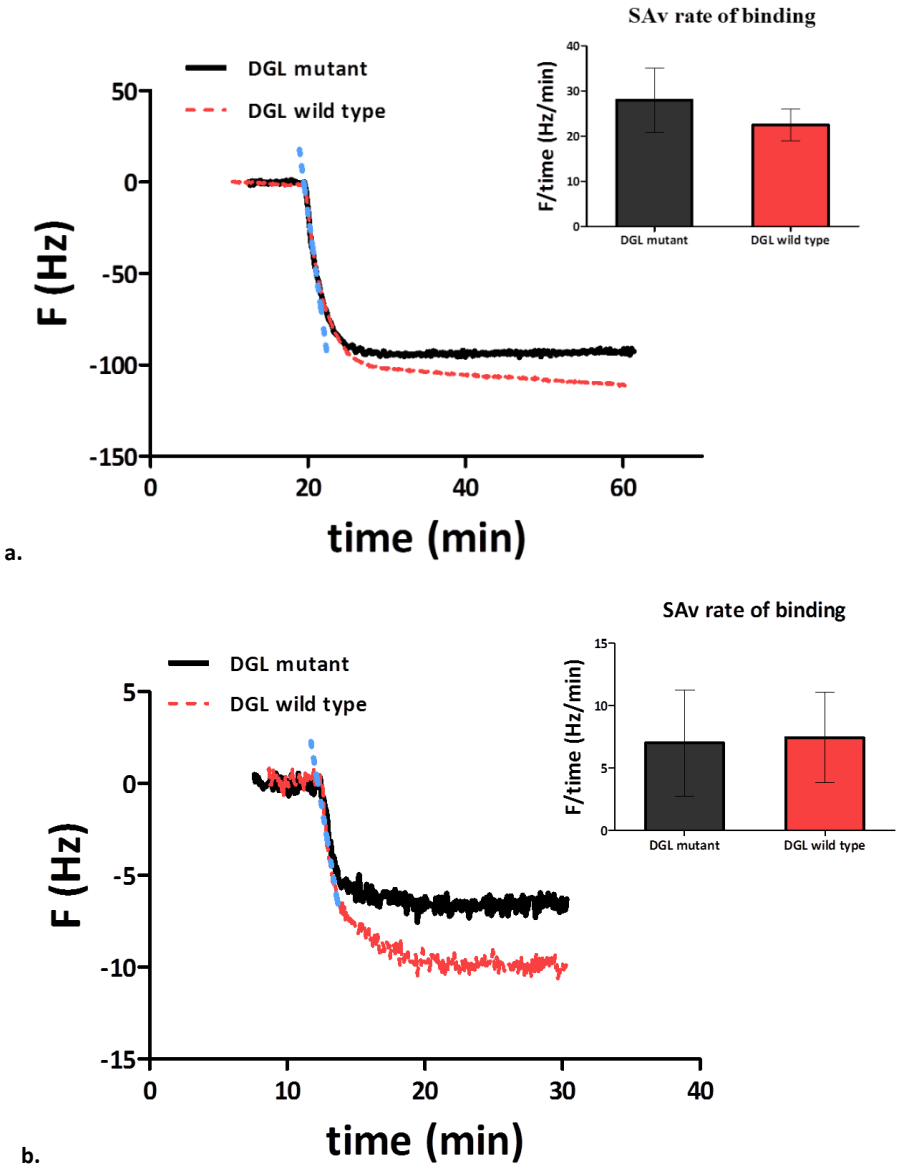


**Figure 72.** Real-time graph depicting the frequency shift upon SAv addition after the treatement of the sensing surface with **a.** K12_2.2 probe and DGL mutant **(black line)** or DGL wild type **(red line)**; **b.** K12_2.3 probe and DGL mutant **(black line)** or DGL wild type **(red line)**. The **blue dashed lines** are the slopes acquired after a linear regression fitting; these slopes represent the initial binding rate of SAv in Hz/min. As can be seen, this rate is almost identical for SAv added on a surface treated with either DGL mutant or DGL wild type reaction. The bar graphs on the top right of each figure depict the rate of binding obtained for SAv in each case. These two bar graphs verify the fact that the rate of binding is the same for SAv added after the DGL reaction with mutant target and the DGL with wild type target addition

Another interesting observation regarding SAv initial binding rate was that the rate increased with the total SAv mass bound on the sensor surface. A higher rate of binding correlated with a higher frequency shift (higher number of Hz obtained) upon SAv addition (Fig. 73).

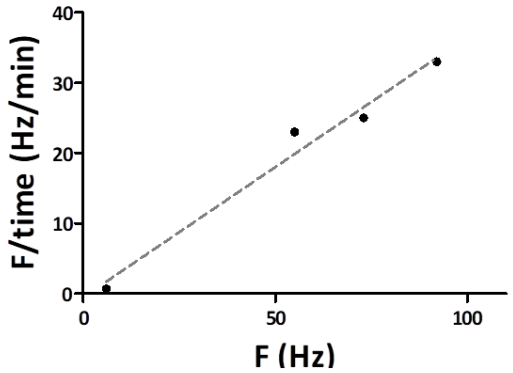


**Figure 73.** Graph representing the rate of binding of SAv on a sensor surface previously treated with the probe K12_2.2 in a 1 : 20 ratio with the 2mer-thiol AA and, consequitively, with a DGL mutant reaction containing 1 µM of the K12_2.2MUT target and 10 µM of the SMART-$A_{biotin}$ nucleobase. The higher the number of Hz obtained upon SAv addition (mass adsorbed on the surface), the higher the binding rate

## 10. Real-time monitoring of the immobilization of biotinylated PNA probes on a 5 MHz QSensor and of the hybridization of short single-stranded mutant targets

In contrast to the case of thiolated DGL probes, this, time, the real-time acoustic detection of the surface-immobilization of the biotinylated probes was achieved. The surface immobilization of the DGL K12_2.4 probe resulted in a frequency decrease of 27 (±5) Hz and in a low dissipation increase of .011 (±0.01) ($10^{-6}$) DU; the acoustic ratio measured was 0.0045 (±0.0012) ($10^{-6}$/Hz). The frequency change recorded is relatively low regarding the concentration of the sample flown over the sensing surface, but it is probably due to the low solubility of the DGL probe in the buffer.

The hybridization of the mutant target to the K12_2.4 probe was also acoustically detected. The average dissipation change obtained upon K12_2.2MUT hybridization to the K12_2.4 probe was 0.23 (±0.01) ($10^{-6}$) DU. The frequency shift was 21 (±1.7) Hz and the ratio was found to be 0.0111 (±0.0016) ($10^{-6}$/Hz). The acoustic ratio is the one expected for a 18 dsDNA attached to the surface through a single biotin.

## 11. Acoustic detection of the DGL reaction completion (SMART-$A_{biotin}$ incorporation) using the biotinylated DGL probes, streptavidin and the QSense Analyzer

Biotin was used to block any holes on both the neutravidin layer and the gold surface, so that streptavidin would not bind to these holes. When the surface was blocked with biotin, before the addition of the DGL reaction on the surface, the addition of SAv resulted in no change in frequency and dissipation (Fig. 73). On the contrary, not blocking the surface with biotin resulted in non-specific binding of SAv, most likely on the bare gold surface. This non-specific frequency shift observed (9 Hz (±1.22)) was the same for DGL containing the mutant and DGL containing the wild-type target (Fig. 74). Once again, the two reactions could not be acoustically discriminated from each other.

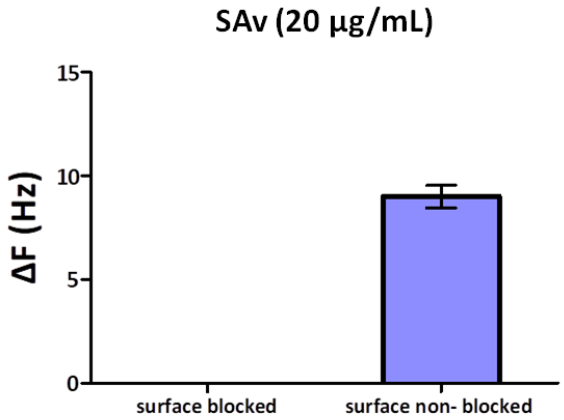


**Figure 74.** Bar graph presenting the frequency increase obtained upon SAv addition after the accomplishment of the DGL reaction on the surface. The left panel depicts the absence of frequency shift upon addition of SAv on a sensing surface blocked with biotin; the right bar includes data obtained from both DGL with the mutant and DGL with the wild-type target, since the two reactions resulted in the same amount of Hz, and could not be discriminated

## 13. Acoustic detection of the DGL reaction completion (SMART-$C_{biotin}$ incorporation) using the PNA chimera complex, streptavidin and the QSense Analyzer

It was calculated that with the aforementioned surface design, the distance of the SMART base incorporation site from the surface was ~5.5 nm. Streptavidin itself however, has a dimension of 5.8 nm x 5.4 nm. This is why a PNA Chimera complex was employed to move the DGL probe and consequently the SMART base incorporation site away from the surface. The new experimental set-up resulted in the distancing of the SMART base incorporation site from the sensor surface at 11 nm (Fig. 75). This DGL probe achieved the discrimination between KWT and K12V included in the DGL reaction. SMART-$C_{biotin}$ recognized the KWT that bares a **G** nucleotide. Differentiation between the two targets could be performed by calculating frequency and dissipation changes, and with the acoustic ratio (Table 4).

PCR-produced RCDestinaWT2 recognized by the SMART-$C_{biotin}$ (referred to here as positive) and PCR-produced G13D not recognized by the SMARTC-$_{biotin}$ (referred to here as mismatch) were also differentiated upon SAv addition. It was shown that 2 ng of the PCR positive are needed in the DGL reaction for detection, with 45 ng allowing for a more stable frequency and dissipation shift. Fewer ng of the PCR positive in the DGL reaction (*i.e.* 0.5 ng) could not be acoustically sensed (Fig. 76). As a matter of fact, preliminary results imply that dissipation shift is more sensitive and specific in differentiating between PCR positive and PCR negative, while frequency change suffers from a small degree of non-specific response (Fig. 76 upper panel).

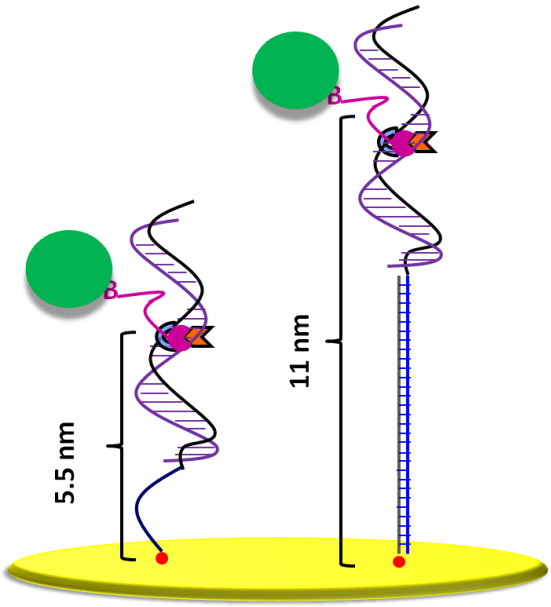


**Figure 75.** Schematic representation of the way the SMART-$C_{biotin}$ incorporation site was moved away from the sensor surface

| Target | ΔD ($10^{-6}$) | F (Hz) | ΔD/ΔF ($10^{-6}$/Hz) |
|---|---|---|---|
| KWT | 0.11 (±0.005) | 9.1 (±0.7) | 0.0127 (±0.016) |
| K12V | 0 | 0-1 (±0.0) | 0 |

**Table 4.** Summary of the frequency and dissipation changes occurring upon SAv addition after the DGL reactions containing either the KWT or the K12V target were flowed over the sensing surface. KWT which is recognized by the SMART-$C_{biotin}$ was acoustically differentiated from the K12V. Calculation of the acoustic ratio also managed to distinguish the KWT from the K12V target

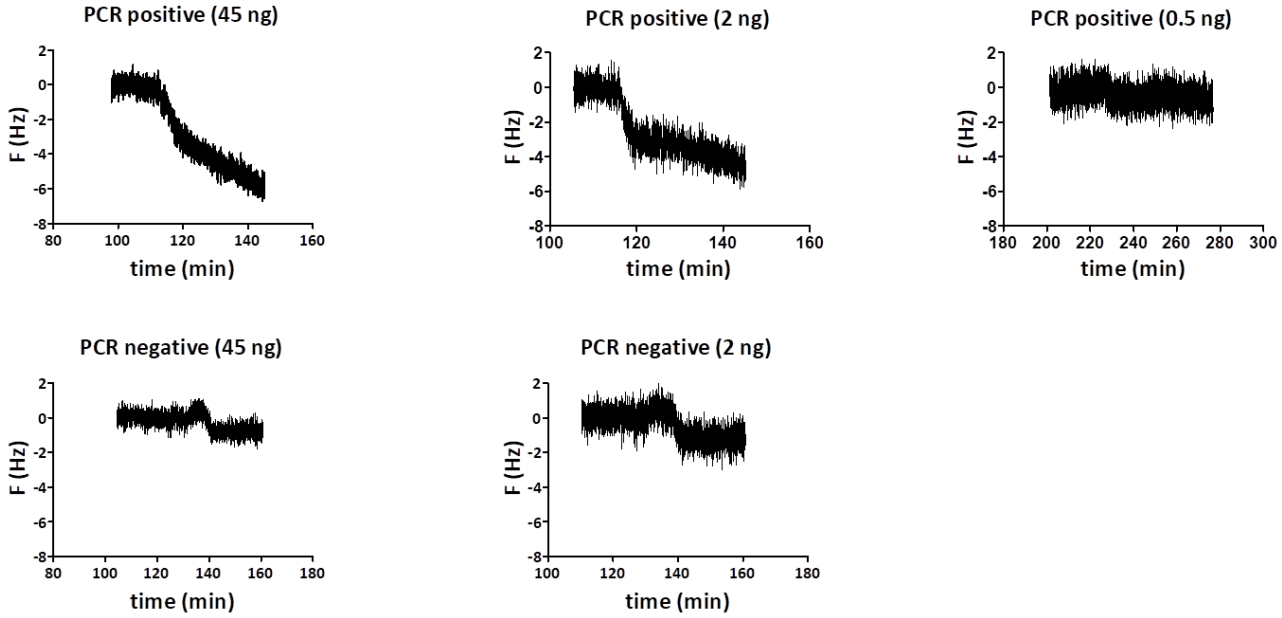

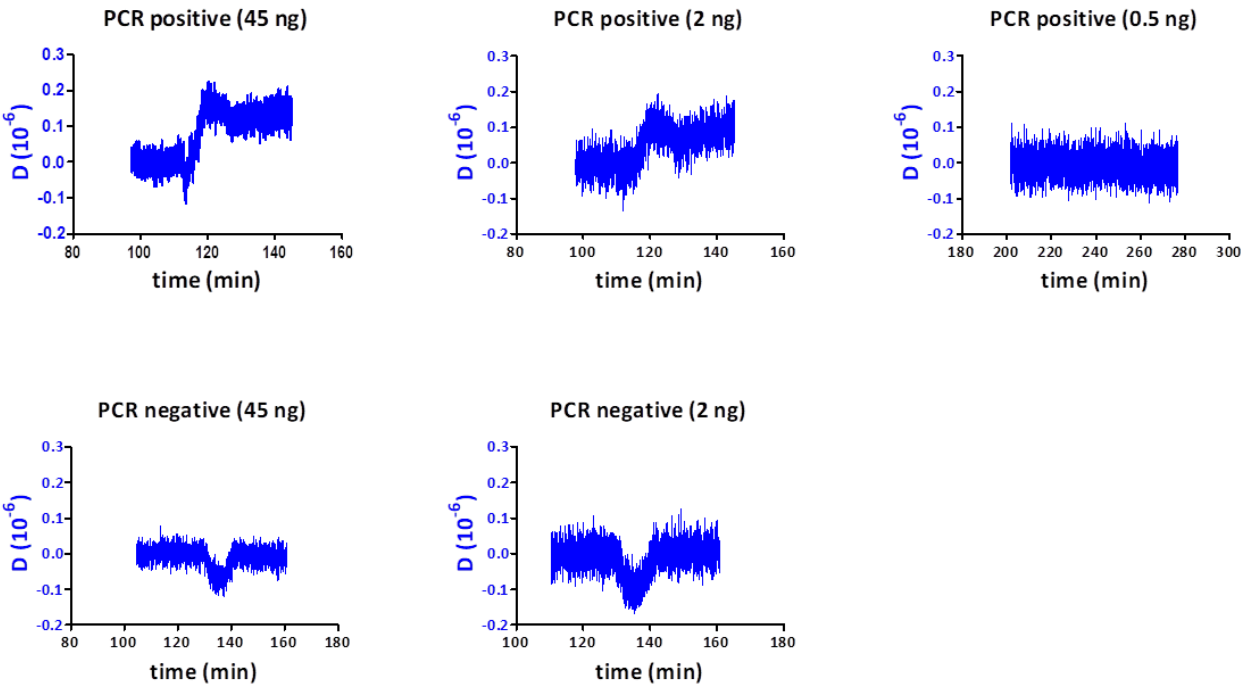


**Figure 76. Upper panel:** frequency changes differentiating PCR positive 45, 2 and 0.5 ng; a non-specific frequency shift was observed for PCR negative 45 and 2 ng; **Lower panel:** dissipation changes differentiating PCR positive 45, 2 and 0.5 ng; no dissipation shift was monitored for PCR negative of 45 and 2 ng

# *Conclusions*

The work presented in this chapter is a proof-of-principle study dealing with the development of an acoustic wave-based bioassay for the detection of KRAS mutations in ctDNA coming from the blood of CRC patients. The assay developed achieved the acoustic detection and discriminationof KRAS mutations present on oligonuclotide mimics of ctDNA. For the first time, acoustic wave sensors were combined with the DGL© technology.

Noteworthy, the bioassay presented achieved the amplification of a KRAS gene mimic both with a conventional PCR and an isothermal RPA. Leaving aside the issue of the non-specific binding of SAv to the surface, the protocol developed achieved the acoustic detection of the PCR-amplified KRAS mimic bearing a T mutation opposite the abasic position of the DGL probe used. The whole duration of the procedure of the PCR amplification, the DGL reaction performance, and the acoustic detection was almost 55 min (less than an hour). The limit of detection achieved was in the range of a few nM (11 nM). These results encourage the belief that the protocol developed can be used for early and fast detection of ctDNA bearing KRAS mutations from a liquid biopsy (blood sample).

The integration of such a bioassay in a user-friendly diagnostic platform that would allow the sensitive, specific, low-cost, rapid, on-site and semi-automated detection of ctDNA with KRAS mutations associated to CRC would be very useful to the field of laboratory medicine. Furthermore, the platform could be used for the monitoring of CRC patients and their response to targeted treatment. ctDNA with KRAS mutations has been found in all patients with metastatic CRC (mCRC) before surgery, and ctDNA exhibited oscillations that correlated with the extend of surgical resection. Patients with detectable ctDNA levels after surgery relapsed with 1 year. The ctDNA was shown to be a much more reliable and sensitive biomarker than the currently used standard carcinoembryonic antigen (CEA) (*215*). Additionally, CRC patients with ctDNA harboring KRAS mutations exhibit resistance to treatment with monoclonal antibodies inhibiting the EGFR (*231-234*). The potential of the application of such a diagnostic platform in the field of “personalized medicine” for CRC patients is, therefore, self-evident.

## *Future perspectives*

The current PhD thesis presented the design and development of acoustic wave-based bioassays for the detection of foodborne pathogens and cancer biomarkers. Acoustic wave biosensors have been undoubtedly established as reliable and sensitive analytical tools. The work presented here has eloquently explained the capacity of acoustic wave biosensors to get integrated in lab-on-chip diagnostic platforms for point-of-care testing. The next big thing in the field of acoustic wave-based biosensors is the development, fabrication and commercialization of such an acoustic wave sensor-based diagnostic platform. In order for such a platform to reach the market, it should fulfill several requirements. Ideally, a reliable acoustic wave-based diagnostic platform would be sensitive, specific, rapid, accurate, robust, small in size, low-cost and easy-to-use by non-skilled personnel. Most of the acoustic wave biosensors reported in the literature satisfy some of these criteria; in general they offer fast, label-free and real-time analyte detection. But, in their majority, they lag behind in sensitivity compared to conventional analytical techniques (PCR, ELISA, DNA sequencing, DNA microarrays) It is anticipated that the application of nanotechnology products, such as gold nanoparticles and liposomes that have been shown to increase the sensor sensitivity will lead to the generation of acoustic wave biosensors which will be able to surpass the limits of detection achieved with conventional diagnostic techniques. Another issue with the development of reliable acoustic wave bioassays is the fact that, a big portion of them, fails whenever tested in field applications and with real complex samples. Nowadays one of the great challenges for the development of successful marketable acoustic wave diagnostic sensors is their miniaturization and integration in automated, high-throughput, cost-effective diagnostic platforms for on-site applications and testing of crude samples (such as blood, urine and saliva). The integration of a piezoelectric device with microfluidics and wireless measurement, and collection of data would be a critical step for the development of the desired acoustic wave-based diagnostic platform. The target market is there and is well defined: food and environmental industries, hospitals and diagnostic centers, biosafety agencies and pharmaceutical industries that need biosensors for drug discovery and screening; what remains is for the right acoustic wave biosensor to appear.

# References


1. Mehrotra P., Biosensors and their applications - a review. *J. Oral Biol. Craniofac. Res.* **6**, 153-159 (2016).
2. Patel S., Nanda, R., Sahoo, S. and Mohapatra, E., Biosensors in health care: the milestones achieved in their development towards lab-on-chip analysis. *Biochemistry Research International* **2016**, (2016).
3. S. Vigneshvar, Sudhakumari, C.C., Senthilkumaran, B., and Prakash, H., Recent advances in biosensor technology for potential applications - an overview. *Front. Bioeng. Biotechnol.* **4**, (2016).
4. Bahadir E.B., Sezgintürk M.K., Applications of commercial biosensors in clinical, food, environmental, and biothreat/biowarfare analyses. *Anal. Biochem.* **478**, 107-120 (2015).
5. Turner A.P.F., Karube I., and Wilson, G.E., *Biosensors: Fundamentals and Applications*. (Oxford University Press, United States, New York, 1987).
6. Bănică F.G., *Chemical Sensors and Biosensors: Fundamentals and Applications*. (WILEY, 2012).
7. Sauerbrey G., Verwendung von schwingquarzen zur wagung dunner schichten und zur mikrowagung. *Zeitschrift fur Physik* **155**, 206-222 (1959).
8. Durmuş N.G., Lin R.L., Kozberg M., Dermici D., Khademhosseini A., and Demirci U., in *Encyclopedia of Microfluidics and Nanofluidics,* L. D., Ed. (2015).
9. Gizeli E., Design considerations for the acoustic waveguide biosensor. *Smart Mater. Struct.* **6**, 700-706 (1997).
10. Ferrari V., and Lucklum R., in *Piezoelectric Transducers and Applications,* A. V.A., Ed. (Springer, 2008).
11. Fogel R., Limson J., and Seshia A.A., Acoustic biosensors. *Essays Biochem.* **60**, 101-110 (2016).
12. Dixon M.C., Quartz crystal microbalance with dissipation monitoring: enabling real-time characterization of biological materials and their interactions. *J. Biomol. Tech.* **19**, 151-158 (2008).
13. Hook F., Kasemo B., Nylander T., Fant C., Sott K., and Elwing H., Variations in coupled water, viscoelastic properties, and film thickness of a Mefp-1protein film during adsorption and cross-linking: a quartz crystal microbalance with dissipation monitoring, ellipsometry, and surface plasmon resonance study. *Anal. Chem.* **73**, 5796-5804 (2001).
14. Janshoff A., Galla H.J., and Steinem C., Piezoelectric mass-sensing devices as biosensors - an alternative to optical biosensors? *Angew. Chem. Int. Ed.* **39**, 4004-4032 (2000).
15. Voinova M.V., Rodhal M., Jonson M., and Kasemo B., Viscoelastic acoustic response of layered polymer films at fluid-solid interfaces: continuum mechanics approach. *Phys. Scr.* **59**, 391-396 (1999).
16. Rodahl M., Hook F., Fredriksson C., Keller C.A., Krozer A., Brzezinski P., Voinova M., and Kasemo B., Simultaneous frequency and dissipation factor QCM measurements of biomolecular adsorption and cell adhesion. *Faraday Discuss.* **107**, 229-246 (1997).
17. Biolin Scientific, QCM-D Measurements. Available at: https://www.biolinscientific.com/measurements/qcm-d. (2018).
18. Tsortos A., Papadakis G., Mitsakakis K., Melzak K.A., and Gizeli E., Quantitative determination of size and shape of surface-bound DNA using an acoustic wave sensor. *Biophys. J.* **94**, 2706-2715 (2008).

19. P. G. Tsortos A., and Gizeli E., Shear acoustic wave biosensor for detecting DNA intrinsic viscosity and conformation: a study with QCM-D. *Biosens. Bioelectron.* **24**, 836-841 (2008).
20. Papadakis G., Tsortos A., Bender F., Ferapontova E.E., and Gizeli E., Direct detection of DNA conformation in hybridization processes. *Anal. Chem.* **84**, 1854-1861 (2012).
21. Papadakis G., Tsortos A., and Gizeli E., Acoustic characterization of nanoswitch structures: application to the DNA Holliday junction. *Nano Lett.* **10**, 5093-5097 (2010).
22. Centers for Disease Control and Prevention (CDC), CDC estimates of foodborn illness in the United States. Available online at: http://www.cdc.gov/foodborneburden/PDFs/FACTSHEET_A_FINDINGS_updated4-13.pdf. (2011).
23. Oliver S.P., Jayarao B.M., and Almeida R.A., Foodborne pathogens in milk and the dairy farm environment: food safety and public health implications. *Foodborne Pathog. Dis.* **2**, 115-129 (2005).
24. Zhao X., Lin C.W., Wang J., and Oh D.H., Advances in rapid detection methods for foodborne pathogens. *J. Microbiol. Biotechnol.* **24**, 297-312 (2014).
25. Scallan E., Hoekstra R.M., Angulo F.J., Tauxe R.V., Widdowson M.A., Roy S.L., Jones J.L., and Griffin P.M., Foodborne illness acquired in the United States - major pathogens. *Emerg. Infect. Diseases* **17**, 7-15 (2011).
26. Yasmin J., Ahmed M.R., and Cho B.K., Biosensors and their applications in food safety: A review. *J. of Biosystems Eng.* **41**, 240-254 (2016).
27. Law J.W.-F., Ab Mutalib N.S., Chan K.G., and Lee L.H., Rapid methods for the detection of foodborne bacterial pathogens: principles, applications, advantages and limitations. *Front. Microbiol.* **5**, (2015).
28. FDA, Food Protection Plan. Department of health and human services. Maryland: U.S. Food and Drug Administration (2007)
29. Velusamy V., Arshak K., Korostynska O., Oliwa K., and Adley C., An overview of foodborne pathogen detection: in the perspective of biosensors. *Biotechnol. Adv.* **28**, 232-254 (2010).
30. WHO, World Health Day 2015: Food safety. Available at: http://www.who.int/campaigns/world-health-day/2015/event/en/. (2015).
31. Regulation EC, No 2073/2005 of the European Parliament and of the Council of 15 November 2005, on microbiological criteria for foodstuffs. (2005).
32. Sharpe A.N., and Jackson A.K., Stomaching: a new concept in bacteriological sample preparation. *Appl. Microbiol.* **24**, 175-178 (1972).
33. Dwivedi H.P., and Jaykus L.A., Detection of pathogens in foods: the current state-of-the-art and future directions. *Crit. Rev. Microbiol.* **37**, 40-63 (2011).
34. Mandal P.K., Biswas A.K., Choi K., and Pal U.K., Methods for rapid detection of foodborne pathogens: an overview. *Am. J. Food Technol.* **6**, 87-102 (2011).
35. Zhou B., Xiao J., Liu S., Yang J., Wang Y., Nie F., Zhou Q., Li Y., and Zhao G., Simultaneous detection of six foodborne pathogens by multiplex PCR with a GeXP analyzer. *Food Control* **32**, 198-204 (2013).
36. Chiang Y.C., Tsen H.Y., Chen H.Y., Chang Y.H., Lin C.K., Chen C.Y., and Pai W.Y., Multiplex PCR and a chromogenic DNA macroarray for the detection of Listeria *monocytogenes*, *Staphylococcus aureus*, *Streptococcus agalactiae*, *Enterobacter sakazakii*, *Escherichia coli* O157:H7, *Vibrio parahaemolyticus*, *Salmonella* spp. and *Pseudomonas fluorescens* in milk and meat samples. *J. MIcrobiol. Methods* **88**, 110-116 (2012).

37. Alves J., Vieira Marques V., Protasio Fereira L.F., Hirooka E.Y., and Moreira de Oliveira C.R. , Multiplex PCR for the detection of *Campylobacter* spp. and *Salmonella* in chicken meat. *J. Food Saf.* **32**, 345-350 (2012).
38. Lee L.H., Cheah Y.K., Noorzaleha A.S., Sabrina S., Sim J.H., Khoo C.H., and Son R., Analysis of *Salmonella* Agona and *Salmonella* Weltevreden in Malaysia by PCR fingerprinting and antibiotic resistance profiling. *Antonie van Leeuwenhoek* **94**, 377-387 (2008).
39. Cheah Y.K., Salleh N.A., Lee L.H., Radu S., Sukardi S., and Sim J.H., Comparison of PCR fingerprinting techniques for the discrimination of *Salmonella enterica* subsp. *enterica* serovar Weltevreden isolated from indigenous vegetables in Malaysia. *World J. Microbiol. Biotechnol.* **24**, 327-335 (2008).
40. Silva D.S.P., Canato T., Magnani M., Alves J., Hirooka E.Y. and de Oliveira T.C.R.M., Multiplex PCR for the simultaneous detection of *Salmonella* spp. and *Salmonella Enteritidis* in food. *Int. J. Food Sci. Technol.* **46**, 1502-1507 (2011).
41. Park Y.S, Lee SR, and Kim Y.G., Detection of *Escherichia coli* O157:H7, *Salmonella* spp., *Staphylococcus aureus* and *Listeria monocytogenes* in *kimchi* by multiplex polymerace chain reaction (mPCR). *J. Microbiol.* **44**, 92-97 (2006).
42. Chen J., Zhang L., Paoli G.C., Shi C., Tu S.I., and Shi X., A real-time PCR method for the detection of *Salmonella enterica* from food using a target sequence identified by comparative genomic analysis. *Int. J. Food Microbiol.* **137**, 168-174 (2010).
43. Wang F., Yang Q., Qu Y., Meng J., and Ge B., Evaluation of a Loop-Mediated Isothermal Amplification suite for the rapid, reliable, and robust detection of Shiga toxin-producing *Escherichia coli* in produce. *Appl. Environ. Microbiol.* **80**, 2516-2525 (2014).
44. Wang L., Shi L., Su J., Ye Y., and Zhong Q., Detection of *Vibrio parahaemolyticus* in food samples using in situ loop-mediated isothermal amplification method. *Gene* **515**, 421-425 (2013).
45. Shao Y., Zhu S., Jin C., and Chen F., Development of multiplex loop-mediated isothermal amplification-RFLP (mLAMP-RFLP) to detect *Salmonella* spp. and *Shigella* spp. in milk. *Int. J. Food Microbiol.* **148**, 75-79 (2011).
46. Han F., Wang F., and Ge B., Detecting potentially virulent *Vibrio vulnificus* strains in raw oysters by quantitative Loop-Mediated Isothermal Amplification *Appl. Environ. Microbiol.* **77**, 2589-2595 (2011).
47. Min J., and Baeumner A.J., Highly sensitive and specific detection of viable *Escherichia coli* in drinking water. *Anal. Biochem.* **303**, 186-193 (2002).
48. Nadal A., Coll A., Cook N., and Pla M., A molecular beacon-based real time NASBA assay for detection of *Listeria monocytogenes* in food products: role of target mRNA secondary structure on NASBA design. *J. MIcrobiol. Methods* **68**, 623-632 (2007).
49. D'Souza D.H., and Jaykus L.A., Nucleic acid sequence based amplification for the rapid and sensitive detection of *Salmonella enterica* from foods. *J. Appl. Microbiol.* **2003**, 1343-1350 (2003).
50. Kim T.H., Park J., Kim C.J., and Cho Y.K., Fully integrated lab-on-a-disc for nucleic acid analysis of food-borne pathogens. *Anal. Chem.* **86**, 3841-3848 (2014).
51. Lutz S., Weber P., Focke M., Faltin B., Hoffmann J., Muller C., Mark D., Roth G., Munday P., Armes N., Piepenburg O., Zengerle R., and von Stetten F., Microfluidic lab-on-a-foil for nucleic acid analysis based on isothermal recombinase polymerase amplification (RPA). *Lab Chip* **10**, 887-893 (2010).
52. Bang J., Beuchat L.R., Song H., Gu M.B., Chang H.I., Kim H.S., and Ryu J.H, Development of a random genomic DNA microarray for the detection and identification of *Listeria monocytogenes* in milk. *Int. J. Food Microbiol.* **161**, 134-141 (2013).

53. Suo B., He Y., Paoli G., Gehring A., Tu S.I., and Shi X., Development of an oligonucleotide-based microarray to detect multiple foodborne pathogens. *Mol. Cell. Probes* **24**, 77-86 (2010).
54. Kumar B.K., Raghunath P., Devegowda D., Deekshit V.K., Venugopal M.N., Karunasagar I., and Karunasagar I., Development of monoclonal antibody based sandwich ELISA for the rapid detection of pathogenic *Vibrio parahaemolyticus* in seafood. *Int. J. Food Microbiol.* **145**, 244-249 (2011).
55. Shen Z., Hou N., Jin M., Qiu Z., Wang J., Zhang B., Wang X., Wang J., Zhou D., and Li J., A novel enzyme-linked immunosorbent assay for detection of *Escherichia coli* O157:H7 using immunomagnetic and beacon gold nanoparticles. *Gut Pathog.* **6**, (2014).
56. Shukla S., Leem H., Lee J.S., and Kim M., Immunochromatographic strip assay for the rapid and sensitive detection of *Salmonella* Typhimurium in artificially contaminated tomato samples. *Can. J. Microbiol.* **60**, 399-406 (2014).
57. Kumar S., Balakrishna K., and Batra H.V., Enrichment-ELISA for detection of *Salmonella typhi* from food and water samples. *Biomed. Environ. Sci.* **21**, 137-143 (2008).
58. Park SH., Aydin M., Khatiwara A., Dolan M.C., Gilmore D.F., Bouldin J.L., Ahn S., and Ricke S.C., Current and emerging technologies for rapid detection and characterization of *Salmonella* in poultry and poultry products. *Food Microbiol.* **38**, 250-262 (2014).
59. Lauri A., and Mariani P.O., Potentials and limitations of molecular diagnostic methods in food safety. *Genes Nutr.* **4**, 1-12 (2009).
60. Tripathi S.M., Bock W.J., Mikulic P., Chinnappan R., Ng A., Tolba M., and Zourob M., Long period grating based biosensor for the detection of *Escherichia coli* bacteria. *Biosens. Bioelectron.* **35**, 308-312 (2012).
61. Zhang D., Yan Y., Li Q., Yu T., Cheng W., Wang L., Ju H., and Ding S., Label-free and high-sensitive detection of *Salmonella* using a surface plasmon resonance DNA-based biosensor. *J. Biotechnol.* **160**, 123-128 (2012).
62. Ohk S.H., Koo O.K., Sen T., Yamamoto C.M., and Bhunia A.K., Antibody-aptamer functionalized fibre-optic biosensor for specific detection of *Listeria monocytogenes* from food. *J. Appl. Microbiol.* **109**, 808-817 (2010).
63. Li Y., Cheng P., Gong J., Fang L., Deng J., Liang W., and Zheng J., Amperometric immunosensor for the detection of *Escherichia coli* O157:H7 in food specimens. *Anal. Biochem.* **421**, 227-233 (2012).
64. Ercole C., Del Gallo M., Mosiello L., Baccella S., and Lepidi A., *Escherichia coli* detection in vegetable food by a potentiometric biosensor. *Sens. Actuator B - Chem.* **91**, 163-168 (2003).
65. Farka Z., Jurik T., Pastucha M., Kovar D., Lacina K. and Skladal P., Rapid Immunosensing of *Salmonella* Typhimurium using electrochemical impedance spectroscopy: the effect of sample treatment. *Electroanal.* **28**, 1803-1809 (2016).
66. Cinti S., Volpe J., Piermarini S., Delibato E., and Palleschi G., Electrochemical biosensors for rapid detection of foodborne *Salmonella*: a critical overview. *Sensors* **17**, 1910-1931 (2017).
67. Singh A., Poshtiban S., and Evoy S., Recent advances in bacteriophage based biosensors for food-borne pathogen detection. *Sensors* **13**, 1763-1786 (2013).
68. Thakur M.S., and Ragavan K.V., Biosensors in food processing. *J. Food Sci. Technol.* **50**, 625-641 (2013).
69. J. C. E. Malik-Kale P., Lathrop S., Winfree S., Luterbach C., and Steele-Mortimer O., *Salmonella* - at home in the host cell. *Front. Microbiol.* **2**, 125-133 (2011).

70. Coburn B., Li Y., Owen D., Vallance B.A., and Finlay B.B., *Salmonella enterica* serovar Typhimurium pathogenicity island 2 is necessary for complete virulence in a mouse model of infectious enterocolitis. *Infect. Immun.* **73**, 3219-3227 (2005).
71. Ahmed A., Rushworth J.V., Hirst N.A., and Millner P.A., Biosensors for whole-cell bacterial detection. *Clin. Microbiol. Rev.* **27**, 631-646 (2014).
72. Gart E.V., Suchodolski J.S., Welsh Jr. T.H., Alaniz R.C., Randel R.D., and Lawhon S.D., *Salmonella* Typhimurium and multidirectional communication in the gut. *Front. Microbiol.* **7**, (2016).
73. WHO, *Salmonella* (non-typhoidal): Fact sheet. Available at: http://www.who.int/mediacentre/factsheets/fs139/en/. (2018).
74. Lindgren S.W., Stojiljkovic I., and Heffron F., Macrophage killing is an essential virulence mechanism of *Salmonella typhimurium*. *Proc. Natl. Acad. Sci. U.S.A.* **93**, 4197-4201 (1996).
75. Ricci F., Volpe J., Micheli L., and Palleschi G., A review on novel developments and applications of immunosensors in food analysis. *Anal. Chim. Acta* **605**, 111-129 (2007).
76. Centers for Disease Control and Prevention (CDC), Timeline for reporting cases of *Salmonella* infection. Available online at: http://www.cdc.gov/salmonella/reporting-timeline.html. (2015).
77. Yoon J.Y., and Kim B., Lab-on-a-chip pathogen sensors for food safety. *Sensors* **12**, 10713-10741 (2012).
78. Prusak-Sochaczewski E., Luong J.H., and Guilbault G.G., Development of a piezoelectric immunosensor for the detection of *Salmonella typhimurium*. *Enzyme Microb. Technol.* **12**, 173-177 (1990).
79. Ye J., Letcher S.V., and Rand A.G., Piezoelectric Biosensor for Detection of *Salmonella typhimurium*. *J. Food Sci.* **62**, 1067-1072 (1997).
80. Park I.S., and Kim N. , Thiolated *Salmonella* antibody immobilization onto the gold surface of piezoelectric quartz crystal. *Biosens. Bioelectron.* **13**, 1091-1097 (1998).
81. Park I.S., Kim W.Y., and Kim N., Operational characteristics of an antibody-immobilized QCM system detecting *Salmonella* spp. *Biosens. Bioelectron.* **15**, 167-172 (2000).
82. Pathirana S.T., Barbaree J., Chin B.A., Hartell M.G., Neely W.C., and Vodyanoy V., Rapid and sensitive biosensor for *Salmonella*. *Biosens. Bioelectron.* **15**, 135-141 (2000).
83. Wong Y.Y., Ng S.P., Ng M.H., Si S.H., Yao S.Z., and Fung Y.S., Immunosensor for the differentiation and detection of *Salmonella* species based on a quartz crystal microbalance. *Biosens. Bioelectron.* **17**, 676-684 (2002).
84. Kim G.H., Rand A.G., and Letcher S.V., Impedance characterization of a piezoelectric immunosensor part II: *Salmonella typhimurium* detection using magnetic enhancement. *Biosens. Bioelectron.* **18**, 91-99 (2003).
85. Su X.L., and Li Y., A QCM immunosensor for *Salmonella* detection with simultaneous measurements of resonant frequency and motional resistance. *Biosens. Bioelectron.* **21**, 840-848 (2005).
86. Olsen E.V., Sorokulova I.B., Petrenko V.A., Chen I.H., Barbaree J.M., and Vodyanoy V.J., Affinity-selected filamentous bacteriophage as a probe for acoustic wave biodetectors of *Salmonella typhimurium*. *Biosens. Bioelectron.* **21**, 1434-1442 (2006).
87. Salam F., Uludag Y., and Tothill I.E., Real-time and sensitive detection of *Salmonella* Typhimurium using an automated quartz crystal microbalance (QCM) instrument with nanoparticles amplification. *Talanta* **115**, 761-767 (2013).

88. Ozalp V.C., Bayramoglu G., Erdem Z., and Arica M.Y., Pathogen detection in complex samples by quartz crystal microbalance sensor coupled to aptamer functionalized core-shell type magnetic separation. *Anal. Chim. Acta* **853**, 533-540 (2015).
89. Trachtenberg S., and Hammel I., The rigidity of bacterial flagellar filaments and its relation to filament polymorphism. *J. Struct. Biol.* **109**, 18-27 (1992).
90. Kanazawa K.K., and Gordon J.G., Frequency of a quartz microbalance in contact with liquid. *Anal. Chem.* **57**, 1770-1771 (1985).
91. Kavita V., DNA biosensors - a review. *J. Bioengineer. and Biomedical Sci.* **7**, 222-226 (2017).
92. Chen S.H., Wu V.C.H., Chuang Y.C., and Lin C.H., Using oligonucleotide-functionalized Au nanoparticles to rapidly detect foodborne pathogens on a piezoelectric biosensor. *J. MIcrobiol. Methods* **73**, 7-17 (2008).
93. Nam J.M., Thaxton C.S., and Mirkin C.A., Nanoparticle-based bio-bar codes for the ultrasensitive detection of proteins. *Science* **301**, 1884-1886 (2003).
94. Chen L., Wei H., Guo Y., Cui Z., Zhang Z., and Zhang X.E., Gold nanoparticle enhanced immuno-PCR for ultrasensitive detection of Hantaan virus nucleocapsid protein. *J. Immunol. Methods* **346**, 64-70 (2009).
95. Bertani G., Lysogeny at mid-twentieth century: P1, P2, and other experimental systems. *J. Bacteriol.* **186**, 595-600 (2004).
96. Hill H.D., Millstone J.E., Banholzer M.J., and Mirkin C.A., The role radius of curvature plays in thiolated oligonucleotide loading on gold nanoparticles. *ACS Nano* **3**, 418-424 (2009).
97. Akbarzadeh A., Rezaei-Sadabady R., Davaran S., Joo S.W., Zarghami N., Hanifehpour Y., Samiei M., Kouhi M., and Nejati-Koshki K., Liposome: classification, preparation, and applications. *Nanoscale research letters* **8**, 102-110 (2013).
98. Shinde S.B., Fernandes C.B., and Patravale V.B., Recent trends in in-vitro nanodiagnostics for detection of pathogens. *J. Control Release* **159**, 164-180 (2012).
99. Patolsky F., Lichtenstein A., and Willner I., Electronic transduction of DNA sensing processes on surfaces: amplification of DNA detection and analysis of single-base mismatches by tagged liposomes. *J. Am. Chem. Soc.* **123**, 5194-5205 (2001).
100. Willner I., Patolsky F., Weizmann Y., and Willner B., Amplified detection of single-base mismatches in DNA using microgravimetric quartz-crystal-microbalance transduction. *Talanta* **56**, 847-856 (2002).
101. Patolsky F., Lichtenstein A., and Willner I., Amplified microgravimetric quartz-crystal-microbalance assay of DNA using oligonucleotide-functionalized liposomes or biotinylated liposomes. *J. Am. Chem. Soc.* **122**, 418-419 (2000).
102. Kim D., and Herr A.E., Protein immobilization techniques for microfluidic assays. *Biomicrofluidics* **7**, 41501 (2013).
103. Rusmini F., Zhong Z., and Feijen J., Protein immobilization strategies for protein biochips. *Biomacromolecules* **8**, 1775-1789 (2007).
104. Zhou L., Wang M.H., Wang J.P., and Ye Z.Z., Application of biosensor surface immobilization methods for aptamer. *Chinese J. Anal. Chem.* **39**, 432-438 (2011).
105. Song S., Wang L., Li J., Fan C., and Zhao J., Aptamer-based biosensors. *Trends Anal. Chem.* **27**, 108-117 (2008).
106. Seo H.B., and Gu M.B., Aptamer-based sandwich-type biosensors. *Journal of Biological Engineering* **11**, 11 (2017).
107. Min K., Cho M., Han S.Y., Shim Y.B., Ku J., and Ban C., A simple and direct electrochemical detection of interferon-γ using its RNA and DNA aptamers. *Biosens. Bioelectron.* **23**, 1819-1824 (2008).

108. Schlensog M.D., Gronewold T.M.A, Tewes M., Famulok M., and Quandt E., A Love-wave biosensor using nucleic acids as ligands. *Sens. Actuator B - Chem.* **101**, 308-315 (2004).
109. Joshi R., Janagama H., Dwivedi H.P., Senthil Kumar T.M., Jaykus L.A., Schefers J., and Sreevatsan S., Selection, characterization, and application of DNA aptamers for the capture and detection of *Salmonella enterica* serovars. *Mol. Cell. Probes* **23**, 20-28 (2009).
110. Poitras C., and Tufenkji N., A QCM-D-based biosensor for *E. coli* O157:H7 highlighting the relevance of the dissipation slope as a transduction signal. *Biosens. Bioelectron.* **24**, 2137-2142 (2009).
111. Olsson A.L., van der Mei H.C., Busscher H.J., and Sharma P.K., Acoustic sensing of the bacterium-substratum interface using QCM-D and the influence of extracellular polymeric substances. *J. Colloid Interface Sci.* **357**, 135-138 (2011).
112. Vaughan R.D., O'Sullivan C.K., and Guilbault G.G., Development of a quartz crystal microbalance (QCM) immunosensor for the detection of *Listeria monocytogenes*. *Enzyme Microb. Technol.* **29**, 635-638 (2001).
113. Jiang X., Wang R., Wang Y., Su X., Ying Y., Wang J., and Li Y., Evaluation of different micro/nanobeads used as amplifiers in QCM immunosensor for more sensitive detection of *E. coli* O157:H7. *Biosens. Bioelectron.* **29**, 23-28 (2011).
114. Dybwad G.L., A sensitive new method for the determination of adhesive bonding between a particle and a substrate. *J. Appl. Phys.* **58**, 2789-2790 (1985).
115. Papadakis G., Tsortos A., Mitsakakis K., and Gizeli E., Characterization of DNA-Hv1 histone interactions; discrimination of DNA size and shape. *FEBS Lett.* **584**, 935-940 (2010).
116. Zanoli L.M., and Spoto G., Isothermal amplification methods for the detection of nucleic acids in microfluidic devices. *Biosensors* **3**, 18-43 (2013).
117. Asiello P.J., and Baeumner A.J., Miniaturized isothermal nucleic acid amplification, a review *Lab Chip* **11**, 1420-1430 (2011).
118. Mullis K.B., and Faloona F.A., Specific synthesis of DNA in vitro via a polymerase-catalyzed chain reaction. *Method. Enzymol.* **155**, 335-350 (1987).
119. Kersting S., Rausch V., Bier F.F., and von Nickisch-Rosenegk M., Multiplex isothermal solid-phase recombinase polymerase amplification for the specific and fast DNA-based detection of three bacterial pathogens. *Microchim. Acta* **181**, 1715-1723 (2014).
120. James A., and Macdonald J., Recombinase polymerase amplification: emergence as a critical molecular technology for rapid, low-resource diagnostics. *Expert Rev. Mol. Diagn.* **15**, 1475-1489 (2015).
121. Compton J., Nucleic acid sequence-based amplification. *Nature* **350**, 91-92 (1991).
122. Notomi T., Okayama H., Masubuchi H., Yonekawa T., Watanabe K., AminoN., and Hase T., Loop-mediated isothermal amplification of DNA. *Nucleic Acids Res.* **28**, e63 (2000).
123. Gusev Y., Sparkowski J., Raghunathan A., Ferguson H. Jr., Montano J., Bogdan N., Schweitzer B., Wiltshire S., Kingsmore S.F., Maltzman W., and Wheeler V., Rolling circle amplification: a new approach to increase sensitivity for immunohistochemistry and flow cytometry. *Am. J. Pathol.* **159**, 63-69 (2001).
124. Vincent M., Xu Y., and Kong H., Helicase-dependent isothermal DNA amplification. *EMBO Rep.* **5**, 795-800 (2004).
125. Piepenburg O., Williams C.H., Stemple D.L., and Armes N.A., DNA detection using recombination proteins. *PLoS Biol.* **4**, e204 (2006).

126. Euler M., Wang Y., Nentwich O., Piepenburg O., Hufert F.T., and Weidmann M., Recombinase polymerase amplification assay for rapid detection of Rift Valley fever virus. *J. Clin. Virol.* **54**, 308-312 (2012).
127. Shen F., Davydova E.K., Du W., Kreutz J.E., Piepenburg O., and Ismagilov R.F., Digital isothermal quantification of nucleic acids via simultaneous chemical initiation of recombinase polymerase amplification reactions on SlipChip. *Anal. Chem.* **89**, 3533-3540 (2011).
128. TwistDx, RPA. The versatile PCR replacement. Available at: https://www.twistdx.co.uk/. (2018).
129. Mayboroda O., Gonzalez Benito A., Sabate del Rio J., Svobodova M., Julich S., Tomaso H., O'Sullivan C.K., and Katakis I., Isothermal solid-phase amplification system for detection of *Yersinia pestis*. *Anal. Bioanal. Chem.* **408**, 671-676 (2016).
130. del Río S.J., Steylaerts T., Henry O.Y., Bienstman P., Stakenborg T., Van Roy W., and O'Sullivan C.K., Real-time and label-free ring-resonator monitoring of solid-phase recombinase polymerase amplification. *Biosens. Bioelectron.* **73**, 130-137 (2015).
131. Santiago-Felipe S., Tortajada-Genaro L.A., Morais S., Puchades R., and Maquieira Á., Isothermal DNA amplification strategies for duplex microorganism detection. *Food Chem.* **174**, 509-515 (2015).
132. Santiago-Felipe S., Tortajada-Genaro L.A., Morais S., Puchades R., and Maquieira Á., One-pot isothermal DNA amplification – hybridisation and detection by a disc-based method. *Sens. Actuator B - Chem.* **204**, 273-281 (2014).
133. Kunze A., Dilcher M., Abd El Wahed A., Hufert F., Niessner R., and Seidel M., On-chip isothermal nucleic acid amplification on flow-based chemiluminescence microarray analysis platform for the detection of viruses and bacteria. *Anal. Chem.* **88**, 898-905 (2016).
134. del Río J.S., Yehia Adly N., Acero-Sánchez J.L., Henry O.Y., and O'Sullivan C.K., Electrochemical detection of *Francisella tularensis* genomic DNA using solid-phase recombinase polymerase amplification. *Biosens. Bioelectron.* **54**, 674-678 (2014).
135. Papadakis G., Friedt J.M., Eck M., Rabus D., Jobst G., and Gizeli E., Optimized acoustic biochip integrated with microfluidics for biomarkers detection in molecular diagnostics. *Biomed. Microdevices* **19**, 1-11 (2017).
136. MItsakakis K., and Gizeli E., Detection of multiple cardiac markers with an integrated acoustic platform for cardiovascular risk assessment. *Anal. Chim. Acta* **699**, 1-5 (2011).
137. Mitsakakis K., Tserepi A., and Gizeli E., Integration of microfluidics with a Love wave sensor for the fabrication of a multisample analytical microdevice. *J. Microelectromech. Syst.* **17**, 1010-1019 (2008).
138. Kordas A., Papadakis G., Milioni D., Champ J., Descroix S., and Gizeli E., Rapid *Salmonella* detection using an acoustic wave device combined with the RCA isothermal DNA amplification method. *Sensing and Bio-Sensing Research* **11**, 121-127 (2016).
139. Yao C., Xiang Y., Deng K., Xia H., and Fu W., Sensitive and specific HBV genomic DNA detection using RCA-based QCM biosensor. *Sens. Actuator B - Chem.* **181**, 382-387 (2013).
140. Prakrankamanant P., Leelayuwat C., Promptmas C., Limpaiboon T., Wanram S., Prasongdee P., Pientong C., Daduang J., Jearanaikoon P., The development of DNA-based quartz crystal microbalance integrated with isothermal DNA amplification system for human papillomavirus type 58 detection. *Biosens. Bioelectron.* **40**, 252-257 (2013).

141. Galán J.E., Ginnochio C., and Costeas P., Molecular and functional characterization of the *Salmonella* invasion gene *invA*: homology of InvA to members of a new protein family. *J. Bacteriol.* **174**, 4338-4349 (1992).
142. Rahn K., De Grandis S.A., Clarke R.C., McEwen S.A., Galán J.E., Ginocchio C., Curtiss R. III, Gyles C.L., Amplification of an *invA* gene sequence of *Salmonella typhimurium* by polymerase chain reaction as a specific method of detection of *Salmonella*. *Mol. Cell. Probes* **6**, 271-279 (1992).
143. Teoh B.T., Sam S.S., Tan K.K., Danlami M.B., Shu M.H., Johari J., Hooi P.S., Brooks D., Piepenburg O., Nentwich O., Wilder-Smith A., Franco L., Tenorio A., and AbuBakar S., Early detection of Dengue virus by use of reverse transcription-recombinase polymerase amplification. *J. Clin. Microbiol.* **53**, 830837 (2015).
144. van der Meulen S.A., Dubacheva G.V., Dogterom M., Richter R.P., and Leunissen M.E., Quartz crystal microbalance with dissipation monitoring and spectroscopic ellipsometry measurements of the phospholipid bilayer anchoring stability and kinetics of hydrophobically modified DNA oligonucleotides. *Langmuir* **30**, 6525-6533 (2014).
145. MItsakakis K., and Gizeli E., Multi-sample acoustic biosensing microsystem for protein interaction analysis. *Biosens. Bioelectron.* **26**, 4579-4584 (2011).
146. U. S. National Center for Health Statistics (US). Health, 2016: With chartbook on long-term trends in health. Hyattsville (MD): National Center for Health Statistics (US); 2017 May. Available from: https://www.ncbi.nlm.nih.gov/books/NBK453378/.
147. Molecular Diagnostics in Cancer - Research Advocacy Network., Available at: http://www.researchadvocacy.org/sites/default/files/resources/MolecularDiagnosticsTutorialFinal.pdf.
148. Jayanthi V.S.P.K. S.A., Das A.B., and Saxena U., Recent advances in biosensor development for the detection of cancer biomarkers. *Biosens. Bioelectron.* **91**, 15-23 (2017).
149. Tothill I.E., Biosensors for cancer markers diagnosis. *Semin. Cell Dev. Biol.* **20**, 55-62 (2009).
150. Wang L., Early diagnosis of breast cancer. *Sensors* **17**, e1572 (2017).
151. Drain P.K., Hyle E.P., Noubary F., Freedberg K.A., Wilson D., Bishai W.R., Rodriguez W., and Bassett I.V., Diagnostic point-of-care tests in resource-limited settings. *Lancet Infect. Dis.* **14**, 239-249 (2014).
152. Office of Biological and Environmental Research of the U.S. Department of Energy Office of Science., Available at: http://www.science.energy.gov/ber/.
153. Soper S.A., Brown K., Ellington A., Frazier B., Garcia-Manero G., Gau V., Gutman S.I., Hayes D.F., Korte B., Landers J.L., Larson D., Ligler F., Majumdar A., Mascini M., Nolte D., Rosenzweig Z., Wang J., and Wilson D., Point-of-care biosensor systems for cancer diagnostics/prognostics. *Biosens. Bioelectron.* **21**, 1932-1942 (2006).
154. Varshney J., and Subramanian S., Small is the new big – interplay of miRNAs in cancer *Curr. Sci.* **107**, 803-814 (2014).
155. Dey S., Preventing breast cancer in LMICs *via* screening and/or early detection: the real and the surreal. *World J. Clin. Oncol.* **5**, 509-519 (2014).
156. Loginov V.I., Burdennyy A.M., Pronina I.V., Khokonova V.V., Kurevljov S.V., Kazubskaya T.P., Kushlinskii N.E., and Braga E.A., Novel miRNA genes hypermethylated in breast cancer. *Mol. Biol. (Mosk)* **50**, 705-709 (2016).
157. Sutcliffe S., Pharoah P.D., Easton D.F., and Ponder B.A., Ovarian and breast cancer risks to women in families with two or more cases of ovarian cancer. *Int. J. Cancer* **87**, 110-117 (2000).

158. Arif S., Qudsia S., Urooj S., Chaudry N., Arshad A., and Andleeb S., Blueprint of quartz crystal microbalance biosensor for early detection of breast cancer through salivary autoantibodies against ATP6AP1. *Biosens. Bioelectron.* **65**, 62-70 (2015).
159. Litton J.K., and Theriault R.L., Breast cancer and pregnancy: current concepts in diagnosis and treatment. *Oncologist* **15**, 1238-1247 (2010).
160. Berkey C.S.B., Tamimi R.M., Rosner B., Frazier A.L., and Colditz G.A., Young women with family history of breast cancer and their risk factors for benign breast disease. *Cancer* **118**, 2796-2803 (2012).
161. Seitz H.K., Pelucchi C., Bagnardi V., and La Vecchia C., Epidemiology and pathophysiology of alcohol and breast cancer: update 2012. *Alcohol Alcohol.* **47**, 204-212 (2012).
162. Smith-Warner S.A., Spiegelman D., Adami H.O., Beeson W.L., van den Brandt P.A., Folsom A.R., Fraser G.E., Freudenheim J.L., Goldbohm R.A., Graham S., Kushi L.H., Miller A.B., Rohan T.E., Speizer F.E., Toniolo P., Willett W.C,, Wolk A., Zeleniuch-Jacquotte A., and Hunter D.J., Types of dietary fat and breast cancer: a pooled analysis of cohort studies. *Int. J. Cancer* **92**, 767-774 (2001).
163. Cleary M.P., and Grossmann M.E., Minireview: obesity and breast cancer: the estrogen connection. *Endocrinology* **150**, 2537-2542 (2009).
164. Lagadec C., Vlashi E., Della Donna L., Dekmezian C., and Pajonk F., Radiation-induced reprogramming of breast cancer cells. *Stem Cells* **30**, 833-844 (2012).
165. Roy R., Chun J., and Powell S.N., BRCA1 and BRCA2: different roles in a common pathway of genome protection. *Nat. Rev. Cancer* **12**, 68-78 (2012).
166. Coleman W.B., Breast cancer personalized medicine: challenges and opportunities. *Am. J. Pathol.* **183**, 1036-1037 (2013).
167. De Abreu F.B., Wells W.A., and Tsongalis G.J., The emerging role of the molecular diagnostics laboratory in breast cancer personalized medicine. *Am. J. Pathol.* **183**, 1075-1083 (2013).
168. Dong H., Lei J., Ding L., Wen Y., Ju H., and Zhang X., MicroRNA: function, detection, and bioanalysis. *Chem. Rev.* **113**, 6207-6233 (2013).
169. Tang J., Ahmad A., and Sarkar F.H., The role of microRNAs in breast cancer migration, invasion and metastasis. *Int. J. Mol. Sci.* **13**, 13414-13437 (2012).
170. Huang S., Chen Y., Wu W., Ouyang N., Chen J., Li H., Liu X., Su F., Lin L., and Yao Y., miR-150 promotes human breast cancer growth and malignant behavior by targeting the pro-apoptotic purinergic $P2X_7$ receptor. *PLoS One* **8**, e80707 (2013).
171. Lawrie C.H., Gal S., Dunlop H.M., Pushkaran B., Liggins A.P., Pulford K., Banham A.H., Pezzella F., Boultwood J., Wainscoat J.S., Hatton C.S., and Harris A.L.. Detection of elevated levels of tumour-associated microRNAs in serum of patients with diffuse large B-cell lymphoma. *Br. J. Haematol.* **141**, 672-675 (2008).
172. Mitchell P.S., Parkin R.K., Kroh E.M., Fritz B.R., Wyman S.K., Pogosova-Agadjanyan E.L., Peterson A., Noteboom J., O'Briant K.C., Allen A., Lin D.W., Urban N., Drescher C.W., Knudsen B.S., Stirewalt D.L., Gentleman R., Vessella R.L., Nelson P.S., Martin D.B., and Tewari M., Circulating microRNAs as stable blood-based markers for cancer detection. *Proc. Natl. Acad. Sci. U.S.A.* **105**, 10513-10518 (2008).
173. Esquela-Kerscher A., and Slack F.J., Oncomirs - microRNAs with a role in cancer. *Nat. Rev. Cancer* **6**, 259-269 (2006).
174. O'Day E., and Lal A., MicroRNAs and their target gene networks in breast cancer. *Breast Cancer Res.* **12**, 201-210 (2010).
175. Madhavan D., Zucknick M., Wallwiener M., Cuk K., Modugno C., Scharpff M., Schott S., Heil J., Turchinovich A., Yang R., Benner A., Riethdorf S., Trumpp A., Sohn C., Pantel K., Schneeweiss A., and Burwinkel B., Circulating miRNAs as surrogate

markers for circulating tumor cells and prognostic markers in metastatic breast cancer. *Clin. Cancer Res.* **18**, 5972-5982 (2012).
176. Liu Q., Shin Y., Kee J.S., Kim K.W., Mohamed Rafei S.R., Perera A.P., Tu X., Lo G.Q., Ricci E., Colombel M., Chiong E., Thiery J.P., Park M.K., Mach-Zehnder interferometer (MZI) point-of-care system for rapid multiplexed detection of microRNAs in human urine specimens. *Biosens. Bioelectron.* **71**, 365-372 (2015).
177. Su L., Zou L., Fong C.C., Wong W.L., Wei F., Wong K.Y., Wu R.S., and Yang M., Detection of cancer biomarkers by piezoelectric biosensor using PZT ceramic resonator as the transducer. *Biosens. Bioelectron.* **46**, 155-161 (2013).
178. Gruhl F.J., and Länge K., Surface modification of an acoustic biosensor allowing the detection of low concentrations of cancer markers. *Anal. Biochem.* **420**, 188-190 (2012).
179. Ding Y., Liu J., Wang H., Shen G., and Yu R., A piezoelectric immunosensor for the detection of alpha-fetoprotein using an interface of gold/hydroxyapatite hybrid nanomaterial. *Biomaterials* **28**, 2147-2154 (2007).
180. Chou S.F., Hsu W.L., Hwang J.M., and Chen C.Y., Development of an immunosensor for human ferritin, a nonspecific tumor marker, based on a quartz crystal microbalance. *Anal. Chim. Acta* **453**, 181-189 (2002).
181. Papadakis G., Tsortos A., Kordas A., Tiniakou I., Morou E., Vontas J., Kardassis D., and Gizeli E., Acoustic detection of DNA conformation in genetic assays combined with PCR. *Sci. Rep.* **3**, 2033 (2013).
182. Yeri A.S., Gao L., and Gao D., Mutation screening based on the mechanical properties of DNA molecules tethered to a solid surface. *J. Phys. Chem. B* **114**, 1064-1068 (2010).
183. Dell'Atti D., Tombelli S., Minunni M., and Mascini M., Detection of clinically relevant point mutations by a novel piezoelectric biosensor. *Biosens. Bioelectron.* **21**, 1876-1879 (2006).
184. Gronewold T.M., Baumgartner A., Quandt E., and Famulok M., Discrimination of single mutations in cancer-related gene fragments with a surface acoustic wave sensor. *Anal. Chem.* **78**, 4865-4871 (2006).
185. Wang J., Nielsen P.E., Jiang M., Cai X., Fernandes J.R., Grant D.H., Ozsoz M., Beglieter A., and Mowat M., Mismatch-sensitive hybridization detection by peptide nucleic acids immobilized on a quartz crystal microbalance. *Anal. Chem.* **69**, 5200-5202 (1997).
186. Premaratne G., Al Mubarak Z.H., Senavirathna L., Liu L., and Krishnan S., Measuring ultra-low levels of nucleotide biomarkers using quartz crystal microbalance and SPR microarray imaging methods: a comparative analysis. *Sens. Actuator B - Chem.* **253**, 368-375 (2017).
187. Palaniappan A., Cheema J.A., Rajwar D., Ammanath G., Xiaohu L., Koon L.S., Yi W., Yildiz U.H., and Liedberg B., Polythiophene derivative on quartz resonators for miRNA capture and assay *Analyst* **140**, 7912-7917 (2015).
188. Plaxco K.W., and Soh H.T., Switch-based biosensors: a new approach towards real-time, in vivo molecular detection. *Trends Biotechnol.* **29**, 1-5 (2011).
189. Lubin A.A., and Plaxco K.W., Folding-based electrochemical biosensors: the case for responsive nucleic acid architectures. *Acc. Chem. Res.* **43**, 496-505 (2010).
190. Wang C., Zhu Z., Song Y., Lin H., Yang C.J., and Tan W., Caged molecular beacons: controlling nucleic acid hybridization with light. *Chem. Commun.* **47**, 5708-5710 (2011).
191. Lai R.Y., Lagally E.T., Lee S.H., Soh H.T., Plaxco K.W., and Heeger A.J., Rapid, sequence-specific detection of unpurified PCR amplicons via a reusable, electrochemical sensor. *Proc. Natl. Acad. Sci. U.S.A.* **103**, 4017-4021 (2006).

192. Chiba J., Akaishi A., Ikeda R., and Inouye M., Electrochemical detection of insertion/deletion mutations based on enhanced flexibility of bulge-containing duplexes on electrodes *Chem. Commun.* **46**, 7563-7565 (2010).
193. Immoos C.E., Lee S.J., and Grinstaff M.W., Conformationally gated electrochemical gene detection. *ChemBioChem.* **5**, 1100-1103 (2004).
194. Idili A., Amodio A., Vidonis M., Feinberg-Somerson J., Castronovo M., and Ricci F., Folding-upon-binding and signal-on electrochemical DNA sensor with high affinity and specificity. *Anal. Chem.* **86**, 9013-9019 (2014).
195. Idili A., Plaxco K.W., Vallée-Bélisle A., and Ricci F., Thermodynamic basis for engineering high-affinity, high-specificity binding-induced DNA clamp nanoswitches. *ACS Nano* **7**, 10863-10869 (2013).
196. Iorio M.V., Ferracin M., Liu C.G., Veronese A., Spizzo R., Sabbioni S., Magri E., Pedriali M., Fabbri M., Campiglio M., Ménard S., Palazzo J.P., Rosenberg A., Musiani P., Volinia S., Nenci I., Calin G.A., Querzoli P., Negrini M., and Croce C.M., MicroRNA gene expression deregulation in human breast cancer. *Cancer Res.* **65**, 7065-7070 (2005).
197. Xia M.H.P., Great potential of microRNA in cancer stem cell. *J. Canc. Mol.* **4**, 79-89 (2008).
198. Wang S., Ma G., Zhu H., Lv C., Chu H., Tong N., Wu D., Qiang F., Gong W., Zhao Q., Tao G., Zhou J., Zhang Z., and Wang M., miR-107 regulates tumor progression by targeting NF1 in gastric cancer. *Sci. Rep.* **6**, 36531 (2016).
199. Martello G., Rosato A. Ferrari F., Manfrin A., Cordenonsi M., Dupont S., Enzo E., Guzzardo V., Rondina M., Spruce T., Parenti A., Daidone M.G., Bicciato S., and Piccolo S., A microRNA targeting dicer for metastasis control. *Cell* **141**, 1195-1207 (2010).
200. Papageorgiou N., Tousoulis D., Androulakis E., Siasos G., Briasoulis A., Vogiatzi G., Kampoli A.M., Tsiamis E., Tentolouris C., and Stefanadis C., The role of microRNAs in cardiovascular disease. *Curr. Med. Chem.* **19**, 2605-2610 (2012).
201. Feng J., Xing W., and Xie L., Regulatory roles of microRNAs in diabetes. *Int. J. Mol. Sci.* **17**, 1729 (2016).
202. Femminella G.D., Ferrara N., and Rengo G., The emerging role of microRNAs in Alzheimer's disease. *Front. Physiol.* **6**, 1-5 (2015).
203. Nadal C., Winder T., Gerger A., and Tougeron D., Future perspectives of circulating tumor DNA in colorectal cancer. *Tumor Biol.* **39**, 1-14 (2017).
204. Dinu D., Dobre M., Panaitescu E., Bîrlă R., Iosif C., Hoara P., Caragui A., Boeriu M., Constantinoiu S., and Ardeleanu C., Prognostic significance of KRAS gene mutations in colorectal cancer--preliminary study. *J. Med. Life* **7**, 581-587 (2014).
205. WHO, Cancer: Fact sheet. Available at: http://www.who.int/mediacentre/factsheets/fs297/en/. (2018).
206. Perakis S., and Speicher M.R., Emerging concepts in liquid biopsies. *BMC Medicine* **15**, 75 (2017).
207. Diaz Jr. L.A., and Bardelli A., Liquid biopsies: genotyping circulating tumor DNA. *J. Clin. Oncol.* **32**, 579-586 (2014).
208. Overman M.J., Modak J., Kopetz S., Murthy R., Yao J.C., Hicks M.E., Abbruzzese J.L., and Tam A.L., Use of research biopsies in clinical trials: are risks and benefits adequately discussed? *J. Clin. Oncol.* **31**, 17-22 (2013).
209. Simonite T., 10 Breakthrough Technologies of 2015: Where are they Now?. Available at: https://www.technologyreview.com/s/544996/10-breakthrough-technologies-of-2015-where-are-they-now/. (2015).
210. Thierry A.R., Mouliere F., El Messaoudi S., Mollevi C., Lopez-Crapez E., Rolet F., Gillet B., Gongora C., Dechelotte P., Robert B., Del Rio M., Lamy P.J., Bibeau F., Nouaille

M., Loriot V., Jarrousse A.S., Molina F., Mathonnet M., Pezet D., Ychou M., Clinical validation of the detection of KRAS and BRAF mutations from circulating tumor DNA. *Nat. Med.* **20**, 430-436 (2014).

211. Heitzer E., Ulz P., and Geigl J.B., Circulating tumor DNA as a liquid biopsy for cancer. *Clin. Chem.* **61**, 112-123 (2015).
212. Phipps A.I., Buchanan D.D., Makar K.W., Win A.K., Baron J.A., Lindor N.M., Potter J.D., and Newcomb P.A., KRAS-mutation status in relation to colorectal cancer survival: the joint impact of correlated tumour markers. *Br. J. Cancer* **108**, 1757-1764 (2013).
213. Molina J.R., and Adjei A.A., The Ras/Raf/MAPK pathway. *J. Thorac. Oncol.* **1**, 7-9 (2006).
214. Loupakis F., Ruzzo A., Cremolini C., Vincenzi B., Salvatore L., Santini D., Masi G., Stasi I., Canestrari E., Rulli E., Floriani I., Bencardino K., Galluccio N., Catalano V., Tonini G., Magnani M., Fontanini G., Basolo F., Falcone A., and Graziano F., KRAS codon 61, 146 and BRAF mutations predict resistance to cetuximab plus irinotecan in KRAS codon 12 and 13 wild-type metastatic colorectal cancer. *Br. J. Cancer* **101**, 715-721 (2009).
215. Diehl F., Schmidt K., Choti M.A., Romans K., Goodman S., Li M., Thornton K., Agrawal N., Sokoll L., Szabo S.A., Kinzler K.W., Vogelstein B., and Diaz Jr. L.A., Circulating mutant DNA to assess tumor dynamics. *Nat. Med.* **14**, 985-990 (2008).
216. Diehl F., Li M., Dressman D., He Y., Shen D., Szabo S., Diaz Jr. L.A., Goodman S.N., David K.A., Juhl H., Kinzler K.W., and Vogelstein B., Detection and quantification of mutations in the plasma of patients with colorectal tumors. *Proc. Natl. Acad. Sci. U.S.A.* **102**, 16368-16373 (2005).
217. Rissin D.M., López-Longarela B., Pernagallo S., Ilyine H., Vliegenthart A.D.B., Dear J.W., Díaz-Mochón J.J., and Duffy D.C., Polymerase-free measurement of microRNA-122 with single base specificity using single molecule arrays: Detection of drug-induced liver injury. *PLoS One* **12**, e0179669 (2017).
218. Wu J.C., Meng Q.C., Ren H.M., Wang H.T., Wu J., and Wang Q., Recent advances in peptide nucleic acid for cancer bionanotechnology. *Acta Pharmacol. Sin.* **38**, 798-805 (2017).
219. Bowler F.R., Diaz-Mochon J.J., Swift M.D., and Bradley M., DNA analysis by dynamic chemistry. *Angew. Chem. Int. Ed.* **49**, 1809-1812 (2010).
220. Pernagallo S., Ventimiglia G., Cavalluzzo C., Alessi E., Ilyine H., Bradley M., and Diaz-Mochon J.J., Novel biochip platform for nucleic acid analysis. *Sensors* **12**, 8100-8111 (2012).
221. Venkateswaran S., Luque-González M.A., Tabraue-Chávez M., Fara M.A., López-Longarela B., Cano-Cortes V., López-Delgado F.J., Sánchez-Martín R.M., Ilyine H., Bradleu M., Pernagallo S., and Díaz-Mochón J.J., Novel bead-based platform for direct detection of unlabelled nucleic acids through single nucleobase labelling. *Talanta* **161**, 489-496 (2016).
222. Luque-González M.A., Tabraue-Chávez M., López-Longarela B., Sánchez-Martín R.M., Ortiz-González M., Soriano-Rodríguez M., García-Salcedo J.A., Pernagallo S., and Díaz-Mochón J.J., Identification of Trypanosomatids by detecting single nucleotide fingerprints using DNA analysis by dynamic chemistry with MALDI-ToF. *Talanta* **176**, 299-307 (2018).
223. Uttenthaler E., Schräml M., Mandel J., and Drost S., Ultrasensitive quartz crystal microbalance sensors for detection of M13-Phages in liquids. *Biosens. Bioelectron.* **16**, 735-743 (2001).
224. March C., García J.V., Sánchez A., Arnau A., Jiménez Y., García P., Manclús J.J., and Montoya A., High-frequency phase shift measurement greatly enhances the sensitivity of QCM immunosensors. *Biosens. Bioelectron.* **65**, 1-8 (2015).

225. García J.V., Rocha M.I., March C., García P., Francis L.A., Montoya A., Arnau A., and Jimenez Y. , Love mode surface acoustic wave and high fundamental frequency quartz crystal microbalance immunosensors for the detection of Carbaryl pesticide. *Procedia Engineering* **87**, 759-762 (2014).
226. Carrascosa L.G., Martínez L., Huttel Y., Román E., and Lechuga L.M., Understanding the role of thiol and disulfide self-assembled DNA receptor monolayers for biosensing applications. *Eur. Biophys. J.* **39**, 1433-1444 (2010).
227. Karamollaoğlu I., Öktem H.A., and Mutlu M., QCM-based DNA biosensor for detection of genetically modified organisms (GMOs). *Biochem. Eng. J.* **44**, 142-150 (2009).
228. Höök F., Ray A., Nordén B., and Kasemo B., Characterization of PNA and DNA immobilization and subsequent hybridization with DNA using acoustic-shear-wave attenuation measurements. *Langmuir* **17**, 8305-8312 (2001).
229. Moreau G., Fourati N.N., Zerrouki C., Mouhsine H., Montes M., Port M., Sylla-Iyarreta Veitía M., Zagury J.F., and Yaakoubi N., Surface acoustic wave biosensors for the quantification of TNF-α/SPD-304 interaction. *Procedia Engineering* **168**, 432-435 (2016).
230. Skládal P., Piezoelectric quartz crystal sensors applied for bioanalytical assays and characterization of affinity interactions. *J. Braz. Chem. Soc.* **14**, 491-502 (2003).
231. Yaeger R., and Saltz L., BRAF mutations in colorectal cancer: clinical relevance and role in targeted therapy. *J. Natl. Compr. Cancer Netw.* **10**, 1456-1458 (2012).
232. Holdhoff M., Schmidt K., Donehower R., and Diaz L.A. Jr., Analysis of circulating tumor DNA to confirm somatic KRAS mutations. *J. Natl. Cancer Inst.* **101**, 1284-1285 (2009).
233. Amado R.G., Wolf M., Peeters M., Van Cutsem E., Siena S., Freeman D.J., Juan T., Sikorski R., Suggs S., Radinsky R., Patterson S.D., and Chang D.D., Wild-type KRAS is required for panitumumab efficacy in patients with metastatic colorectal cancer. *J. Clin. Oncol.* **26**, 1626-1634 (2008).
234. Karapetis C.S., Khambata-Ford S., Jonker D.J., O'Callaghan C.J., Tu D., Tebbutt N.C., Simes R.J., Chalchal H., Shapiro J.D., Robitaille S., Price T.J., Shepherd L., Au H.J., Langer C., Moore M.J., and Zalcberg J.R., K-ras mutations and benefit from cetuximab in advanced colorectal cancer. *N. Engl. J. Med.* **359**, 1757-1765 (2008).

# Publications Appendix

**1.** A. Grammoustianou, E. Gizeli. Acoustic wave-based immunoassays: Vashist S., Luong J. (Ed): Handbook of Immunoassay Technologies, Approaches, Performances and Applications, Chapter 9, *Elsevier Academic Press*, 2018

**2.** A. Grammoustianou *et al.* Solid-phase isothermal DNA amplification and detection on Quartz Crystal Microbalance using liposomes and dissipation monitoring. *IEEE Sensors Letters*, **1**(5), 2017

**3.** K. Tsougeni *et al.* Plasma nanotextured polymeric lab-on-chip for highly efficient bacteria capture and lysis. *Lab on a Chip*, **16**, 2016

**4.** M. Gianneli *et al.* Nanostructured PMMA-coated Love wave device as a platform for protein adsorption studies. *Sensors and Actuators B*, **236**, 2016

**5.** A. Tsortos *et al.* The detection of multiple DNA targets with a single probe using a conformation-sensitive acoustic sensor. *Chemical Communications*, **51** (57), 2015